UNIVERSITÀ DELLA CALABRIA

Dipartimento di Biologia, Ecologia e Scienze della Terra

Scuola di Dottorato in Scienze e Ingegneria dell'Ambiente, delle Costruzioni e dell'Energia (SIACE) – XXXVI Ciclo

LATE PLEISTOCENE COASTAL SEA SURFACE TEMPERATURE AND ENVIRONMENTAL RECONSTRUCTION FOR A POST GLOBAL-WARMING CLIMATE MODELLING IN THE CENTRAL MEDITERRANEAN

Settore Scientifico Disciplinare (04/GEOS-02/A)

Coordinatore: *Prof. Salvatore Critelli*

Salvatore Critelli
09.09.2024 08:17:43
GMT+01:00

Supervisore: *Prof. Edoardo Perri*

Cosupervisore: *Prof.ssa Maria Pia Bernasconi*

Dottorando: *Pierluigi Santagati*

Index

PREFACE

This PhD thesis collects the results of the research activities conducted between 2020 and 2023 in the PhD course in Environmental, Construction and Energy Sciences and Engineering (SIACE) at the University of Calabria (UNICAL). This study focuses on the palaeoenvironmental characterization, comprising palaeoecological and palaeoclimatic topics, of two Late Pleistocene fossiliferous deposits, located in the Central Mediterranean (Calabria and Apulia, Southern Italy), both related to the Marine Isotope Stage (MIS) 5, which is the Last Interglacial sensu lato. A multidisciplinary approach was adopted, using techniques and topics from palaeontology, palaeoecology, carbonate sedimentology, and geochemistry, all with the aim to characterize the past palaeoenvironmental settings in the studied area during the Last Interglacial.

The last interglacial, in particular its first substage known as MIS 5e (about 125 ka ago), is the last warm period before the current interglacial. During this short time of span, higher global temperatures (globally estimated at +1-2 °C), higher sea levels, reduced ice caps that the current interglacial took place, accompanied also by changes in the latitudinal distribution of living species. Due to its recent age, the last interglacial is often considered as a good model for understating the current global warming.

The aim of the thesis is to contribute to the knowledge of the palaeoenvironmental dynamics that took place in the Central Mediterranean during the Last Interglacial, hoping that such data, being relative to a recent warm period, with a slightly different climate than today, can give a contribution to understanding how current marine systems respond to the ongoing global warming.

Below a short summary of the chapters of the thesis that are subdivided into a: state of the art and methodologies in palaeoclimatology (*Chapters 1 to 3*); results achieved (*Chapters 4 to 8*) mainly based on research papers published or submitted to international or national journals (including some work in progress), with their related conclusions; and finally, a general conclusion part (Chapter 9).

Chapter 1 (*Cenozoic to Tyrrhenian palaeoclimate history*) summarizes some of the main topics of palaeoclimatology, with reference to the Late Pleistocene and to the Last Interglacial, in order to give a climatic and chronologic framework for the studied sites.

Chapter 2 (*Main Causes of Climate changes*) deals with the main causes of the Cenozoic climate changes.

Chapter 3 (*Methods of study and analysis in palaeoclimatology*) discuss the most used geological, geochemical, and palaeoecological approaches in palaeoclimatology, focused on the palaeotemperature estimations.

Chapters 4, 5 and *6* deal with the palaeoecological, palaeoclimatic, and petrographic study of a MIS 5e calcarenite coming from the coastline of the Mar Piccolo of Taranto (TA, Apulia). The topics of these chapters are partially published in the following contributes:

1. **Santagati P**., Edoardo Perri E., Maria Pia Bernasconi M.P., Borrelli M., Guerrieri S., Critelli S. (**2024a**). MIS 5e Sea Surface Temperature estimation; a multi-proxy approach using a marine macrofossil assemblage (Mar Piccolo, Gulf of Taranto, Southern Italy). *Journal of palaeogeography, 2024.*

2. **Santagati P**., Borrelli M., Guerrieri S., Perri E. (**2024b**). Early diagenetic microbial induced cementation in Late Pleistocene (Mis 5e) shallow-water marine deposits of the Taranto Gulf (South Italy). *Rendiconti Online Società Geologica Italiana.*
3. **Santagati P**., Borrelli M. Bernasconi M.P., Perri E. (**2023a**). Fossil fauna in MIS 5e deposits of Mar Piccolo basin (Taranto, Southern Italy) suggests new palaeoclimatic constraints. *Rendiconti Online Società Geologica Italiana*, 59, 16-20.
4. **Santagati P.**, Borrelli M., Bernasconi M.P., Perri E. (**2023b**). Geochemical proxies of sea surface temperature from MIS 5e marine fossils in the Taranto Gulf (Ionian Sea, Southern Italy). *Rendiconti Online Società Geologica Italiana,* 59, 9-15.

Chapter 7 is focused on the understanding the environmental and diagenetic dynamics of biosedimentary deposits from Capo Colonna (KR, Calabria) through the study of the microfacies. These results are partially published in:

1) Guerrieri S., **Santagati** P., Borrelli M., Perri E. (**2024**). Depositional and diagenetic facies of Late Pleistocene (MIS 5) shallow-marine carbonates of the Capo Colonna Terrace, Crotone Basin, Southern Italy (preliminary data). *Rendiconti Online Società Geologica Italiana.*
2) **Santagati** P., Salvatore Guerrieri G., Mario Borrelli M., Perri E. (**2024c**). Calcareous bioconstructions formation during the last interglacial (MIS 5) in the Central Mediterranean: a consortium of algal, metazoan, and microbial framebuilders (Capo Colonna - Crotone Basin - South Italy). Submitted to *Marine and Petroleum Geology.*

Chapter 8 presents an introduction of a work in progress study.
Finally, *Chapter 9* presents the general conclusions derived from the results of the present study, useful for modelling of the near time global warming effects in the Central Mediterranean.

Abstract

The Last Interglacial (MIS 5) is a warm period within the Late Pleistocene. In particular, its first substage (MIS 5e) is the last warmer than today period before the present-day Interglacial, therefore it is considered a good analogue for assessing future climate responses to global warming. The present work focuses on two shallow marine deposits cropping out along the Ionian Sea coastline, central Mediterranean: 1) a MIS 5e fossiliferous calcarenite from Taranto (Apulia), and 2) MIS 5a/c bioconstructed deposits from Capo Colonna (Calabria). These deposits were studied for a paleoenvironmental characterization, which included the paleoecology of benthic associations, paleotemperature estimates and early diagenetic phenomena, with the aim of providing new data on the response of these systems to climatic variations.

The MIS 5e calcarenite from Taranto, sampled in three related sites cropping out along the Mar Piccolo (MP) coastline (Masseria La Penna, Mass. S. Pietro, and Il Fronte), returned a rich molluscan fauna consisting of 120 extant species and 5174 individuals, including four of the tropical Senegalese Fauna, today absent in the Mediterranean. The molluscan assemblages were used for a refined quantitative palaeoenvironmental reconstruction; as a whole, the fauna represents an autochthonous-parautochthonous assemblage coming from a sandy-vegetated infralittoral bottom, locally accompanied by coarser and less finer sediment fractions, and characterized by slight lateral variability, shifting from more sheltered and exposed areas, and from finer and coarser bottoms, suggesting a heterogeneous and well-structured palaeoenvironment during MIS 5e.

The same molluscan assemblage was used for a multi-proxy palaeoclimatic study. The biogeographic-climatic affinity of the assemblage shows, compared to today, a double percentage of warm affinity species, while the cold affinity species are similarly represented, indicating a warmer but not strictly tropical Sea Surface Temperature (SST). This is confirmed by the most recurring preferred SST ranges of the assemblage, indicating an average of 20 °C. The skeletal compositions of five well-preserved molluscan and coral specimens were analyzed for trace elements and stable isotopes for further mean SST estimations. From the comparison of the results of several equations available in literature, it appears that only some SST estimations are realistic, converging into similar values of, on average, 20.8 ± 0.9 °C. Considering all the used proxies, the MIS 5e SST difference compared to today falls in the range 1.2 - 2.0 °C for the Gulf of Taranto (GT) (being a more reasonable scenario) and 2.0 - 2.8 °C for the MP. This is not a firmly tropical-like SST setting as suggested by the sole Senegalese fauna, indicating at least 2.7 °C to 3.5 °C more than to today's GT and MP, respectively. The approximations and assumptions made for obtaining SST values with any single proxy indicates the need of a multi-proxy approach to define the best SST estimation.

Cemented samples of the same MIS 5e calcarenite were analyzed through optical and SEM analyses. Clasts mostly consist in medium to coarse sandy size skeletons and fragments of skeletons of a variegated biota together with mainly large mollusks shells that inhabited the sediment and a very minor amount of siliciclastic. Micritization variably affects most of the bioclasts while cements are constituted by a microcrystalline texture with various micro-morphologies and fabrics: not-isopachous aphanitic and filamentous rims, vacuolar peloidal meniscus, aphanitic micro-mounds, and aphanitic porosity-filling matrix. Cements are constituted by sub-micron sized anhedral to nanospheroidal crystals of low Mg calcite, mixed with a minor amount of irregular platy crystals of saponite. All fabrics of cement are rich of mineralized filamentous, tubular, and sub-spherical bacteria bodies that imply the presence of a microbial community forming an epilithic to endolithic biofilm that stabilized the incoherent sediment and mediated the early precipitation of cements. This process led to the synsedimentary hardening of some parts the mobile sandy substrate, allowing the settlement of sessile taxa - such as *Spondylus gaederopus*, oysters, serpulids and barnacles.

The Last Interglacial (MIS 5) transgressive-regressive deposits of the Capo Colonna marine terrace provide a good fossil example of a Central Mediterranean infra/circa-littoral setting, characterized by both calcareous coralline algae-dominated low-relief bioherms and biostromes, analogous respectively to the present coralligenous and mäerl habitats. The skeletal primary framework of the bioherms consists of laminar to massive encrusting coralline red algae acting as main bioconstructors, with minor bryozoans, encrusting foraminifera and serpulids as secondary frame-builders. Whereas the autochthonous mäerl tabular beds are mainly composed of free-branched coralline red algae rudstones. A variable amount of sandy bioclastic sediment is laterally interbedded with the bioconstructions and tends to be entrapped in their cavities and pockets. All sedimentary sub-facies of the bioconstructions and associated sediment, are rich in

autochthonous syn-sedimentary microbial-mediated micrite, forming aphanitic, peloidal, clotted peloidal, and filamentous fabrics. Microbial micrite can also trap and bind a variable amount of grains or being a secondary component of the sandy detrital sediment with micritic rims surrounding the clasts. All these early-lithified micrites show the typical nanostructure of the primary microbial-mediated carbonates, rather than a detrital mud particles accumulation, as they consist of nanospheres coalescing into subhedral microcrystals, replacing, and mineralizing both microbial cells (present with several morphological types) and extracellular substances. This in turn implies the widespread presence of benthic lithifying microbial biofilms that colonized both the cavities of the skeletal framework of the bioconstructions, and the intergranular space of the associated sediment. These microbial communities, thanks to the metabolic processes of the microorganisms that induced the carbonate precipitation, significantly contributed to the early cementation of all the studied deposits.

In conclusion, the results of the work were used to infer possible effects of climate change in similar Mediterranean contexts. The diversity and temperature preferences of the MIS 5e molluscan assemblage from Taranto show no significant differences compared to modern analogous faunas from some Southern Italy sites reported in the literature, which could show a resilient response to an SST increase of +2 °C, already experienced during MIS 5e and expected in the next decades. This, however, does not consider the different causes, the current higher warming rates, as well as the human impact, which could affect faunas more than the temperature itself. Today, microbial induced micritic cementation processes, similar to those reported in the studied MIS 5 deposits, are observed in tropical/subtropical carbonate platform realms and have not been indicated for similar infra-circalittoral beds of the modern Mediterranean. Their occurrence in MIS 5 deposits confirms the warmer SST during MIS 5e and suggests a persistently warm SST at the end of MIS 5. However, as these cements have been associated with an estimated SST of just +2 °C compared to modern times, it is suggested that early cementation could become common in the Mediterranean mobile bottoms already in the near future as an effect of the global warming.

CHAPTER 1 - THE QUATERNARY PALAEOCLIMATE

1.1 Introduction to the Quaternary palaeoclimate

Climate is commonly defined from the average atmosphere meteorological conditions, averaged over a time scale of at least 30 years, and it is the result, on a global level, of the interaction between atmosphere, hydrosphere, cryosphere, and biosphere (Joussaume and Duplessy, 2021). Climatology therefore studies the processes controlling the states of the global system.

Similarly, *palaeoclimatology* is the study of past climate, prior to instrumental recording, of past climate changes, occurring on historical, millennial, and million-year time scales, and of their causes.

Palaeoclimate is one of the most important topics in the Quaternary research. The Quaternary, the last period of the Cenozoic Era (66 – 0 Ma), spans from 2.58 million years ago to today, and it is composed of two epochs: 1) the Pleistocene (2.58 Ma – 11.7 ka) and 2) the Holocene (11.7 ka – today). According to an updated chronostratigraphic scheme (**Fig. 1**), the Pleistocene is further divided into Gelasian (2.58 – 1.80 ma), Calabrian (1.80 – 0.774 a), Chibanian (0.774 – 0.129 ma), and a not yet formalized Late Pleistocene (0.129 – 0.0117 ma). The Holocene is also further divided into Greenlandian (11.7 – 8.2 ka), Northgrippian (8.2 – 4.2 ka), and Meghalayan (4.2 – 0 ka) **Fig. 1**).

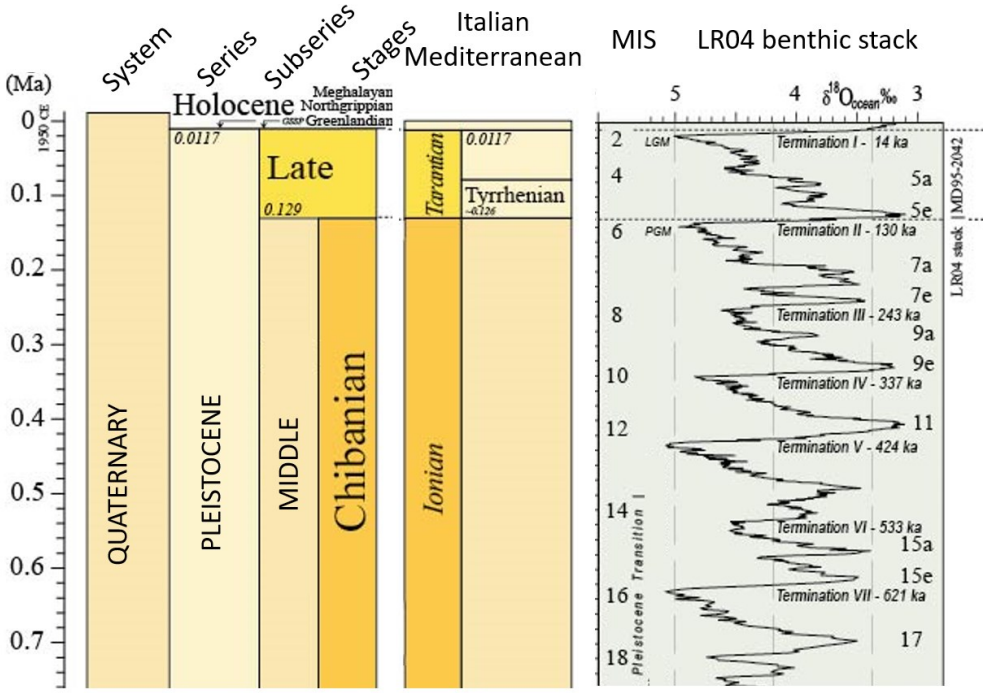

Figure 1. Upper Middle-Late Pleistocene and Holocene chronostratigraphic chart with global and Italian Mediterranean subdivision, and marine oxygen isotope palaeoclimatic curves. Mod. after Cohen and Gibbard (2022).

1.2 Long term cooling during the Cenozoic era

The Quaternary and the present-day climate are the result of a long-term decreasing of average global temperatures that took place during most of the Cenozoic era, shifting the global conditions from two climatic extremes: from a warm "*greenhouse* Earth", with no polar ice caps, to a cold

"*icehouse* Earth" with stable polar ice caps and a strong millennial cyclic variability (glacial/interglacial cycles), well established in the last million years (Caley *et al.*, 2021) (**Fig. 1**).

The first part of the Cenozoic (**Fig. 2**) was considerably warmer than today, also characterized by an abrupt and intense warming event that occurred around 55 Ma ago, named "*Paleocene-Eocene thermal maximum*" (Zachos *et al.*, 2001; Jansen *et al.*, 2007), followed by a constantly warm period known as *Eocene climate optimum.* After this warm phase, global climate started a progressive cooling around 50 ka, with a marked deterioration around 40 ka due to the Antarctic ice cap development (that reached up to 50% of its current extension) (Caley *et al.*, 2021) (**Fig. 2**). This event started the ongoing Icehouse period, even if briefly interrupted by two warmings and subsequent reductions of the Antarctic ice sheet at the end of the Oligocene and in the Middle Miocene. Then, in the upper part of the Miocene (14 ka), a new rapid cooling led to a further growth of the Antarctic ice sheet (up to 85% of the current extent) (Caley *et al.*, 2021; Fluteau and Sepulchre, 2021).

In the meanwhile, the north pole was ice free. Indeed, only around 5.5 Ma ago a new, more intense climatic deterioration would have started the northern hemisphere glaciation, with ice cap stabilization at about 3.2 Ma ago (Jansen and Sjoholm, 1991) (**Fig. 2**).

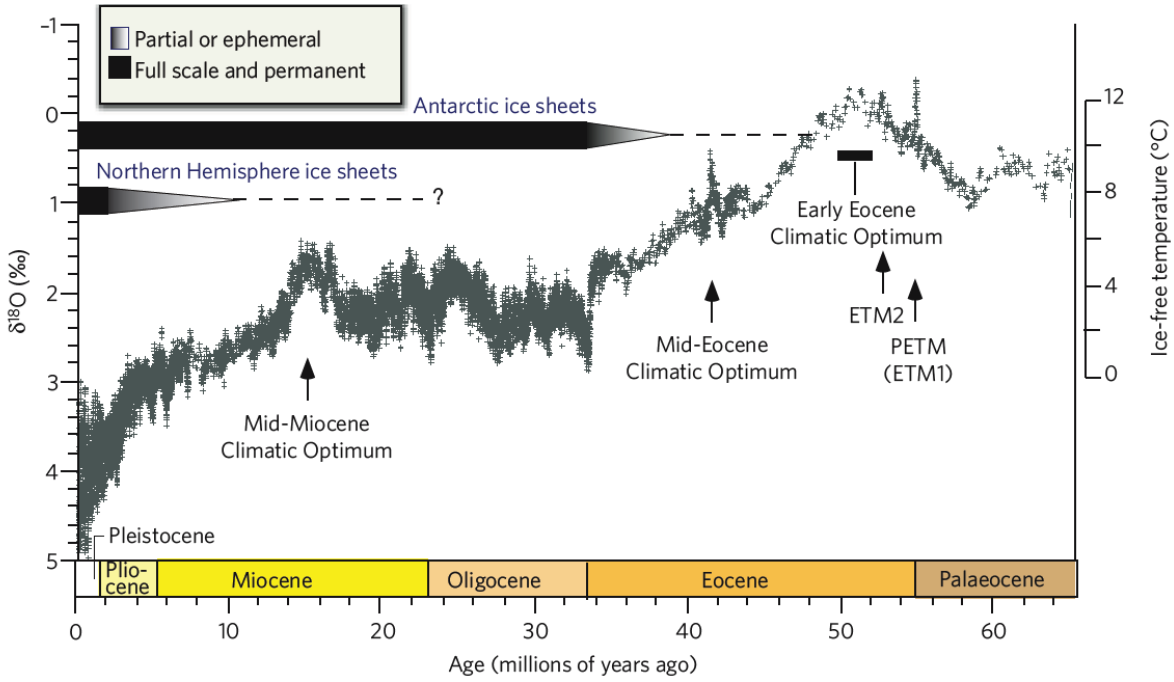

Figure 2. Cenozoic climatic data showing the Eocene warm climate and the progressive cooling trend toward modern times. Mod. after Zachos *et al.* (2008).

The presence of two iced hemispheres created the necessary conditions for the establishment of a strong glacial/interglacial climatic cyclicity, consisting in alternating expansions and reductions of the ice caps, which was superimposed to the continuing global cooling trend (Fluteau and Sepulchre, 2021). During the Pliocene, the global climatic variations, reconstructed from benthic foraminifera isotopes, during the Pliocene climate were characterized by small glacial/interglacial variability (with a 41-ka period). Then, the beginning of the Pleistocene (2.6 Ma ago) led to the strongest cooling (Caley *et al.*, 2021), also accompanied by a progressive increasing of the periodicity of the glacial/interglacial cycles (from 41 to 100 ka) and amplitude of the related climatic variations (i.e.,

the so-called *Middle Pleistocene transition*, around 1.2 - 0.6 Ma) (**Fig. 3**) (see *Chapter 2* for more details). After this transition, the global climate resulted colder, with more severe glacial conditions than in the Pliocene.

For the last million years (Middle-Late Pleistocene) the most detailed climate reconstructions are available (Joussaume and Duplessy, 2021). During this time of span, the 100 ka cyclicity resulted in short interglacial periods and about 10 times longer glacial periods, peaking every 100 ka (**Fig. 3**). The ends of each cold period were marked by a rapid warming partially melting the ice sheets, while the subsequent cooling was more progressive, showing an alternation between relatively cool (stadials) and warm phases (interstadials) (**Fig. 3**). The glacial-interglacial variations also coincided with rises and falls of the eustatic sea level, with an amplitude of roughly 120-130 in the Late Pleistocene (from -120 m than today during the Last Glacial maximum, and e.g. at most around + 6 m than today during the Last Interglacial maximum) (Dutton and Lambeck, 2012; Caley *et al.*, 2021).

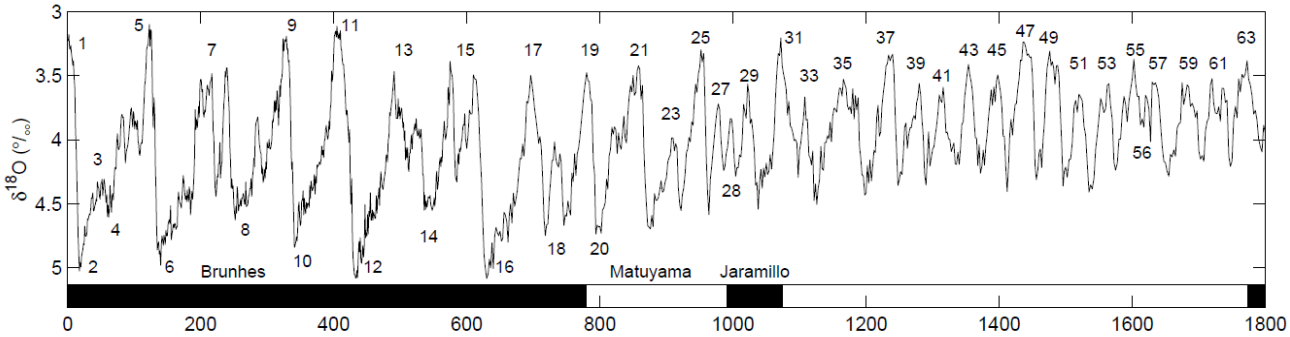

Figure 3. Upper-middle Pleistocene (Calabrian) to present day (Holocene) $\delta^{18}O$ benthic stack showing the alternance of glacial (even number) and interglacial (odd number) peaks. Mod. after Lisiecki and Raymo, (2005).

1.3 Climate during the Late Pleistocene: the last Glacial cycle

The last glacial cycle (MIS 5-MIS 2; **Fig. 3**; **4**) coincides with the Late Pleistocene (129 Ma – 11.7 ka) that, therefore, is comprised between the two climatic extremes: the first substage of MIS 5, i.e. the warmest MIS 5e, marking its beginning, and the coolest MIS 2, or Last Glacial Maximum, characterizing its end (Lisiecki and Raymo, 2005).

MIS 5, first recognized by Emiliani (1955), is the Last Interglacial "sensu lato", was then subdivided in 5 warmer and cooler substages (MIS 5e to MIS 5a from the oldest to the youngest) by Shackleton (1969).

The warmest peak of the Last interglacial is represented by the MIS 5e (Last Interglacial "sensu stricto"), a short warm period comprised between 129 to 116 ka (according to Dutton *et al.*, 2015) or, in other schemes, between 135 to 116 ka (Shackleton *et al.*, 2003) (**Fig. 4**). As indicated by several marine, continental, and ice proxies, the MIS 5e global climate was similar or, at most, +1-2 °C warmer than today (Guiot *et al.*, 1989; Jouzel *et al.*, 1987; Rohling *et al.*, 2008; Dutton and Lambeck, 2012; Dutton *et al.*, 2015; Hoffman *et al.*, 2017; Fischer *et al.*, 2018). Warming also affected ocean temperature, from + 0.4 °C in the deep Atlantic waters to +1–2 °C in the surfaces of high latitude oceans in respect to the Holocene (Duplessy et al, 2007; Capron *et al.*, 2014; Hoffman *et al.*, 2017;

Caley *et al.*, 2021). This warming was concomitant with a higher eustatic sea level (ca. +6 to +9 m) related to an important ice-cap retreat (affecting Greenland and West Antarctica ice caps) (Dutton *et al.*, 2009; Antonioli, 2012; Dutton and Lambeck, 2012; Sánchez-Goñi *et al.*, 2012; Dutton *et al.*, 2015). As to the reasons of such warming, the causes are not found in atmospheric CO_2 (i.e., the greenhouse effect), which was similar to today, but in a stronger insolation at high northern latitude (Caley *et al.*, 2021; see also *Chapter 2*).

MIS 5e was followed by other substages (**Fig. 4**): MIS 5d and MIS 5b represent cooler stadials, MIS 5c and MIS 5a are relatively warmer interstadials that briefly interrupted the climatic cooling towards the last glacial maximum (Thompson and Creveling, 2021, and ref. therein). As shown by $\delta^{18}O$ curves and sea level estimations, ice caps were wider than today, and global sea level was lower than today (e.g., estimated around – 40 to – 20 m; Caley *et al.*, 2021; Thompson and Creveling, 2021, and ref. therein). Indeed, climate was cooler than today in all the Late Pleistocene except for the warmer MIS 5e. Consequently, there is not agreement on the duration of the Last Interglacial (Helmens, 2014), as not an unambiguous definition of what an Interglacial is (Kukla *et al.*, 2002). In Its original definition by Emiliani (1955), the last Interglacial coincided with the whole MIS 5, but later Shackleton (1969) subdivided it into five stages (i.e. MIS 5e to MIS 5a).

In a first view, the Last Interglacial should be correlated only to the warmest MIS 5e peak (Last Interglacial *sensu stricto*), related to the warm Eemian in the pollinic continental stratigraphy (Martinson *et al.* 1987; McManus *et al.* 2002; Cutler *et al.* 2003). In this case, the start of the last glacial period is placed with the onset of MIS 5d, considered an early glacial period (Kukla *et al.*, 2002), characterized by a sensibly cooler that today climate in the northern hemisphere (Stirling *et al.*, 1998; Jansen *et al.*, 2007, Ovtos, 2015).

In a second way, the Last Interglacial refers to the whole MIS 5 as in Emiliani's original definition, e.g. a Last Interglacial *sensu lato,* or MIS 5 interglacial complex (e.g. McIntyre and Ruddiman, 1972; McManus *et al.*, 1999; Oppo *et al.*, 2006; Martrat *et al.*, 2007; Bigelow, 2013; Helmens, 2014; Columbu *et al.*, 2019; Dumitru *et al.*, 2020; Ryan *et al.*, 2021). This view is supported by the indications of an overall mild, temperate MIS 5 climate conditions, contrasting with the much more severely cold conditions the MIS 4-2 interval (Helmens, 2014), and by local conditions of MIS 5a and 5c interstadials, which were regionally warm or warmer than today (e.g. Väliranta *et al.*, 2009; Ilyashuk, *et al.*, 2020). In this case, the start of the Last glacial is represented by MIS 4. Accepting this view, another consideration arises: the duration of the MIS 5 is similar to MIS 4-2 interval, i.e. 50 ka in both cases, overpassing the classic idea of shorter interglacials and longer glacial periods (Guiter *et al.*, 2003; Helmens, 2014).

MIS 4 (71 – 57 ka; Doughty *et al.*, 2021), the first true glacial peak, making the Last Glacial period to start definitively. During this period much more important global glacier extension than during the MIS 5 stadials happened: MIS 4 glacial conditions are also comparable with the coldest MIS 2 (Doughty *et al.*, 2021), e.g. having led to a global sea level drop down to around – 100 m in respect to today (De Deckker *et al.*, 2019).

MIS 3 (29-57 ka; Doughty *et al.*, 2021) is interposed between the glacial phases MIS 4 and MIS 2 and is an anomalous isotope stage: even it should represent an interglacial, MIS 3 did not reach interglacial isotopic values (Emiliani, 1972); therefore, it is now considered a relatively warm interstadial in between of the Last Glacial Period (Paillard, 2021). In addition, MIS 3 climate was

highly variable, but always sensibly cooler than today, with a variable global sea levels generally constrained at – 30 to – 90 m or even lower than today (Shackleton, 1987; Rohling *et al.*, 2008; Siddal et al, 2008; Spratt and Lisiecki, 2016).

The Last Glacial Maximum (LGM), corresponding to MIS 2 (29-14 ka; Doughty *et al.*, 2021), represents the cool extreme in the near time climate variations, whose maximum was reached about 20,000 years ago (**Fig. 4**). Today, the Antarctic ice cap is the most extensive (28 km^3) while the Greenlandic one is very reduced (1 km^3) ; during the Last Glacial, instead, northern glaciers expanded through Canada and Europe (up to 50 km^2 in extension forming the Laurentide ice sheet) (Joussaume and Duplessy, 2021). As result, sea level has dropped to at least -120 m compared to today (Caley *et al.*, 2021). CO_2 was around 100 ppmv less than pre-industrial level (Petit *et al.*, 1999), and temperatures cooled by 10 °C to 2 °C in the northern Atlantic and in the Antarctic Ocean, respectively (MARGO Project Members, 2009). Tropical ocean SST were around 2-3 °C cooler than present (Jansen *et al.*, 2007). The Last Glacial climate was highly variable, as rapid climate changes are known. The *Heinrich events* are the result of rapid warmings, which led to ice-sheet destabilization and iceberg rafting (identified by glacial debris carried at low latitudes); the ice melting altered the ocean thermohaline circulation, leading to new cooling in the N hemisphere. The *Dansgaard-Oeschger events* (found in the isotopic record of Greenland ice cores) are interstadial-stadial cycles of rapid warmings (8-16 °C in few decades) followed by much slower cooling, yet not unanimously explained (Jansen *et al.*, 2007; Joussaume and Duplessy, 2021).

The deglaciation lasted from 20 to 8 thousand years ago, between the Pleistocene-Holocene transition; during this period, a warm peak, the Bolling-Allerød interstadial, and a last glacial cooling phase, the recent Dryas stadial (about 13 – 11.7 ka ago), happened (Maslin *et al.*, 2001, and ref. therein). This unstable phase was then followed by the Holocene Interglacial (MIS 1), characterized by a relatively stable warm, with a climate optimum between about 9.000 and 5.000 years ago, and a peak around 6 ka ago (Jansen *et al.*, 2007; Caley *et al.*, 2021).

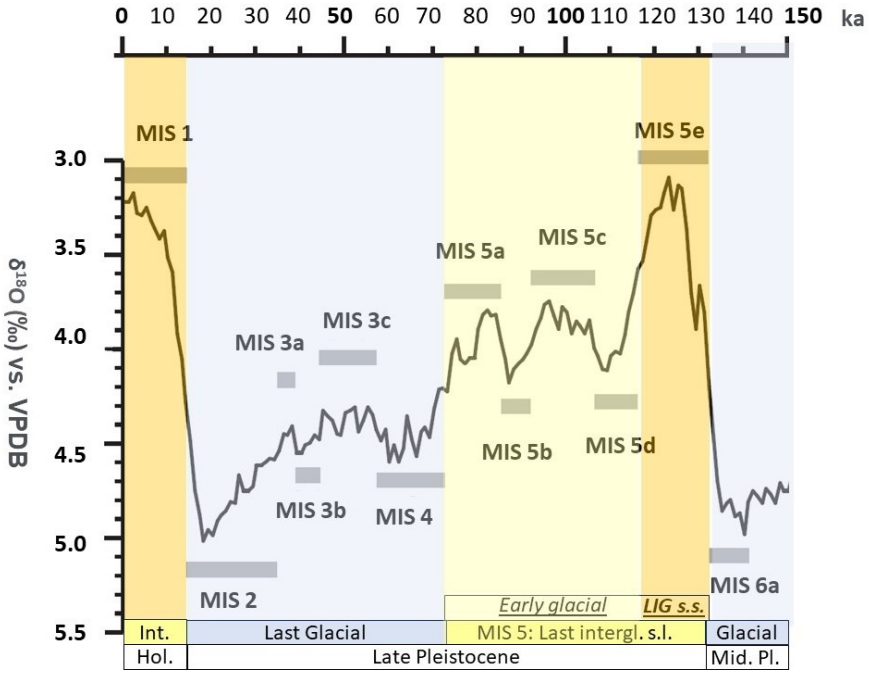

Figure 4. Last Glacial Cycle (Late Pleistocene) substages. Mod. after Railsback *et al.* (2015).

1.4 The Last Interglacial "Tyrrhenian" in the Mediterranean Basin

The Last Interglacial is frequently known as Tyrrhenian in the Mediterranean area. Originally, the term *Tyrrhenian* was proposed by Issel (1914) to formalize the time span between the Sicilian and the Holocene, i.e. the plane corresponding to the Middle-Late Pleistocene, used first in the Mediterranean area and then throughout the world (Cita *et al.*, 2005). Formulated in a such way, the Tyrrhenian includes the last interglacial and the last two glaciations (Cita, 2008). To date, the Middle Pleistocene, one named Ionian in the Mediterranean area, has been formalized as Chibanian, while the Late Pleistocene remains uncovered (**Fig. 1**).

It has been discussed if using the term Tyrrhenian or not for the formalization of the Late Pleistocene (Cita *et al.*, 2005). Indeed, for the definition of the Tyrrhenian, Issel used sedimentary deposits containing a peculiar fauna, with a "warm" character, located in Cagliari (Sardinia). This fauna is the *Senegalese Fauna*, defined just a year earlier by Gignoux (1913) and traditionally regarded as an important palaeoclimatic indicator (see ahead). The lack of formalization of the Tyrrhenian led to a different use over time, when in chronostratigraphic and when climatostratigraphic sense. Therefore, Cita *et al.* (2005) proposed either to restrict the "Tyrrhenian" to MIS 5e interval, i.e. the warmest part of the Last Interglacial (climatostratigraphic sense), or to extend it to all that part of the Pleistocene not yet formalized, i.e. from termination II (between MIS 6 and 5) and termination I (between MIS 2 and 1) (roughly corresponding to the Late Pleistocene) (chronostratigraphic sense).

Subsequently, a proposal was made to replace the term Tyrrhenian with the term *Tarantian* to refer to the Late Pleistocene (Antonioli *et al.*, 2008; Cita, 2008; Amorosi *et al.*, 2014; Negri *et al.*, 2015), using the section of Il Fronte, near the Mar Piccolo of Taranto. This is reported in recent scheme for the Mediterranean (Cohen and Gibbard, 2022), which also uses the term *Tyrrhenian* for the whole MIS 5, as synonym of the last interglacial sensu lato (**Fig. 1**). Anyway, to date, the Late Pleistocene remains globally unformalized.

The MIS 5e sea level rise (estimated of + 6 ± 3 m a.s.l.), led to the deposition of several marine terraced, today raised all over the Mediterranean coastline (e.g., Ferranti *et al.*, 2006; Zecchin *et al.*, 2020), which return examples of the tropical Senegalese fauna, traditionally considered indicator of the Tyrrhenian (Gignoux, 1913). This fauna, being represented by warm water molluscan species absent at present in the Mediterranean but still living along the tropical West African Province, is considered a key palaeoclimatic indicator of generalized warm and tropicalized conditions (Amorosi *et al.*, 2014; Negri *et al.*, 2015). Considering the whole MIS 5 interglacial, MIS 5e transgressive terraced deposits with *Thetystrombus latus* (known in the past literature with the synonym of *Strombus bubonius*), have also been called "*Eutyrrhrenian*" while the younger phases (i.e., MIS 5c and 5a) where called "*Neotyrrhenian*" (e.g., Bonifay and Mars, 1959; Dai Pra and Stearns, 1977). Anyway, the presence of *T. latus* and other Senegalese species was then recognized also in *Neotyrrhenian* deposits (MIS 5a or 5c of Capo Colonna, Calabria, Southern Italy, Nalin *et al.*, 2012) and in "*Palaeotyrrhenian*" older ones (i.e., MIS 7 of Spain; De Torres *et al.*, 2010), indicating a more complex colonization history. Nonetheless, the Senegalese fauna in raised terrace deposits remains emblematic of MIS 5e (Ferranti *et al.*, 2006).

1.5 MIS 5e and today's global warming

One of the main topics of climatologic research is the ongoing global warming, conventionally started around in 1850 due to increasing of human activities, above all the emission of greenhouse gases such as CO_2, which is increasing global average temperatures and sorting various climatic and environmental effects worldwide (IPCC 2007, 2023). Since the Holocene is a warm interglacial period, probably about to become even warmer soon due to human activity (IPCC, 2023), particular interest is placed in the previous Tyrrhenian interglacial. Although there were past intervals much warmer than the Last Interglacial (e.g., the Pliocene), and although the causes of warming were different (orbital forcing rather than increase in CO_2), the MIS 5e interval is often regarded as a good model for understanding modern (i.e., expected for the end of century) climate change effects, such as temperature increase, ice sheet melting, and sea level rise (Overpeck *et al.*, 2006; Rohling *et al.*, 2008; Siddall and Valdes, 2011; Antonioli *et al.*, 2017; Fischer *et al.*, 2018; IPCC, 2023).

Land-surrounded basins, such as the Mediterranean, are more sensitive to the climate change and undergo a more rapid warming, up to 4 times the rate of global warming (Belkin, 2009). For example, while in 2018 global atmospheric temperature has increased of about 1 °C in respect to the 1890-1899 period, the Mediterranean basin experienced an increasing of 1.5 °C (Cramer *et al.*, 2018). Moreover, oceanographic data indicate a warming of the first 150 m of sea water of about + 0.5 °C in 1980-2000 (Rixen *et al.*, 2005); in the 1982 – 2018, mean superficial SST increase of +1.5 °C (Pisano *et al.*, 2020).

From a biogeographical perspective, the Mediterranean Sea has already been a tropical sea in the geological past (e.g., Monegatti and Raffi, 2001). Among the most recent warm episodes, the tropical Senegalese fauna entering in the Mediterranean during MIS 5 stands out. This entering was allowed by the weakening of the cold upwelling current of the Canaries, which took place during the Last Interglacial, which today prevents the northward dispersion of these species (Taviani *et al.*, 2015). Once entered, warm enough SST matching the thermal tolerance of these species would have led to the successfully colonization of these species, even if an acclimatization toward cooler temperatures cannot be excluded (Monegatti and Raffi, 2001; Taviani *et al.*, 2015). Nowadays, global warming effects on the Mediterranean are changing its biota, as warm water southern species are migrating northwards (the so called *southernization*), and tropical Atlantic and Indo-Pacific alien species, entered through the Strait of Gibraltar and the artificial Suez Canal respectively, and ship unintentional transport, are successfully acclimatizing (the so called *tropicalization*) (Bianchi and Morri, 2003; Albano *et al.*, 2021, 2024). In order to assess the impact of the tropical species, the Tyrrhenian is an important window on future faunal changes, as such warm water incursion in the Mediterranean Sea has already happened (Albano *et al.*, 2024).

CHAPTER 2 – THE MAIN CAUSES OF PAST CLIMATIC CHANGES

2.1 Climate forcing

The energy reaching the Earth surface, on which the climate depends, derives from the Sun activity, and is thus expressed in terms of *insolation* (W/m^2). Earth temperature depends also on the balance of absorbed and reflected heat. On one hand, atmospheric *greenhouse gases* (mainly H_2O, CO_2, CH_4, and N_2O) cause the so-called greenhouse effect, which is trapping part of the solar radiation in the atmosphere, maintaining average global temperature around 14 °C (that is + 33 °C in respect what would occur with a totally transparent atmosphere) (Jansen *et al.*, 2007; Joussaume and Duplessy, 2021; Bertini *et al.*, 2022). On the other hand, the *albedo* is the ratio between reflected and absorbed radiation (and deriving heat): withe reflecting objects have a high albedo (more heat reflected than absorbed), whereas black ones have a low one (more heat absorbed than reflected) (Joussaume and Duplessy, 2021).

On larger time scales (from millennia to millions of years), various phenomena external to the climate system occur which, being able to influence its characteristics, are therefore called "*external forcing*". The main external forcings are 1) variations in the sun activity; 2) variation in earth orbital parameters, 3) tectonic processes, all acting together on different timescales. The climate system variation is called “response”. The relationship between forcing a response can be explained through four alternative *theoretical models*: 1) linear and synchronous response (a direct and proportional relation); 2) muted or limited response (a reduced response to a strong forcing); 3) delayed or non-linear response (a response in delay with the forcing, proceeding in a nonlinear way); 4) threshold response (no response after the reaching of a threshold, then, possibly, an intense and fast response in respect to the forcing) (Maslin *et al.*, 2001).

2.2 The role of sun and astronomical motions in the past climatic changes

Sun radiation is the source of energy reaching the Earth surface, especially high at low latitudes, then distributed and exchanged through oceanic and atmospheric circulation to high latitudes. Short term variations on Sun activity (e.g. solar spots cycle) can influence the climate over yearly (most importantly, the 11-year cycles) to century or millennial time scale (e.g., prolonged minima and maxima are known for the historic times), albeit in a small extent (Joussaume and Duplessy, 2021).

Over thousand and hundred-thousand-year time scales, periodic variations in insolation are controlled by the changes in the earth’s orbital parameters, rather than to variations in the solar output. These so-called *millenary motions*, related to the gravitational effects of Solar System objects on the Earth, represent the primary factor in the triggering and in the timing of past climate change, which is the glacial-interglacial cycles. There are three orbital cycles with a total of five periods: eccentricity (400 and 100 ka), obliquity (41 ka), and precession (23 and 19 ka) (Zachos *et al.*, 2001) (**Fig. 1**).

- *Eccentricity* expresses the Earth's orbit shape (today’s *e* is equal to 0.0167), varying from nearly circular (e = 0) to a low flattened ellipse (e = 0.06) every 100.000 and 400.000 ka. Although the average insolation increases by decreasing the eccentricity, deriving Earth mean temperature

variations between the two extreme cases are negligible. Albeit ineffective to directly affect the climate, the eccentric cycles modulate the effect of the effects of the other millennial motions on the climate (Paillard, 2021).

- *Obliquity* is the inclination of the Earth's axis with respect to the orbital plane (ecliptic). The axis tilt (today 23°27') oscillates between 21.9° and 24.5° every 41,000 years, due to the attraction of the moon, and less of the Sun, on the equatorial bulge of the Earth. Since the axial tilt determines the existence of the seasons (e.g., in a given hemisphere, summer occurs when the axis points towards the sun, and vice versa for winter), and controls the width of the tropical and polar belts, any variation in obliquity changes the insolation at high latitudes, modifying the climate: high obliquity values increase the seasonal contrast, while low values decrease it (Paillard, 2021).
- *Precession* is the progressive clockwise rotation of the direction of the Earth's axis through consecutive passages at the same orbital points (e.g., the equinoctial points). Precession produces a double-cone motion, with an average periodicity of 21,000 years, reversing the orientation of the axis every half cycle. This period results from the combination of two components, one relating to the Earth's axis motion (period of 25,700 years), and another relating to the rotation of the Earth's orbit (the anti-clockwise precession of the perihelion, with a period of 112,000) (Paillard, 2021; Joussaume and Duplessy, 2021). The periodicity of the precession is also modulated by the eccentricity cycle, resulting in the double cyclicity of 19,000 and 23,000 years (average 21,000 years) (Paillard, 2021). Precession controls the seasonal contrast: in a given hemisphere, it is greater when summer is at perihelion and winter is at aphelion (hot summers and cold winters), and vice versa (milder winters and cooler summers). The two scenarios will reverse due to the precession cycle, as a given hemisphere will reverse its orientation relative to the Sun when the Earth is at aphelion and perihelion, reversing the seasons and affecting the climate. For example, 10 ka ago northern summers happened in perihelion (rather than in aphelion as today), resulting warmer than today (Joussaume and Duplessy, 2021). Finally, the effects of precession are modulated by the eccentricity cycle, as the related seasonal variations in insolation are stronger during high eccentricity periods than low eccentricity ones (Jansen *et al.*, 2007).

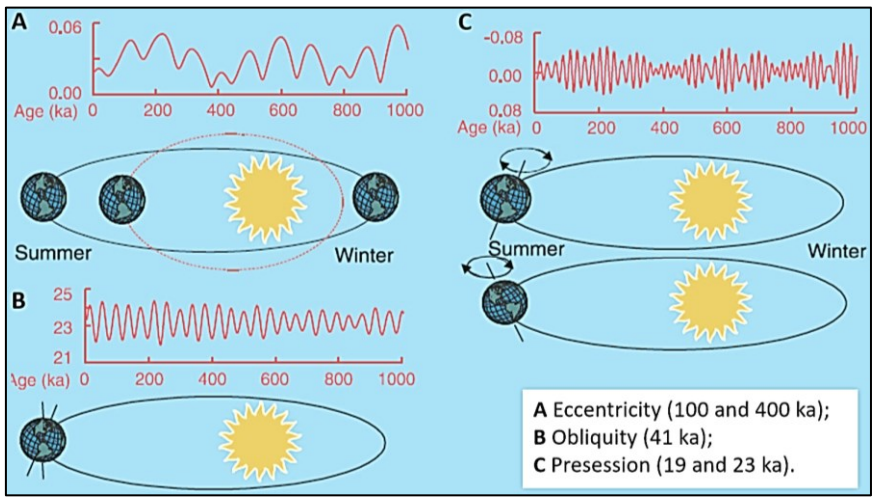

Figure 1. A synopsis of the millenary orbital motions. Mod. after Zachos *et al.* (2001).

Several theories were proposed to explain the past climatic variations with the millenary motions since the mid-1800s. Firstly, it was proposed that glaciations were triggered by winters coinciding with aphelion, considered either particularly longer (Adhémar, 1842) or colder due to less insolation received (Croll, 1864).

However, the modern views are mostly founded on the keystone work of Milankovitch (1941). In this model, although each of these three motions can affect the global climate, it is their combination (either in phase and in phase opposition), which can be defined as "astronomical forcings of the climate," that controls the seasonal insolation irradiating the Earth surface (**Fig. 2**). Milankovitch quantified the variations of the summer insolation at high latitude (65°N) for the last 600.000 years, concluding that any glaciation is triggered by those parameter combinations that decreases summer insolation at the considered latitude. This generates longer and cooler summers that are corresponded by shorter and milder winters. Such a decreased seasonal contrast is favourable for positive *snow balance*: the heat received during any summer cannot melt all the snow and ice deposited during the previous winter, so that this can persist in form of ice during the years. Conversely, other combination of the three motions that increases seasonal contrast and summer insolation at high latitudes, triggers deglaciations. For example, the warmer than today's MIS 5e global climate was the result of a combination of high orbital eccentricity, strong obliquity, and the passage of the earth near the summer solstice, which increased the amount of summer solar radiation in the northern hemisphere (where ice forms) by 30 W/m^2 higher than today (Caley *et al.*, 2021).

In both cases, glaciation/deglaciations are favoured by positive feedback with the albedo (Joussaume and Duplessy, 2021): in the presence of an expanding ice cap, albedo increases sensibly, enhancing the reflected heat and favouring a cooling process; on the contrary, when an ice cap starts to melt, albedo decreases, increasing the absorption of heat and thus warming. Summarizing, the orbital forcing is the main cause of the climate change, but its effects are critically amplified through positive feedback between ice and global mean temperature (Joussaume and Duplessy, 2021). Feedback with the ocean dynamics and carbon cycle (involving the greenhouse gas CO_2) are also crucial in the amplification the astronomically driven climate changes *(see next paragraph*).

The astronomic theory was not widely accepted due to the incompleteness of the geological record, until that Emiliani (1955) evidenced how global climate variations could be reconstructed from the geochemical composition of deep-sea cores, showing the alternance of "cold" and "warm" climatic phases that were related to glacial and interglacial stages (*see Chapter 3*). As demonstrated by Hays *et al.* (1976), these deep-sea core records respond to different cycles with periods of 23, 41 and 100 ka for the last 450 ka period, fitting with the astronomical frequencies predicted by the Milankovitch's theory.

2.3 Greenhouse gas variations

Carbon has crucial role in regulating the global temperature, especially in form of atmospheric CO_2, the most effective modulator of the greenhouse effect (Maslin *et al.*, 2001), and CH_4. This phenomenon is today well known due anthropogenic CO_2 emissions that, in 2019, surpassed the maximum known in the last 800.000 years, leading to an increase of +1 °C in the global average

temperature compared to the pre-industrial era (i.e., 1850) (Joussaume and Duplessy, 2021). The role of CO_2 greenhouse effect is crucial both in near time (glacial/interglacial time scales) and in deep time (e.g., Cenozoic time scale) global climatic variations, respectively as a key contributing cause of other external forcing, and as main trigger of long-term climatic changes (*see next sections*).

CH_4 is the most effective greenhouse gas after CO_2. It is mainly produced by microbial activity in wetlands and then stored in permafrost in periglacial areas or fixed in methane hydrates on the oceanic bottom. Warming phases and oceanic eruptions, and related causes, can release the stored CH_4 (Jansen *et al.*, 2007; McInerney and Wing, 2011; Fluteau and Sepulchre, 2021, and ref. therein), increasing the greenhouse effect. For example, the abrupt Paleocene-Eocene thermal maximum (ocean SST raised up to 8 °C; Dickens, 2003), and the sharp Late Pleistocene glacial-interglacial changes are suggested to be caused by oceanic CH_4 releases (Kennet *et al.*, 2003).

2.3.1 Glacial/interglacial CO_2 changes

Although the main causes of glacial/interglacial cyclicity are found in the astronomical cycles (Hays *et al.*, 1976), these alone cannot explain all the reconstructed palaeoclimatic changes, making necessary to consider also changes in the biogeochemical carbon cycle, varying the CO_2 level in the atmosphere (Paillard, 2009). The role of CO_2 variations in the ice age development, first quantified by Arrhenius (1896) for the Last Glacial period, was also considered to explain on its own all the past climatic variations without requiring any astronomical forcing (Paillard, 2021, and ref. therein). Today, the astronomical and the geochemical theories are considered complementary rather than incompatible, as both the forcings are required to explain the palaeoclimatic variations, although their relationships have still to be understood (Paillard, 2021).

CO_2 past variations are directly measured in air bubbles trapped in polar ice cores up to 800 ka (Petit *et al.*, 1999; Monnin *et al.*, 2001), or can be inferred from carbonate carbon isotopes ($^{13}C/^{12}C$), such as from planktic foraminifera, dependent on CO_2 water and atmosphere concentration (Jansen *et al.*, 2007; Joussaume and Duplessy, 2021). A clear correlation between the carbon cycle and the climate is evident along 800.000 years Ice-core archives: the atmospheric CO_2 and temperature variations fluctuated in a parallel pattern, evidencing low values (190 ppm) during cold periods and high values (280 ppm) during warm periods (Siegenthaler *et al.*, 2005; Jansen *et al.*, 2007; Joussaume and Duplessy, 2021) (**Fig. 2**). This strong covariation is explained by the dependence of the atmosphere-ocean CO_2 exchange from phenomena (e.g., ocean circulation and ice sheet dynamics) that are both controlled by the orbital parameters (Petit *et al.*, 1999; Joussaume and Duplessy, 2021).

Thus, even if at this timescale the CO_2 variations are not the direct cause of the climatic changes (e.g., estimated temperature rises precede the CO_2 rises by hundreds of years during deglaciations) (Caillon *et al.*, 2003; Jansen *et al.*, 2007), these strongly affect climate through positive feedback processes that intensify the effects of the orbital forcing (Maslin and Ridgwell, 2005; Köhler *et al.*, 2005; Jansen *et al.*, 2007; Francés *et al.*, 2018). For example, when a glacial period starts, multiple phenomena decrease the atmospheric CO_2, weakening the greenhouse effect, and favouring further cooling and ice sheet growth.

The processes that modify the atmospheric CO_2 content involve the carbon cycle (carbon transfer and storing between lithosphere, atmosphere, biosphere, and hydrosphere) and particularly the

oceanic processes, considered the primary source of glacial/interglacial CO_2 variations (Jansen *et al.*, 2007 and ref. therein). CO_2 solubility in water is inversely related to temperature, therefore decreased superficial and deep ocean temperature absorb more CO_2 from the atmosphere (Jansen *et al.*, 2007). Cooler water is also more saline, and thus less able to store CO_2, but the overall CO_2 absorption increases during cold times, thanks to enhanced phytoplankton carbon absorbing and storing activity (Fluteau and Sepulchre, 2021). This is explained by an increment of nutrients and therefore of the oceanic productivity, which are favoured during glacial (e.g. due to greater dust production in cold-arid continental environments, and due to the increasing of CO_2 -consuming chemical weathering of shelves, exposed after sea level fall). The organically fixed carbon is then sunk and stored on deep seafloors (Jansen *et al.*, 2007; Joussaume and Duplessy, 2021).

Ice caps also favour the carbon storing. First, the initial decrease in atmospheric CO_2 facilitates the expansion of the ice cap via feedback processes; their development increases the salinity and density of the surrounding waters, leading to the stratification of water masses; this slows down and limits the upwelling, preventing carbon release from the deep ocean to the atmosphere (Paillard and Parrenin, 2004; Jansen *et al.*, 2007). This lasts until the glacier occupies the whole shelf; then, it is interrupted, ceasing the stratification of water, and releasing the CO_2 into the atmosphere, promoting a rapid global warming during the deglaciation (Paillard and Parrenin, 2004).

Other than in form of organic matter, part of the carbon is stored by calcium-carbonate fixing organisms (Jansen *et al.*, 2007). Changes in $CaCO_3$ equilibrium with water contributed to the observed changes (Jansen *et al.*, 2007), e.g. the dissolved CO_2 increases $CaCO_3$ dissolution that, in turn, increases the atmospheric CO_2 oceanic absorption.

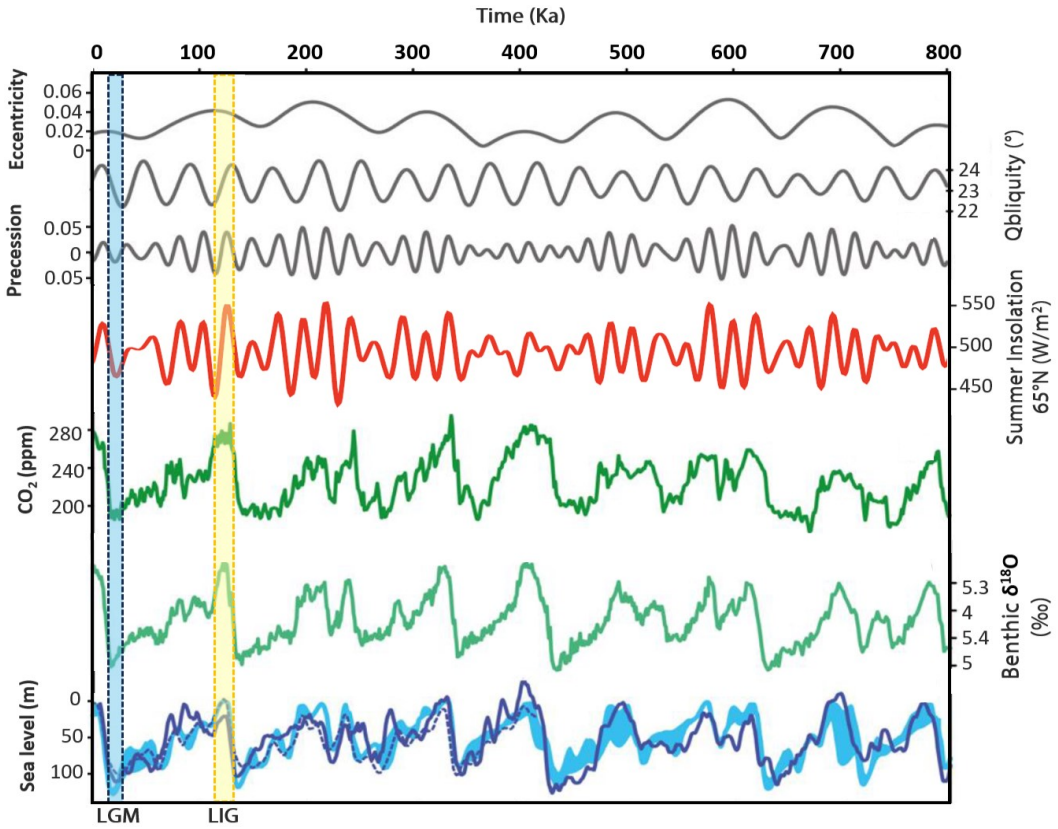

Figure 2. A comparison between the three orbital motions, the CO_2, $\delta^{18}O$, and sea level covariations the last 800 ka; LGM: Last Glacial Maximum (MIS 2); LIG: Last Interglacial (MIS 5e). Curves from Berger and Loutre (1991), Laskar *et al.* (2004), Lisiecki and Raymo (2005), Francés *et al.* (2018) and ref. therein.

2.3.2 Long time CO_2 variations

A strong CO_2-temperature relationship is known for the entire Phanerozoic (Royer, 2006). Considering the Cenozoic era, the long-term CO_2 decrease is the most evident climate-forcing trend. CO_2 levels dropped by very high values (*at least* ca 1000 ppmv in the Eocene or much more), correlated to higher than today average temperatures and ice-free poles (greenhouse climate), to low values (e.g. down to 300 ppmv in the Neogene), accompanied by a progressive drop of temperatures and ice sheet development (icehouse climate) (Zachos *et al.*, 2008). On these longer million-year time scales, the atmospheric CO_2 levels are balanced by tectonic processes, such as the emission by the so-called *degassing* (volcanic and mantle activities), and its removal (consumption due to the silicate weathering promoted by orogenesis, and organic carbon burial in the deep ocean sediments) (Jansen *et al.*, 2007; Zachos *et al.*, 2008; Fluteau and Sepulchre, 2021; Joussaume and Duplessy, 2021).

Concerning the emissions, while short volcanic eruptions can cool the climate after emitting debris and sulphur dioxide that reduce the insolation, intense large scale tectono-magmatic processes (e.g., Deccan traps, Late Cretaceous) can release enormous volumes CO_2 in the atmosphere, enhancing the greenhouse effect (Francés *et al.*, 2018; Joussaume and Duplessy, 2021).

The efficiency of chemical weathering that consumes CO_2 is controlled by precipitation and temperature, regulating the climate through feedback processes: an initial warm-humid climate favours the chemical weathering, consequently reducing CO_2 levels, the greenhouse effect and global temperatures (Fluteau and Sepulchre, 2021, and ref. therein; Scotese *et al.*, 2021). For example, this climatic driver was proposed the Himalayan orogeny and the uplift of the Tibetan Plateau, considered as the main driver of Cenozoic cooling: first, the action of the warm-humid Asian monsoon facilitated chemical weathering on uplifted silicate rocks and then, as the orogen rose, increased uptake of atmospheric CO_2, promoting global cooling (Raymo *et al.* al., 1988; Scotese *et al.*, 2021). Furthermore, huge amounts of removed CO_2 were sequestered in the sediments of the Bay of Bengal, whose effect was estimated to be 2-3 times greater than that of atmospheric agents (France-Lanord and Derry 1997). Finally, Guo *et al.* (2021) demonstrated how variations in magmatic-metamorphic emissions, linked to the India-Asia collision, were the main factors controlling CO_2 changes during the Cenozoic.

2.4 Changes in continents and oceans

Other than changing the atmosphere composition over long time scales, tectonic affects climate system by altering the regional and global geography, such as the location and shape of oceans and of continental masses and their reliefs, controlling the energy and heat flow in the oceans and atmosphere. The major Phanerozoic icehouse-greenhouse shifts, for example, were linked to the major accretion and breakages of the supercontinents (Scotese *et al.*, 2021, and ref. therein). In addition, it has been supposed that the major glaciations were favoured by the poleward shift of the major land masses, making the necessary conditions for several other factors to trigger glaciations (Beaty, 1978, and ref. therein; Francés *et al.*, 2018). For the Cenozoic cooling, this process was probably a minor trigger cause, as the latitudinal drift of the northern continents was relatively small during this Era, indicating that other processes had a major climatic effect.

Concerning the oceanic dynamics, changes in the oceanic circulation may have contributed to the climatic cooling (Fluteau and Sepulchre, 2021). In fact, the global oceanic circulation or *thermohaline circulation* (i.e., produced by latitudinal water temperature and salinity variations), is the key factor transporting heat along latitudinal gradients, and any alteration thereof implies a change in the distribution of heat along the high latitudes (Caley *et al.*, 2021; Joussaume and Duplessy, 2021). Thus, alongside theories that focus on CO_2 – which is however strongly linked to ocean dynamics (Paillard and Parrenin, 2004) – others seek the main reasons for Cenozoic climate change in changes in ocean circulation (Goddéris *et al.*, 2021).

The growth of Ice caps has been related to the openings and closure of oceanic passages due to the continental drift. This is the case of the Drake Passage and of the Tasman Gateway development, related to the Australia northward drift, which established the Antarctic Circumpolar Current. This, by reducing latitudinal circulation and heat exchanges, caused a notable drop in temperature until the Antarctic ice sheet stabilized during the Eocene and Oligocene (Zachos *et al.*, 2001; Francés *et al.*, 2018; Caley *et al.*, 2021; Fluteau and Sepulchre, 2021; Scotese *et al.*, 2021). Similarly, the Artic glaciation was related to the formation of the isthmus of Panama and related changes in oceanic circulation: by interrupting the Atlantic-Pacific interchange and establishing the warm Gulf Stream, the moisture increased at the Arctic, increasing the snow production and the ice sheet grow (Scotese *et al.*, 2021). This hypothesis has also been criticized because the uplift of the isthmus had occurred earlier in the Miocene and, therefore, is not related to glaciation. For this, the North Hemisphere glaciation was probably enhanced by declining CO_2 values, increased N deep-water formation, and circulation changes combined (Francés *et al.*, 2018; Caley *et al.*, 2021, and ref. therein).

2.5 The Middle Pleistocene Transition and the "100 ka problem"

The Middle Pleistocene Transition (MPR) is a change in shape and duration of the glacial-interglacial cycles. For the Pliocene and Lower-Middle Pleistocene, the reconstructed glacial-interglacial cycles were almost symmetrical, with a relatively small amplitude, and with a period of 41 ka, indicating a linear response to the 41 ka cyclicity orbital forcing (the obliquity cycle). Around 1 Ma, the 41-ka periodicity changed into a 100 Ka periodicity, which dominated representing the most relevant timing of the Middle-Late Pleistocene glacial-interglacial cycles of the last 800 ka (Berger and Jansen, 1994; Maslin and Ridgwell, 2005) (**Fig. 3**). After this, an increased amplitude and cycle asymmetry (slow glaciation leading to 90.000 ka glacial periods, and rapid deglaciations leading to shorter 10.000 ka interglacials) is observed.

This strong 100 ka frequency apparently corresponds to the 100-ka eccentricity cycle which, alone, is too weak to produce relevant effects on the climate, resulting inadequate to explain the palaeoclimate record. This aspect is known as the "*100 ka Problem*" and represents a still unclear topic of the astronomical theory (Imbrie *et al.*, 1993; Paillard, 1998).

Various hypotheses have been proposed to explain the Middle Pleistocene transition and the onset of the present day "100 ka world". Some invocate a nonlinear response of the global climate to the eccentricity cycle (Maslin and Ridgwell, 2005, and ref. therein), while others suppose that the 100-ka periodicity is an average between different astronomical cycles rather than eccentricity (Paillard, 2021). For example, the 100-ka periodicity has been related to 4^{th} or 5^{th} period precession

cycles (Maslin and Ridgwell, 2005), and to double or triple period obliquity cycles, entering the climate system in a chaotic phase with different, non-linear climate response to the forcing periodicities (Huybers and Wunsch, 2005; Huybers, 2009).

Otherwise, it has been proposed that external linear forcings, alone, may have only a weak climatic, but they can be amplified if combined with internal (stochastic) forcings, causing the climate to oscillate between two extreme modes (glacial- interglacial) (Benzi *et al.*, 1982). It is suggested that climate shifts between the two extremes only when certain critical thresholds (relative to insolation values and ice volume) are exceeded, resulting in a rapid, non-linear response in respect to the forcing (e.g. Paillard, 1998). For example, it has been proposed that the reaching of a critical size of the Northern Hemisphere ice cap changed the global climate response, producing a non-linear response between the weak 100 ka orbital cycle and the stronger climate response (Imbrie *et al.*, 1993). Alternatively, the 100-ka world can be the result of a long-term cooling that allowed the ice volume to overpass a critical threshold that made it persist longer for 80-100 ka, making the 41-ka orbital forcing ineffective on controlling climate changes (Abe-Ouchi, 1996; Raymo, 1997). Possibly, this was favoured by tectonic processes: after the development of the Greenland-Scotland submerged ridge, dated at around 1 Ma ago, the consequent changes in the thermohaline circulation and consequent heat flow, made it easier to lock the climate system in a glacial mode rather than in interglacial one (Denton, 2000).

As already mentioned, the long-term cooling could have been triggered also by the atmospheric CO_2 decreasing trend due to the increased chemical weathering, resulting from the uplift of Cenozoic orogens (Raymo *et al.*, 1988). Other studies suggest that the onset of the 100-ka glacial cycle, and related global cooling, were triggered by the progressive erosion and removal of regolith layer under flowing ice sheets, resulting in a slower flow and melting, allowing ice sheet to persist longer (Clark and Pollard, 1998). Finally, recent studies (Willeit *et al.*, 2019, and ref. therein) suggest that both the processes (atmospheric CO_2 decrease and regolith removal) acted together.

Concluding, the 100-ka problem clearly indicates that astronomical theory can only a part of the last million-year climate change, since variations in CO_2 and other internal forcings, linked to bio-geochemical cycles, oceanic and tectonic processes, are also very important contributing causes of climate change, amplifying the climatic effects triggered by the astronomical motions.

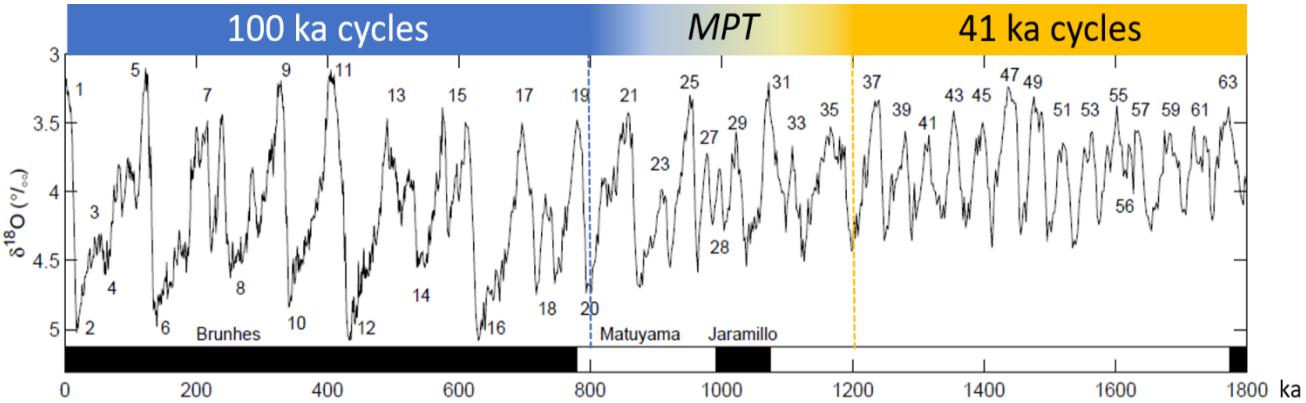

Figure 3. Lower Pleistocene to Holocene benthic stack showing the Middle Pleistocene Transition (MPT) from the 41 ka cyclicity to the 100 ka cyclicity. Mod. after Lisiecki and Raymo (2005).

CHAPTER 3 - GEO-BIOLOGICAL PROXIES FOR ASSESSING PALAEOTEMPERATURES

3.1 Archives and proxies for palaeotemperature reconstructions

In the palaeoclimatic and palaeoceanographic research, the palaeotemperatures of the air and of the sea (including the Sea Surface Temperature or SST) are important climate parameters, frequently estimated from a variety of natural archives and proxies. There are several natural *archives* that can record the palaeoenvironmental and palaeoclimatic variations during their formation (Bertini *et al.*, 2022). Natural archives are represented by both inorganic and organic, marine, and continental ancient materials. Natural archives record a series of *proxies,* "substitute" data that can be used for indirect qualitative or quantitative estimations of palaeoclimatic or other palaeoenvironmental parameters (e.g., palaeotemperature, ice volume, sea level, salinity, etc.) (Bertini *et al.*, 2022). Following, the main palaeoclimatic archives are listed, grouped into inorganic and biological, together with the registered proxies (synthesis after Bertini *et al.*, 2022).

Inorganic (geo-glaciologic) archives are:

1) ***Sedimentary record***: coastal, pelagic, and lacustrine sedimentary sequences and cores, recording environmental variations of, potentially, the whole Earth story, through a multitude of proxies such as: a) geo-lithological proxies (lithologies indicators of climate), b) geochemical composition of microfossils, c) faunal composition of marine assemblages, both micro and macrofossils; d) pollen, e) vegetation macro and microfossils, f) insects and other continental organisms.
2) ***Speleothems and tufa***: carbonate continental deposits, recording environmental parameters through geochemical proxies during their deposition.
3) ***Ice cores****:* found in polar ice sheets, constitute a nearly 1 Ma record of geochemical proxies, dust levels, and past CO_2 and CH_4 atmospheric concentrations, trapped into air bubbles.

Biotic archives, are:

1) ***Hard shelled or skeletal marine macrofossils*** (e.g., molluscs, brachiopods, corals, recording geochemical and other proxies related to the skeletal growth);
2) ***Ancient wood***: ancient (Ka aged) wood recording in the tree rings geochemical and other physical proxies related to the wood growth;
3) ***Midden***: accumulation deposits made on long times by rodents, recording continental fauna and flora proxies (e.g., pollen, insects, etc…).

Each of these archives can record palaeoenvironmental and palaeoclimatic variations over different time spans, and with different time resolutions (**Fig. 1**). The following part deals with the most used proxies used to inferring past water or air palaeotemperatures, with mention to the importance of some of these proxies to evidencing past global changes.

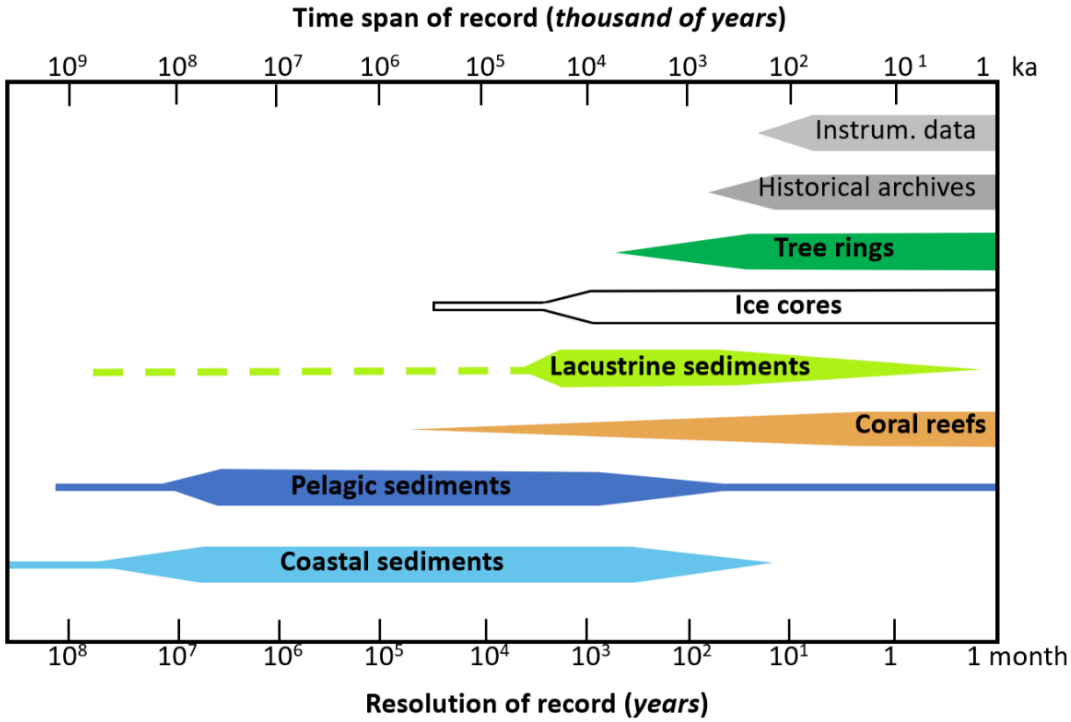

Figure 1. Time span of record and resolution of the main archives. Mod. after Bertini *et al.* (2022).

3.2 Lithological proxies

Sedimentary deposits can archive peculiar lithologies that can be used as qualitative climate proxies, requiring precise climatic conditions to be developed. The most common cases include *tillites* (deposited in cold periglacial environments), *coal beds* (derived from vegetal accumulations in warm-humid climate), *evaporites* (generally deposited in warm-arid marine or continental environments), *loess* (aeolian dusts deposited in arid continental environments), *palaeosoils* (linked to humid climate), whose alternation are also related to glacial/interglacial cycles (Bertini *et al.*, 2022).

3.3 Geochemical and biogeochemical proxies for global climate and palaeotemperatures

During time, several kinds of geochemical proxies for palaeoclimate analyses were identified. Some of the most important geochemical proxies are represented by oxygen and carbon isotopes, as well as by trace elements ratio, allowing direct palaeotemperature estimates and to trace palaeoclimatic-palaeoenvironmental changes (Bertini *et al.*, 2022). These proxies can be measured in a series of different natural archives.

First, the isotopic composition of ice cores can be used for calculating atmospheric temperature during the precipitation. Speleothems, freshwater tufa, calcareous skeletons, and tree wood, grows through consecutive bands during the year, producing temporal growths that can be dated and analysed for geochemical composition, used for reconstructing palaeoenvironmental and palaeoclimatic parameters, such as temperature or precipitation (Bertini *et al.*, 2022). In particular, SST estimations are commonly derived by microfossil (planktic foraminifera, calcareous nannoplankton) and macrofossil record (including, among others, calcareous algae, arthropods,

echinoderms, brachiopods, and frequently molluscs and corals; Wierzbowski, 2021; Bertini *et al.*, 2022). Moreover, the bulk isotope composition of benthic foraminifera shell from deep cores, instead, provides continuous isotopic record of the palaeoclimate changes, in terms of deep temperature and polar ice volume variations (Emiliani, 1955; Lisiecki and Raymo, 2005; Railsback *et al.*, 2015; West *et al.*, 2018).

3.3.1 Stable isotopes

When involved in physical-chemical processes, isotopes - atoms of a same element with different mass (i.e., with a different number of neutrons) - follow different fractionating phenomena that are environmentally controlled. For this, oxygen stable isotopes are widely used in palaeoclimatic, palaeoceanographic, and palaeoecologic research. In particular, the oxygen isotopic composition of a substance is expressed as $\delta^{18}O$ (isotopic ratio of "heavy" ^{18}O oxygen and "light" ^{16}O oxygen, normalized with respect to an appropriate standard). The $\delta^{18}O$ is used both for palaeotemperature estimations on fossil carbonates (Epstein *et al.*, 1953) and for evidencing the global climatic variations in the geological past, resulting also in a high-resolution isotopic stratigraphy (e.g., Emiliani, 1955; Lisiecki and Raymo, 2005; Railsback *et al.*, 2015).

After the early works (Urey, 1947; McCrea, 1950; Epstein *et al.*, 1953) it is well known that the biogenic carbonate oxygen isotopic ratio ($\delta^{18}O_c$, normalized to the PDB standard) is a function of both the isotopic composition ($\delta^{18}O_w$, normalized to the SMOW standard) and of the temperature (T, °C) of the water solution in which the carbonate precipitated. These relationships are formalized in several *palaeotemperature formulas* (e.g., Epstein *et al.*, 1953), used for calculating the temperature of formation of a skeletal carbonate for a given $\delta^{18}O_w$ value. In particular, $\delta^{18}O_w$ and $\delta^{18}O_c$ are in direct relationship, i.e. the change in the composition of the water is directly recorded in the calcareous skeleton. Conversely, the relationship between T and $\delta^{18}O_c$ is inverse: according to the classic equation of Epstein *et al.* (1953) the increase of 1 °C leads to a decrease of 0.23 ‰ in $\delta^{18}O_c$.

Stable carbon isotopes are also used in palaeoceanographic and palaeoclimatic analyses. Changes in the $\delta^{13}C$ ratio ($^{13}C/^{12}C$, normalized in respect to the PDB standard) derived from marine archives are related to main changes in the dissolved carbon, depending on the carbon biogeochemical cycle (e.g., production and sequestration of organic matter and carbon) that, in part, are linked by global climatic and oceanographic events (Goddéris *et al.*, 2021).

3.3.1.1 Oxygen palaeoclimatic curves and Marine Isotopic Stages

After the development of the palaeotemperature formula (Epstein *et al.*, 1953), an important application of the oxygen stable isotopes was made by Emiliani (1955) who, for the first time, identified and quantified Late Quaternary cyclical climate variations in the oxygen isotopic composition of planktonic foraminifera fossil tests, sampled from oceanic cores in the Caribbean Sea. He interpreted the succession of high and low values of $\delta^{18}O_c$ as global sea surface palaeotemperature variations, with amplitudes estimated in the order of 5-10 °C, matching the alternation of glacial and interglacial intervals, convincingly demonstrating the usefulness of isotopes for reconstructing past climatic variations, theorized in the astronomical theory of

Milankovitch (1941). Most importantly, Emiliani proposed for the first time an isotopic stratigraphy still used and improved (e.g. Lisiecki and Raymo, 2005; Railsback *et al.*, 2015), based on the division of geological time into the so called "*Marine Isotope Stages*" (*MIS*), numbered from the present day warm period, the MIS 1 interglacial: starting from this and going deep into the near past, the other warm interglacials are identified with odd numbers (e.g. MIS 5), and the cold glacial stages with even numbers (e.g., MIS 2). The points of transition between glacial and interglacial stages are called *terminations* (Lisiecki and Raymo, 2005). So far, 104 MISs have been defined for the Quaternary, up to about 2.6 Ma and other, even if identified by different acronyms, for the Pliocene, up to 5.2 Ma (Lisiecki and Raymo, 2005). Minor peaks, stadials and interstadials, identify minor substages related to less pronounced climatic oscillations, labelled both with numbers or letters (e.g., MIS 5.5 or MIS 5e) (Shackleton, 1969; Railsback *et al.*, 2015).

In the 1950s it was known – as indeed formalized in the palaeotemperature equation of Epstein *et al.* (1953) – that the composition of carbonates depended both on the carbonate formation temperature and on $\delta^{18}O_w$; however, it was still unclear which of the two factors played the biggest role in determining the mineral $\delta^{18}O$ composition. Emiliani (1955) assumed that the signal recorded by the foraminifera represented mostly palaeotemperature variations between glacial and interglacial, attributing a low contribute (< 0.4 ‰) to the variations in $\delta^{18}O_w$, linked to the expansion and contraction of ice sheets (Shackleton and Opdyke, 1973). In contrast, as estimated by Olausson (1965), this value had varied considerably during glacial and interglacial cycles, i.e. around 1 - 1.1 ‰) (representing the glacial-interglacial difference for the Upper Pleistocene; Shackleton and Opdyke, 1973), coupled with large oceanic salinity and sea level variations (Thunell and Williams, 1989; Caley *et al.*, 2021).

In the late ’60s, a reinterpretation of the isotopic curves meaning was provided by Shackleton (1967), who analysed benthic foraminifera from the same core of the Emiliani’s planktonic foraminifera. He found that benthic foraminifera, albeit living under the thermocline (i.e., at rather constant temperature between glacials and interglacials), net of different absolute values, recorded the same variations found in the planktonic foraminifera, previously interpreted as SST temporal variations. Thus, Shackleton (1967) demonstrated precisely that the changes in ocean water composition (dependent on the greater or lesser extraction of light oxygen by expanding/melting glaciers during glacial/interglacial stages) constitute the main source of the signal of the planktonic and benthic foraminifers, and that therefore the climatic curves should be rethought: "*extensive glaciation*" in place of “cold”, and “*reduction of glaciers*" instead of “warm” (Shackleton, 1967), as confirmed by subsequent papers (Duplessy *et al.*, 1970; Shackleton and Opdyke, 1973).

Anyway, Shackleton (1967) initially assumed that the variation of the water composition during the glacial/interglacial cycles was the only recorded signal, assuming a constant deep oceanic temperature. Nevertheless, relevant glacial/interglacial deep-water temperature changes were then discovered worldwide, i.e. with interglacial values similar to the modern ones, and cooler glacial values (Labeyrie *et al.*, 1987). This is explained with different oceanographic conditions for the formation of deep oceanic water during glacials and interglacials. For example, the North Atlantic deep water (the main modern source of global deep water) forms in the Norwegian Sea at low temperatures (-1.9 °C). Before sinking into the ocean basin, it crosses a shallow sill, mixing with warmer shallow waters and reaching around 3 °C. Instead, during the Last Glacial, as these waters

formed directly in the Atlantic, they sank without warming, at around close to the freezing point (-1 °C) (Labeyrie *et al.*, 1987; Caley et al, 2021). Thus, at Glacial/Interglacial scale, deep foraminifera also record temperature variations, which should be corrected for reconstructing the global variations in the ice volume signal, possibly with Mg/Ca or clumped analysis that allow water-independent temperature estimations (Caley et al, 2021).

3.3.1.2 The palaeotemperature formula

Oxygen stable isotope analyses ($\delta^{18}O$) have been widely used for SST estimates on skeletal carbonates, e.g., derived from the widely used equation of Epstein *et al.* (1953), for calcitic fossil carbonates, and of Grossman and Ku (1986) for aragonitic ones.

Anyway, as known, any $\delta^{18}O$-SST relationship requires the two values of the isotopic composition of the skeletal carbonate and of the seawater where the organism lived. The isotopic composition of the seawater, being dependent on time, latitude, and local environment (e.g., evaporation or freshwater inputs), is almost never known and represents the main bias for an accurate SST result estimation (Jarret, 2009; West *et al.*, 2018; Caley *et al.*, 2021; Wierzbowski, 2021; Huntington and Petersen, 2023). For instance, the unknown $\delta^{18}O_w$ can be derived from independent SST estimates, using other geochemical or biological proxies (e.g., Pérèz-Folgado *et al.*, 2004).

In addition, different taxa can exert a specific biological control ("vital effect"), secreting their skeleton out of isotopic equilibrium with the $\delta^{18}O_w$ of marine waters (Wierzbowski, 2021). Foraminifera and molluscs generally deposit their shell in isotopic equilibrium with seawater (Wierzbowski, 2021); bivalves, for example, are useful even without disposing a specific equation (Ragaini *et al.*, 2019), but disequilibria were recently reported for some species due to ontogenetic or metabolic controls (Wierzbowski, 2021, and ref. therein). Instead, for other molluscan species, as *Thetystrombus latus*, strong isotopic variations in living individuals from the same locality are reported (De Torres *et al.*, 2010), making it risky for SST estimations.

3.3.2 Clumped isotope analysis

Clumped isotope analysis is a newer geochemical method for palaeotemperature estimations, based on both oxygen and carbon stable isotopes on biogenic, abiogenic, marine, and continental carbonates (Ghosh *et al.*, 2006). The method is based on the Δ47 parameter, representing the abundance of heavy ^{13}C and ^{18}O isotopes, bonded (clumped) in the same CO_3^{2-} ionic group (i.e., the mass 47 isotopologue), relative to a stochastic distribution; clumping is inversely related to the formation temperature through the system entropy (Wierzbowski, 2021; Anderson *et al.*, 2021; Huntington and Petersen, 2023). As the technique involves only single-phase (carbonate) isotopic exchanges, water-carbonate isotopic equilibria are not considered. Thus, clumped analysis returns direct SST estimations, requiring no assumption for the past $\delta^{18}O_w$ of the seawater and overpassing the limits of the traditional isotopic palaeotermometry. Therefore, clumped-derived SST values are also useful for estimating $\delta^{18}O_w$ through the traditional palaeotemperature equation (Anderson *et al.*, 2021; Huntington and Petersen, 2023). Anyway, also clumped analysis on biogenic carbonates can be biased by non-equilibrium calcification and related vital effects, which must be known and corrected for (e.g., corals; Spooner *et al.*, 2016, and ref. therein).

3.3.3 Trace element analysis

Metallic cations as Mg and Sr among others, can vicary Ca in the crystal lattice of calcium carbonate polymorphs, in an extent being related to the solution temperature. Based on this, trace elements ratio such as Mg/Ca and Sr/Ca versus SST relationships were established for different calcareous shelled taxa as, among others, bivalves (Freitas *et al.*, 2005), corals (Silenzi *et al.*, 2005; Rosenthal and Linsley 2006; Montagna *et al.*, 2007; Royle *et al.*, 2015a), foraminifera and ostracods (Rosenthal and Linsley, 2006), and coralline red algae (Ragazzola *et al.*, 2020). The main advantage of trace element analysis is that the knowledge of the seawater composition is not required, and the calibrated equations return a direct SST estimation. Albeit the method uses taxon-specific equations, these proxies can suffer biases, too. For example, coral Sr/Ca relationships can be influenced by disequilibria offset, varying between corals of the same species, even living in proximity (Rosenthal and Linsley, 2006). This effect is demonstrated for the Mediterranean coral *C. caespitosa,* for which different calibrated equations have been proposed (Silenzi *et al.*, 2005; Montagna *et al.*, 2007) that, due to a colony-specific unpredictable vital effect, might return unrealistic results (Royle *et al.*, 2015b).

3.3.4 Biochemical proxies: alkenones

Coccolithophorids calcareous plates, most notably those of the cosmopolitan species *Emiliana huxleyi,* contain organic molecules (biomarkers) known as *alkenones*, i.e., long-chained molecules with 37 carbon atoms and 2-3 double bonds, whose number, expressed by an undersaturation index, is related to the temperature during the time of synthesis, estimated via linear calibrations (e.g., Prahl and Wakeham, 1987; Prahl *et al.*, 1988; Müller *et al.*, 1998). This approach is useful for estimating mean annual SST of the shallow water mass (Rohling *et al.*, 2002; Kandiano *et al.*, 2014).

3.4 Biological and Palaeoecological proxies

As palaeoclimatology (i.e., climatology of the past), also palaeoecology is defined from its modern counterpart: *ecology* is the study of the interactions between organisms with each other and with their environment, including all biotic and abiotic aspects, thus *palaeoecology* is "*the ecology of the past*" (Birks and Birks, 1989; Bottjer, 2016). Considering the ecology research topics, palaeoecology is also defined as: "*the reconstruction and study of past ecosystems, including the relations between organisms and their environments*" (Roberts, 1998). Due to the link between organism and environment, palaeoecology is a useful tool for the palaeoenvironmental reconstructions, based on the knowledge of the autoecology of fossil taxa, derived from their current analogues on the assumption that they have changed over time (principle of actualism and taxonomy of uniformitarianism).

For example, marine palaeoecology uses *biofacies* and *ichnofacies* (based on body and trace fossils record, respectively) for characterizing the palaeoenvironment. Marine biofacies are strongly controlled by physical environmental factors, such bathymetry, hydrodynamics, and substrate or, in other words, to the sedimentary regime, making also sedimentological features of the fossil-bearing assemblage an important tool for interpreting past environments (e.g., Bernasconi and Robba,

1993) (see also *Chapter 4* for more details). In continental settings, most of the palaeoecological reconstructions are based on pollen and fossil plant analysis, among the main proxies for palaeoclimate and palaeoecology (Peppe *et al.*, 2018).

Although palaeoecology and palaeoclimatology are two different branches of palaeosciences whit two different aims (Rull, 2010), these two fields of research are intimately related. In palaeoenvironmental research, in fact, some parameters that concern the palaeoecology of fossil species and palaeocommunities, and for extension of a palaeoenvironments, are also fundamental palaeoclimatic parameters (for example, atmospheric temperature, sea surface temperature, salinity, etc.). Describing a palaeoenvironment cannot ignore palaeoclimatic conditions, with all palaeontological data to be framed in their epochal and geographical context. Therefore, a correct palaeoecological analysis considers biostratigraphic, palaeobiogeographic, and palaeoclimatic analysis (Raffi and Serpagli, 1994). On a wider ecological scale, changes in past ecosystems are strongly linked to palaeoclimate changes (Sepulchre, 2002). Over millions of years, therefore, continental and marine ecosystems respond to both evolutionary processes and global climatic changes (Joussaume and Duplessy, 2021), so that macroevolutionary processes can also be constrained by long-term palaeoecological data and by abiotic factors, i.e. tectonics and climate (Sepulchre, 2002).

3.4.1 Coral reefs and warm water species

A clear example of palaeoecology and palaeoclimate link comes from shallow water Scleractinia reefs: modern shallow water coral reefs are highly diverse habitats, restricted to regions characterized by a tropical climate, i.e. with mean annual temperature between 25 – 29 °C (Bottjer, 2016), representing a distinct tropical climate proxy (Rosen, 1999; Veron, 2000; Vertino *et al.*, 2014). In the Mediterranean, the tropical/subtropical reefs disappeared during the Pliocene, due to the climatic deterioration. The only survived zooxanthellate coral, i.e. *Cladocora caespitosa,* remained an important reef constructor during warmest periods of the Plio-Pleistocene (Vertino *et al.*, 2014). Similarly, the distribution of another warm-affinity coral, the non-constructive *Astroides calycularis,* today limited to the warmer south-eastern Mediterranean, was wider that today in response to past warmings (Vertino *et al.*, 2014, and ref. therein).

3.4.2 Marine plankton as SST proxy

The marine palaeoecology mostly focuses on benthos and plankton, with the former traditionally used for palaeoenvironmental reconstructions, and the latter for palaeoceanographic reconstructions (e.g., past water temperature and salinity) (Raffi and Serpagli, 1994). Indeed, in deep and shallow water sediments, fossil assemblage of coccolithopohorids, foraminifera, and radiolarians, are used in palaeoclimate. Other than an archive for $\delta^{18}O$ and trace elements, SST estimations are made using the ecological preferences of the identified species, e.g. using the latitudinal dispersion along the modern biogeographic oceanic provinces (i.e. polar, temperate, subtropical, tropical) (Bertini *et al.*, 2022). Foraminifera assemblage variations register changes in water masses proprieties, such variations in SST, productivity, and pycnocline (Kandiano *et al.*,

2014). Palaeotemperaturure estimates from marine plankton can be derived by using different statistical approaches: transfer functions, equations based on the number of species with different ecological preference, first used for SST estimation by Imbrie and Kipp (1971). These empirically derived equations assume that biological responses are function of one or more palaeoenvironmental parameters, such as seasonal mean water temperature; for this, transfer functions are calibrated on the present-day taxa ecological and climatic preference, i.e. using a uniformitarian approach. Other approaches for SST reconstructions are the modern analogue technique (Hutson, 1980; Prell, 1985) and the revised analogue technique (Waelbroeck *et al.*, 1998).

3.4.3 Molluscan palaeobiogeography and ecological proxies

The distribution of the molluscan species among different latitude bioprovinces is mainly a function of the climate since the boundaries of each marine bioprovince match those of climatically different areas (Hall, 1964; Raffi *et al.*, 1985) each with its typical SST setting mainly defined by the duration of critical SST values during the year (Garilli, 2011). On this base, fossil molluscs can be used for obtaining palaeo-SST estimations through the study of their climatic/biogeographic affinity. Addicott (1969), for example, reconstructed the Oligocene to Pleistocene climatic variations in the northeastern Pacific using the northward and southward shifts of selected extant warm water species, by reconstructing the latitudinal shifting of the related bioprovinces.

The presence of fossil molluscs that are locally extinct but nowadays living in areas with a different SST is the main indicator of climate changes, even if this approach is also potentially limited by pure actualistic and uniformitarian assumptions, which exclude the possibility that the species can develop adaptation to climate changes (Monegatti and Raffi, 2001; Meco *et al.*, 2002; Garilli, 2011; Montesinos *et al.*, 2014; Ávila *et al.*, 2015). This is the case of the Senegalese Fauna: the northward expansion of the Senegalese fauna during the Tyrrhenian reflects warm generalized conditions from the Canaries to the Mediterranean, where today such fauna is not present (Gignoux, 1913; Meco *et al.*, 2002; Garilli, 2011).

Other approaches for palaeoclimate characterization, less used in recent literature (e.g., Gliozzi, 1987; Aguirre, 2003; Aguirre *et al.*, 2006), assume the temperature as the main controlling factor on the species distribution (e.g., Aguirre, 2003), and that the quantitative variation of species groups, distinguished in the function of their modern biogeographic distribution, can be used for inferring climatic conditions in the past (Aguirre *et al.*, 2006). Essentially, a warmer or cooler SST setting is here inferred by a comparison between the taxonomic composition of the fossil assemblage with the modern counterpart of the study area. However, it must be considered that the taxonomic composition of the fossil assemblage may depend also on other palaeoecological factors, as bathymetry and type of community (Gliozzi, 1987), and thus misinterpretations on the SST characterization could result.

3.4.4 Skeletal Growth rates

It is well known that the SST variations can affect the growth rate of many marine invertebrates (such as corals), which can be recorded in their skeleton structures. For example, for *C. caespitosa*

corallites, the relationship between the growth rate and SST was investigated on living individuals, to calibrate specific relationships (e.g., Peirano *et al.*, 2009, and Kružić *et al.*, 2012) but, also in this case as for trace elements, equations are different and results divergent, suggesting caution should be exercised in a general application of such relationships. Moreover, when used to back-calculate SST, the application of the actualism principle for the species *C. caespitosa* is questionable, since its thermal tolerance is most probably changed through time. In fact, palaeontological evidence (i.e., occurrence of the largest bioconstructions during the warmer Plio-Pleistocene phases) suggests a decreasing of *C. caespitosa* thermal tolerance during the Holocene, as mortality events have been observed during prolonged SST rises, and a wide spectrum of other environmental factors can influence thermal tolerance of this species of coral (Zanchetta *et al.*, 2019, and ref. therein).

3.4.5 Pollen and palynomorphs

Microfossils made of cuticle are known as *palynomorphs*; among these, pollen is the most important proxy for continental palaeoecological and palaeoclimatic reconstructions. Indeed, the pollinic record reflects the vegetation association of the study area, which permits to reconstruct the regional climate based on its ecological and geographical affinity of the taxa (determined at genus or family level) (e.g., Guiot *et al.*, 1989; Seppä and Bennett, 2003; Bertini and Martinetto, 2011; Helmens, 2014; Miao *et al.*, 2015; Peppe *et al.*, 2018; Bertini *et al.*, 2022). Many of the Quaternary continental stages, as the Eemian (= Last Interglacial sensu stricto or MIS 5e), and even the Holocene (= MIS 1), were defined through the pollen record. On one hand, the recognition of a certain vegetation (e.g., warm/humid taxa or cold/arid taxa) can give qualitative palaeoclimate data (Caley *et al.*, 2021). On the other hand, statistical methods were also set (e.g., transfer function and modern analogues) for quantitative estimations, based on the number of species with a different climatic meaning, among others (Guiot *et al.*, 1989).

3.4.6 Vegetal macro rests and wood

Considering vegetal macrofossils, also the association of macro vegetal remains (i.e., in lacustrine sediment archives) is a valid palaeoclimate proxy. For example, the functional morphology of fossil leaves can also be used in palaeoclimatology: the number of leaf stomata is inversely proportional to the atmospheric CO_2 concentration, and the percentages of sooth and jagged margined species is used to estimate the average annual air temperature, while the area can indicate mean annual precipitation (Bottjer, 2016, and ref therein; Peppe *et al.*, 2018; Bertini *et al.*, 2022). Ancient wood provides a high-resolution record, through well differentiated annual growth rings, which can be even dated (dendrochronology) or analysed with the aims of palaeoenvironmental and palaeoclimatic inferences (dendroclimatology) (Bertini *et al.*, 2022). Cellulose is an archive for stable oxygen and carbon isotopes, and physical and growth parameters of the wood, e.g. density and width of growth bands, are proxy for temperature, humidity, and cloudiness (Edwards and Fritz, 1986; Battipaglia *et al.*, 2008; Bertini *et al.*, 2022).

3.4.7 Other biological proxies

In marine and continental settings, non-pollen palynomorphs or NPC (diatoms, dinoflagellate, etc), which are organic-walled microfossils generally found during pollen analysis, are used as palaeoenvironmental and palaeoclimatic indicators (e.g., Limaye *et al.* 2007; Miao *et al.*, 2015; Bertini *et al.*, 2022). Other palaeoenvironmental and palaeoclimatic proxies used in continental deposits are represented by the phytoliths (silica deposits within plant cells, another proxy for vegetation) (e.g., Biswas *et al.*, 2021; Liu *et al.*, 2021). In continental freshwater deposits, fossil insects are useful biological proxies: Coleoptera and Diptera (family Chironomidae) assemblages can be used for palaeoecological and palaeoclimatic reconstructions, such as, mean annual air temperature and mean water temperature, the latter based on modern chironomids larvae analogues (e.g., Brooks, 2006; Coope, 2010; Plikk *et al.*, 2019).

3.5 Concluding remarks

The marine and continental stratigraphic record provides palaeoenvironmental and paleoclimatic archives, thanks to changes in the lithological, geochemical, and biological features. For example, palaeoecology and geochemistry aspects of fossil assemblage can be used to define paleoenvironmental and paleoclimatic aspects, through a purely actualistic view (e.g., Cornu *et al.*, 1993; Freitas *et al.*, 2005; Jarret, 2009; Garilli, 2011; Royle *et al.*, 2015a, West *et al.*, 2018). However, no paleoclimate proxy or method is free from bias (Jansen *et al.*, 2007). Most of the SST estimations of the past marine ecosystems are based on a single proxy, for instance, a single species or taxon, or a single methodology (Judd *et al.*, 2022, and ref. therein). Even if the single methods can lead to well-constrained results, there is a possibility to obtain unreliable SST estimations since various methodologies could be singularly affected by biases or based on unknown or too many approximate variables (e.g., salinity, isotopic fractionation, etc.) (e.g., Royle *et al.*, 2015b). Multi-proxy-based SST estimations are attempted to avoid uncertainty, compare different results, and evaluate their convergence or divergence (e.g., Dowsett and Robinson, 2009; Kandiano *et al.*, 2014; Cisneros *et al.*, 2016; Finné *et al.*, 2019).

CHAPTER 4 - A FOSSIL MOLLUSCAN ASSEMBLAGE FROM THE MAR PICCOLO OF TARANTO (APULIA, SOUTHERN ITALY): A PALAEOENVIRONMENTAL RECONSTRUCTION DURING MIS 5E

Abstract. *This chapter reports a quantitative palaeoecological study focused on the macrobenthic molluscan assemblages collected from a MIS 5e calcarenite sampled at three sites of the Mar Piccolo di Taranto (MP) coastline (Masseria La Penna, Mass. S. Pietro, and Il Fronte), for a refined palaeoenvironmental reconstruction during the warmest peak of the Last Interglacial. A total of 5174 individuals, belonging to 120 species of Bivalvia, Gastropoda, and Scaphopoda, indicate an autochthonous-parautochthonous assemblage coming from a shallow, photophilic subtidal bottom. The palaeoenvironmental interpretation of the molluscan fauna indicates a locally vegetated and mostly sandy mobile bottom, locally accompanied by either a coarser and finer fraction, and characterized by lateral variability, shifting from more sheltered and exposed areas, and from finer to coarser sites, suggesting a heterogeneous well-structured palaeoenvironment during MIS 5e.*

Keywords*: MIS 5e; Last Interglacial*; *Calcarenite; Palaeoecology; Molluscan assemblage.*

4.1 INTRODUCTION

In this chapter, the fossiliferous content of the MIS 5e calcarenite of Taranto, which will also be investigated for the palaeotemperature estimation in *Chapter 5*, is here studied for a refined palaeoecological study, whit the aim of defining the local mean palaeoenvironmental conditions during the warmer peak of the Last Interglacial (MIS 5e), which was warmer than today as indicated by sea levels, biological, and geochemical proxies (Cornu *et al.*, 1993; Cita, 2008; Garilli, 2011; Dutton and Lambeck, 2012; Montesinos *et al.*, 2014; Ávila *et al.*, 2016).

4.1.1 Geological and stratigraphic setting

The study area, which includes the city of Taranto and the coastal area around the Mar Piccolo (MP) (a semi-closed marine basin), is located in the Gulf of Taranto (GT) (Ionian Sea, Southern Italy). The stratigraphic framework of the area consists of a basal Mesozoic limestone (Murge Limestones, part of the Apulian platform domain), covered by Pliocene to Lower Pleistocene marine deposits (argille subappennine unit laterally passing into the Gravina Calcarenite Fm) (**Fig. 1**). These units are overlaid by two orders of marine terraces: one, Middle Pleistocene in age, related to the MIS 11; another, Late Pleistocene in age, related to the MIS 5e, very well exposed along the coastal area (Amorosi *et al.*, 2014; Negri *et al.*, 2015), comprised in the Monte Castiglione Fm (Martinis and Robba, 1975) (**Fig. 1**; **2A-D**). Since the last century several works focused on the stratigraphy of these Late Pleistocene deposits (Gignoux, 1913; Belluomini, 2002; Dai Pra and Stearns, 1977; Hearty and Dai Pra, 1992). Recently, much effort was focused on the 'Il Fronte' section (**Fig. 1**; **3**), which preserves a complete MIS 5e stratigraphic record, for a GSSP formal proposal of the Upper Pleistocene boundary, also known as Tarentian Stage (Antonioli *et al.*, 2008; Amorosi *et al.*, 2014; Negri *et al.*, 2015).

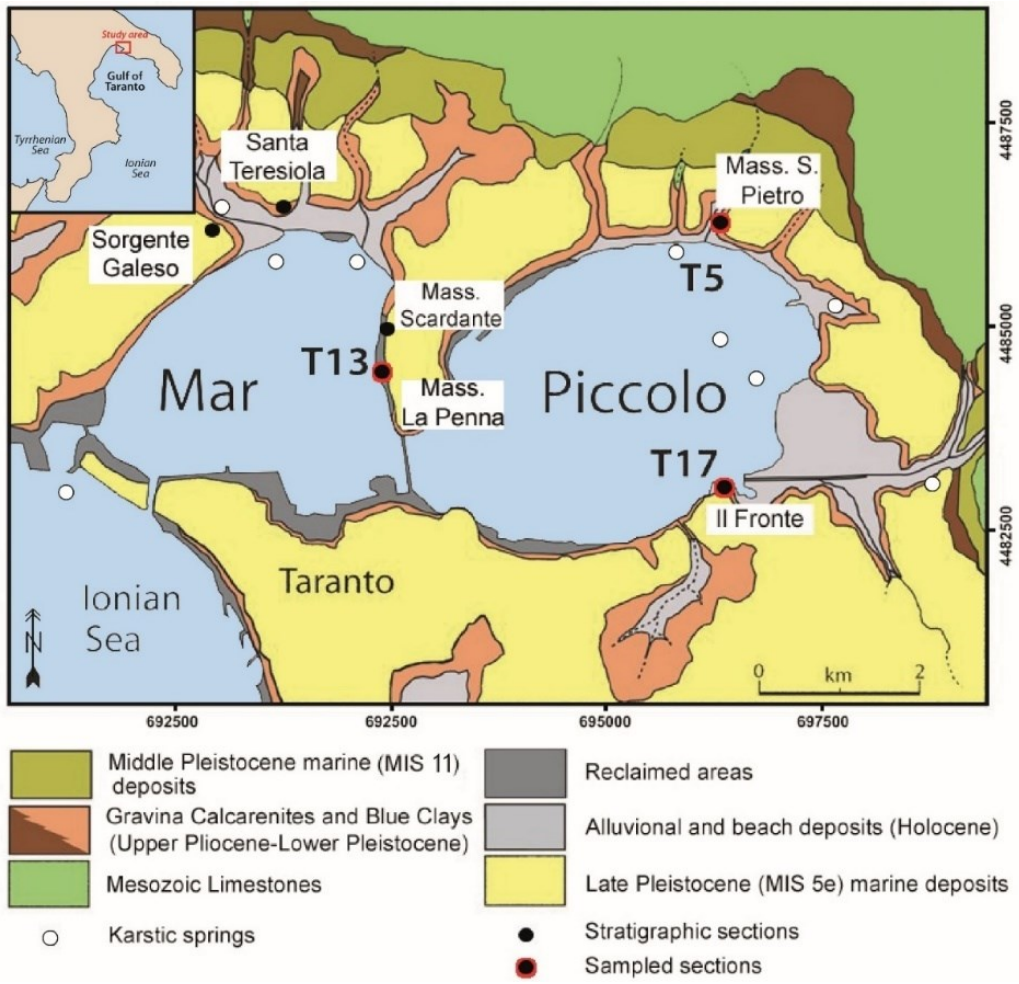

Figure 1. Geological Map of the MP and location of the sampled sections. Mod. after Amorosi *et al.*, (2014).

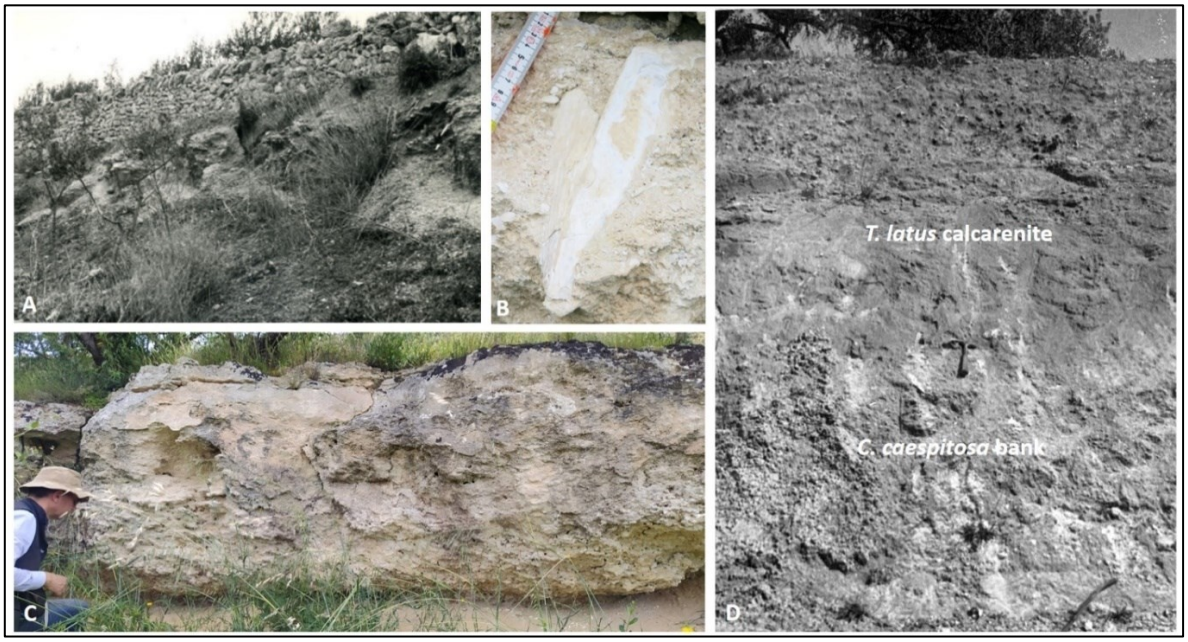

Figure 2. **(A)** Old photograph of the T5 outcrop. **(B)** *Pinna nobilis* specimen in life position from the T5 outcrop; **(C)** Recent photo on T5 outcrop; T13; old photograph showing the today-dismantled calcarenite level on T13 site, with *Cladocora caespitosa* level at the bottom and the calcarenite with *Thetystrombus latus* at the top.

A total of six stratigraphic sections, oriented along an ideal W-E transect (**Fig. 3**), were studied, integrating the data and observations published in the previous works, excluding Masseria La Penna section that was never described (Dai Pra and Stearns, 1977; Hearty and Dai Pra, 1992; Amorosi *et al.*, 2014). All the sections show a very good lateral continuity, being well correlated thanks to lithostratigraphy, biostratigraphy, and absolute age dating (see **Fig. 3** caption for details). Following the Amorosi *et al.* (2014) stratigraphic scheme, defined at the Il Fronte section, five main stratigraphic units can be recognized and correlated along the considered W-E transect (**Fig. 3**). A basal unit (U1) made by continental to marine deposits erosively overlays a basement represented by the argille subappennine unit. The marine facies of the Unit 1 record brackish to nearshore palaeoenvironments, with common shells of the genera *Cerastoderma* and *Ostrea* (Dai Pra and Stearns, 1977; Amorosi *et al.*, 2014). Eastward, such marine/transitional deposits make transition to continental alluvial sandy facies, which in turn grade laterally and upward to palustrine tufa deposits. The thickness of this basal unit is very variable, since it is about 2 meters to the west (Sorgente Galeso section), it reduces to circa 25 cm to the east (Il Fronte section), while it is absent in the middle areas (Masseria Scardante and Masseria La Penna section).

The second unit (U2) is characterized by grey marls with the very common presence of *Cladocora caespitosa* bioconstructions (Dai Pra and Stearns, 1977; Amorosi *et al.*, 2014). This unit is well exposed at the Santa Teresiola section where it shows a maximum thickness of circa 1 m, whereas is absent in the Sorgente Galeso section, and is representative of a lagoonal (Peirano *et al.*, 2009) to shallow marine stable palaeoenvironment (Amorosi *et al.*, 2014) (**Fig. 3**). This level was dated at Il Fronte, returning an age consistent with the initial phase of the MIS 5e (137 ± 6 ka near the base to 124 ± 4 ka in the middle; Amorosi *et al.*, 2014).

Unit 2 passes upward to the Unit 3 (U3) composed mainly of calcarenite with less sandstones, rich of fossils and representing the studied level of the present work. This calcareous layer shows a good lateral continuity since it is generally well exposed in the study area, with a thickness ranging from 1 to 2 m. Unit 3 is dominantly defined by a characteristically and heterogeneously cemented bioclastic calcarenite (**Fig. 2A-D**) with sometimes cross-bedded sedimentary structures, especially developed in the eastward part of the studied transect (Il Fronte section). Argillaceous sandstones deposits also occur in this unit at some localities as Santa Teresiola. This unit is rich among others of in situ fossils of *C. caespitosa* and bivalves with both disarticulated and in life positions shells, such as *P. nobilis* (Hearty and Dai Pra, 1992; Amorosi *et al.*, 2014) (**Fig. 2B**). Examples of the MIS 5e typical Senegalese fauna as *Thetystrombus latus* are also present in this unit. Palaeoecological studies carried out on this unit indicate a shallow littoral to sublittoral depth deposition (Boenzi *et al.*, 1985; Caldara, 1986; Amorosi *et al.*, 2014; Negri *et al.*, 2015). In addition to these studies, a detailed analysis of molluscan fauna from the calcarenitic U3 is provided in the present chapter, allowing also to contextualize subsequent palaeoclimatic inferences presented in *Chapter 5*. This level was dated at Sorgente Galeso and at Il Fronte returning respectively an age of 134 ka and 123 ± 4 ka (Hearty and Dai Pra, 1992).

The stratigraphic succession continues with the mud-dominated Unit 4 (U4), with a thickness of about 2.5 m, followed by a second calcarenitic level (U5), very similar to the calcarenite of the U3. The boundary between the Unit 4 and 5 is constrained at 120 ka (**Fig. 3**, section Il Fronte), which implies the MIS 5e isotopic peak should correspond with the middle part of the Unit 4 as showed by

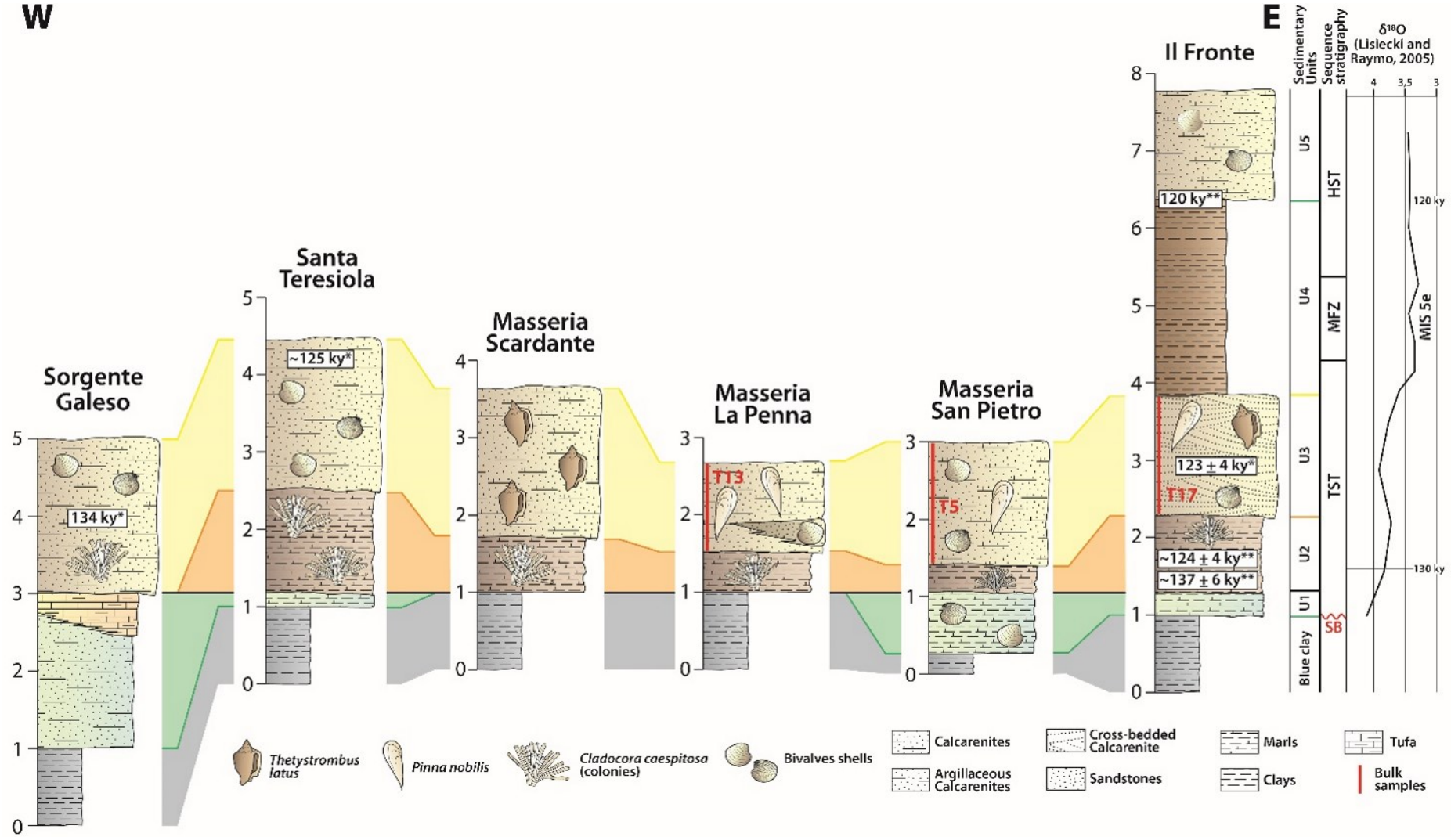

Figure 3. Stratigraphic sections along a WE transect in the MP area, showing the lateral continuity of the *T. latus* bearing calcarenite and the location of the three bulk samples (T5, T13, and T17). Sequence stratigraphy and units based on Il Fronte section, after Amorosi *et al.* (2014). Masseria Scardante and Masseria San Pietro sections are modified after Dai Pra and Stearns (1977); Sections Sorgente Galeso, Santa Teresiola, and Il Fronte mod. after Amorosi *et al.* (2014); section Masseria la Penna from field notes taken during sampling in 1976. Absolute ages from: * Hearty and Dai Pra (1992); ** Amorosi *et al.* (2014).

the global $\delta^{18}O$ curve (Amorosi et al 2014) (**Fig. 3**). Finally, from a sequence stratigraphy point of view, the succession comprised between U1 to the lower part of U4, records a deepening upward trend of the facies, passing from alluvial/transitional marls (U1) to marine marls (U2) and calcarenites (U3) up to marine clays (U4) (**Fig. 3**), indicating a transgressive system tract. Whereas, as the upper part of Unit 4 and Unit 5 show a shallowing upward trend of the facies (**Fig. 3**), they define a highstand system tract (Amorosi *et al.*, 2014).

4.2 MATERIALS AND METHODS

The work was carried out on three selected volumetric samples, one per site (each contained in a 3 dm^3 sampling bag). The material was extracted by A. D'Alessandro and colleagues in 1976 from the less cemented lithotype of the *T. latus* bearing calcarenite at the following sections, listed from east to west (see **Fig. 1**): 1) Mass. La Penna locality (40°29'12.00''N 17°16'2.63''E) (Sample T13) (**Fig. 2D**); 2) 500 m south of Mass. S. Pietro (40°30'8.52"N 17°18'45.74"E), from a "very soft calcarenite" (Sample T5) (**Fig. 2A-C**); 3) "Il Fronte'' cliff (40°28'31.20"N 17°18'48.56"E) (Sample T17), from a whitish calcarenite characterized by common presence of in situ *C. caespitosa* small colonies associated to pycnodontids shells (D'Alessandro, field notes). Since that time, many sites were not more accessible or even exposed, as the T13 sample (see **Fig. 2D**), today testified by few remnant blocks of calcarenite and in situ *C. caespitosa* colonies entombed in a grey marl at the base. Nevertheless, the researchers' notes and schemes were used for integrating data related to the samples within the stratigraphic sections checked in the field (see **Fig. 3**).

4.2.1 Preparation of the samples, identification, and counts

Each of the three bulk-samples consist of loose bioclastic calcarenites, made all almost of sand to gravel sized calcareous bioclast, including dominant molluscan shells. Due to the presence of several granulometric fractions, it was decided to work on the one greater than 2 mm in size, corresponding to the molluscan macrobenthos (*sensu* Di Geronimo and Robba, 1976), which represents the most abundant fraction of each sample. Furthermore, each sample was enriched by larger (centimetric-to-decimetric) specimens, not included in the volumetric sampling due to their size, which were considered to avoid possible loss of their palaeoenvironmental information. Due to the high fossil density in each sample, it was superfluous to add further material for the study.

Molluscan specimens were identified at specific level, adopting the synonymy and the systematics of the World Register of Marine Species database (WoRMS Editorial Board, 2022) (see Appendixes I and III). As sole exception, owing to the high shell variability among the *Pusillina* species, and in view of their similar ecological meaning, we refer to them as "*Pusillina* group", as already suggested in other studies (Scotti *et al.*, 1995; Basso *et al.*, 2008).

For each species, the number of individuals (*abundance*) was estimated following the criteria of Di Geronimo and Robba (1976): 1) for bivalves, all the articulated specimens, all the complete disarticulated valves, and all the incomplete ones retaining the beak and/or hinge, were counted; the abundance was calculated as: *A= n valves of the most represented type + n/2 least represented valves + n whole individuals*; 2) for gastropods, all whole and incomplete specimens were counted only if preserving protoconch or the opening plus at least 2/3 of the teleoconch; 3) a similar criterion

was here adopted for scaphopods, i.e. at least 2/3 of the shell with apex. Then the *relative abundance* (A %), representing the number of a species on the total number of individuals of each sample, was calculated to directly compare the three samples, being equal in size, but different in total number of individuals.

4.2.2 Diversity structure of the fossil assemblages

Using the number of species (S) and of individuals (N), monovariate indexes, graphic diversity plots, and multivariate analysis, were performed to characterize and compare the diversity structure of the three samples. The PAST software was used for calculating monovariate indexes – Margalef's species Richness (d), Shannon index (H'), and the Pielou's evenness (J') – and to plot rarefaction curves, these used for a graphical comparison of the diversity structures, and to check the appropriateness of the sampling for the quantitative study (Hammer and Harper, 2006).

In addition, rank-abundance plots (e.g. Whittaker, 1965) were calculated (through the software R) and compared to the classical ecological abundance models, in order to identify the best-fitting model and characterized the environmental conditions (Hammer and Harper, 2006).

4.2.3 The Palaeobiocoenotic Approach

For the palaeoecological reconstruction, the palaeobiocoenotic approach was used, being one of the most used methods in the palaeoecology of the Neogene-Quaternary palaeocommunities of the Mediterranean basin (e.g., Bernasconi and Robba, 1993; Bernasconi and Stanley, 1997; Basso *et al.*, 2008; Gianolla *et al.*, 2010; Bernasconi and Stanley, 2014; Melis *et al.* al., 2015). The method consists in the comparison between the benthic palaeocommunities with the biocoenoses of the present-day Mediterranean Sea, the latter based on the Benthic Bionomy model (Pérès and Picard, 1964; Picard, 1965; Pérès, 1967; Carpine, 1970; Pérès, 1982; Picard, 1985), which uses biological features for the environmental description (Montefalcone *et al.*, 2021).

Each biocoenosis is defined starting from its characteristic zoo- and phytobenthos, and on the type of sediment that also gives the original French name of the biocoenosis (e.g., "SFBC": *Biocoenoses de le Sables Fin Bien Classé*: Biocoenosis of the Fine Well Sorted Sands).

Five species-specific autecological data are needed for the application of the palaeobiocoenotic approach, consisting of:

1) ***biocoenotic meaning,*** the species affinity for a biocoenosis that can be (following Pérès, 1982): *characteristic exclusive,* limited of a certain biocoenosis; *characteristic preferential,* present in a high number in a certain biocoenosis, but not limited to it; *accompanying,* or ubiquitous species; *accidental,* excl. of a certain biocoenosis and accidentally present in another one;
2) ***bathymetric distribution*** through the benthic zones of Pérès and Picard (1964) (i.e., mesolittoral, infralittoral, circalittoral, bathyal);
3) ***textural* affinity,** indicating the species preference for a certain substrate type: *psephophylic* (gravel-related species), *psammophylic* (sand-related spp), *pelophylic* (mud-related spp), *mistophylic* (species related to unsorted-mixed sediments), *solid-substrate* related species;
4) ***feeding type,*** indicating the trophic strategies of the species: *deposit feeders* (including detritus, deposit, and herbivore feeders, feeding on organic particles deposited on or inside

the substrate, or on vegetate substrates); *filter feeders* (filter feeders and suspension feeders filtering and capturing organic particles from water, respectively); *carnivores* (including necrophages and, plus ectoparasites due their negligible percentage);

5) ***habitus,*** defining the way of living of a species: *endobenthos* (living inside the substrate, including semi-endofaunals), and *epibenthos* (living on the substrate). Mobility faculties were not considered.

These data were collected for each species from several scientific papers on both fossil and modern molluscan assemblages (Corselli, 1981; Benigni and Corselli, 1981; Biagi and Corselli, 1984; Boenzi *et al.*, 1985; Caldara, 1986; Caldara and Laviano, 1986; Spano, 1989; Bernasconi and Robba, 1993; Dominici, 1994; Bernasconi and Stanley, 1997; Piazza and Robba, 1998; Brambilla *et al.*, 1998; Basso and Corselli, 2002; Spano *et al.*, 2002; Basso and Brusoni, 2004; Poggiani *et al.*, 2004; Ferrero *et al.*, 2005; Brunetti, 2011; Repetto *et al.*, 2017; La Mesa *et al.*, 2019; Bracchi *et al.*, 2020; Pavia *et al.*, 2022). For the quantitative and graphic palaeoecologic reconstruction, the relative abundances of the species of the same autecological class were summed together. Together with the autecological analysis, it was checked the presence of allochthonous elements, using different taphonomic evidence, and checking the ecological incompatibility of the species.

4.3 RESULTS

4.3.1 Macrofossils found in the calcarenite

Considering the taphonomic framework of the assemblage, the general conditions observed in the field and the state of preservation of the fossils suggest absence of relevant transport (e.g., absence of relevant fragmented and worn shells, contemporaneous occurrence of all-sized fossils, both of the same and of different species); this, together with evidence of autochthonism of some species (e.g., *Pinna nobilis* in life position; **Fig. 2B**) indicates that the assemblage is mostly autochthonous-parautochthonous.

Concerning the studied fraction (> 2 mm), molluscan represented the dominant component of the loose calcarenite, both as countable fossils and bioclastic fragments. The three molluscan samples yielded a total of 120 species (S) (S_{T5} = 83; S_{T13} = 89; S_{T17} = 51), of which just 32 are common to all samples, and a total of 5174 specimens (N) (N_{T5} = 3059; N_{T13} = 1580; N_{T17} = 535) (Appendix I-III). Individuals belongs to the classes of Bivalvia (relative abundances of 70 to 79%), Gastropoda (relative abundance 20 to 25 %), and Scaphopoda (relative abundance 1 to 6 %).

All the species are Mediterranean or Mediterranean-Atlantic (Appendix II), expect four of the identified species that are representative of the Senegalese fauna (Gignoux, 1913), found in the T13 and 17 samples: *Thetystrombus latus* (Gmelin, 1791), *Conus ermineus* Born, 1778, *Hyotissa hyotis* (Linnaeus, 1758), and *Cardita rufescens* Lamarck, 1819 (**Fig. 4**), well known in these deposits.

Other than molluscs, other taxa were recognized, and briefly listed as follows: rare to common corallites of *Cladocora caespitosa* (both found as corallites dispersed in the sediment and small colonies); rare barnacles and polychaete tubes encrusting few molluscan shells or sediment; rare fragments (dactyla and thoracic segment) of decapods; bryozoans, both as encrusting colonies and erect branched (cf. *Myriapora*); benthic and encrusting foraminifera (including some specimens of *Miniacina miniacea*); rare sub-centimetric complete irregular echinoid tests and articles; two tiny

bones (i.e. a fish jaw bone and a micromammal scapula); common coralline algae branched nodules (especially in T13, cf. *Lithothamnion* sp.). Sponge-related ichnogenus *Entobia* sp. was also found on large molluscan shells.

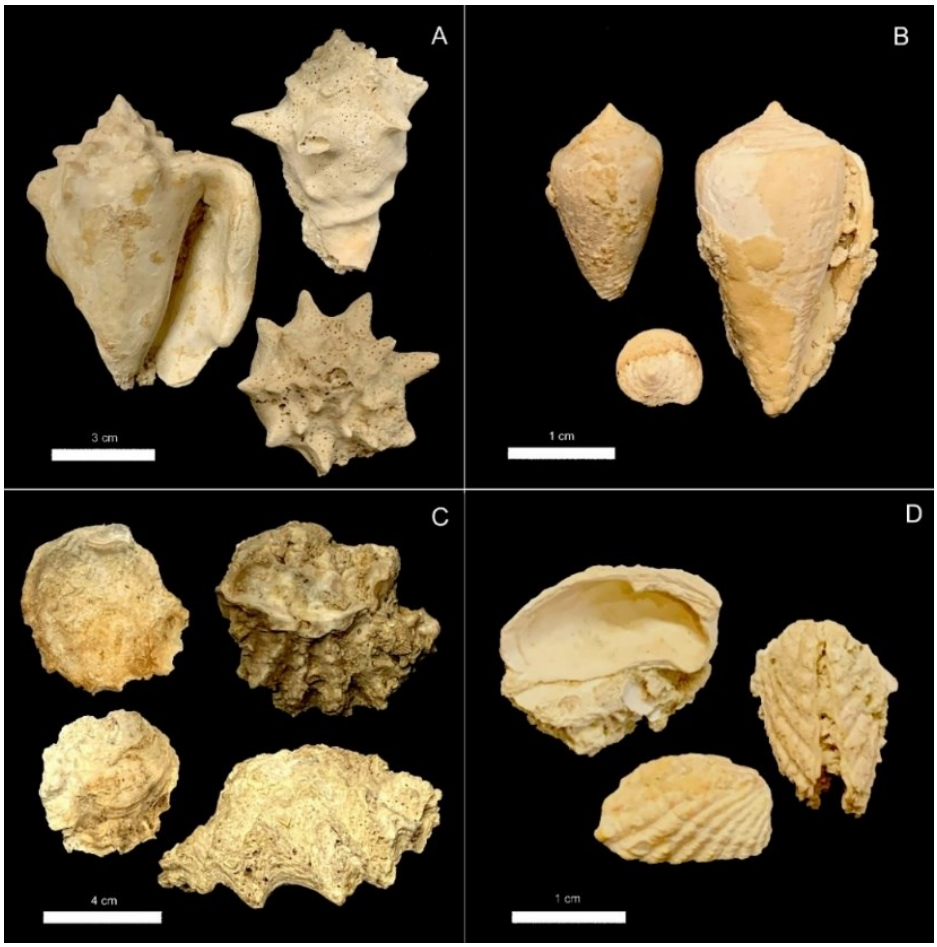

Figure 4. Senegalese Guests found in the studied material; **(A)** *Thetystrombus latus* (Gmelin 1791); **(B)** *Conus ermineus* Born, 1778; **(C)** *Hyotissa hyotis* (Linnaeus, 1758); **(D)** *Cardita rufescens* Lamarck 1819

4.3.2 Diversity structure of the molluscan assemblages

The molluscan Margalef's richness index (d) reaches its maximum values in T13, followed by T5 (d_{T13} = 11.95; d_{T5} = 10.22), and the minimum in T17 (d_{T7} = 7.96); evenness (J') is higher in T17 (J'_{T17} = 0,80), followed by T13 (J'_{T13} = 0.76), and is minor in T5 (J'_{T5} = 0.65); the overall diversity (H') is higher in T13 (H'_{T13} = 3.40) than in T17 (H'_{T17} = 3.15) and in T5 (H'_{T5} = 2.87) that, albeit more species-rich, has a unevener distribution than T17 (**Tab. 1**).

The individual rarefaction curves show graphically the diversity of the three samples (**Fig. 5**): T13 appears as the most diverse sample as its curve start flattening off after a greater number of species, while T5 and T17 start flattening earlier. Despite the different species richness (Taxa S) and absolute specimen abundances, all the curves show an asymptotic pattern by increasing the number of individuals (i.e., sample size). This indicates that almost all the common species present in the sites have been recovered, and only some rarer species are missing (Hammer and Harper, 2006). The T17 sample returned the minor number of species and individuals, as possibly biased by a greater extent of cemented calcarenite portion in the sampling bag that may have prevented the finding of most

species. Nevertheless, it is acceptable for quantitative study as its rarefaction curve shows a moderate pendency in its terminal part (**Fig. 5**), indicating that only few rare species would be added into the sample by adding further loose material. Instead, the more species and individuals rich T13 and T5 samples show a slightly higher slope of the terminal tract: possibly, some rarer species are missing but, overall, all the curves are well developed and acceptable (**Fig. 5**). Summarizing, all the samples are suitable for quantitative palaeoecology.

Finally, as shown in **Figure 6**, the theoretical model that better describes the structural diversity pattern of the three assemblage is the log-normal model (Preston, 1948), with a typical S-shaped pattern, as all the samples features few dominant species, followed by several co-dominant and a very high number of rarer species, contributing to the diversity structure of the assemblages (see also **Fig. 7**).

Sample	S	N	d	J'	H'
T5	83	3059	10.22	0.65	2.87
T13	89	1580	11.95	0.76	3.40
T17	51	535	7.96	0.80	3.15
tot	*120*	*5174*	*13.92*	*0.71*	*3.38*

Table 1. Monovariate indexes of the three molluscan palaeocommunities and of the three samples considered as a whole. S: number of species; N: number of individuals; d: Margalef's Species Richness; J': Pielou evenness index; H': Shannon Diversity index.

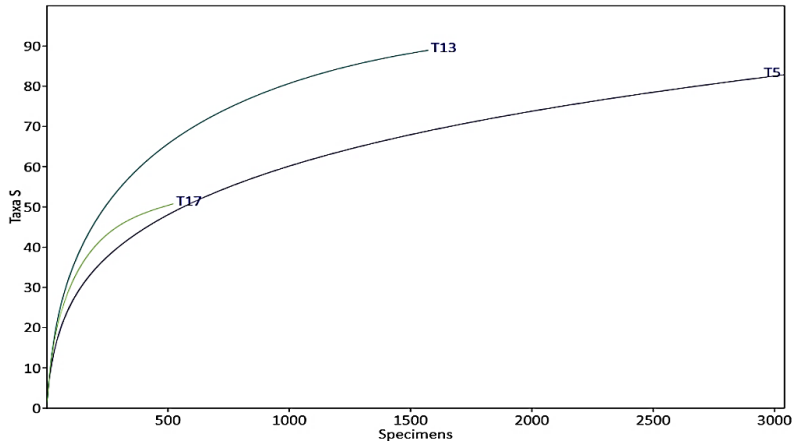

Figure 5. Individual rarefaction curves of the three samples.

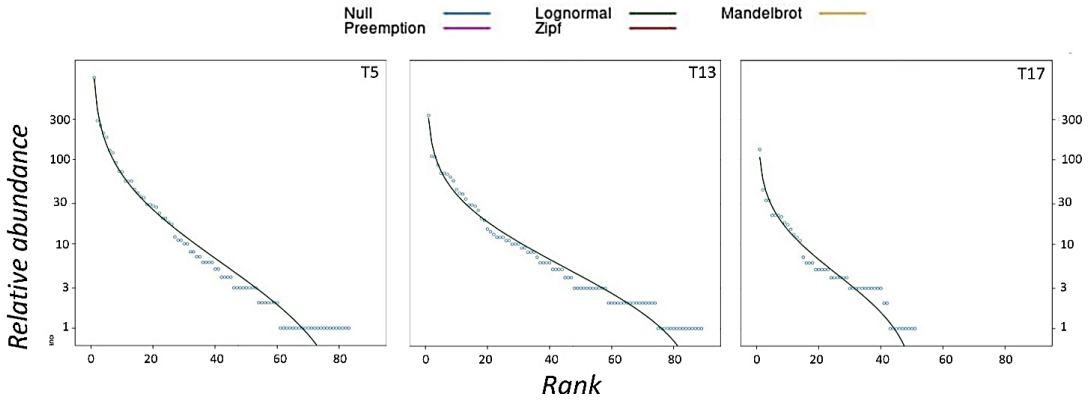

Figure 6. Rank abundance models of the three samples (Y-logged axis).

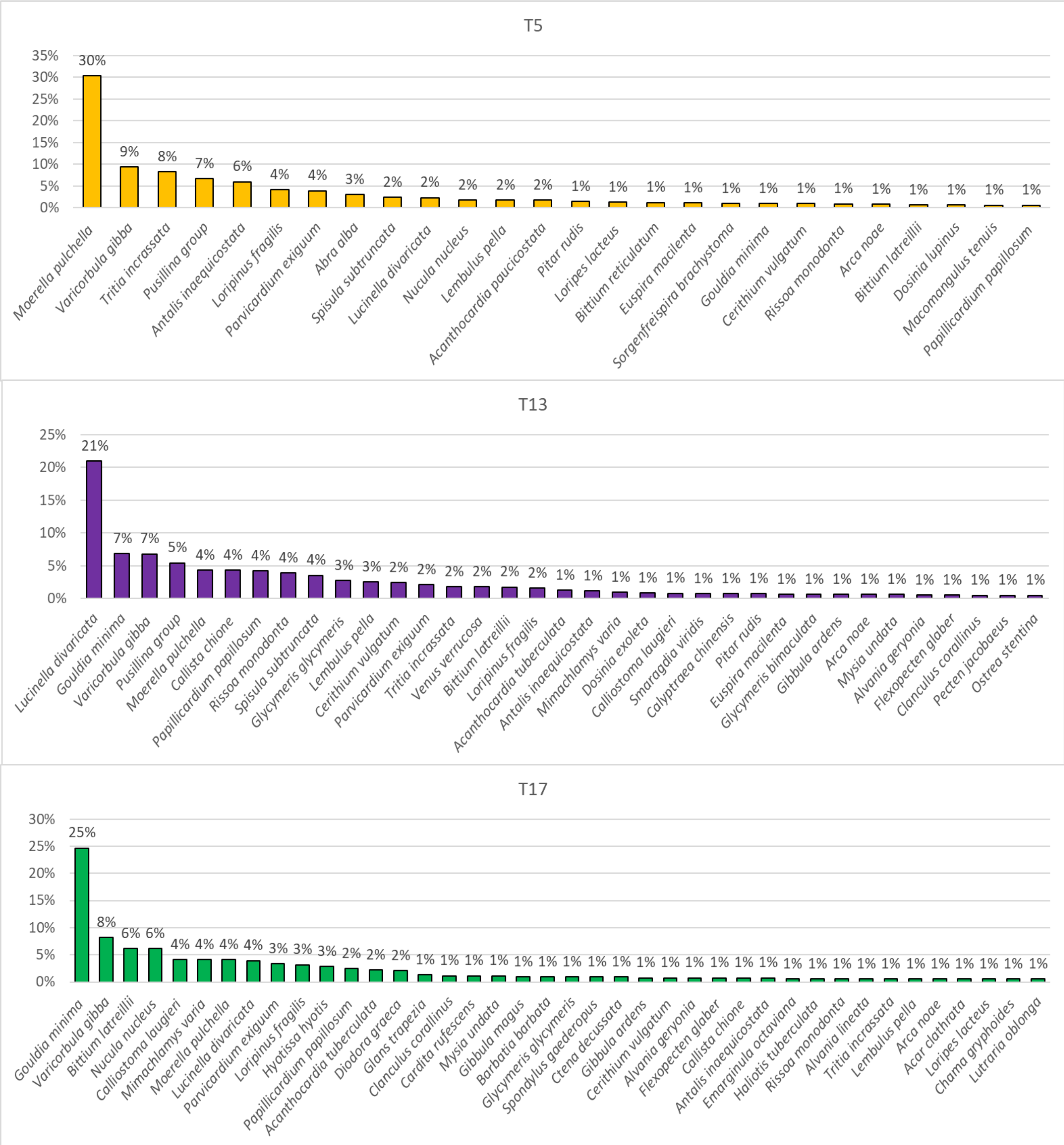

Figure 7. Relative abundances (%) of common species (cut off 1 %) in the three samples.

4.3.3 Palaeoecology of the molluscan assemblages

The palaeobiocoenotic analysis shows a general similarity of the three palaeocommunities as regards the bathymetric range and life-habit of the molluscan species. First, an infralittoral location is indicated by the relative abundance values (from 97.0% to 99.0 %) of species living in this shelf sector. In all the samples, the infauna always prevails (from 68.0 % to 85.0 %) on the epifauna (from 32.0 % to 15.0 %). Nevertheless, subtle differences are recognizable when the ecological meaning (Fig. 8), substrate preference and feeding type of taxa are considered (Fig. 9**A, B**).

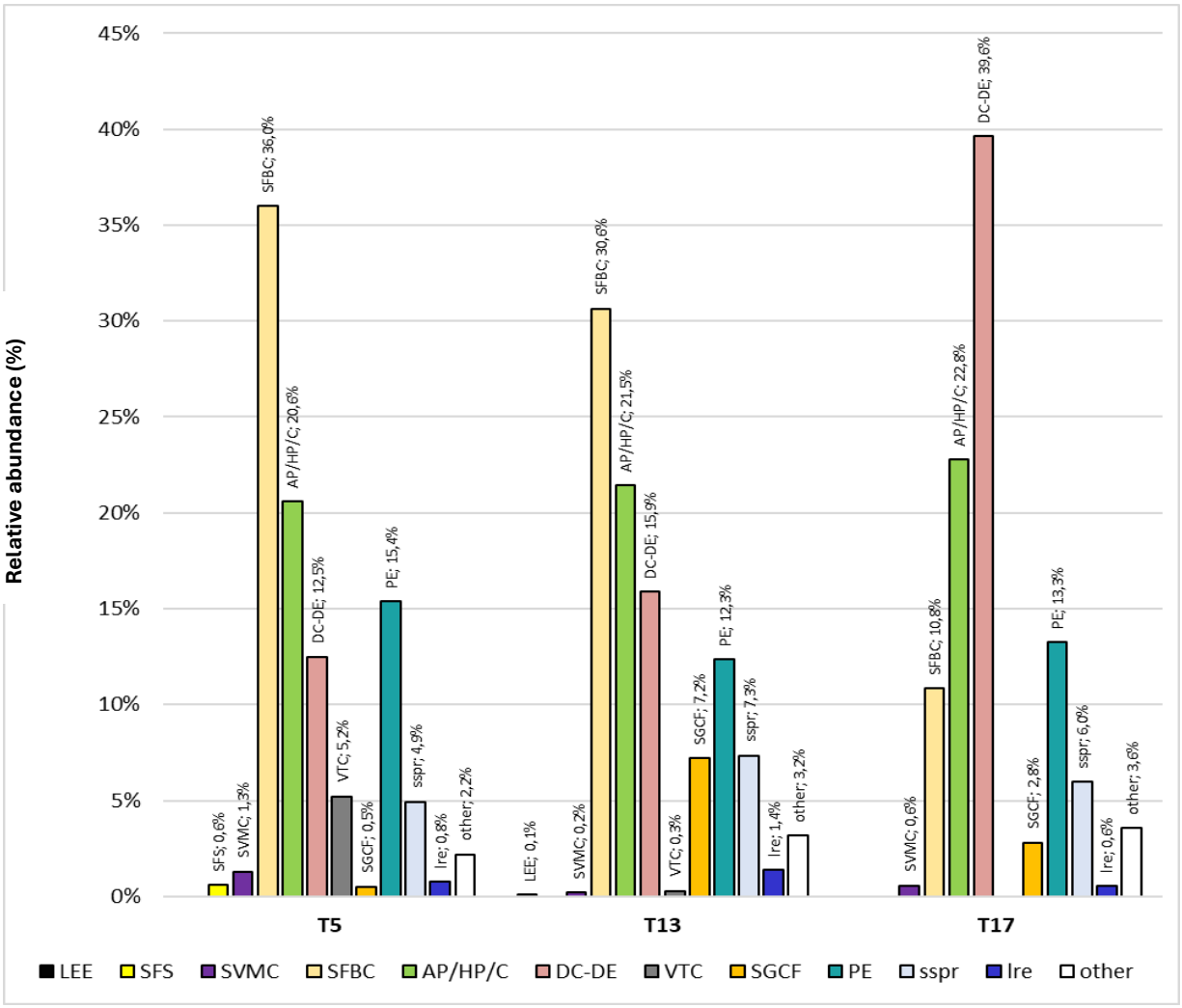

Figure 8. *Palaeoecological characterization: Ecological meaning of the molluscan assemblages* Biocoenosis of Eurythermal and Euryhaline Lagoons (LEE), B. of Superficial Fine Sands (SFS); B. of Superficial Muddy Sands in Sheltered Areas Of Fine Well Sorted Sands (SMVC), B. of Fine Well Sorted Sands (SFBC) B. of Photophilic Algae (AP), Posidonia Meadows (HP)] Coralligenous (C), B. of Coastal Detritic and Muddy Detritic (DC-DE), B. of Coastal Terrigenous Muds (VTC), B. of Coarse Sands under Bottom Currents (SGCF), Heterogeneous Community (PE), species lacking a precise ecological meaning (sspr), species with a wide ecological distribution (lre).

In samples T13 and T5, the most represented biocoenoses are those of Fine Well Sorted Sands (SFBC) (30.6%, 36.0%) and of vegetated bottoms [i.e. Photophilic Algae (AP), *Posidonia* Meadows (HP), plus negligible coralligenous species] (21.5%, 20.6%) (**Fig. 8**). The SFBC biocoenosis is inferred by several exclusive characteristic species: the bivalves *Lucinella divaricata* (dominant species in T13), *Moerella pulchella* (dominant species in T5), *Acanthocardia tuberculata*, and *Spisula subtruncata*, and the gastropods *Tritia mutabilis*, *Mangelia attenuata*, and *Acteon tornatilis*, and by the preferential characteristic bivalve *Dosinia lupinus* (**Fig. 7**).

The Photophilic vegetated AP-HP biocoenoses are represented by the exclusive characteristic gastropods *Smaragdia viridis*, *Diodora italica*, and *Conus ventricosus*, and by a stock of preferential

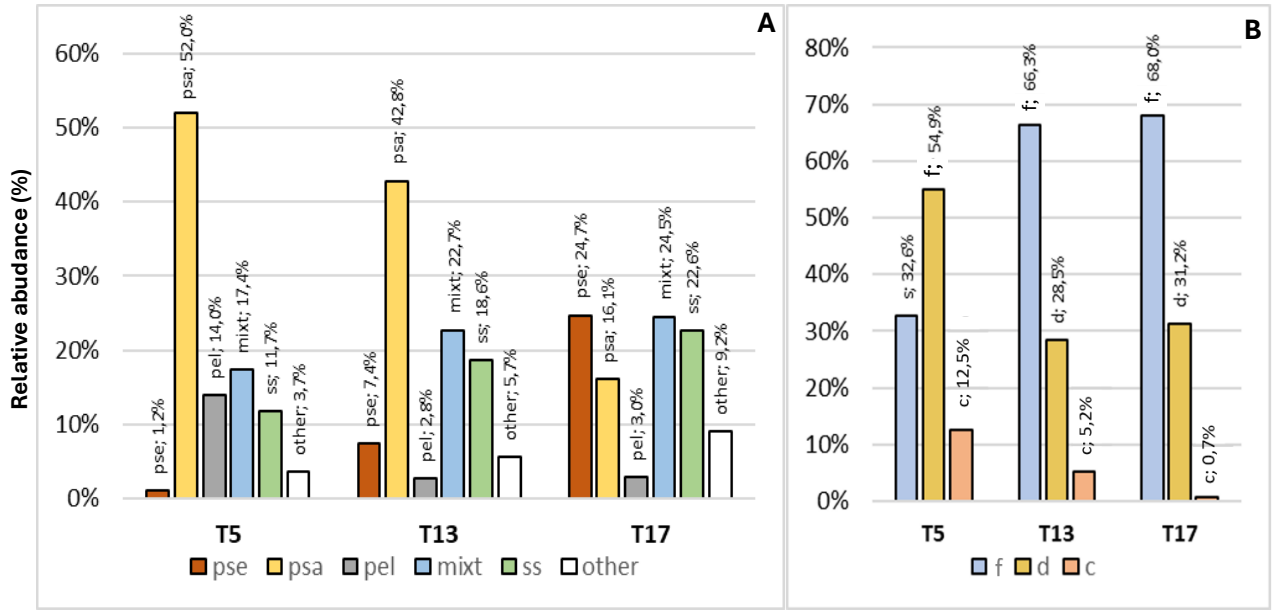

Figure 9. *Palaeoecological characterization*. (**A**) *sediment preference*: gravel related species (pse), sand-related species (psa), mud-related species (pel), mixed substrate-related species (mixt), hard substrate-related species (ss); (**B**) *Feeding type*: suspension/filter feeders (f), deposit/detritus feeders (d), carnivores/necrophages/parasites (c).

taxa: among these are the gastropods *Diodora graeca, Tricolia pullus pullus, Rissoa monodonta, R. violacea, Tritia incrassata, Columbella rustica,* and the bivalves *Arca noae, Barbatia barbata, Pinna nobilis, Spondylus gaederopus,* and *Chama gryphoides*. Several other species are commonly associated to vegetated bottoms (the gastropods *Clanculus corallinus, Jujubinus striatus, Bittium reticolatum, B. latreilii, Cerithium vulgatum, Alvania* spp., *Pusillina* spp., *Stramonita haemastoma*) (**Fig. 7**).

In samples T13 and T5, species indicative of Coastal Detritic and Muddy Detritic biocoenoses (DC-DE) (15.9%, 12.5%) are detected (**Fig. 8**). This stock is represented by preferential species (the bivalves *Nucula nucleus, Mimachlamys varia, Myrtea spinifera, Acanthocardia echinata, Papillicardum papillosum, Azorinus chamasolen, Timoclea ovata, Gouldia minima, Pitar rudis,* the gastropods *Gibbula magus and Sorgenfreispira brachystoma,* and the scaphopod *Antalis inaequicostatua*), and few strictly circalittoral species (the DC exclusive bivalves *Flexopecten flexuosus, Pecten jacobaeus,* and *Gari fervensis,* the gastropod *Turritella turbona*, and the preferential gastropod *Calliostoma zizyphinum*), and the preferential scaphopod *Antalis inaequicostata* (**Fig. 7**).

T13 and T5 are also characterized by species related to the Heterogeneous Community (PE) (12.3%, 15.4%) are also present (**Fig. 8**), testified by the bivalves *Lembulus pella, Ctena decussata, Parvicardium exiguum, Varicorbula gibba, Moerella distorta,* the gastropod *Euspira guillemini*, and the scaphopod *Fustiaria rubescens* (**Fig. 7**). As expected, sand-related species dominate (42.8 %, 52.0%), followed by mixed substrate-related (22.7%, 17.4%) and hard substrate-related taxa (18.6 %, 11.7%) (**Fig. 9A**); carnivores are better represented in T5 (12.5%) than in T13 (5.2%) (**Fig. 9B**).

In the T13, a significant relative abundance (7.2%) pertains to the biocoenosis of Coarse Sands under Bottom Currents (SGCF) (**Fig. 8**); this biocoenosis is testified by the exclusive characteristic bivalves *Glycymeris glycymeris, Venus casina,* and *Dosinia exoleta,* and the preferential *Glycymeris*

bimaculata and *Laevicardium crassum,* and *Venus verrucosa, Glans trapezia* and *Venericardia antiquata* (**Fig. 7**). Gravel-related (7.4%) are more represented than mud-related (2.8%) taxa (**Fig. 9A**). Filter feeders prevail over deposit feeders (66.3% and 28.5%, respectively) (**Fig. 9B)**.

In sample T5, smaller percentages pertain to the biocoenoses of Coastal Terrigenous Muds (VTC) (5.2%), which is testified by the preferential characteristic gastropod species *Turritelinella tricarinata, Eulima glabra,* the bivalves *Acanthocardia paucicostata* and *Abra alba* (that is commonly associated with); it is recognized also the Superficial Muddy Sands in Sheltered Areas (SVMC) (1.3%) biocoenoses (testified by the exclusive bivalve *Loripes lacteus*) (**Fig. 7**; **Fig. 8**). Mud-related (14.0%) dominate over gravel-related (1.2%) species (**Fig. 9A**). Deposit feeders prevail over filter feeders (54.9% and 32.6%, respectively) (**Fig. 9B**).

The T17 shares almost all the species with T13 and T5: just 5 species, as the AP exclusive gastropod *Haliotis lamellosa,* were found just in this sample. Albeit this, significantly different relative abundance values of these species make the DC-DE stock prevailing (39.6%) on the AP/HP (22.8%), PE (13.3%), SFBC (10.8%) and SGCF (2.8%) (**Fig. 8**). Gravel-related (24.7%) and mixed substrate-related species (24.5%) dominate, followed by hard substrate-related species (22.6%), sand-related species (16.1%), and mud-related (3.0%) species (**Fig. 9A**). As in T13, suspension-feeders prevail over deposit-feeders (68.0 % and 31.2 %, respectively) (**Fig. 9B**). The relative abundance of the DC biocoenosis and gravel related species is mostly related to the DC preferential psephophilic and rheophilic *Gouldia minima* that is the dominant species of this sample (**Fig. 7**).

4.4 DISCUSSION

4.4.1 Diversity structure

The palaeobiodiversity analyses indicate a similar structural diversity framework for the three samples, represented by moderately-to-high diverse molluscan assemblages (**Fig. 5**; **Fig. 6**). The graphic comparison of the structural diversity also indicates a similar setting, as in all the cases the log-normal model of Preston (1948) is the model that better describes the structure of the three samples (**Fig. 6**). This pattern is indicative of diverse communities in stable (non-stressed and resource rich), heterogeneous environments (May, 1981; Hammer and Harper, 2006). This pattern also corresponds to communities in equilibrium controlled by various environmental factors, generated by a process in which each species randomly occupies a niche and enters in competition with other species (Sugihara, 1980). One of the three samples (i.e. T17) has a minor correspondence to this model, which nevertheless remains the only that efficiently describes its pattern (**Fig. 6**). All considering, monovariate indexes and the rank-abundance analysis indicate that the three sites were similar each other and no substantial environmental differences existed in the three sites.

Anyway, even if in a similar palaeoenvironmental framework, some slight differences occurred between the three sites. Indeed, the indexes' values and the rank-abundance patterns featured some slight differences: T5 and T13 are similar for species richness, but different for diversity and evenness; T13 and T17 are similar for evenness and diversity, but different for species richness. These minor differences are also suggested by partially different taxonomic composition of the three samples, as only 32 species common to all samples, even with significantly variable relative abundances values (see **Fig. 7** and Appendix I).

4.4.2 Palaeoecological interpretation

Also, palaeoecological data suggest that, although in a similar framework, the three sites were characterized by slightly different environmental parameters, which can be highlighted for a refined palaeoenvironmental reconstruction. As stated by Amorosi *et al.* (2014), the association is made up of species coming from different nearby palaeobiotopes but as shown by the subsequent reconstruction, not ecologically incompatible. The fossil community, overall, therefore represents an autochthonous-parautochthonous assemblage. It should be noted that any estimate of diversity and the variety of palaeobiocoenotic analysis results may also be, at least in part, related to the taphonomy of the assemblage, i.e. the mixing and condensation of different thanatocoenoses developed in space and time. Therefore, the palaeoecological interpretation should be more properly considered as representative of the mean palaeoenvironmental conditions during MIS 5e at the three studied sites.

In accordance with previous literature contributions, mollusc autecological data indicate that the three assemblages inhabited a shallow infralittoral bottom, testified by high relative abundance values either of species with a purely infralittoral depth range, and by the SFBC and AP/HP biocoenoses, both strictly related to this relatively shallow setting (**Fig. 8**).

The sandy bottom SFBC biocoenosis dominates in T13 and T5. The right/left valves ratios of the dominant SFBC exclusive species, which are *M. pulchella* in T5 and *L. divaricata* in T13 (**Fig. 7**) are close to 1 (1.1, and 1.0, respectively). This indicates that these species, and therefore the whole SFBC stock, are residual and autochthonous (e.g. Aberhan and Fursich, 1991; Ragaini and Mariani, 1992). The SFBC is significantly represented also in T17, but it is not the dominant biocoenosis. Nevertheless, at this site, the psammophylic SFBC-related *Lutraria* spp was reported in life position (Amorosi *et al.*, 2014), suggesting the occurrence of an SFBC bottom also at this site, coherent with the lithology of the calcarenitic bed. According to the high relative abundance of species SFBC, T5 and T13 are also dominated by sand-related species, accompanied by mixed substrate-related species indicating an overall heterogeneous bottom; sand-related species are detected also in T17, where gravel and mixed substrate-related species dominate (see below). If the MP calcarenite hosted an in situ SFBC bottom, the present-day range of this biocoenosis can be used to better constrain the palaeodepth estimation that, therefore, would result between 2.5 and 25 m (UNEP/MAP-RAC/SPA, 2015).

The commonly associated photophilic vegetated AP-HP biocoenoses are well represented in all the samples (on average 21.6 % of the association), as expected in an infralittoral palaeoenvironment. As the SFBC, also the AP-HP stock can be interpreted as a residual community. This is exemplified by *P. nobilis* shells that, according to field notes and photographs taken during the sampling and our field observation, were recovered in life position (i.e. with downward antero-umbonal margin) in all the samples. Today, this semi-infaunal bivalve is commonly associated to *Posidonia oceanica* and/or other phanerogams meadows, and its bathymetric range usually coincides with those of these plants (Guallart and Templado, 2012; Bracchi *et al.*, 2020). Moreover, the abundant presence of Pinnidae in life position is also considered as a possible indicator of sea-grass palaeoenvironments (Reich *et al.*, 2015; Bracchi *et al.*, 2020; Tomassetti *et al.*, 2022). For this reason, this species was considered as preferential for the HP. In support to this point, other AP-HP

related species (e.g. *A. noae* and *C. vulgatum*) have been found inside *P. nobilis* in situ articulated shells, strengthening this association.

The characteristic *Glans trapezia, Venericardia antiquata,* and *Venus verrucosa* are good HP indicators, being part of the matte endofauna; anyway, their relative abundance was counted among the SGCF stock (see below). Another species commonly found in the HP, i.e., *Callista chione*, has been counted among species lacking an ecological meaning (sspr) having been considered both as characteristic of HP (La Mesa *et al.*, 2019) and of SFBC (Dauvin *et al.*, 2017); anyway, its presence well fits in a such sandy-vegetated bottom. Finally, among vegetated habitats, the circalittoral Coralligenous (C) exclusive *Barbatia clathrata* found in the material, is likely accidental or indicative of small sciaphilic enclaves.

The warm water Senegalese species *Thetystrombus latus,* a detritivorous-herbivorous requiring mobile substrates often with algal meadows, and also *Cardita rufescens*, can be associated with these vegetated contexts (Barrier *et al.*, 1990; Repetto *et al.*, 2020).

Among the AP-HP stock, some AP exclusive species figure (e.g., *H. lamellosa*), indicating the co-occurrence of seagrasses, to be expected in a mobile infralittoral bottoms, and seaweeds, typically related to hard infralittoral bottoms. Most of these species require solid substrates. These, at least in part, were provided by plant leaves (e.g. small epiphytic species) or by other small objects, such as large shells lying on the seafloor. Anyway, some large species, as the situ articulated AP preferential *Spondylus gaederopus*, typically require rocky bottoms. This species presents a good overall preservation, with both right and left valves keeping delicate spines intact. Having not been identified rocky substrates in the MP deposits (Caldara and Laviano, 1980), and as these species were found with the encrusting right valve directly overgrown on the calcarenite, possible local early cemented sediment patches are suggested. The same indication is provided by oysters, rare barnacles, and serpulids, found in the calcarenite without encrusting any hard substrate. For a further explanation of this point, see *Chapter 6*.

The current-dominated SGCF biocoenosis as well as abundant rheophilic species are significantly detected in T13 and T17. Nowadays, the SGCF biocoenosis is often mixed with other infra-circalittoral biocoenosis, such as HP bottoms, as it can be located inside the current-dug intermatte channels (Corselli, 1981). As mentioned, the HP-related bivalves *Glans trapezia, Venericardia antiquata,* and *Venus verrucosa* are all present in the T13 sample. These species typically live intermatte channels under strong current action, developing a SGCF community, which is not always clearly distinguishable from a true matte fauna (Pérès and Picard, 1964; Corselli, 1981). Indeed, *V. verrucosa* was considered in literature both HP and SGCF exclusive (Harmelin and Schlenz, 1964; Biagi and Corselli, 1984). Albeit their strong relationship with HP bottoms, these species were counted among SGCF stock with the aim to better emphasize environmental (i.e., hydrodynamic) differences among the different sites. Due to the recognition of a vegetated HP assemblage, this is the most likely scenario for the MP assemblage. Indications of bottom currents are provided also by *Gouldia minima,* the dominant species of the T17 sample (see below).

The upper circalittoral gravelly to muddy bottom DC-DE stock dominates the T17 assemblage, and it is also found in the other samples with a significant relative abundance value (**Fig. 8**). Anyway, the exclusively circalittoral species sum a very low percentage (around 1 %). Concordantly, these biocoenoses are mostly represented by DC preferential characteristic species (pure DE indications

are negligible) that can live both in the infralittoral and in the circalittoral, not precluding the infralittoral location for this site. In support of this hypothesis, some significant DC preferential species can be contextualized in the recognized infralittoral biocoenoses. For example, *Mimachlamys varia*, regarded as DC preferential (e.g. Basso and Brusoni, 2004; Pavia *et al.*, 2022) is also considered indicative of HP bottoms (Bracchi *et al.*, 2020). The same can be said on the gravel related *Gouldia minima*: albeit often regarded as lacking a precise ecological meaning, it has been considered as DC characteristic preferential (Basso and Brusoni, 2004), and can also be an abundant accessory species in vegetated bottoms (Spada, 1970; Tomašových *et al.*, 2019). Being the dominant species of the T17 sample (**Fig. 7**), and even autochthonous as suggested by the r/l ratio close to 1 (i.e., 1.1), this species possibly indicates a more important influx a close DC community (also supported by the other preferential species) on the infralittoral vegetated community.

The DC relative abundance values, together with the high percentage of infra-circalittoral species, indicates that the T17 palaeobiotope was probably located towards the lower portion of an SFBC-HP bottom, passing to and coarser DC-like bottom, probably made of a more important accumulation of bioclastic gravel, likely represented by part of the shells found in the material. Moreover, even if *G. minima* is not characteristic of the SGCF community, where can be also found, this species is considered an indicator of bottom currents (Caldara, 1986; Dominici, 1994). This is consistent with modern findings, i.e., lower infralittoral with coarser bottoms influenced by currents (Spada *et al.*, 1973). Therefore, its relative abundance suggests a relatively higher energy at the T17 site.

Finally, there are some minor indications of other habitats, which may indicate neighbouring biocoenoses or small mixed enclaves. A low but significant (> 1%) percentage of the SVMC biocoenoses (represented by the exclusive *Loripes lacteus*) is significantly detected in the T5 (**Fig. 7**), likely associable to sheltered areas that, given the palaeobiocoenotic indications, possibly could be set behind a *posidonietum*. Some negligible indications of the Superficial Fine Sands (SFS) biocoenosis (testified by the exclusive *Macomangulus tenuis*) are found in the T5 site (**Fig. 7**). Finally, in T13 not significant indication of the Euryhaline and Eurythermal Lagoons (LEE) biocoenosis comes from two worn valves of the exclusive *Cerastoderma glaucum*, likely transported and allochthonous. The fast-deposited fluvial mud-related VTC biocoenosis is significant (5.2 %) only in T5 (**Fig. 8**), indicating the occurrence of fluvial mud deposition in low energy areas located near the T5 site. This biocoenosis can fade into SFBC bottoms, recognized at the T5 site, as it can form ecotones with its lower part (Benigni and Corselli, 1981; Koulouri *et al.*, 2006).

The PE, found with a significant percentage (on average, about 14 %), establishes and becomes dominant under increased turbidity periods that favour tolerant opportunistic species (Di Geronimo and Robba, 1989). Some of the identified PE species (*Varicorbula gibba*, associated to *S. subtruncata, A. inaequicostata, A. alba,* and *N. nucleus*) were reported at the limit of the infralittoral, favoured by momentaneous mud increasing (Benigni and Corselli (1981). This, possibly, may have occurred in SFBC-VTC ecotones located close to the T5 site. Anyway, in all the samples, this community does not reach dominant value, suggesting an overall stable palaeoenvironment with only moderate mudding.

4.4.3 Lateral variability

Summarizing, the calcarenitic level deposited under very similar palaeoenvironmental conditions at the three sites investigated, i.e. a dominantly sandy/gravelly vegetated, relatively stable infralittoral bottom, as indicated by the similar percentages of SFBC, AP-HP, DC, and PE (**Fig. 8**). Endofaunals molluscs dominate over the epifaunal in all the samples, as expected by soft bottom settings, with only local small solid substrate. Despite these similitudes, the three samples are characterized by minor differences concerning palaeobiocoenotic, trophism, substrate preference, and life habit, testifying slightly different hydrodynamics between the sites (**Figg. 7-9**). On one hand, in the T5, SVMC and VTC biocoenoses, detected as accessory components of the fossil assemblage, indicate respectively shallow and deeper bottoms with low water energy, allowing some mud and fine organic particles deposition. According to this indication, deposit feeders, requiring such low energy conditions for the deposition of organic detritus (e.g., Koulouri *et al.*, 2006), dominate over filter feeders. Not surprisingly, a consistent mud related species percentage (i.e. 14%) is reached only in the T5, while gravel-related species are very poorly represented (1.2%). The low relative abundance of gravel related species is also linked to the highest percentage of endofaunals (84.8 %). All these indications indicate an overall slightly more sheltered seafloor near the T5 site. On the other hand, the current related SGCF biocoenosis and the relative abundance of rheophilic species are significantly represented in the T13 and T17. As expected by more energetic waters, filter feeders dominate over deposit feeders (representing more than 2/3) in both samples. Gravel-related species percentage is consistent in the T13 (7.4%), and also the dominant ones (in the T17 (24.7%). By contrast, mud related species sum up a little percentage (on average, 2.9%) in both the samples. The lowest percentage of endofaunals (i.e. 68,4 %) is found in the T17 (i.e. where gravel related species dominate). All these indications indicate an overall more exposed seafloor, likely to current actions, near the T13 and T17 sites. In addition, as already suggested, the T17 was probably slightly deeper than T13 and T5 due to dominant DC preferential species percentages.

4.5 CONCLUSION

The study of three bulk samples of the *T. latus* calcarenite from three sites of the MP (T5, T13, T17) led to the identification of a rich molluscan taxa, composed of 120 species (including 4 of the well-known Senegalese fauna), of which 32 are common to all the samples. The three assemblages are well diversified, indicating a relatively stable and variegated palaeoenvironmental conditions during the deposition of the MIS 5e calcarenite. The mean palaeoenvironmental conditions inferred can be depicted as a mostly sandy to gravelly bioclastic mobile bottom, located in an infralittoral/lower infralittoral setting. By terms of biocoenotic affinities, the whole fauna is indicative of a mixed Well Sorted Fine Sands (SFBC) mixed with a Photophilic Algae and *Posidonia* meadows (AP/HP) biocoenoses, with minor contribution from neighbouring biocoenoses. In the T17 site, a major number of species preferential for upper circalittoral biocoenoses, mostly Coastal Detritic (DC), indicates the proximity to circalittoral deeper and coarser bottom, suggesting a slightly deeper lower infralittoral location than T5 and T13. T13 and T17 areas were more exposed to bottom currents and/or waves, while the T5 area resulted more protected allowing more finer particles deposition. Therefore, the goal of this contribute is adding a new quantitative refinement about the palaeoenvironmental conditions during MIS 5e of the Taranto Area.

CHAPTER 5 - MIS 5e SEA SURFACE TEMPERATURE ESTIMATION; A MULTI-PROXY APPROACH USING A MARINE MACROFOSSIL ASSEMBLAGE (MAR PICCOLO, GULF OF TARANTO, SOUTHERN ITALY)

Abstract. *It is reported a multi-proxy palaeoclimatic study conducted on a MIS 5e calcarenite from the Mar Piccolo Basin (MP), Gulf of Taranto (GT) (Central Mediterranean). The calcarenite returned a rich malacofauna consisting of 120 extant species, including four of the tropical Senegalese Fauna, today absent in the Mediterranean. The biogeographic-climatic affinity of the assemblage shows, compared to today, a double percentage of warm affinity species, while the cold affinity species are similarly represented, indicating a warmer but not strictly tropical SST. This is confirmed by the most recurring preferred SST ranges of the assemblage, indicating an average of 20 °C. The skeletal compositions of five well-preserved molluscan and coral specimens were analysed for trace elements and stable isotopes for further mean SST estimations. From the comparison of the results of several equations available in literature, it appears that only some SST estimations are realistic, converging into similar values of, on average, 20.8 ± 0.9 °C. Considering all the used proxies, the MIS 5e SST difference compared to today falls in the range 1.2 - 2.0 °C for the GT (being a more reasonable scenario) and 2.0 - 2.8 °C for the MP. This is not a firmly tropical-like SST setting as suggested by the sole Senegalese fauna, indicating at least 2.7 °C to 3.5 °C more than to today's GT and MP, respectively. The approximations and assumptions made for obtaining SST values with any single proxy indicates the need of a multi-proxy approach to define the best SST estimation.*

Keywords: *MIS 5e; Sea Surface Temperature; Palaeoclimate proxy; Fossil Fauna; Gulf of Taranto.*

5.1 INTRODUCTION

As wrote in *Chapter 1*, MIS 5e is a good analogue for the present-day global warming future development. Hence the importance of using the geo-palaeontologic archive for obtaining palaeoclimatic inferences, starting with the estimate of the Sea Surface Temperature (SST), the rise of which is one of most direct effect on marine waters of global warming. With this purpose and with the goal of adding new palaeoclimatic insights into MIS 5e in the Gulf of Taranto (South Italy - Central Mediterranean), a multi-proxy-based approach was used to estimate the SST from a marine macrofossil assemblage. This assemblage was used here for a multi-proxy study based on biogeographical data, i.e. species climatic affinity, preferred SST range, and thermal constraints, and on geochemical data, i.e. major and trace elements, and oxygen stable isotopes composition. The study was focused on molluscs and coral fossils since both taxa are commonly used as palaeoclimatic indicators and archives (see *Chapter 3*).

5.1.1 Geological and stratigraphic setting

See *Chapter 4*.

5.1.2 Oceanographic setting

The modern MP is a shallow semi-closed basin, strongly affected by freshwater inputs from the so called "Citri" karstic springs. Based on historical data from 1922 to 2014 (https://va.mite.gov.it/File/Documento/293172), its mean superficial salinity (SSS) is generally lower than the open sea one, with an average of about 36.3 psu, while the mean annual SST is around 18.0 °C ranging from the mean monthly SSTs of 11 to 25 °C.

The MP is connected, through the adjacent Mar Grande, to the wider Gulf of Taranto (GT), which represents the northernmost part of the Ionian Sea. Out of the MP, average SSS values range from 37.8-38 psu in the nearby Mar Grande (Alabiso *et al.*, 2005; Di Leo *et al.*, 2014; Cardellicchio *et al.*, 2015), up to 38.2 psu in the northern Ionian Sea (corresponding to a $\delta^{18}O_w$ of 1.4 ± 0.1 ‰ ; Grauel and Bernasconi, 2010), resulting in average ca. 38 psu, which is the average SSS of the entire Mediterranean (Garilli, 2011; Nessim *et al.*, 2015; Danovaro, 2019). In the Northan Ionian Sea (GT), mean winter and summer SST are about 14 °C and 25 °C, respectively, and the average annual SST is around 18.8 °C (Shaltout and Omstedt, 2014).

5.2 MATERIALS AND METHODS

The studied fossil assemblage was selected from three highly fossiliferous bulk-samples of sediment, about 3 dm^3 each, enriched by coarse specimens with larger fossils. Samples named T5, T13, and T17, were originally collected by A. D'Alessandro and colleagues in 1976, along the MP coastline at the following sites: sample T13 comes from Masseria La Penna (40°29'12.00''N 17°16'2.63''E), sample T5 from south of Masseria S. Pietro (40°30'8.52"N 17°18'45.74"E), and sample T17 from Il Fronte cliff (40°28'31.20"N 17°18'48.56"E) (see *Chapter 4,* **Fig. 1**). Six stratigraphic sections were documented, including the ones from which the samples were collected (see *Chapter 4,* **Fig. 3**) Unfortunately, since many years have passed after the sampling, Masseria La Penna section is no longer well exposed; nevertheless, the section was reconstructed according to researchers' field notes taken during sampling in 1976, integrated with some new observations. Each sample comes from the same stratigraphic level (see *Chapter 4,* **Fig. 1**): the heterogeneously cemented MIS 5e calcarenite bed, 1.5 m thick on average, a value that represents the whole stratigraphic thickness of the bed in the three sites of sampling. The analyses on the bulk samples were focused on the mollusc macrobenthos (shell coarser than 2 mm in size) - representing the most abundant fraction of the fossil material – that were identified at species level. The material is stored at the Palaeoecology Laboratory of Calabria University.

5.2.1 Biogeographical analysis and thermal constraints

The modern biogeographical distribution of the here-identified fossil species out of the Mediterranean Sea was collected (see Appendix II) from malacological literature (Parenzan, 1974; Tebble, 1976; Sabelli, 1980; Eisenberg, 1983; Graham, 1988; Wye, 1991; Dance, 1992; Ardovini and Cossignani, 2004; Gofas *et al.*, 2011), checklists (Rosewater, 1975; Høsæter, 1986; Hannson, 1998; Palerud *et al.*, 2004; HELCOM, 2012; Cordeiro *et al.*, 2015), websites (Oliver *et al.*, 2016), and scientific papers (Lemche, 1948; Ghisotti, 1968; Ghisoti and Melone, 1975; Piani, 1984; Voskuil and

Onverwagt, 1989; Oliver and Cosel, 1992; Kellner, 2003; Borghi and Vecchi, 2005; Cosel, 2006a,b; Rueda *et al.*, 2009; Lopes, 2010; Michel *et al.*, 2011; Marina *et al.*, 2012; Brunetti and Vecchi, 2011; 2014; Dell'Angelo *et al.*, 2017; Delongueville *et al.*, 2019; Dominici *et al.*, 2020; Delongueville *et al.*, 2021; Russo, 2021).

As a reference, the following biogeographical provinces were considered (simplified after Hall, 1964, and Raffi *et al.*, 1985): 1) Cool temperate Boreal-Celtic Province; 2) Warm temperate/subtropical Lusitanian Province (including the Mediterranean Sea); 3) Tropical Mauretanic-Senegalese Province. On this basis, three biogeographical and/or climatic groups were adopted in order to define the climatic affinity of the whole assemblage examined: a) warm or southern affinity species group (W) (i.e. taxa living in the warm temperate/subtropical Lusitanian Province and/or in the tropical Mauretanic-Senegalese Province); b) cold or northern affinity species group (C) (i.e. taxa diffused in the warm temperate/subtropical Lusitanian Province and in the cool temperate Boreal-Celtic Province); c) group of species lacking a warm or cold affinity with respect to the present day Mediterranean (N) (i.e. characterized by cosmopolitan taxa distributed in the warm and cold Atlantic waters, and by Lusitanian/Mediterranean taxa indicative of the present day Mediterranean SST).

In addition, the climatic character of the molluscan assemblage was also defined by checking the preferred SST ranges of each species on the OBIS database (OBIS, 2023); the database provides 5 °C-wide SST ranges where each species was observed. For each species, a "1" was attributed to each SST interval in which the presence of that species was indicated. Subsequently, the occurrences of all species along the SST intervals were summed together, obtaining a histogram showing the recurrence of the various SST intervals. The most recurring SST intervals are assumed to be indicative of the SST setting during MIS 5e.

Moreover, the present-day SSTs of the studied area (MP; GT, derived from Shaltout and Omstedt, 2014) were compared to the well-known thermal constraints of the "Senegalese" gastropod *Thetystrombus latus* (Gmelin, 1791) (= *Strombus bubonius* Lamarck, 1822) (Meco *et al.*, 2002; Meco, 2008; Garilli, 2011; Harzhauser and Kronenberg, 2013; Ávila *et al.*, 2015, 2016; Chakroun and Zaghbib-Turki, 2017), to define the minimal SST increase with respect to today, with a pure actualistic point of view.

5.2.2 Geochemical analysis

The ultrastructure of selected fossils (*Cladocora caespitosa, Pinna nobilis, Spondylus gaederopus,* and *Thetystrombus latus*) was investigated to discard the presence of diagenetic alterations through standard petrographic analyses on thin sections, stereo microscopy, and Scanning Electron Microscope. In addition, the original biominerals composition was checked by X-Ray Diffraction (XRD) analysis, which was made through a Philips PW1730 diffractometer.

The Sr, Mg and Ca content of an antero-umbonal fragment of a *P. nobilis* shell (PN13 from sample T13) and fossil specimens of *C. caespitosa* (corallites CL5 from sample T5, CL13 from sample T13, Cl17 and CL17_alt from sample T17) were analysed using a JEOL JXA-8230 electron probe micro-analyser (EPMA) with wavelength-dispersive spectrometers (WDS) at the Calabria University laboratory. The analysis was performed on polished and cleaned surfaces along the growth direction

of the skeletons with a constant sampling step varying from 100 to 250 µm. The measurements were performed using mineral standards (Calcite for Ca, Diopside for Mg, and Celestite for Sr; SPI Supplies, 02757-AB 59 Metals and Minerals Standard, Serial 4SK) and the instrumental precision better than 0.001 %. In particular, the Sr/Ca and Mg/Ca ratios in calcitic and aragonitic carbonate of the studied samples were used to estimate the SST during the carbonate precipitation. These ratios are commonly used in the existing literature (Freitas *et al.*, 2005; Silenzi *et al.*, 2005; Montagna *et al.*, 2007) but they are commonly derived from Inductively Coupled Plasma Mass Spectrometry (ICP-MS) that has a major precision in measuring the concentration of elements (up to ppb). However, we decided to use EPMA (as Ragazzola *et al.*, 2020), because: 1) EPMA allows a much higher resolution in the measurement points, with respect to ICPMS-LA, as the probed mineral volume is submicrometric; 2) the ICPMS-LA precision up to ppb, results superfluous in our case, because minimal trace element relative abundance is near 1 %.

The $\delta^{18}O$ and $\delta^{13}C$ determinations were performed at the DiSTeM of the University of Palermo on selected fragments of *Thetystrombus latus* from T13 (TL), *Spondylus gaederopus* from T5 (SG), *Venus verrucosa* from T13 (VV), *Pinna nobilis* from T5 (PN), *Cladocora caespitosa* from T17 (CC), since all these species have been already used for SST palaeotemperature estimations in the Quaternary (Cornu *et al.*, 1993; Kennedy *et al.*, 2001; Maier and Titschack, 2010; Royle *et al.*, 2015a; Uvanović *et al.*, 2021).

The selected fossils were sectioned, ultrasonically cleaned and micro-drilled. The methods were repeated to obtain 3 to 9 powder samples from each fossil (8–10 mg), except for CC that was micro-drilled on the cleaned external surface to avoid internal detrital filling. These powder samples were then dissolved in 100 % HCl for 12 h at 25 °C and analysed through a Thermo Scientific Delta V Advantage continuous flow isotope ratio mass spectrometer. Results are expressed in delta notation (δ) relative to the Vienna Pee Dee Belemnite (V-PDB). Precision of the oxygen and carbon isotope ratios for duplicates was better than 0.1 ‰.

5.3 RESULTS

The studied samples returned a rich molluscan fauna (Appendix I), i.e., 5174 individuals belonging to 120 molluscan species (mainly gastropods and bivalves, plus a few scaphopods), including four species of the warm water Senegalese fauna: *Thetystrombus latus* (Gmelin, 1791), *Conus ermineus* Born, 1778, *Hyotissa hyotis* (Linnaeus, 1758), and *Cardita rufescens* Lamarck, 1819 (see *Chapter 4,* **Fig. 4**). Except for the four Senegalese species found, all the other identified species are still present in the Mediterranean biota.

Figure 1 (next page). (A) Geographical distribution of the east Atlantic provinces surrounding the Mediterranean with indication of the areas of distribution of warm-affinity (orange circle) vs cold-affinity (blue circle) species, as considered in this paper; **(B)** Species (%) grouped by their climatic affinity: warm (W), cool (C) or without climatic meaning respect to the Mediterranean modern climate (N); **(C)** Incidence (%) of the SST intervals, resulting from the overlapping of typical SST optimal ranges of each species in the whole fossil assemblage. The polynomial 4° trend line, showing the SST trend, is reported (R^2 = 0.99). >

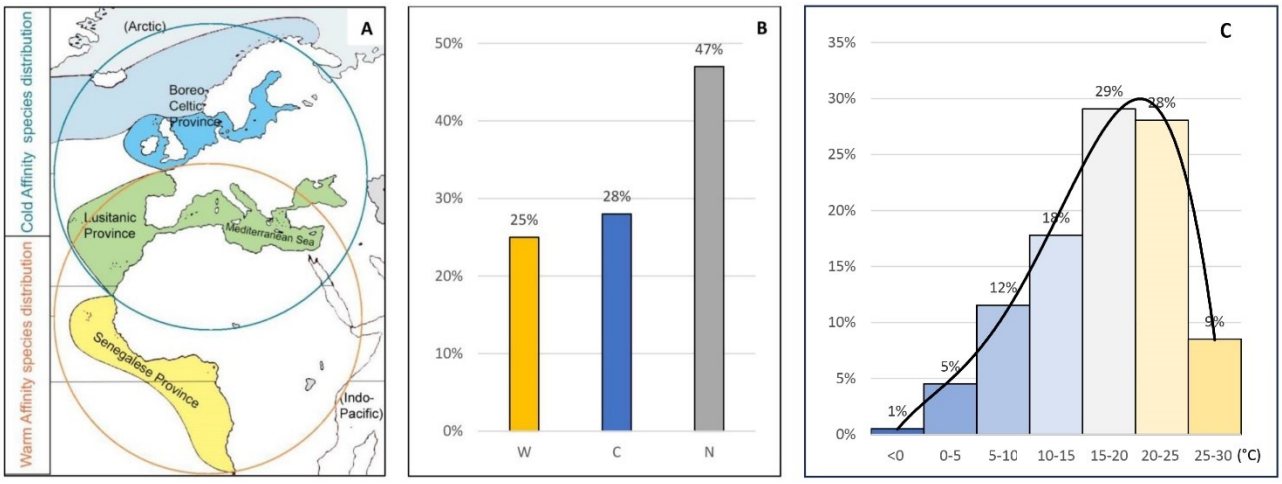

5.3.1 Biogeographical analysis and thermal constraints

The biogeographical analysis revealed a substantial evenness between the percentages of species with warm affinity (W) and cold affinity (C), accounting for 25 % and 28 %, respectively. The remaining percentage (47 %) is represented by species lacking a warm or cold affinity with respect to concerning the Mediterranean (N) (**Fig. 1A, B**). Regarding the preferred SST ranges of each species, checked on OBIS (2023), the representativeness of each range results in a unimodal asymmetrical distribution with the most recurring range of 15-20 °C (29 %), closely followed by the 20-25 °C (28 %). A small percentage (9 %) deals with ranges indicating higher SST (25-30 °C), while those indicating cooler SSTs (< 15 °C) are progressively less represented (17 % to 1 % decreasing the SST) but span over a wide SST range (-5 – 15 °C) (**Fig.1C**).

5.3.2 Geochemical analysis

XRD and microscopy analyses showed an overall good preservation of the selected fossils (**Fig. 2; Fig. 3**). For *C. caespitosa,* the CC sample, selected for isotopic analysis, is aragonitic, as just minor calcite peaks were found, possibly deriving from external or internal debris (**Fig. 2A**). Further samples were observed in thin section, showing the pristine aragonitic spherulitic structure, only locally partially dissolved (**Fig. 3A**), and through SEM during Sr/Ca analysis (samples CL), which shown the absence of neomorphic recrystallizations (**Fig. 3B**).

For *P. nobilis,* sample PN from sample T5, selected for isotopic analysis, resulted almost entirely pristine aragonitic (**Fig. 2B**). A second sample, PN13, selected for Mg/Ca analysis and sampled in the calcitic layer, showed no recrystallization evidence at SEM (**Fig. 3C**).

T. latus (TL) and *S. gaederopus* (SG) shown a dominant aragonitic composition, but also associated calcite presence (**Fig. 2C, D**) This is not necessarily a symptom of diagenesis as minor calcite quantities are naturally associated with the aragonite of *T. latus* (De Torres *et al.*, 2010), and the shell of *S. gaederopus* is bimineralic (Maier and Titschack, 2010), so some calcite may have been intercepted during sampling of the aragonitic layer. This is likely as the selected SG sample still retain its original reddish coloration, clearly pointing toward a good preservation. It is worth nothing, anyway, that during powder sampling, to avoid sampling different layers or external contaminants,

the fossils were sectioned in order to sample fresh surfaces. The same applies to *V. verrucosa* (VV), for which no further analyses are available.

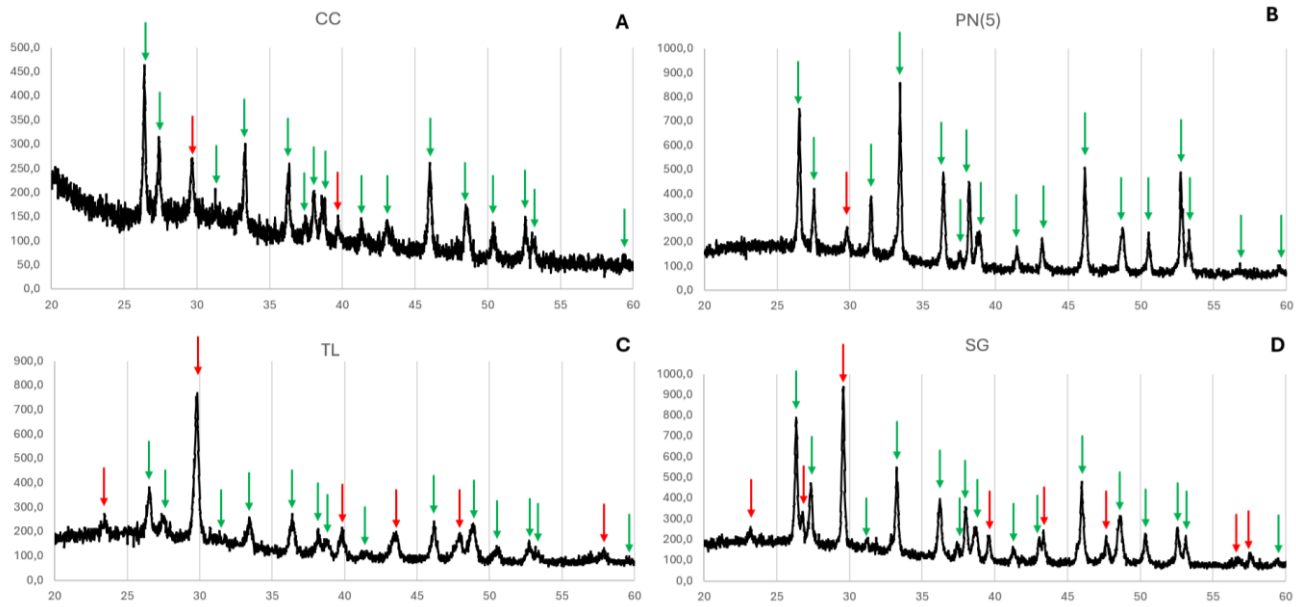

Figure 2. XRD spectra of CC **(A)**, PN **(B)**, TL **(C)** and SG **(D)** with major peaks of pristine aragonite (green arrows) and subordinate secondary or external calcite (red arrows).

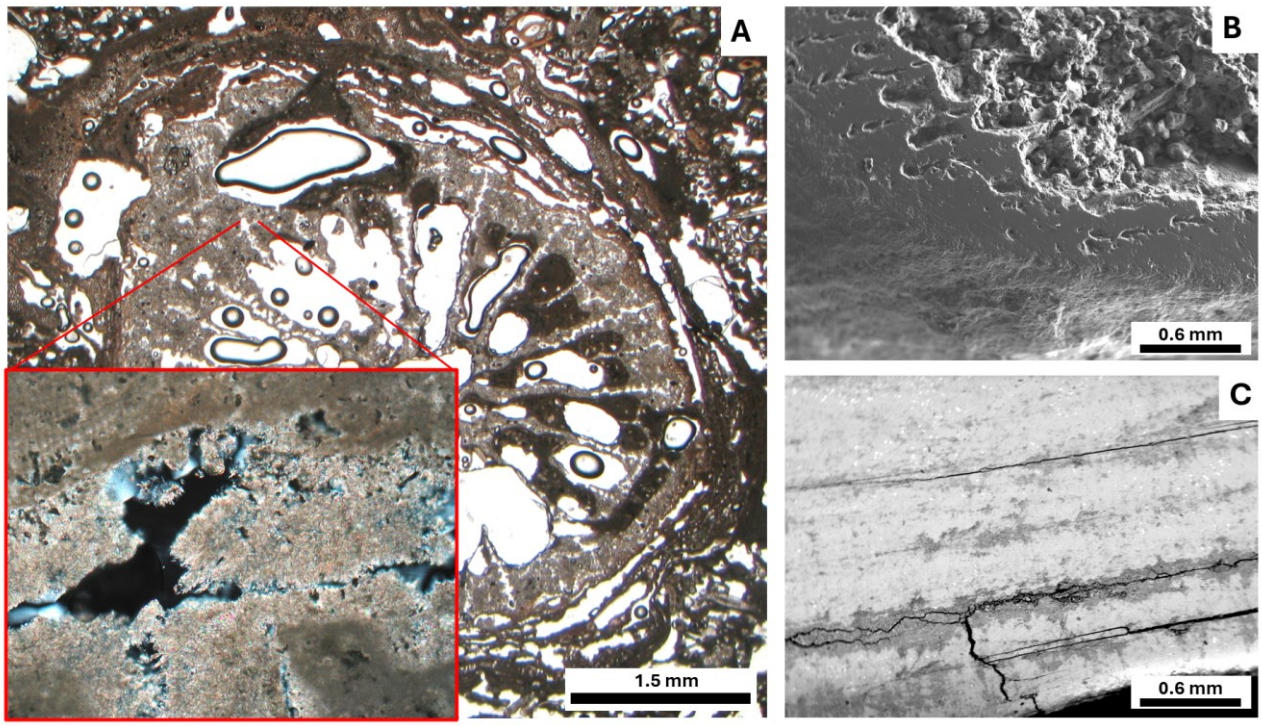

Fig. 3. (A) Thin section of *Cladocora caespitosa* from site T17 showing pristine aragonitic skeletal structure, only locally dissolved (red square); **(B)** SEM view of another corallite from same site, with unaltered surfaces; **(C)** SEM view of *Pinna nobilis* sample (PN13).

The Mg/Ca ratio of the calcitic shell of *P. nobilis* (PN13) revealed a relatively high range of variation comprised between 7.5 to 77.1 mmol mol^{-1}, with an average value of 34.5 ± 18 mmol mol^{-1}. Considering the equation of Freitas *et al.* (2005) based on measures of modern shells of *P. nobilis*, a

mean SST of 21.6 ± 18.4 °C can be estimated for the MIS 5e sample. Obviously, the large variation range of the Mg/Ca values implies a very high standard deviation of SST values, suggesting caution in the use of this result (see discussion).

The Sr/Ca values in the aragonitic skeleton of *C. caespitosa* corallites show a range of values spanning from 4.27 to 16.08 mmol mol^{-1}, with a mean value of 9.58 ± 1.02 mmol mol^{-1} (**Tab. 1**). According to the equations for SST estimation published by Silenzi *et al.* (2005) (*Sr/Ca (mmol/mol) = 11.25 – 0.079*SST (°C)*) and Montagna *et al.* (2007) (*Sr/Ca (mmol/mol) = 10.50 – 0.073*SST (°C)*), calibrated on modern and Pleistocene *C. caespitosa* corallites, the resultant mean SST turns out respectively 21.1 ± 13.0 °C and 12.6 ± 14.0 °C (**Tab. 1**); again, a consistent standard deviation characterizes the results.

Sample	Sr/Ca (mmol mol^{-1})	Mean SST (°C) (Silenzi *et al.*, 2005)	Mean SST (°C) (Montagna *et al.*, 2007)
CL5	9.37 ± 0.56	23.8 ± 7.1	15.5 ± 7.7
CL13	10.08 ± 0.85	14.8 ± 10.7	5.8 ± 11.6
CL17	9.28 ± 1.46	25.0 ± 18.4	16.8 ± 20.0
CL17_alt	9.60 ± 0.87	20.9 ± 11.0	12.4 ± 11.9
MEAN ± S.D.	***9.58 ± 1.02***	***21.1 ± 13.0***	***12.6 ± 14.0***

Table 1. Mean of SST values obtained from the Sr/Ca ratio; S.D.: standard deviation.

Sample	GR (mm yr^{-1})	SST (°C) (Peirano *et al.*, 2009)	SST (°C) (Kružić *et al.*, 2012)
CL5	2.2	14.4 / 21.6	11.6
CL13	4.2	18.0	19.5
CL17	3.8	16.6 / 19.5	17.9
CL17_alt	3.8	16.6 / 19.5	17.9
MEAN ± S.D.	***3.5 ± 0.9***	***16.4 ± 1.5 / 19.6 ± 1.5***	***16.7 ± 3.5***

Table 2. Estimated mean growth rate (GR) and relative SST values of the *C. caespitosa* corallites. S.D.: standard deviation.

Plotting the same Sr/Ca values, which were taken with a regular step along the growth direction of the *C. caespitosa* corallite, against the length of the corallite itself, a curve with alternating negative and positive peaks is derived (**Fig. 4**). These latter can be related to the seasonal SST variations: winters = maximum Sr/Ca values while summers = minimum Sr/Ca values (Royle *et al.*, 2015b). With the aim to better show the background seasonal signal, the Sr/Ca curves were smoothed using moving averages (from the third to fifth period depending on the sample) (**Fig. 4**). Measuring the distance between the lowest Sr/Ca peaks (corresponding to the summer periods) along the growth direction of the corallite, mean annual growth rate (GR, in mm/year) of four corallite was estimated. The growth rate was obtained as average of the distance of consecutive

summer peaks, corresponding to an annual growth (also observed on the external wall of the corallites as thinner/thicker bands). Summer peaks were chosen since they provide a clearer seasonal signal than the winter ones. The mean growth rate estimations of the four corallites returned the values of 2.2 mm yr^{-1} (CL5), 3.8 mm yr^{-1} (CL17, CL17_alt), and 4.2 mm yr^{-1} (CL13), with a general mean value of 3.5 ± 0.9 mm yr^{-1} (**Tab. 2**). These values are all reliable since they are included in the modern *C. caespitosa* growth rate range of 1.36 - 5.2 mm yr^{-1} (Royle *et al.*, 2015b, and ref. therein).

The obtained mean growth rate values were then used for SST estimation using the equations proposed by Peirano *et al.* (2009) and Kružić *et al.* (2012). The first equation (Peirano *et al.*, 2009: *GR (mm/y) = -0.1491*SST^2 (°C) + 5.3681*SST (°C) - 44.21*) is a quadratic relationship, and thus returned two SST estimations for each growth rate value: the value of 2.2 mm yr^{-1} returns 14.4 or 21.6 °C (CL5); the value of 3.8 mm yr^{-1} returns 16.6 or 19.5 °C (CL17, CL17_alt); the value of 4.2 mm yr^{-1} (CL13), instead, returns a single SST estimation of about 18 °C, representing the optimal growth SST according to this relationship. Using these values, two mean SST values are calculated on the base of the lowermost and uppermost SST values giving 16.4 ± 1.5 and 19.6 ± 1.5 °C, respectively (**Tab. 2**). Finally, the linear equation of Kružić *et al.* (2012) *(GR (mm/y) = -0.6987 + 0.25976*SST (°C))* returned a mean SST estimation of 16.7 ± 3.5 °C (**Tab. 2**).

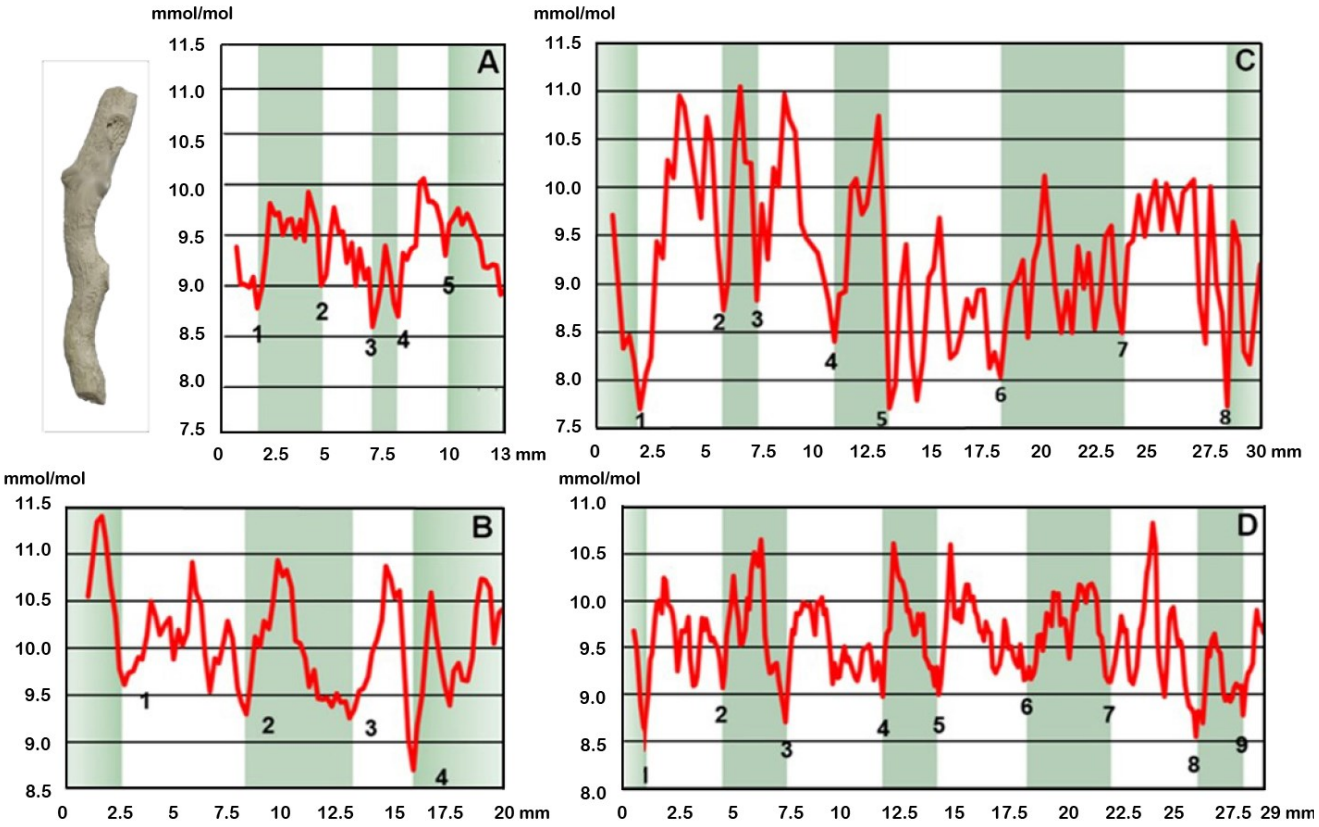

Figure 4. Sr/Ca (mmol mol-1) profiles along the growth direction of *C. caespitosa* corallites with minimum (=summer) peaks identified (progressive numbers). Inferred annual growth bands evidenced with alternate colours. **(A)** CL5 (sampling step of 200 µm, 3rd period moving averages curve); **(B)** CL13 (sampling step of 200 µm, 4th period moving averages curve); **(C)** CL17 (sampling step of 250 µm, 3rd period moving averages curve); **(D)** CL17_alt (sampling step of 100 µm, 5th period moving averages curve).

PN13 sample also showed a similar variations of Mg/Ca values, which were not included in this work as no equations linking growth rate and SST, like for *C. caespitosa,* were found.

The variability of the $\delta^{18}O$ and $\delta^{13}C$ values of each fossil species (**Fig. 5**; **Tab. 3**) is very similar to the range reported for recent to modern samples of the same species (Cornu *et al.*, 1993; Kennedy *et al.*, 2001; Silenzi *et al.*, 2005; De Torres *et al.*, 2010; Freitas *et al.*, 2005; Maier and Titschack, 2010; Bajnóczi et al., 2014; Royle *et al.*, 2015a; Zanchetta *et al.*, 2019; Uvanović *et al.*, 2021; Peharda *et al.*, 2022; Prada et al., 2019), as expected from the good preservation of the analysed fossils.

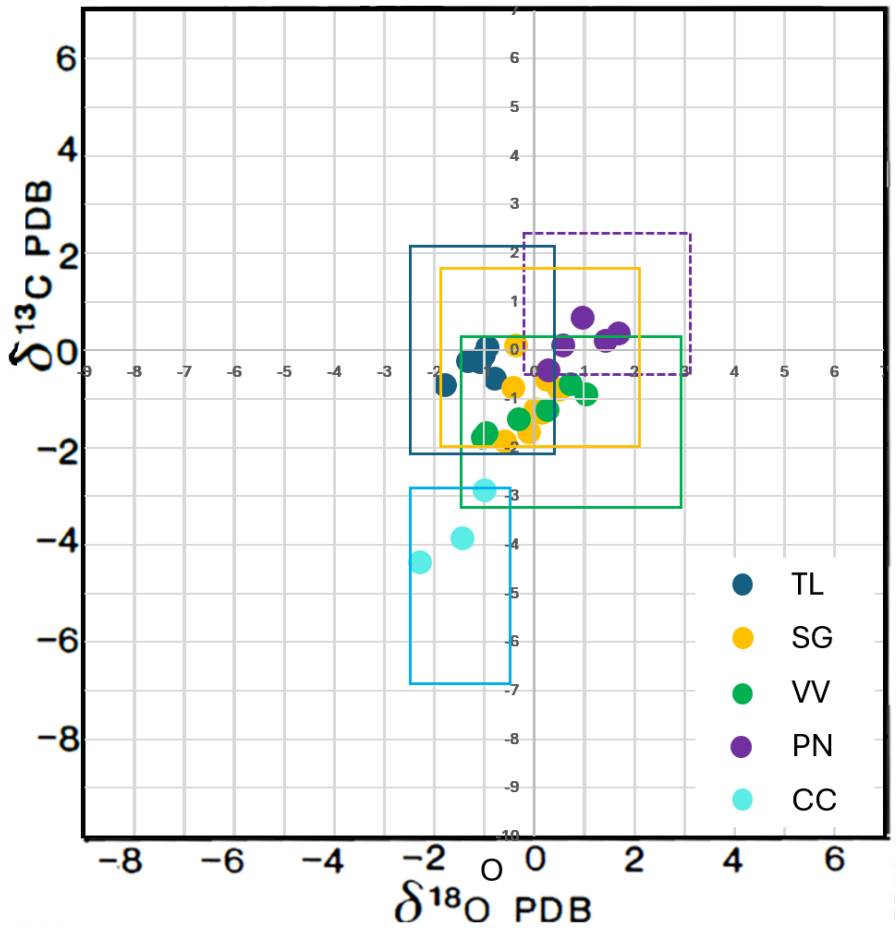

Figure 5. Cross plot showing the $\delta_{13}C$ and $\delta_{18}O$ values of the analysed fossils: TL (*Thetystrombus latus*); SG (*Spondylus gaederopus*); VV (*Venus verrucosa*); PN (*Pinna nobilis*); CC (*Cladocora caespitosa*). The rectangles indicate the variability of the isotopic composition reported for recent samples of aragonitic samples, with the exception of PN, whose values are referred to calcite samples (see text for references).

As all the molluscan sampled shells are aragonitic, the Grossman and Ku (1986) equation (in the corrected form reported in Wierzbowski, 2021: $T(°C) = 20.6 - 4.34*(\delta^{18}O_{aragonite} - \delta^{18}O_{water} + 0.2)$, was used to obtain an estimation of SST. Instead, for *C. caespitosa*, a specific equation was used from Royle *et al.* (2015a) $(SST\ (°C) = 20.60 - 4.34*(\delta^{18}O_{aragonite} + 3.5 - (\delta^{18}O_{water} - 0.20)$. Since both equations require a value of the oxygen isotopic composition of the coeval sea water ($\delta^{18}O_w$, expressed in V-SMOW), three possible scenarios have been considered (see below): 1) $\delta^{18}O_w$ analogous to the modern MP; 2) $\delta^{18}O_w$ equal to the modern GT; 3) a depleted $\delta^{18}O_w$ with respect to the modern central Mediterranean value, related to different hydrological conditions of MIS 5e

(Thunell and Williams, 1989). Moreover, the present day $\delta^{18}O_w$ values are closely related to SSS following an equation valid for the Mediterranean Sea (Pierre, 1999).

For the scenario 1, a $\delta^{18}O_w$ = 0.9 ‰ value was used, obtained from the SSS of 36.3 psu for the MP. This value is lower than the adjacent GT, where the SSS reaches a mean value of 38 psu, due to the freshwater karstic inputs (Cardellicchio *et al.*, 2015) (see *Chapter 4*, **Fig. 1**). However, it must be considered that during the MIS 5e the MP was not a semi-closed lagoon like the basin as today (see Dai Pra and Stearns, 1977; Valenzano *et al.*, 2018), and thus the freshwater effect on the seawater composition was probably limited or even absent.

For the scenario 2 it is considered the mean SSS of 38 psu based on the modern open sea of the GT, which led to $\delta^{18}O_w$ = 1.36 ‰ (Alabiso *et al.*, 2005; Di Leo *et al.*, 2014; Cardellicchio *et al.*, 2015). For

Sample	$\delta^{13}C$ (‰)	$\delta^{18}O$ (‰)	Scenario 1 (°C)	Scenario 2 (°C)	Scenario 3 (°C)
TL1	0.07	*-0.95*	27.8	29.8	25.4
TL2	-0.24	*-1.10*	28.4	30.4	26.1
TL3	-0.22	*-1.34*	29.5	31.5	27.1
TL4	-0.12	*-1.02*	28.1	30.0	25.7
TL5	-0.71	*-1.81*	31.5	33.5	29.1
TL6	-0.57	*-0.80*	27.1	29.1	24.8
TL mean ± S.D.	*-0.30 ± 0.29*	*-1.17 ± 0.36*	*28.7 ± 1.6*	*30.7 ± 1.6*	*26.4 ± 1.6*
SG1	-0.77	*-0.42*	25.5	27.5	23.1
SG2	-0.60	*0.23*	22.6	24.6	20.3
SG3	-1.88	*-0.59*	26.2	28.2	23.9
SG4	0.10	*-0.37*	25.2	27.2	22.9
SG5	-1.68	*-0.12*	24.2	26.2	21.8
SG6	-0.80	*0.50*	21.5	23.5	19.1
SG7	-1.29	*0.14*	23.0	25.0	20.7
SG8	-1.20	*0.02*	23.6	25.6	21.2
SG mean ± S.D.	*-1.02 ± 0.64*	*-0.08 ± 0.37*	*24.0 ± 1.6*	*26.0 ± 1.6*	*21.6 ± 1.6*
VV1	-1.24	*0.26*	22.5	24.5	20.2
VV2	-1.71	*-0.95*	27.7	29.7	25.4
VV3	-0.69	*0.73*	20.5	22.5	18.1
VV4	-0.91	*1.05*	19.1	21.1	16.7
VV5	-1.80	*-1.02*	28.1	30.1	25.7
VV6	-1.42	*-0.30*	24.9	26.9	22.6
VV mean ± S.D.	*-1.30 ± 0.44*	*-0.04 ± 0.86*	*23.8 ± 3.7*	*25.8 ± 3.7*	*21.5 ± 3.7*
PN1	0.20	*1.43*	17.4	19.4	15.1
PN2	0.35	*1.70*	16.3	18.3	13.9
PN3	0.67	*0.98*	19.4	21.4	17.1
PN4	-0.42	*0.29*	22.4	24.4	20.0
PN5	0.10	*0.59*	21.1	23.1	18.7
PN mean ± S.D.	*0.18 ± 0.40*	*1.00 ± 0.58*	*19.3 ± 2.5*	*21.3 ± 2.5*	*17.0 ± 2.5*
CC1	-3.9	*-1.44*	16.4	18.4	14.0
CC2	-2.88	*-1.00*	14.4	16.5	12.1
CC3	-4.35	*-2.30*	20.2	22.2	17.8
CC mean ± S.D.	*-3.70 ± 0.75*	*-1.58 ± 0.58*	*17.0 ± 2.9*	*19.0 ± 2.9*	*14.6 ± 2.9*
MEAN ± S.D.	**-1.00 ± 1.19**	**-0.27 ± 0.98**	**23.4 ± 4.4**	**25.4 ± 4.4**	**21.0 ± 4.4**

Table 3. Isotopic and related SST data. TL (*Thetystrombus latus*); SG (*Spondylus gaederopus*); VV (*Venus verrucosa*); PN (*Pinna nobilis*); CC (*Cladocora caespitosa*). Mean results and standard deviation (S.D.) as variability index. Mean values for each sampled fossils in italics; mean value based on all data in bold.

the assessment of the depleted scenario 3, we used the determined $\delta^{18}O_w$ values of the sapropel level called "S1", dated at 8,000 years, which can be assumed as representative also of the MIS 5e (125,000 years) (Cornu *et al.*, 1993). More specifically, Thunell and Williams (1989) provided two averaged $\delta^{18}O_w$ depletion values with respect to the modern values, one for the Western Mediterranean (-0.8 ‰) and another for the Eastern Mediterranean (-1.2 ‰). Being the GT located in the Central Mediterranean, in our work we adopted a mean depletion value of -1 ‰, obtained by averaging the two previous mean values, and applied only to the $\delta^{18}O_w$ of the Scenario 2 since the present-day MP (scenario 1), due to the considerable freshwater input, which is not a good analogue of the MIS 5e palaeoenvironment. The depleted value resulted in a $\delta^{18}O_w$ value of 0.36 ‰ which defined the Scenario 3. Using these values in the palaeotemperature equations, three mean average SST values were obtained: 1) 23.4 ± 4.4 °C (Scenario 1); 2) 25.4 ± 4.4 °C (Scenario 2); 3) 21.0 ± 4.4 °C (Scenario 3). Complete $\delta^{13}C$, $\delta^{18}O$, and SST results with relative standard deviation as variability index, are listed in **Table 3**.

5.4 DISCUSSION

5.4.1 Biogeographical analysis and ecological proxies

The palaeoclimatic analysis based on biogeographic data of species, shows a similar percentage of warm and cold affinity species during the MIS 5e in the studied area (25 % and 28 % respectively) (**Fig. 1A, B**). The warm affinity species percentage is more than twice as many as the mean Mediterranean value of 11.6 % at today (Gliozzi, 1987, and ref. therein). Consequently, considering the present-day amount of warm affinity species as related to the SST, the studied fossil assemblage could indicate a warmer than today's SST setting with an annual variability of maxima and minimal temperature still tolerated by the few species of tropical fauna (see below for further details). Moreover, the lack of a dominance of the warm affinity species to the cold ones, implies that the MIS 5e SST, in the studied area, did not reach the typical values of a strictly tropical climate as proposed by several Authors (e.g., Cita, 2008; Amorosi *et al.*, 2014) because the simple presence of the Senegalese Fauna.

A possible alternative explanation of these apparently contrasting data (lack of dominance of warm-water affinity fauna vs presence of tropical species) could be found in local factors. For example, Peirano *et al.* (2009) estimated a relatively low annual SST (a mean of 17.6 °C) studying the growth pattern of a *C. caespitosa* bank in the MIS 5e deposits of S.ta Teresiola (see *Chapter 4,* **Figs. 1, 3**). Such a low annual SST was explained with cooler freshwater inputs form the "Citri" karstic springs in a lagoonal-like setting. These springs are today suspected to influence both salinity and SST of the MP (Cardellicchio *et al.*, 2015). However, albeit it is a realistic scenario, modern data shows no strong SST difference between the MP and the neighbouring GT (Alabiso *et al.*, 2005), as the temperature of the freshwater (constantly around 18 °C) is similar to the mean annual SST of the MP (18 °C).

For a further SST characterization, the preferred SST of the fossil assemblage was compared to the modern SSTs of the study area. Present day mean annual SST in the MP is 18 °C, with mean SSTs of about 12 °C and 24 °C in winter and summer respectively. The facing open sea setting, as the GT, experiences today slightly warmer SSTs, i.e., a mean annual SST of about 18.8 °C, ranging from about

14 °C to 25 °C in winter and summer respectively (data derived from 1982-2012 averaged values, reported by Shaltout and Omstedt, 2014). The preferred SST range indicated by the whole fossil fauna shows a high representativeness (i.e., 57 % together) of the 15-25 °C interval (**Fig. 1C**). Considering the near-equal percentages of the 15-20 and 20-25 °C ranges, a mean SST of roughly 20 °C can be supposed. Moreover, assuming that the extreme values 15 °C and 25 °C are representative of winter and summer mean SSTs, a seasonal variability of 10 °C can be inferred, which is similar to the today seasonality of about 11 °C (Shaltout and Omstedt 2014). Anyway, the wide array of cooler SSTs ranges (< 15 °C), due to the good percentage of species living also in cooler waters, can confirm a not extreme warmth. These results agree with those obtained by the comparison of warm and cold affinity species. The warm affinity species, about double than today, are probably related to warmer SSTs, but the equal presence of cold affinity species points to reconsider the idea of a strictly tropical warm climate.

The thermal vital constraints of the Senegalese *Thetystrombus latus* can be used for an additional SST estimation. This species nowadays needs the following SST conditions:

1) although its optimal climatic preference is the area of Cape Verde that has an average annual SST of 23.5 °C (Bardaji *et al.*, 2009; Garilli, 2011), it was also reported in cooler areas of the tropical West Africa with a mean annual SST of 21.5 °C (Meco *et al.*, 2002, 2008; Harzhauser and Kronenberg, 2013; Ávila *et al.*, 2016);
2) a winter mean SST of at least 19 °C (Ávila *et al.*, 2015; Garilli, 2011);
3) not less than 16 °C in average during the coldest month (Harzhauser and Kronenberg, 2013; Chakroun and Zaghbib-Turki, 2017);
4) a period of seven months with SST > 20 °C (Meco *et al.*, 2002; Ávila *et al.*, 2016).

This thermal requirements would imply that during MIS 5e: a) the annual SST mean could have been at least 3.5 °C or 2.7 °C higher than today when compared respectively to the MP (i.e., 18 °C) and to the GT (i.e., 18.8 °C; Shaltout and Omstedt, 2014); b) winter mean SST was at least 7 °C warmer compared to the MP (about 12 °C), or at least 5 °C warmer if compared to the GT (about 14 °C; Shaltout and Omstedt, 2014); c) the coldest month SST mean was, at most 5 °C higher, relative to February mean SST of the MP (i.e., about 11 °C); d) in any case, the presence of *T. latus* indicates that mean SST reached 20 °C for at least seven months, thus indicating longer summers than today, in accordance with Garilli (2011).

5.4.2 Geochemical proxies

Regarding the SST estimations based on the Mg/Ca ratio, the equation of Freitas *et al.* (2005) for P. nobilis returned a reasonable mean SST of 21.6 °C ± 18.4 °C. Still, the large variability of the values in the sampled fossil shell (PN13) leads a wide standard deviation. This latter is responsible for an unrealistic SST variability, making it necessary to take caution with these results. Nonetheless, the use of EPMA highlights possible real and unexpected microscale variations of the skeletal composition not yet known in the literature. If one accepts the as reasonable the mean SST result (21.6 °C), the MIS 5e SST would have been 3.6 °C higher than today in the MP (as the modern mean

is 18° C) or 2.8 °C in the GT (as 18.8 °C is the today mean) (**Table 4**). The 21.6 °C value is also consistent with the minimal annual SST required by *T. latus* (i.e., 21.5 °C; Meco *et al.*, 2002).

The mean SST estimated from the Sr/Ca values on *C. caespitosa* skeletons are different depending on the used equation: 21.1 ± 13.0 °C and 12.6 ± 14.0 °C from the equation of Silenzi *et al.* (2005) and Montagna *et al.* (2007) respectively. Again, in both cases, a very large standard deviation results were obtained, which led to unrealistic SST estimations. The mean result returned by the Montagna *et al.* (2007) equation (12.6 °C) is even cooler than the lowest monthly SST tolerated by *T. latus* (i.e., 16 °C; Harzhauser and Kronenberg, 2013; Chakroun and Zaghbib-Turki, 2017), while the one returned by the Silenzi *et al.* (2005) equation (21.1 °C) is just slightly cooler than the minimal annual mean SST tolerated by this species (i.e., 21.5 °C; Meco *et al.*, 2002), and thus more reliable. This value (21.1 °C) leads to + 3.1 °C than the modern mean SST of the MP, or +2.3 °C with respect to the GT mean SST (Table 4). The biases affecting the use of the *C. caespitosa* skeletal Sr/Ca ratio as palaeothermometer were already highlighted by Royle *et al.* (2015b), who demonstrated a strong colony-specific variability of the Sr/Ca versus temperature relationships, making this proxy inaccurate for absolute SST determinations.

As seen, the Sr/Ca pattern-derived growth-rate (GR) of the analysed *C. caespitosa* corallites (**Fig. 4**) can further be used for SST estimations, but it must be firstly considered that modern *C. caespitosa* calcifies in an SST range spanning from about 14/15 °C to 24 °C (Montagna *et al.*, 2007; Royle *et al.*, 2015a, and ref. therein). For this reason, we here consider more likely the mean SST estimation obtained with the equation of Peirano *et al.* (2009), because all the obtained SST values (from 14.4 to 21.6 °C) fall completely into this range; on the contrary, the values returned by the equation of Kružić *et al.* (2012) (i.e., from 11.6 to 19.5 °C) are not all reasonable in this context. Moreover, the equation of Peirano *et al.* (2009), being quadratic, returned two SST values for each growth rate value (Table 2) thus, considering a warmer MIS 5e than today, which we assume as more likely SST estimations pointing towards warmer conditions with respect to the present SST means (i.e. MP, 18 °C and GT, 18.8 °C): 18 °C (CL13), 19.5 °C (CL17, CL17_alt), and 21.6 °C (CL5). It must be noted that only the CL5 corallite gave an SST value of 21.6 °C, in accordance with the minimal annual SST required by *T. latus* (i.e., 21.5 °C). Finally, a general mean SST of 19.6 ± 1.5 (Tables 2-4) can be proposed, which is 1.6 °C higher than that of today's MP, or 0.8 °C than GT (Table 4). However, an inferred increase of temperatures is not enough to support the presence of *T. latus*. For the estimations of the mean SST using the oxygen stable isotope data, three $\delta^{18}O_w$ scenarios were adopted based on different mean SSS values. Although different from each other, all three scenarios provide realistic mean SSTs even if only scenario 3 is reasonably considered for the study area (Table 3): scenario 1 gives a mean SST of 23.4 °C, indicating + 4.6/5.4 °C with respect to modern means of GT and MP, while scenario 2 gives a mean SST of 25.4 °C (+6.6/7.4 °C more than today); scenario 3 gives a mean SST of 21.0° C that means +2.2/3 °C warmer than today. Both scenarios 1 and 2 would indicate a not realistic SST during the MIS 5e in the central Mediterranean being similar, or even slightly higher, than the modern annual mean of Dakar (Senegal) (i.e., 24 °C; Bardají *et al.*, 2009). Conversely, scenario 3 indicating an average of 21 °C, would suggest a moderate warming of a few degrees with respect to today of the MIS 5e SST (Table 4), still acceptable with respect to the minimal annual SST required by *T. latus* (21.5 °C).

Furthermore, in order to confirm this scenario as the most probable, it can be considered that the SSS during the MIS 5e in the central/eastern Mediterranean was considerably lower than today, as indicated by the presence of the Senegalese fauna, which requires 34-36 psu (typical of West African seawater, Bardají *et al.*, 2009; Garilli, 2011; Albano *et al.*, 2024). The equation of Pierre (1999) was used to back-calculate the SSS from the $\delta^{18}O_w$ value of the scenario 3 (0.36 ‰), resulting in a value of 34.3 psu, falling in the range indicated by the Senegalese fauna. All considered, scenario 3 with an SST of 21.0 ± 4.4 °C (**Table 3**), being the cooler among the three calculated scenarios is the most probable, which is also similar to those obtained with other methods (Table 4).

Finally, on average, the most likely mean MIS 5e SST obtained from all the different geochemical proxies converges on a mean value of 20.8 ± 0.9 °C, which would imply + 2.8 ± 0.9 °C with respect to the MP scenario, and + 2.0 ± 0.9 °C with respect to present day's GT scenario that is the most reasonable (**Table 4**).

Method	SST (°C)	MIS 5e SST increment with respect to present day's MP (°C)	MIS 5e SST increment with respect to present day's GT (°C)
Mg/Ca	21.6 ± 18.4	+ 3.6	+ 2.8
Sr/Ca	21.1 ± 13.0	+ 3.1	+ 2.3
GR	19.6 ± 1.5	+ 1.6	+ 0.8
$\delta^{18}O$	21.0 ± 4.4	+ 3.0	+ 2.2
MEAN ± S.D.	***20.8 ± 0.9***	***+ 2.8 ± 0.9***	***+ 2.0 ± 0.9***

Table 4. More likely results obtained from the following methods: Mg/Ca derived SST with the Freitas *et al.* (2005) equation; Sr/Ca derived mean SST with the Silenzi *et al.* (2005) equation; growth rate (GR) derived SST with the Peirano *et al.* (2009) equation; $\delta^{18}O$ mean SST derived, assuming a depleted $\delta^{18}O_w$ of 0.36 ‰ (Scenario 3). Present day MP SST: 18 °C; Present day GT SST: 18.8 °C.

5.4.3 Final remarks

Both the results of the biogeographical analysis and of the preferred SST ranges of fossil species indicate that the fossil assemblage features a warmer climatic affinity than today. In fact, a mean SST of roughly 20 °C can be supposed, albeit with a seasonality of about 10 °C, similar to today. The results of the geochemical proxies converge toward similar results, which indicate 20.8 ± 0.9 °C SST. Lastly, an SST increment in the range of 1.2-2.0 °C, warmer than today, is inferred, with an open sea scenario of the area during the MIS 5e and considering an SST of 18.8 °C like the modern GT. The results are not indicative of strictly warm tropical conditions, for a comparison, the tropical mean annual SST in Dakar (Senegal) is 24 °C (Bardají *et al.*, 2009).

Despite the general interest in the palaeoclimatic reconstructions of the MIS 5e in a global scale, quantitative estimations of the SST in coastal settings of the Mediterranean are quite rare. For example, Cornu *et al.* (1993) estimated for the western Mediterranean an increment of the mean annual SST during the MIS 5e with respect to the modern temperature of about 3 °C, and a seasonal variability of 7 °C to 9 °C. This value is not far from our estimation of a mean value in the range of 1.2-2.0 °C with a seasonality variation of 10 °C.

Area	Core/archive	Method	Mean annual SST in the 127-119 ka period (°C)	Reference
Alboran Sea	ODP-976	A	22	Martrat *et al.*, (2014)
	ODP-977	F	19	Pérez-Folgado *et al.* (2004)
	ODP-977A	A	22	Martrat *et al.* (2004, 2014)
Balearic Sea	OPD Leg 161	F	20	Kandiano *et al.* (2014)
		A	21	Kandiano *et al.* (2014)
Ionian Sea	KS205	A	21	Rohling *et al.* (2002)
	Outcr. deposit	M	*21*	***This work***
Aegean Sea	LC21	A	20	Marino *et al.* (2007)
Levantine Sea	ODP-971A	A	20	Rohling *et al.* (2002)
	SL104	A	21	Obreht *et al.* (2022)
	ODP-967C	A	21	Rohling *et al.* (2002)
Global mean SST			**21 °C**	

Table 5. Mean annual SST during the 127-119 ka period in Mediterranean basins. A: Alkenone SST; F: Foraminifera SST; M: Macrobenthos.

Garilli's (2011) biogeographical data on molluscan fauna, stated for the MIS 5e a mean winter SST of 2-4 °C higher than today in the eastern Mediterranean, and of 4-6 °C in western Sicily sea, with a seasonality variation of 6-7 °C. To compare our estimation with those of Garilli (2011) an average of + 4 °C should be considered, as our study area is located about equidistant from the two studied by the Author. Moreover, assuming a + 4 °C for the mean winter SST with respect to the present-day one, which is about 14 °C in the GT, a mean winter SST of about 18 °C, and an annual average of about 21 °C, is obtained for the MIS 5e in the study area on the basis of Garilli's (2011) data. Our estimation of a winter SST mean in the MIS 5e is about 15 °C, which is not in accordance with Garilli's (2011) value, being 3 °C cooler. Garilli (2011) also estimated a seasonality of 6-7 °C for the MIS 5e, lower than the current one of 11 °C, and again quite different from our estimation of the seasonality of about 10 °C. However, the annual mean SST inferred from Garilli's (2011) data of about 21 °C is closer to our estimation of 20.8 °C. In addition, the mean annual SST estimates are available for the pelagic Mediterranean domain, derived from foraminifera-based statistical methods and alkenone palaeothermometry during the 127-119 ka interval, which is the time interval studied in the present work (Table 5). In this period, in the Alboran Sea, foraminifera returned a mean annual SST of nearly 19 °C (Pérèz-Folgado *et al.*, 2004), while alkenones indicate a higher SST of nearly 22 °C (Martrat *et al.*, 2004, 2014). In the Balearic Sea, winter and summer foraminifera averaged data (Kandiano *et al.*, 2014) indicate winter and summer mean SST of about 16 °C and 24 °C, respectively, leading to an approximate mean annual SST of 20 °C, while alkenone mean annual SST is about 21 °C (Kandiano *et al.*, 2014). For the NW Ionian Sea, average alkenone data indicate a mean annual SST of about 21 °C (Rohling *et al.*, 2002), consistent with the mean annual SST of about 21 °C (i.e., 20.8 °C) derived in the present work for the coastal setting. In the eastern Mediterranean Sea, alkenone SST is about 20 °C in the western Levantine Sea (Rohling *et al.*, 2002). SST is about 20 °C in the southern Aegean Sea, NE of Crete (Marino *et al.*, 2007), and 21 °C in the Levantine Sea, SE of Crete (Obreht *et al.*,

2022). In the eastern Levantine Sea, South of Cyprus, alkenone data indicate a mean SST of about 21 °C for the considered period (Rohling *et al.*, 2002).

In this framework, our result of mean annual SST of around 21 °C perfectly matches the mean results of these proxies (i.e. 21 °C with a range between 19 to 22 °C), even if derived from different archives and proxies (open sea plankton versus coastal benthos). Consequently, excluding low-amplitude intra-interglacial climatic variability (Kandiano *et al.*, 2014; Obreht *et al.*, 2022), it can be affirmed that the mean annual SST was rather homogeneous along the eastern and western Mediterranean during the considered time span (127-119 ka), which correspond to the MIS 5e peak. This value, representing a possible mean SST for the MIS 5e in the Mediterranean Sea, is consistent with a slightly warmer SST with respect to the modern mean Mediterranean SST that is about 20 °C (Shaltout and Omstedt, 2014); confirming that the MIS 5e can be considered a good analogue for the incoming next expected warming of the Mediterranean.

5.5 CONCLUSIONS

The biogeographical-based palaeoclimatic analysis and the preferred SST ranges of the molluscan assemblage indicate a slightly warmer than today's scenario for the MIS 5e, with an annual mean of 20 °C and a seasonal variability of 10 °C, which results in + 1.2 °C with respect to today's GT and + 2.0 °C with respect to today's northern Ionian Sea annual mean.

The geochemical analyses give different ranges of SST values depending on the methods, but all returned close values of the mean SST for the MIS 5e, indicating a possible mean SST of 20.8 ± 0.9 °C, which again suggests a moderate warming of the SST of + 2.8 °C with respect to today's MP and + 2.0 °C higher than today's GT. However, an open sea scenario of the study area is the most likely morphological scenario of the studied area during the MIS 5e, with respect to a semi-closed basin as the modern MP.

The final value of the mean SST during the MIS 5e returned from this multiproxy analysis, is circa 20.4 °C, which is 1.2 - 2.0 °C warmer than today's open seawater of the GT. This is not a firmly warmer tropical-like SST setting as it would be derived from the mere presence of the Senegalese fauna.

In conclusion, the number of assumptions and approximations made for performing any applied method points out that the values of SST obtained with a single proxy-based method may be affected by variable incertitude. This strongly indicates the necessity of a multi-proxy approach to compare the results obtained from each methodology and to define the best SST estimation.

CHAPTER 6 – MICROBIAL MEDIATED HARDENING OF A CENTRAL MEDITERRANEAN UPPER SHELF SEAFLOOR DURING THE MIS 5e; A POSSIBLE POST GLOBAL WARMING SCENARIO?

Abstract. Higher sea level and sea surface temperature than at present are inferred for the Last Interglacial (MIS 5e, 135-116 ky), which can be a good analogue for modelling environment's climate response to global warming in the near future. With the aim of predicting the possible evolution of some central Mediterranean shallow sandy seabed, a MIS 5e biocalcarenite was investigated (Gulf of Taranto, Italy). Limited post-depositional diagenesis affected this deposit, which represents an infralittoral sandy seabed, with local vegetation and relatively high energy conditions. Medium-coarse sand sized bioclasts, with a negligible quantity of siliciclastic, compose the sediment that guests also large shells of autochthonous molluscs. Micritic cements are widespread, often in continuum with the micritized part of the shells, showing various micromorphologies and fabrics: non-isopachous aphanitic and filamentous rims, aphanitic micro-mounds, vacuolar peloidal meniscus, and aphanitic pore-filling matrix. All these cements consist of submicrometric anhedral or nanospheroidal crystals of low-Mg calcite, mixed with a smaller amount of irregular plate-like crystals of saponite. Micritic cements are also rich in mineralized filamentous, tubular, and subspherical bacterial bodies, highlighting the occurrence of an epilithic and endolithic microbial community and forming a biofilm that stabilized the mobile sediment as consequence of the microbial mediated early cement precipitation. This process led to the synsedimentary hardening of some parts the mobile sandy substrate, allowing the settlement of sessile taxa - such as *Spondylus gaederopus*, oysters, serpulids and barnacles, together with endofaunal organisms. Early micritic cementation is common in modern tropical climate, whereas is substantially absent in the modern Mediterranean. Consequently, its presence in the MIS 5e deposits confirms warmer sea water temperature compared to today (estimated at ca +2 °C) and suggests a possible substantial increase of the hardening of mobile substrates in the next future in response to the global warming.

Keywords: *MIS 5e, Last Interglacial; Calcarenite; Micrite; Early cementation; Microbial community.*

6.1 INTRODUCTION

In tropical and sub-tropical marine carbonate depositional systems, primary (synsedimentary or early) cementation is a relatively rapid and initial diagenetic phenomenon, widely documented from very shallow to deep-water settings (Purdy, 1963; Fabricius, 1977; Moore, 1977; Chafetz, 1986; Whittle *et al.*, 1993; Morad, 1998; Folk and Lynch, 2001; Hillgärtner *et al.*, 2001; Flügel, 2004; Van der Kooij *et al.*, 2010; O'Reilly *et al.*, 2017; Diaz and Eberli, 2022). Reefs and other relatively hard substrates are preferential formation sites of early marine cements, which significantly contribute to the further hardening of the buildups' framework, and the seabed in general (Westphal *et al.*, 2010; Riding, 2011; Seard *et al.*, 2011; Perri *et al.*, 2024a). However, lithification due to synsedimentary cementation can take place even in mobile seabed of moderate to low-energy areas

(e.g. ooid/bioclastic shoals) where sand-sized particles are typically merged together (e.g. grapestone belts) (Bathurst, 1974; Flügel, 2004; Diaz and Eberli, 2022).

Mineralogy of modern early carbonate cements varies from high-Mg calcite to aragonite, while the fabric is often characterized by isopachous rims, botryoidal structures in phreatic contexts, and meniscus or microstalactitic in vadose zones (Scholle and Ulmer-Scholle, 2003).

The precipitation of primary cements is largely considered a process due to oversaturated water conditions in respect to Ca-carbonate as consequence of evaporation, loss of CO_2, or ions supply. However, it is also well assessed that biological processes, linked to the presence of living microbial communities, can play a crucial role in mediating the precipitation of primary cement, similarly to other microbial carbonates (Hillgärtner *et al.*, 2001; Riding, 2011; Russo *et al.*, 2006; Dupraz *et al.*, 2009; Perri *et al.*, 2017, 2024b; Gindre-Chanu *et al.*, 2020; Borrelli *et al.*, 2021). In particular, autotrophic or heterotrophic metabolic activities of many microorganisms (i.e. bacteria, algae, fungi, and even viruses) can produce local super-saturation of the micro-environment surrounding the cells, inducing mineral precipitation and/or promoting mineral nucleation and cation concentration along the cell walls and within the extracellular polysaccharides (Konhauser *et al.*, 2005; Perri *et al.* 2022).

Bio-mediated early cements are commonly characterized by a micritic texture with fabrics varying from isopachous rim to pillar and meniscus. The meniscus-type morphology is common in vadose diagenetic environments and, thus, it has been for long time regarded as indicators of meteoric diagenesis. However, it is now widely accepted that this micritic cement type can also develop in marine phreatic zone through microbial mediation processes (Hillgärtner *et al.*, 2001). Moreover, biomediated micritic primary cements can be precursor for subsequent primary isopachous sparry cements, including fibrous aragonite (Diaz and Eberli, 2022). Finally, in the same marine settings, the formation of early marine micritic cement is often accompanied by the coeval inward microboring and destruction of the biota skeletal structure, with the resulting replacing of the skeletal tissue by micrite. Such a process is known as "micritization" of bioclasts, and the formation of this type of (replacive) micrite is actively or passively due to microbial activities (Reid and Macintyre, 2000; Flügel, 2004). Consequently, this microbial micrite is actually indistinguishable from the primary microbial micritic cement, at least in term of fabric and microstructure, but not in terms of morphology as the latter is an overgrowth on the skeletal grain (Kobluk and Risk, 1977; Perry, 1999; Hillgärtner *et al.*, 2001).

The above-described phenomenon of mobile seafloor hardening in warm climates is believed to be substantially absent in cold or even temperate contexts such as higher latitude sedimentary systems like in the Mediterranean (e.g., Betzler *et al.*, 1997; Perry, 1999). In particular, in the non-tropical mid-latitude shallow water carbonate realms, the early marine cementation and micritic rim formation are considered to be much rarer than in tropical waters, due to minor water temperature and lower Ca-carbonate saturation (Nelson, 1988; Betzler *et al.*, 1997; Fornos and Ahr, 1997; Reijmer, 2021). Nevertheless, ancient shallow marine phreatic calcitic cements are sporadically reported for mid-latitude non-tropical areas, indicating that these phenomena could be not exclusive of tropical waters (Nelson and James, 2000; Christ *et al.*, 2015). For example, subtidal phreatic early cements characterized by bladed or isopachous rims of both sparry and micritic calcite, are reported for Late Pleistocene MIS 5 deposits of the Mediterranean, including its western

(Kindler *et al.*, 1997; El-Shazly *et al.*, 2016) and central (Bracchi *et al.*, 2014; *Chapter 7*) settings. Moreover, early cementation due to both micritic and sparitic cements, are reported for non-tropical mid Tertiary and Pleistocene carbonate ramps of the Central Mediterranean (e.g., Mutti and Bernoulli, 2003; Gruszczynki *et al.*, 2008) and of New Zealand shelves (Nelson and James, 2000). In the current Mediterranean, early cementation of mobile substrata along the subtidal shelves by high Mg-calcite precipitation, was limitedly observed to the internal sediment that infills calcareous algal skeletal framework cavities (Alexandersson, 1969; Bracchi *et al.*, 2022), while in bathyal deep-sea settings further cases were reported (Christ *et al.*, 2015, and ref. therein).

The present study deals with a bioclastic calcarenitic shallow littoral to sublittoral deposit (i.e. an original mobile sandy seafloor), cropping out in the Gulf of Taranto (central Mediterranean) and dated to the Last Interglacial warmest peak MIS 5e (135-116 ky) (Amorosi *et al.*, 2014; Negri *et al.*, 2015; *Chapters 4 and 5*). New insights obtained from the microfacies study of this deposit allowed to investigate the inferred process of microbial mediated early cementation that affected this mobile seafloor substrate during the MIS 5e. This finding reaches a major interest in the view of predicting the possible evolution of this type of central Mediterranean seafloor in response to the ongoing global warming. In fact, the MIS 5e is considered a good analogous model of the next-future climate, since higher sea level and sea surface temperature (SST) (ca +2 °C) than at present were estimated (Overpeck *et al.*, 2006; Rohling *et al.*, 2008; Siddall and Valdes, 2011; Antonioli *et al.*, 2017; Fischer *et al.*, 2018; IPCC, 2023; Albano et al., 2024; *Chapter 5*).

As shown in *Chapter 4*, the studied level is made of a bioclastic calcarenite body (**Fig. 1A**), with rarer cross bedding in the eastern sections, with subordinate argillaceous sandstones, showing a good lateral continuity and ranging from 1 to 2 m of thickness. This unit has an absolute age ranging from around 134 ky and 123 ± 4 ky (Hearty and Dai Pra, 1992). The calcarenite hosts a variegated macrofauna, dominated by very abundant molluscs (**Fig. 1B**); the dominant species are: *Moerella pulchella* (sample T5) and *Lucinella divaricata* (Sample T13), indicative of shallow water sandy palaeobiotopes, and *Gouldia minima*, preferring coaster sandy-gravelly substrates (**Fig. 1C-E)**. In all the sites, about ¼ of the molluscs recovered indicates the occurrence of vegetated (seagrasses and /or seaweeds) substrates (see *Chapter 4*). Warm water mollusk species nowadays absent in the Mediterranean, such as the Strombidae *Thetystrombus latus,* are also present (**Fig. 1F**). These, as the equivalent modern tropical fauna, are collectively known as the "Senegalese Fauna" (Gignoux, 1913). Large specimens of molluscs were found in life position within the calcarenite bed, including both endofaunals or semi-endofaunals, such as in-situ *Pinna nobilis* (**Fig. 1G**) or cemented epifaunals, notably *Spondylus gaederopus,* ostreids, rare barnacles and serpulids (**Fig. 1H-J**). Common corallites and algal nodules are also found (**Fig. 1K**). The calcarenite facies represents a shallow littoral to sublittoral deposit, interpreted as a bioclastic sandy-detrital vegetated seafloor, with minor variations from more sheltered to higher energy conditions. The sea surface temperature (SST) was estimated of circa 20.8 °C as annual average, which is + 2 °C than the modern one in the Taranto Gulf, with a seasonal variation similar to today. This implies a possible warmer climate condition in respect to today, but far from real tropical conditions (*Chapter 5*).

6.1.1 Geological and stratigraphic setting

See *Chapter 4*.

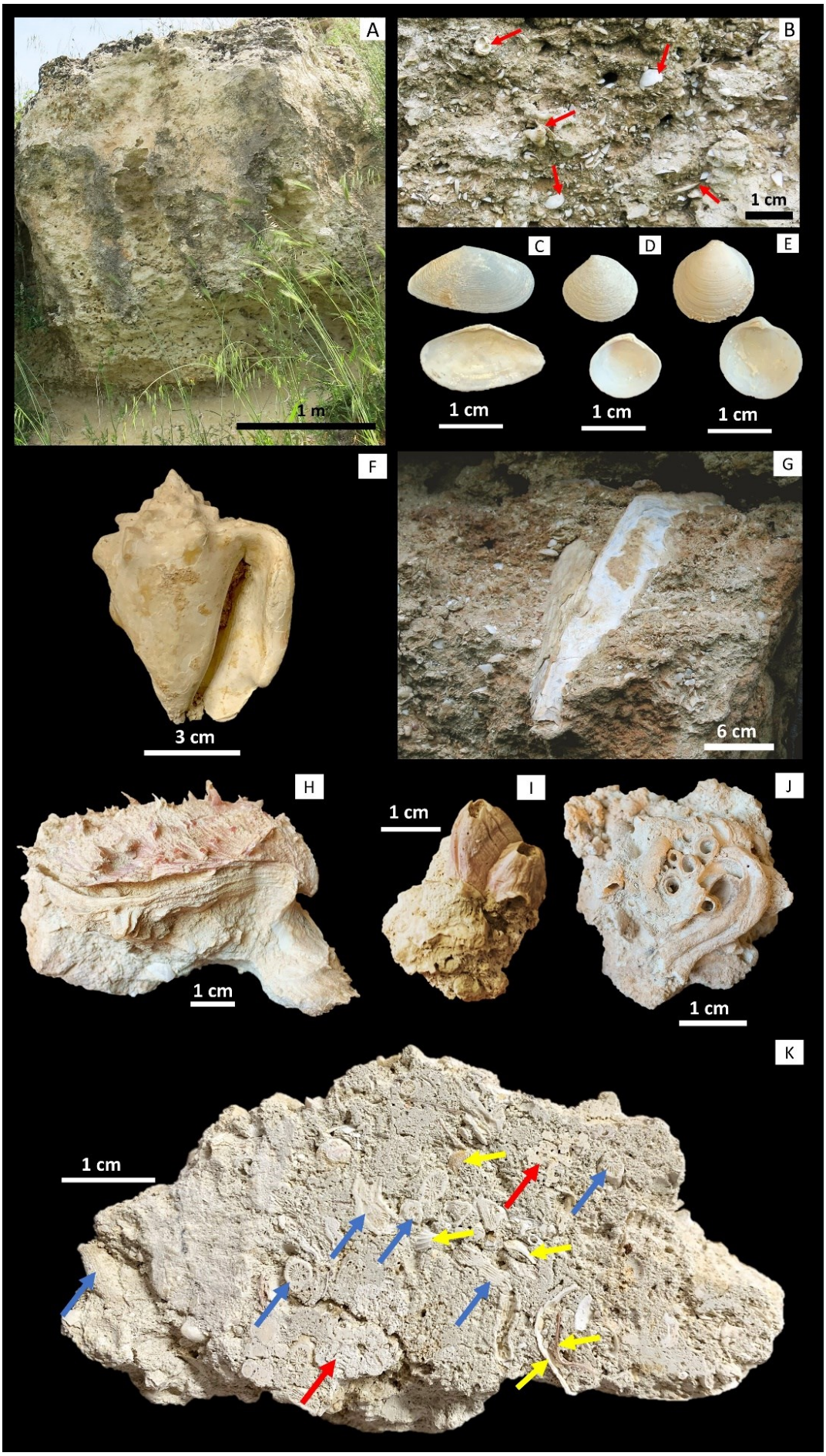
A
1 m
B
1 cm
C
D
E
1 cm
1 cm
1 cm
F
3 cm
G
6 cm
H
1 cm
I
1 cm
J
1 cm
K
1 cm

< Figure 1 (previous page). (A) Field view of the studied calcarenite at Mass. S. Pietro Section; **(B)** Close-up view of the same calcarenite showing the very common occurrence of fossils mainly consisting of molluscan shells and fragments (red arrows): **(C)** Dominant bivalve species at Mass. San Pietro (sample T5): *Moerella pulchella;* **(D)** Dominant bivalve species at Il Fronte (sample T17): *Gouldia minima;* **(E)** Dominant bivalve species at Mass. La Penna (sample T13): *Lucinella divaricata;* **(F)** Senegalese *Thetystrombus latus* at Mass. La Penna section; **(G)** In situ *Pinna nobilis* near Mass. S. Pietro section; **(H)** Articulated in situ *Spondylus gaederopus*; **(I)** Serpulids; **(J)** Barnacles. **(K)** Slab of a hand specimen of the calcarenite from Il Fronte Section, with easily distinguishable *Cladocora caespitosa* corallites (blue arrows), mollusk shells (yellow arrows), and calcareous red algae (red arrow).

6.2 METHODS

The calcarenite was sampled at three key locations, where the stratigraphic sections were measured and described: Masseria La Penna (sample T13), Masseria S. Pietro (Sample T5), and Il Fronte (Sample T17) (**Fig. 1, Fig. 3**; *Chapter 4*). Five thin sections were obtained after resin embedding through traditional protocol and studied using an optical polarizing microscope (Zeiss Axioscop – 40). In addition, Scanning Electron Microscopy (SEM) analysis was performed using a ZEISS Crossbeam 350, operating in a range of 5 to 20 kV with a working distance between 6mm and 15mm at the Università della Calabria, on Carbon coated fresh surfaces of rock samples. Geochemical signatures of the calcarenite, and in particular of the micritic cements, were obtained with and Energy Dispersive Spectrometer (EDS) EDAX OCTANE Elite Plus operating at 20 kV with a working distance of 12 mm, during SEM sessions. The bulk mineralogic composition of the calcarenite was checked by X-Ray Diffraction (XRD) analysis, using a Philips PW1730 diffractometer.

6.3 RESULTS

6.3.1 Petrography and composition of the deposit

The calcarenite is composed of a bioclastic framework with primary porosity (both intergranular and intragranular) partially occupied by micrite with various fabrics (below described in detail). Grains consist of fine to coarse brownish to whitish bioclastic sand (**Fig. 2A-I**), with a negligible siliciclastic component mostly represented by angular quartz and very fine clay minerals. Bioclasts consist of reworked and worn fragments of:

- various types of calcareous red algae: geniculate, free branched and non-geniculate lithothamnii forms, or even encrusting other bioclasts (**Fig. 1K**, **Fig. 2C, D**);
- bryozoans, like the erect and branched cf. *Myriapora* (**Fig. 2C**);
- loose *Cladocora caespitosa* corallites (**Fig. 1K**, **Fig. 2E**);
- Anellida (calcareous tubes of Polychaeta indet.) (**Fig. 2F**), Crustacea (rare barnacle plates), echinoid test fragments and radiola, and rare scaphopod tubular shells.
- Benthic foraminifera are well represented in the sandy-sized bioclastic component of the calcarenite, both as encrusting forms (e.g. *Planorbulina mediterranensis,* **Fig. 2G**), common free forms like hyaline (e.g., *Elphidium* cf *crispum;* **Fig. 2H**) and porcelaneous foraminifera (e.g., *Quinqueloculina* sp. (**Fig. 2I**). Planktonic foraminifera (e.g., *Globigerina* sp.) are also sporadically present.

The calcarenite also includes entire macrofossils shells (some in life position) or large fragments of bivalves (**Fig. 1K**; **Fig. 2A**) and gastropods (**Fig. 2B**) that, most probably, inhabited the sediment.

The preservation of the original texture and composition of the bioclasts is variable, ranging from well preserved to fragmented, bioeroded, and partially to completely micritized (**Fig. 2A-F, I; Fig. 3A, C, D**). Moreover, effects of dissolution processes are found, as some bioclasts are partially to totally dissolved, resulting in large intra-skeletal porosity. Other clasts, instead, show evidence of a moderate neomorphic recrystallization (see below). In addition, intra and inter-skeletal cavities are

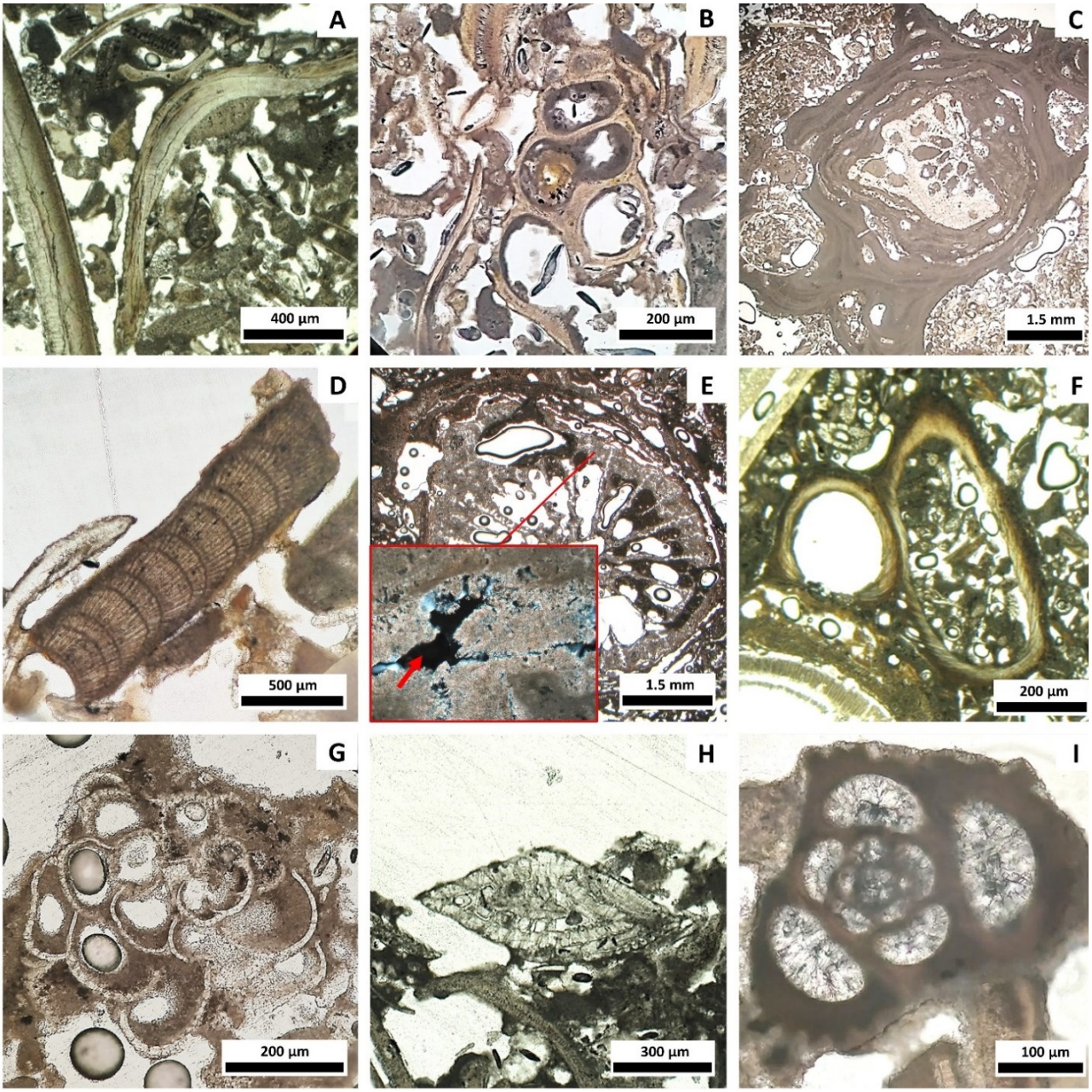

Figure 2. Common bioclasts**. (A) Bivalves; (B) Gastropods; (C) Coralline red algae (in the example shown** encrusting a bryozoan bioclast); **(D)** Articulated coralline red algae fragment; **(E)** *Cladocora caespitosa* showing the spherulitic skeletal aragonite microstructure locally affected by partial dissolution (red arrow); **(F)** Polychaetes tubes; **(G)** Encrusting foraminifera (*Planorbulina mediterranensis*); **(H)** Hyaline foraminifera (*Elphidium* cf *crispum*); **(I)** Porcellanaceous foraminifera (*Quinqueloculina* sp.).

partially to totally filled by micrite (Fig. 2**A, E, F**) or, more rarely, by secondary sparry cements (Fig. 2**I**). Very rare early diagenetic cements consisting of isopachous rims of fibrous sparry calcite were also found. Despite these localized diagenetic alterations, the calcarenite is overall affected by limited post-depositional alteration. This is testified by the good preservation of aragonitic *C. caespitosa* skeletons, which retain their pristine aragonitic fibrous and spherulitic microstructure of corallite walls and septa, excluding some minor dissolution voids (Fig. 2**E**).

6.3.2 Micrite

Micrite is often abundant, resulting as a widespread component of the calcarenite. It shows various micro-morphologies and fabrics, grouped into two main categories, as follows: 1) Rims and crusts enveloping the bioclasts; 2) Intergranular voids-infilling micrite.

a) **Rims and crusts enveloping the bioclasts**. Isopachous to irregular dark rims and crusts, showing a variable thickness of tens of microns and enveloping the bioclasts are very common (Fig. 3**A, C**). In some bioclasts, the external micritic crusts make inward transition to micritized areas, which exhibit the same petrographic features (and also microstructure as showed below) of the crust (Fig. 3**D**). In other cases, the micrite surrounds the bioclasts forming outward thickened micro-mounds (from 20 to 100 µm) (Fig. 3**E, F**), or even connects adjacent bioclasts with narrow meniscuses or elongated columns/pillars (about 100-150 µm) (Fig. 3**B**; Fig. 4**B-D**). The petrographic fabrics of these micrites are commonly aphanitic and subordinately peloidal or filamentous (Fig. 4**B, C**). Peloidal fabric is composed of 10 to 30 µm in size irregular dark micritic clots surrounded by microsparite (Fig. 4**B**). Filaments, observed in thin section are around 10 µm in diameter and 50-100 µm in length, with a curved and meandering shape (Fig. 4**C**). However, further filamentous structures have been detected with SEM analyses (e.g. Fig. 4**D**), as reported in detail below.

b) **Intergranular voids-infilling micrite.** Micrite can partially to totally occupy intergranular pores among the bioclasts, commonly showing aphanitic or micropeloidal fabric that can include trapped fine detrital grains, and form packstone-wackestone pockets in the calcarenite (Fig. 4**E, F**).

Figure 3 (next page). (A) General thin section view of the calcarenite structure and micrite cements; note: micritized grains (yellow arrows), columnar bridge cements (red arrows); non-isopachous micritic envelopes (blue arrows), local thickenings (purple arrow), dissolution cavities (green arrows); **(B)** SEM view of the calcarenite; note micritic crusts around the grains biding them through envelopes and pillars (red arrows); (**C)** Microphotograph of micritic rim cements (yellow arrows) binding bioclasts. Thin section view; **(D)** Micritic envelope on micritized grain (red arrows) and grain micritization (green arrow). Thin section view; **(E)** Anisopachous micritic rim cement (yellow arrows) and micro-mounds (red arrows). Thin section view; **(F)** Micritic micro-mounds over a *Lucinella divaricata* valve (yellow arrows). SEM view**.** **>**

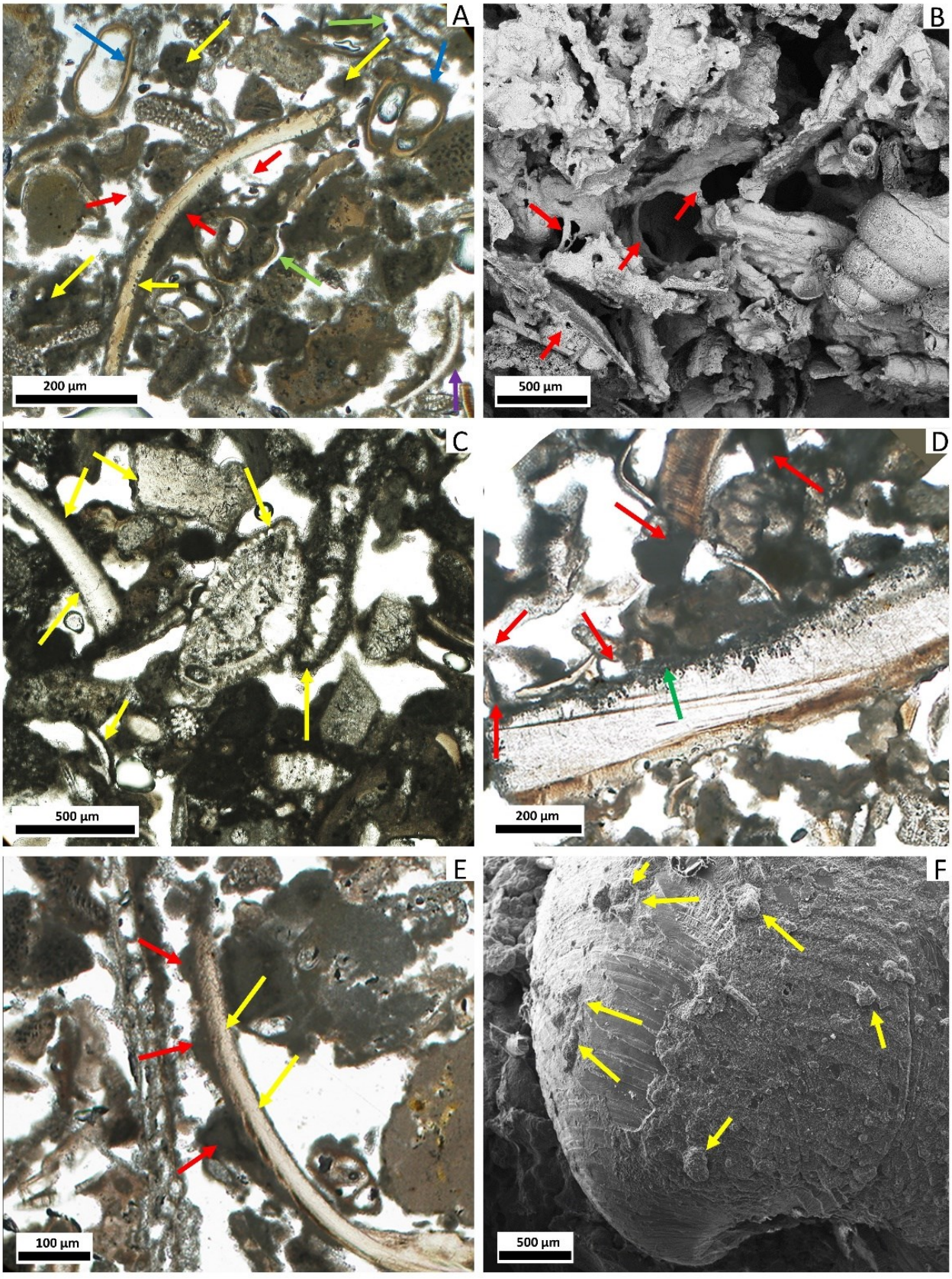
A
200 µm
B
500 µm
C
500 µm
D
200 µm
E
100 µm
F
500 µm

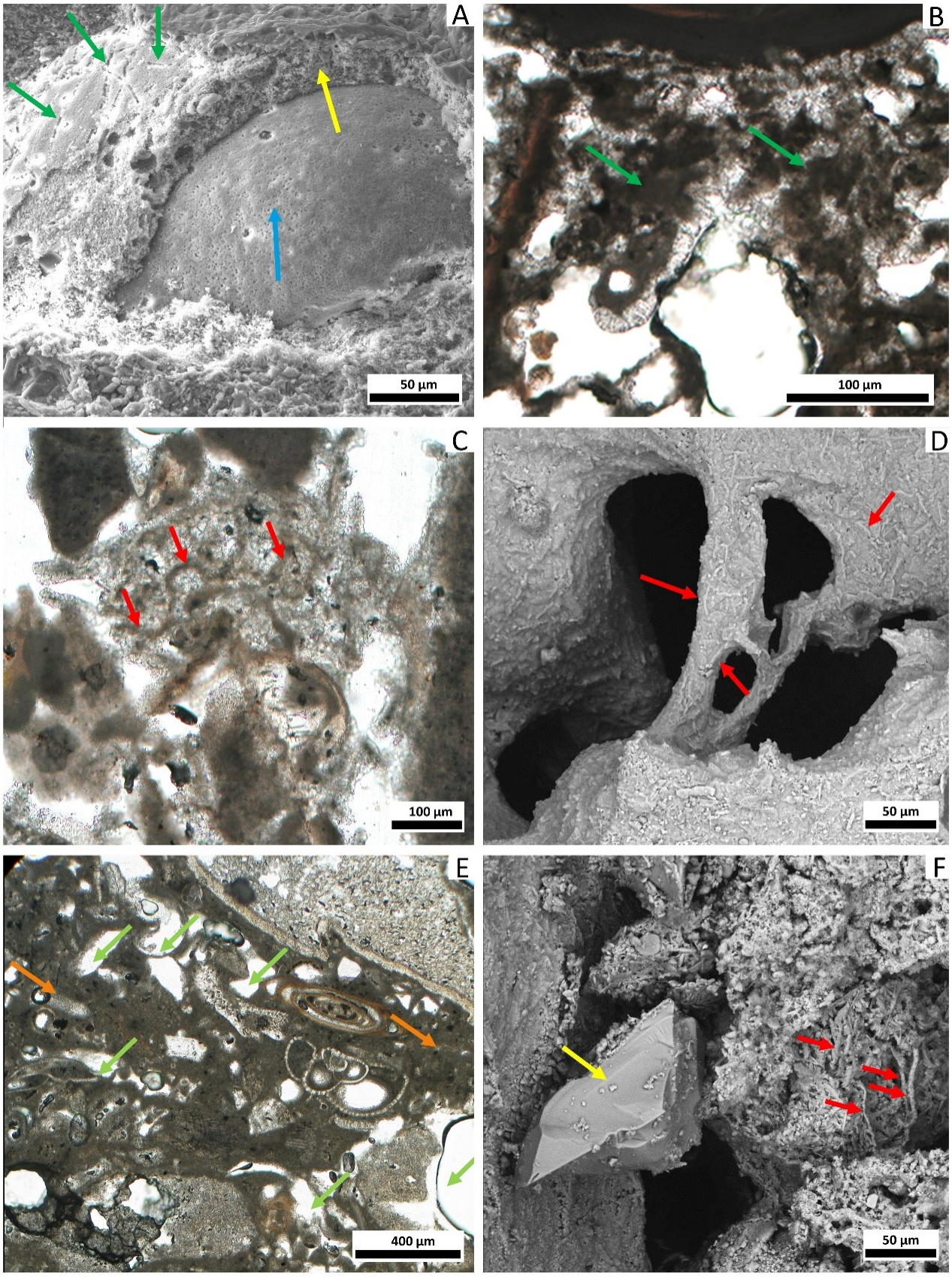
A
50 µm
B
100 µm
C
100 µm
D
50 µm
E
400 µm
F
50 µm

< Figure 4 (previous page). (A) Micritic rim (yellow arrow) enveloping a bioeroded (micritized) bioclast (blue arrow), note numerous bacterial moulds (green arrows). SEM view; **(B)** Pillar cement with clotted peloidal fabric (green arrows). Thin section view; **(C)** Pillar cement with filamentous fabric (red arrows). Thin section view; **(D)** SEM view of pillar micritic cement with finer filamentous mineralized structures (red arrows); **(E)** Void-filling micrite (orange arrows) and dissolution cavities (green arrows). Thin section view; **(F)** Void-filling micrite surrounding a quartz grain (yellow arrow). Note mineralized curved filaments (red arrows). SEM view.

6.3.3 Ultrastructure and composition of micrite

Despite the different micro-morphologies, the ultrastructure of all the described types of micrite, including the one derived from micritized grains, is substantially equal. It is, in fact, composed of sub-micron sized, anhedral to subhedral crystals of Ca-carbonate mixed with a variable minor amount of clay microcrystals (**Fig. 5A**). In particular, the calcite shows a moderate amount of Mg (4-6 moles %, excluding C and O), whereas the clay mineral shows a mean composition of Si: 34 moles %, Al: 12 moles %, Mg: 6 moles %, K: 4 moles % (**Fig. 5B, C**), which is in accordance with the standard mean composition of saponite (Barrios *et al.*, 2001). The presence of saponite, associated with the calcite, is further confirmed by the XRD analysis that shows a minor amount of aragonite, probably deriving from unaltered skeletal grains, and quartz deriving from terrigenous clasts (**Fig. 5D**).

In detail, the calcite shows a specific nanostructure consisting of nanospheres, 100 to 300 nm in size, which aggregate to form larger micritic crystals (around 1-4 µm) which, in turn, can develop a sub-euhedral habitus (**Fig. 6A, B**). Saponite crystals show a variable dimension and a sheet-like habitus. They can form very large sheets enveloping the micrite crystals themselves as well as being dispersed in the micritic matrix (**Fig. 6C, D**). For both the two minerals, micrite and saponite, no evidence indicating a detrital origin (e.g., fractured and smoothed surfaces of irregular grains) was detected in all the studied portions of the calcarenite.

Under the SEM the micrite reveals a widespread presence of fossilized (calcified) organic material, or empty cavities, possible molds of organic components (**Fig. 6E**). In particular, very common filamentous structures (as already seen in optical microscopy, **Fig. 4C**), and rarer sub-spherical structures, also occur. In detail, these mineralized structures can be classified in three morphological types:

1. rod-like, around 10-20 µm long and 3-5 µm wide mineralized bodies, locally very densely occurring (**Fig. 6E**; **Fig. 7A**);
2. longer (around 50 µm) and thicker (up to 10-15 µm), sometimes curved, filamentous mineralized bodies, in some cases tubular, with a decreasing diameter, and with a thick wall (around 5 µm) (**Fig. 6E**; **Fig. 7B**);
3. mineralized subspheres (cocci-like) up to 5 µm in size (**Fig. 7C**).

Empty cavities, more common in the micritized part of bioclasts, show tubular or spherical shape with dimension in the ranges of the equivalent mineralized structures (**Fig. 8A-D**). Moreover, irregular often sheet-form masses have been found, appearing like a thin mineralized crusts developed over the grain surfaces and closely associated with the mineralized filaments and spheroids (**Fig. 6E**). Finally, the micrite often includes dispersed dehydrated organic matter remains, as sheets and filaments, which sometimes appear from partially up to not mineralized by the calcareous nanospheres (**Fig. 8E, F**).

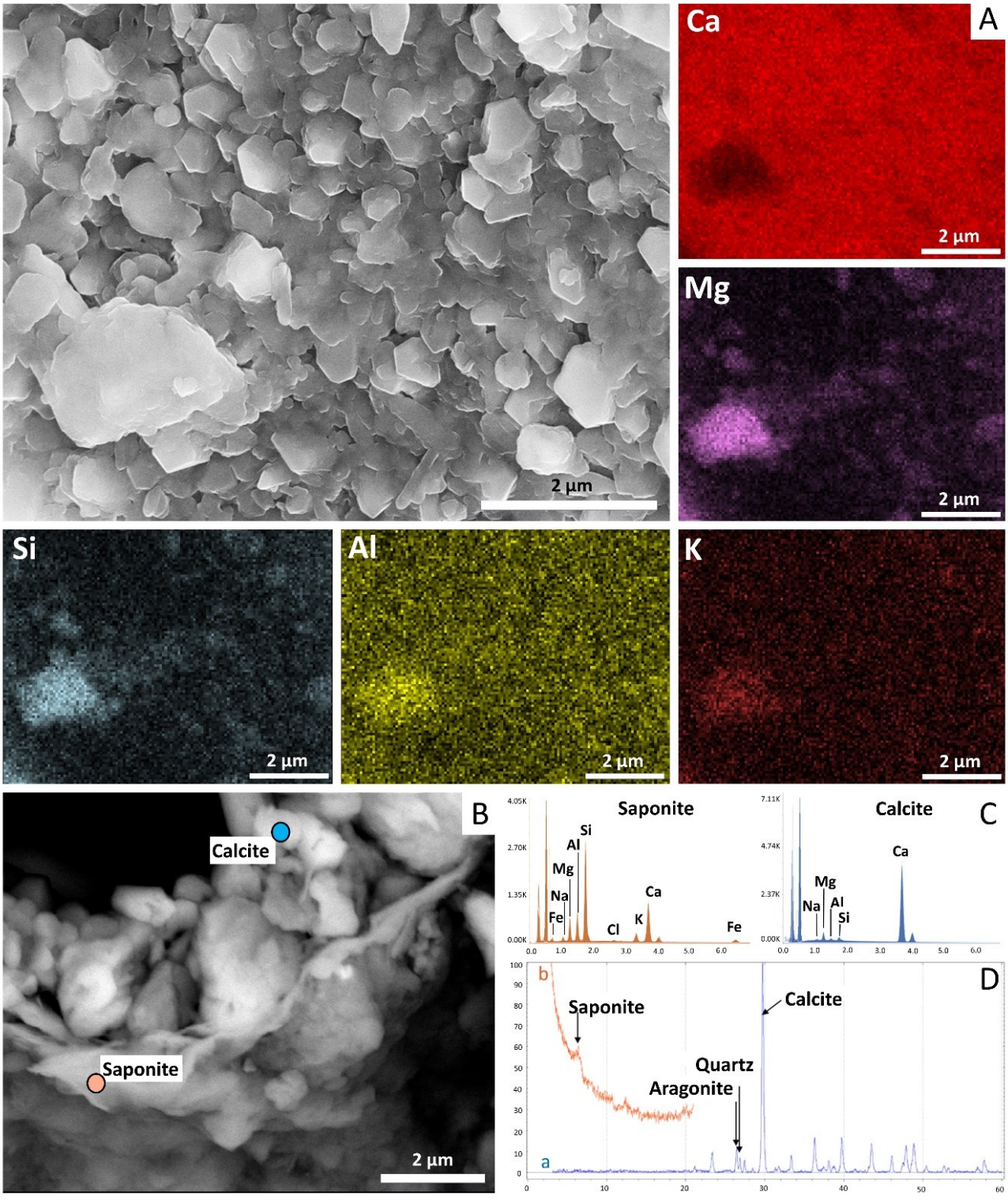

Figure 5. (A) SEM view and EDS elemental maps map of micrite and clay minerals making the cement. The Ca-carbonate crystals are recognizable in respect to clay crystals, comparing the distribution of Ca with those of Si, Al, K, and Mg. **(B-C)** SEM view and EDS spot analyses on the calcite and saponite mineral cements and relative elemental spectra. **(D)** XRD spectra of a calcarenite bulk sample. The spectrum (a) shows the main peaks of calcite, aragonite (deriving from the micrite and the skeletal components) and quartz (from rare siliciclastic grains). The spectrum (b) is limited to $2\theta = 20.5°$ to amplify the clay mineral peaks, and to define the presence of saponite, which is contained in the micrite, as main argillaceous mineral (see Discussion).

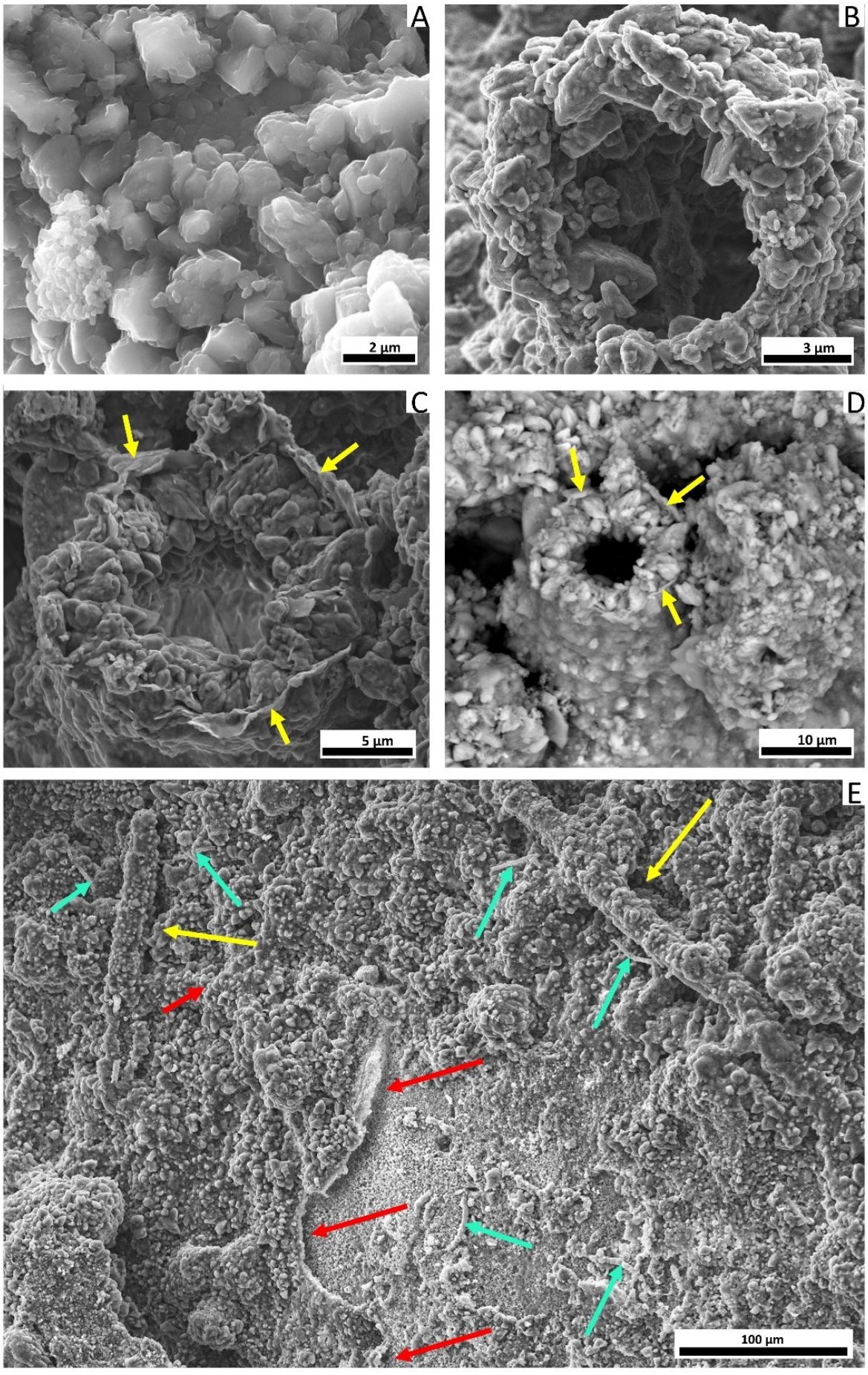
A
2 µm
B
3 µm
C
5 µm
D
10 µm
E
100 µm

< Figure 6 (previous page). Nanostructure of micrite cement. **(A)** Nanospheres typically composing the micrite cement. SEM view in secondary electrons; **(B)** Filament's ghost highlighted by the micrite developed along its surroundings, formed by the aggregation of nanospheres. SEM view in secondary electrons; **(C)** SEM secondary electrons view and **(D)** back scattered electron view of a mineralized filament with saponite platy crystals (yellow arrows); **(E)** SEM view of sheet like mineralized crust (red arrows) associated with large (yellow arrows) and thin mineralized filaments (blue arrows).

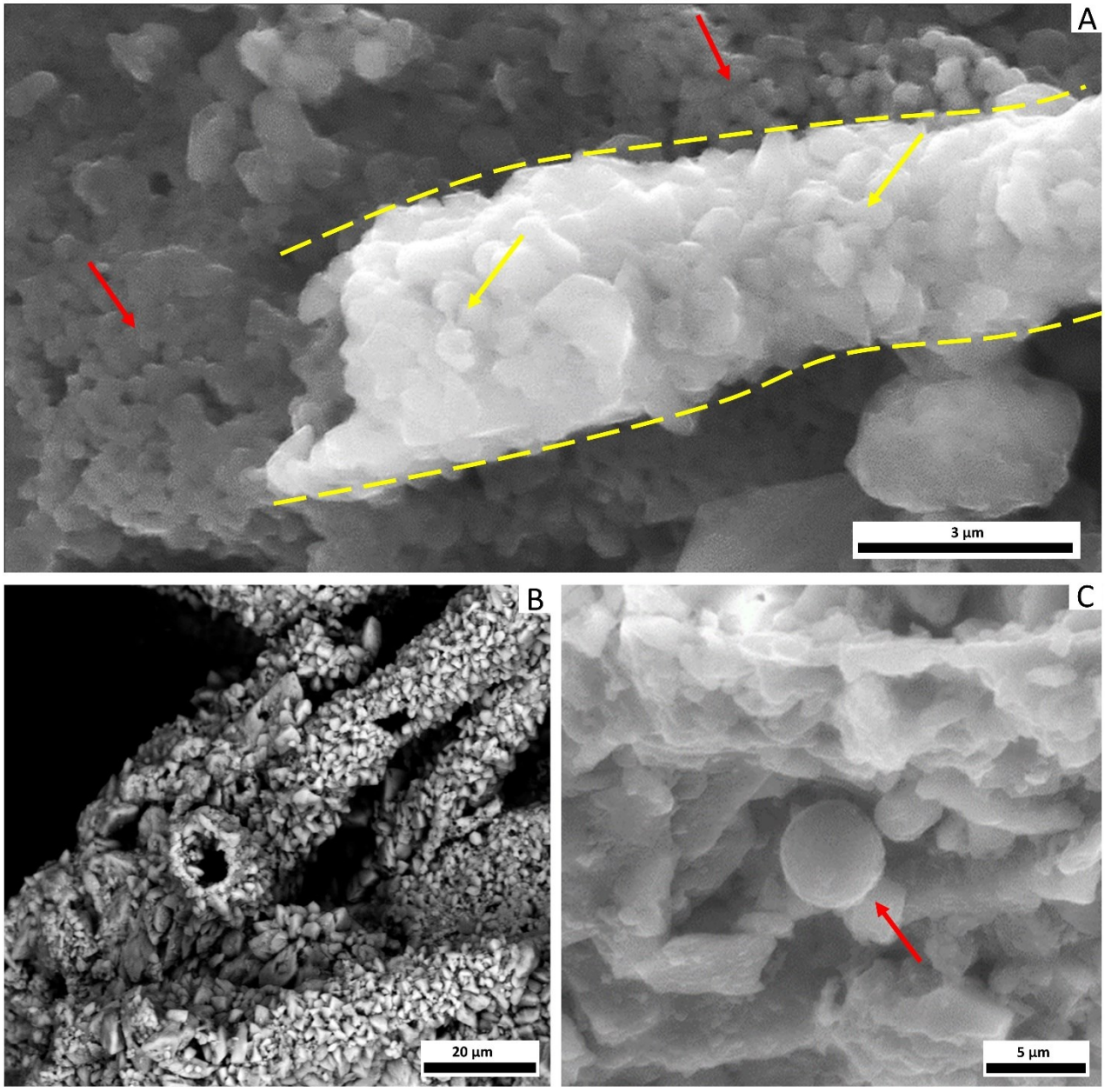

Figure 7. SEM views of mineralized filaments and cells. **(A)** Rod-like mineralized filament (yellow arrows and lines) and extracellular micrite (red arrow) (see Fig. 8D for location of the picture); **(B)** Large tubular mineralized filament, possibly representing plant root hair ghosts*;* **(C)** Mineralized spheroidal bacterial cell (red arrow).

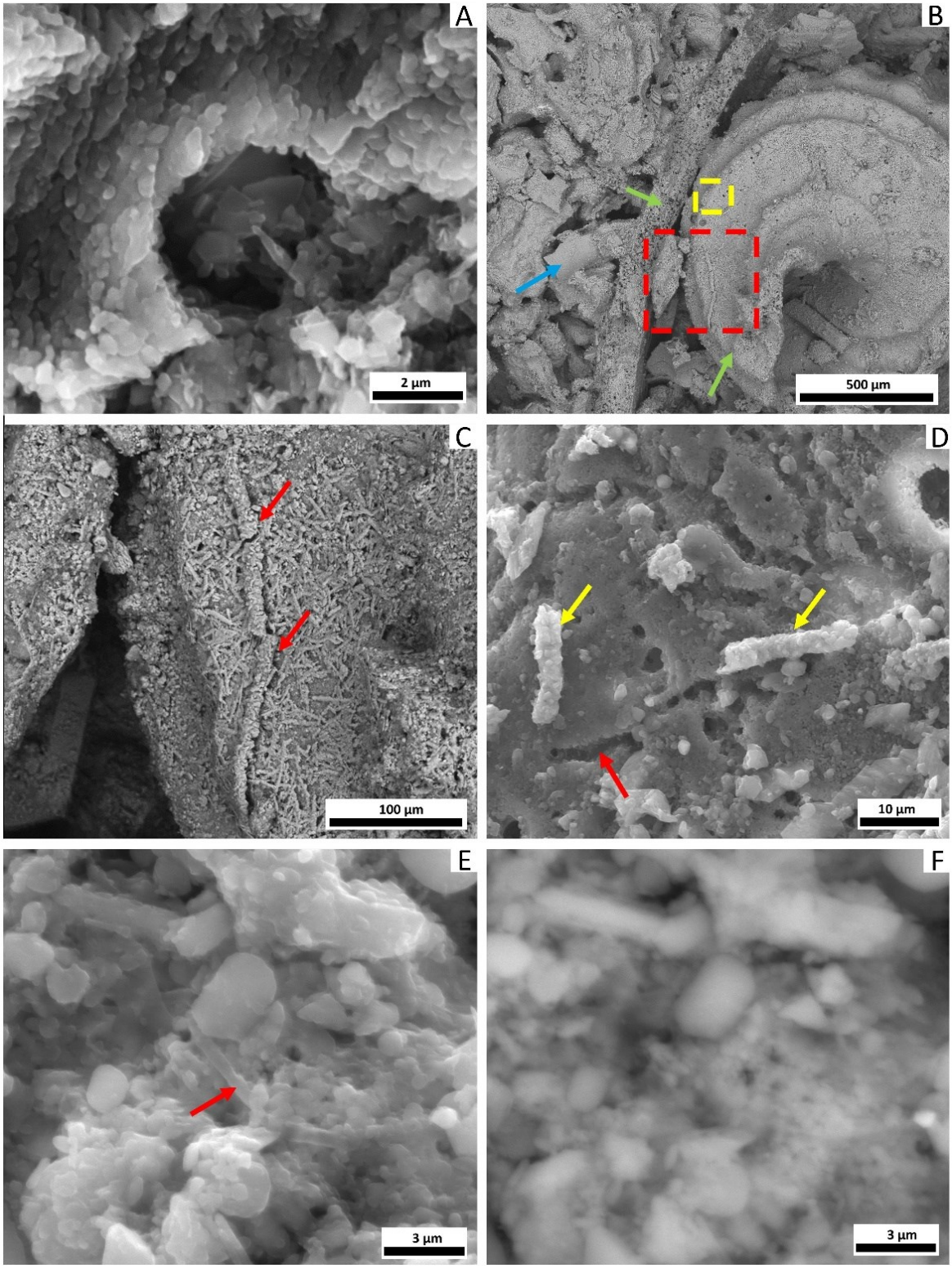

Figure 8. SEM views of fossilized microorganisms in the micrite**. (A)** Empty mould of possible bacterial cell in the micrite; **(B)** Micritized molluscan shells (green arrows) and unaltered bioclasts (blue arrows); the red square indicates the position of Fig. 8C, while the yellow one indicates the position of Fig. 8D; **(C)** Surface of micritized bioclast, with rich association of large filaments, possibly plant root hair (red arrows) and diffuse thin filaments; **(D)** Detail of microboring channels on the surface of a bioclast (red arrow), associated with external micrite nanospheres including thin mineralized filaments (yellow arrows). **(E-F)** Mummified organic matter remains (note a bacterial filament, indicated by the red arrow), in secondary electron view (E), resulting transparent when observed in back scattered electron view (F).

6.4 DISCUSSION

In the studied bioclastic calcarenite, the abundance of calcareous red algae fragmented thalli, together with the abundance of shallow water benthic foraminifera, such as porcelaneous miliolids, and rare planktic forms, is consistent with a very shallow water setting such as a shallow subtidal environment (or infralittoral zone). Moreover, the presence of the foraminifera *Planorbulina mediterranensis* (**Fig. 2G**) is a good proxy to also infer the possible presence of *Posidonia* meadows (Mariani *et al.*, 2022). The molluscan assemblage is also in accordance with a sandy vegetated shallow bottom, being dominated by the characteristic species (*M. pulchella, L. divaricata*) typical of the fine well sorted sands (SFBC) biocoenosis (Pérès and Picard, 1964), accompanied by rheophilic gravel related species (*G. minima*), and by characteristic species of the photophilic algae and *Posidonia* meadows (AP/HP) biocoenoses (**Fig. 1**) (see also *Chapter 4*).

Considering the very low Mediterranean tide excursion (few decimetres in average), a depth range comprised between ca. 0.5 m and 25 m (corresponding to the typical maximum depth of the SFBC biocoenosis) can be proposed for the inferred environment, also considering the common fragmentation and abrasion of the bioclasts, consistent with a relatively energetic wave agitated setting.

Micrite is very abundant in the studied deposit, showing various micro-morphologies and fabrics that are consistent with a synsedimentary precipitation (i.e. autochthonous micrite), rather than a detrital origin. First of all, the presence of typical microbial fabrics, such as peloidal and filamentous, characterizing most of the micrite, confirms the biological mediation in their formation (**Fig. 4B-D, F**) (Chafetz, 1986; Riding, 2000; Konhauser and Riding, 2012). Moreover, the irregular thickness and geometries of the micritic cements (i.e., non-isopachous wavy rims locally with outward convexities, e.g. **Fig. 3A, E, F**) together with their anti-gravitative pattern, is further evidence of their biologically controlled synsedimentary deposition, which also reminds intra-porosity micro-reefs formation (Flügel, 2004; Perri *et al.*, 2019). Indeed, the best evidence of the authigenic bio-mediated deposition of this micrite is its particular mineral nanostructure and the presence of many fossilized microbial cells and organic matter. In fact, all types of the observed micrite are constituted of a typical an in-situ precipitation framework characterized by the hierarchical pattern starting from sub-micron in size nanospheroidal crystals (**Fig. 6A, B**; **Fig. 7A**), which typically aggregate to form larger carbonate crystals. It is widely accepted that these nanospheres, also termed as “amorphous calcium carbonate” (ACC), represent the result of a microbial-mediated genesis (Perri and Spadafora, 2011; Perri *et al.*, 2012a, 2012b; Ihli *et al.*, 2014; Diaz and Eberli, 2022). The crystal structure of these crystals in fact, is different from the euhedral "solid" structure of the pure inorganic precipitates (Niederberger and Colfen, 2006). It is important to underline that such a nanostructure also characterizes the aphanitic void-filling micrite, which commonly incorporates detrital clasts (**Fig. 4E, F**). More in detail, the nucleation of nanospheres forming the described micrites, as well as the associated micritized skeletons, can be promoted within the microbial mucilaginous film (composed by the microbial community that includes bacteria, algae, fungi, and vesicles, viruses) embedded in the Extracellular Polymeric Substances (EPS), which act as precursors for the cement precipitation. This process is favoured by the accumulation of cations and by the progressive degradation and replacement by mineral precipitates, which often involves the microbial cells incorporated into them (Van Lith *et al.*, 2003; Benzerara *et al.*, 2006, 2010; Perri and

Tucker, 2007; Perry *et al.*, 2007; Bontognali *et al.*, 2008; Pedley *et al.*, 2009; Sánchez-Román t al., 2008; Manzo *et al.*, 2012; Bahniuk *et al.*, 2015; Perri *et al.*, 2022; Słowakiewicz *et al.*, 2023).

In addition, the micrite commonly hosts both rod-like and filamentous fossils of mineralized microorganisms. This provides a further key evidence of the presence of a microbial community forming a widespread biofilm among the grains (**Fig. 9A**). The shape and size of subspherical cells (**Fig. 7C**) and tubular or solid calcified filamentous structures (about 5 µm in diameter, tens of µm in length) (**Fig. 6E**; **Fig 7A**) is compatible with fossil bacteria (Perry, 2007; Perri and Spadafora, 2011; Perri *et al.*, 2012a; Diaz and Eberli, 2022). The only exception regards the largest calcified filaments (200 µm in length and 10-15 µm in diameter) which are too large to represent a bacterial-like organisms. They most probably fall within the range of possible fine root hairs of seagrasses (**Fig. 6E**; **Fig. 7B**), whose presence in the studied sediment is indicated by plant-related mollusk species, as detected through the palaeoecological study (*Chapter 4*). Indeed, the average shape and width of *Posidonia oceanica* root hairs is reported to be around 12 µm (Zenone *et al.*, 2020) that is very similar to our mineralized largest tubiform structures.

The presence of hollow tubular and subspherical empty cavities within the micrite **(Fig. 6B-D**; **Fig. 7B**) indicates that most of the microbial cells are preserved as molds, suggesting that the process of crystal nucleation takes places mostly in the EPS and less on external cell wall (**Fig. 6E**; **Fig. 7A**). This is further supported by local remnants of non-mineralized organic matter associated with the micritic precipitates (**Fig. 8E, F**).

As seen, the formation of the above described microbial micritic cement is commonly associated with the micritization of many bioclasts. In fact, a gradual transition from the micritic cement up to the microbored and micritized zones of the bioclast, and the equal fabric of both micrites, are often observable (**Fig. 3A, D**; **Fig. 8B-D**). It is thus evident the direct link between micritization of the skeleton and their external encrustation, pointing towards a linked biogenic genesis of both processes, as already suggested in marine systems (Reid and Macintyre, 2000; Diaz and Eberli, 2022, and ref. therein) (**Fig. 9**). As micritization is one of the earliest marine diagenetic processes affecting bioclasts, it is therefore demonstrated that also the formation of the associated micritic cement took place very early and in a marine environment. This is also testified by the even slight Mg presence in the calcite of micrite (4-6 moles %; **Fig. 5B-C**), consistent with a marine environment rather than in a tardive continental vadose setting (Tucker and Wright, 1990).

Some Authors (e.g., Perry 1999; Hillgärtner *et al.*, 2001) distinguished between destructive and constructive micrite envelopes, the former resulting from an inward microboring activity and cement infilling (e.g., Reid and Macintyre, 2000), and the latter resulting from an external microbial mediated precipitation and sediment trapping. Moreover, other Authors (Kobluk and Risk, 1977; Scholle and Ulmer-Scholle, 2003) suggest that the same microbial communities can accomplish both the processes coupled together. Congruently to these literature data, our results show that external cement precipitation is not always clearly distinguishable from the inward micritized areas, pointing toward the close genetic association between micritization and micritic cementation phenomena (**Fig. 3D**; **Fig. 8B-D**).

Finally, the saponite associated with the micrite can be also considered authigenic, even if subsequent to the calcite, also considering the morphology of the crystals that can envelope mineralized calcareous filaments (**Fig. 5B**; **Fig. 6C, D**). The authigenic precipitation of saponite, and

similar clay minerals, is documented in literature in association with marine carbonate microbialites (e.g. Perri *et al.*, 2018; Suosaari *et al.*, 2022).

The synsedimentary growth of micritic cements enveloping the grains in subtidal environments was traditionally thought to require a calm, not permanently moving substrate, such as that associated to seagrass-stabilized biotopes (Perry, 1999, and ref. therein; Reich *et al.*, 2015). Recently, Diaz and Eberli (2022) found microbial early diagenetic cements, very similar to those observed in our study, in shallow high energy mobile sandy shoal bottoms of tropical modern carbonate platforms. They demonstrated that microcrystalline meniscuses, crusts, and pillar micritic cements, often considered in literature to be indicative of marine tidal vadose or quiet subtidal phreatic zones, can also develop in high energy shallow marine phreatic environments under a microbial control. Thanks to the microbial mat growth, the sediment is relatively quickly stabilized allowing the precipitation of the microbial micritic cement. This is in accordance with the occurrence of similar microcrystalline cements in a variety of marine environments, even into energetic mud-free grain-supported sediments (e.g., grainstone sense Dunham, 1962) (Flügel, 2004). The overall palaeoecological inferences derived from the molluscan assemblage that characterize the calcarenite (*Chapter 4*) confirm the relatively moderate to high energy setting sandy palaeobiotope, with local presence of seagrasses and/or seaweeds. The presence of seagrass is fundamental to stabilize the substrate and to reduce the hydrodynamic energy on the water-sediment interface, promoting the accumulation of fine and organic matter and the development of microbial biofilms and cementation (Reich *et al.*, 2015).

A further indication of this synsedimentary microbial cementation is provided by the endofaunal species, typical of mobile sandy to gravelly substrates, accompanied by a good percentage of epifaunal species, including those living on hard substrates. The occurrence of large rock-encrusting epifaunal species in life position, such as the AP (Photopilic Algae biocoenosis) characteristic *Spondylus gaederopus*, implies the presence of a rocky substrate, which is apparently in contrast with the general seabed proposed reconstruction. However, this is solved by the demonstrated early cementation of the sandy substrate by the microbial mediated micrite precipitation, which justify presence of such species. The same is found for smaller epibenthic taxa, such as barnacles and polychaetas (**Fig. 1I, J**), which can directly encrust patches of locally hardened bioclastic sand. It should be considered that the cementation phenomena were non-pervasive (like an extended hardground), as many soft-bottom infaunal molluscs still thrived into the sediment (*Chapter 4*).

According to the literature data, microbial cements and related early lithification phenomena, analogously to what found in MIS 5e of Taranto, are typically associated with warm subtropical/tropical waters, such as those found in the Bahamas and Northwest Australia (Diaz and Eberli, 2022). Consequently, they are not typical of the modern non-tropical Mediterranean at comparable infralittoral shallow depths, where only a very negligible microbial cementation may occur (Betlzer *et al.*, 1997).

Excluding intertidal and deep-sea early cements, comparable subtidal phreatic early cements, varying from sparry to microcrystalline cements, are reported for MIS 5e deposits of western Mediterranean (Sardinia, Kindler *et al.*, 1997; El-Shazly *et al.*, 2016), and also younger bioconstructed and detrital facies of central Mediterranean (Calabria, Bracchi *et al.*, 2014; Borrelli *et al.*, 2024; *Chapter 7*). In the MIS 5e Taranto calcarenite, the recognition of such early lithification

by these warm water cements matches warmer sea surface temperatures (SST) compared to today, estimated +2 °C in the same deposits (*Chapter 5*) (**Fig. 9**). Considering the high warming rates of surface waters of the Mediterranean Sea (in the Ionian Sea being 0.037 °C/year; Pisano *et al.*, 2020), MIS 5e -like sea surface temperatures are expected in the second half of the present century. Consequently, it is possible to infer that such shallow marine cementation will become increasingly common in the modern Mediterranean due to ongoing global warming, causing similar early cementation phenomena like those inferred for the MIS 5e calcarenite of Taranto. Moreover, if SST will overpass the estimated palaeotemperature, this cementation process may even become more widespread and pervasive, possibly causing relevant environmental changes.

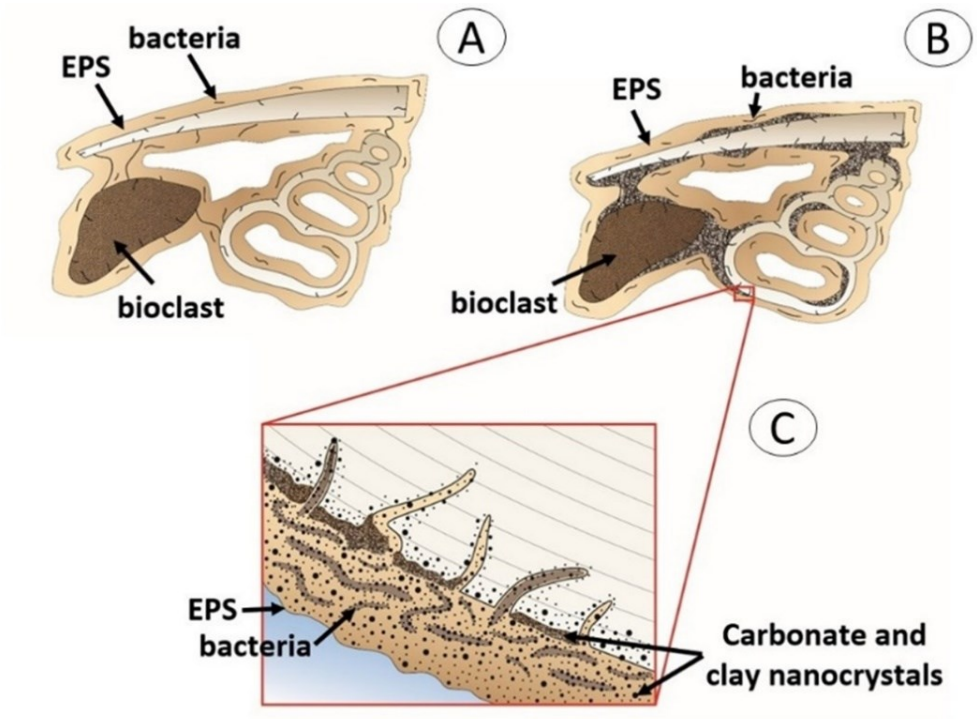

Figure 9. Diagram showing the formation of micritic cements after the coating of grains by organic EPS **(A)** and bioerosion due to bacteria **(B-C).**

6.5 CONCLUSION

A possible trend of a central Mediterranean sandy littoral/sublittoral seafloor adaptation, in response to the ongoing global warming, expected to carry on an increase of ca +2 °C of the SST at the end of the century (Pisano *et al.*, 2020) similarly to the MIS 5e (135-116 ky) time (*Chapter 5*), is here proposed. The model derives from the study of a well-preserved biocalcarenite deposit, cropping out in the Gulf of Taranto, which is characterized by the following features:

- the studied calcarenite (grainstone/packstone) is almost entirely made by bioclasts, such as mollusk shells and fragments, constituting the coarser fraction, together with calcareous red algae, benthic foraminifera, corals, bryozoans, polychaetas and crustaceans;
- overall, the fossils are well preserved, although fragmentation and micritization, and they are consistent with a very shallow-water environmental setting of deposition;

- micrite is widespread in the calcarenite as syn-sedimentary marine cements, both coating the grain surfaces and locally completely filling the intergranular primary spaces;
- no evidence of detrital origin of micrite was found;
- on the contrary, micrite show an evident autochthonous origin as a microbial mediated precipitate;
- the microbial origin of micrite is witnessed by typical microbial fabrics, such as the mineral nanostructure characterized by submicron nanospheres replacing the original organic matter that aggregate to form larger crystals and the widespread occurrence of several types of mineralized microbial cells.

All these features suggest the presence, during the MIS 5e, of a lithifying microbial mat that could, at least partially, stabilize the sandy substrate, even in a relatively energetic shallow, locally vegetated paleoenvironment. In particular, it can be very likely supposed that hardened patches of the seafloor progressively appeared and, consequently, they were used as substrate by epilithic taxa, typic of hard seafloor settings. Notably, the presence of these cements in this mid-latitude sand during a slightly warmer period, in respect to today, suggests a possible future appearance and potential increase of this very early cementation processes triggered by the global warming. This could potentially impact the ecological evolution of marine environments in warm temperate regions like the Mediterranean.

CHAPTER 7 – CALCAREOUS BIOCONSTRUCTIONS FORMATION DURING THE LAST INTERGLACIAL (MIS 5) IN THE CENTRAL MEDITERRANEAN: A CONSORTIUM OF ALGAL, METAZOAN, AND MICROBIAL FRAMEBUILDERS (CAPO COLONNA - CROTONE BASIN - SOUTH ITALY)

Abstract. The last interglacial (MIS 5) transgressive-regressive deposits of the Capo Colonna marine terrace provide a good fossil example of a Central Mediterranean infra/circa-littoral setting, characterized by both calcareous coralline algae-dominated low-relief bioherms and biostromes, analogous respectively to the present coralligenous and mäerl habitats. The skeletal primary framework of the bioherms consists of laminar to massive encrusting coralline red algae acting as main bioconstructors, with minor bryozoans, encrusting foraminifera, and serpulids as secondary frame-builders. Whereas the autochthonous mäerl tabular beds are mainly composed of free-branched coralline red algae rudstones. A variable amount of sandy bioclastic sediment is laterally interbedded with the bioconstructions and tends to be entrapped in their cavities and pockets. All sedimentary sub-facies of the bioconstructions and associated sediment are rich in autochthonous syn-sedimentary microbial-mediated micrite, forming aphanitic, peloidal, clotted peloidal, and filamentous fabrics. Microbial micrite can also trap and bind a variable amount of grains or be a secondary component of the sandy detrital sediment with micritic rims surrounding the clasts. All these early-lithified micrites show the typical nanostructure of the primary microbial-mediated carbonates, rather than a detrital mud particles accumulation, as they consist of nanospheres coalescing into subhedral microcrystals, replacing and mineralizing both microbial cells (present with several morphological types) and extracellular substances. This in turn implies the widespread presence of benthic lithifying microbial biofilms that colonized both the cavities of the skeletal framework of the bioconstructions, and the intergranular space of the associated sediment. These microbial communities, thanks to the metabolic processes of the microorganisms that induced the carbonate precipitation, significantly contributed to the early cementation of all the studied deposits.

Keywords*: Late Pleistocene; Bioconstructions; Coralligenous; Mäerl; Micrites; Microbialites.*

7.1 INTRODUCTION

7.1.1 Introduction and Geological framework

Late Pleistocene global climate shifted from the warm Last Interglacial, corresponding to the Marine Isotope Stage (MIS) 5, to the cold Last Glacial (MIS 2) (Shackleton, 1969; Helmens, 2014, and ref. therein). The MIS 5 is considered a good analogue of the ongoing global climate change, as the warmest period is represented by the first substage MIS 5e (ca 125 ky), which was few degrees warmer than today, while, after this peak, the decrease in global temperatures took place with the alternance of two relatively colder periods: MIS 5d (ca 110 Ky) and 5c (ca 100 Ky), and two warmers: MIS 5b (ca 90 Ky) and 5a (ca 80 Ky) (Railsback *et al.*, 2015). MIS 5 climate variations are potentially

recorded in the corresponding geological record, which is considered a good potential archive of data to predict the possible effects of the modern climate change (e.g., Overpeck *et al.*, 2006; Rohling *et al.*, 2008; Antonioli *et al.*, 2017; Albano *et al.*, 2024).

MIS 5 terraced marine deposits widely crop out in the central Mediterranean as well as along the coasts of southern Italy, where they are particularly well exposed along the Ionian Sea coastline around Taranto (Puglia) and Crotone (Calabria) areas (e.g., Amorosi *et al.*, 2014; Nalin *et al.*, 2020; Zecchin *et al.*, 2020). In particular, in the Crotone area five orders of Middle to Late Pleistocene (including a complete MIS 5 warm phases sequence) carbonate-siliciclastic raised marine terraced deposits have been recognized, topping a Neogene-Quaternary sedimentary succession (Gliozzi, 1987) (**Fig. 1A**). The Crotone basin originated during the development of the Southern Italy orogen and is linked to the eastward migration of the Calabrian Arc towards its present-day location, after the opening of the Tyrrhenian back-arc basins (e.g., Critelli, 1999; Zecchin *et al.*, 2012; Critelli *et al.*, 2013, 2017; Gindre-Chanu *et al.*, 2020; Borrelli *et al.*, 2022, 2023a). The five orders of terraces, resulting from the combination of regional uplift (from 0.70 to 1.25 m/ky) and glacio-eustatic fluctuations (Zecchin *et al.*, 2016) are spread along the southern Crotone area (**Fig. 1A**) and are unconformably transgressive on the Piacenzian – Calabrian Cutro marly clay Formation. The Cutro marine terrace represents the first terrace order, being associated with the MIS 9 (Palmentola *et al.*, 1990), or with the MIS 7 (Nalin *et al.*, 2020). The second terrace order is represented by the Campolongo terrace, undoubtedly dated to MIS 5e, while the Capo Cimiti terrace is representative of the third terrace order, probably characteristic of the MIS 5c (Mauz and Hassler 2000; Zecchin *et al.*, 2004; Nalin *et al.*, 2012). The fourth terrace order is found both in the Capo Rizzuto area and along the Capo Colonna Peninsula, which is object of the present work, is considered MIS 5a in age, as revealed by stratigraphic correlations, and aminostratography, U/Th, and optically stimulated luminescence dating (Gliozzi, 1987; Belluomini *et al.*, 1988; Nalin, *et al.*, 2006; Nalin and Massari, 2009; Nalin *et al.*, 2020). However, for the same terrace was also proposed a MIS 5c dating, on the base of other stratigraphic correlations (Palmentola *et al.*, 1990; Zecchin *et al.*, 2004; 2009). Finally, the Le Castella terrace (the fifth and the youngest) was dated at MIS 3 (Bracchi *et al.*, 2016, and ref. therein).

The Capo Colonna terrace extends along a W/O oriented peninsula with a planar surface sloping about 1 degree toward East. The deposits show a maximum thickness of 10 meters and are well exposed along the sea cliff that limits the terrace (**Fig. 1**); they generally are composed by mixed carbonate and siliciclastic deposits that unconformably cap the Cutro marly clay Formation. Zecchin *et al.* (2009) identified two different high frequency transgressive-regressive cycles, the second of which, much better preserved, is the object of this study and. In such second cycle Nalin and Massari (2009) defined a palaeoenvironmental West to East gradient from proximal to distal sedimentary facies, while Bracchi *et al.* (2014) carried out an in-depth palaeoecological and stratigraphical analysis, better defining and characterizing the main autochthonous carbonate deposits, consisting of coralline red algae dominated facies.

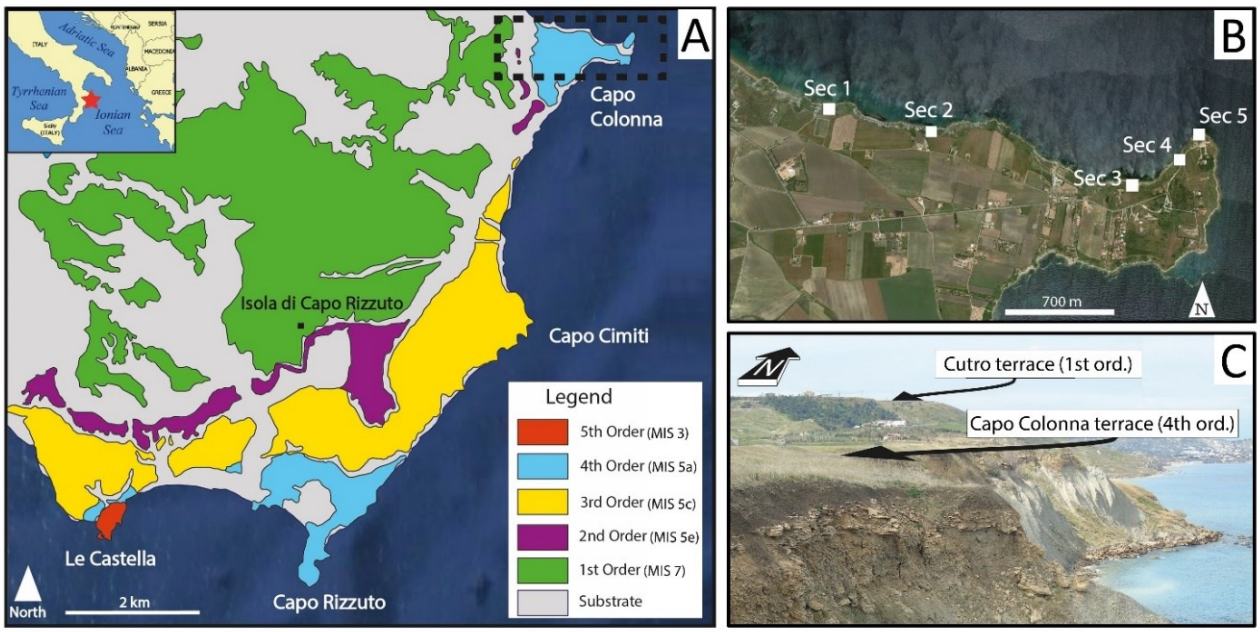

Figure 1. **(A)** Simplified map of the Quaternary marine terraces of the Crotone Peninsula (mod. after Bracchi *et al.*, 2014). The dashed black rectangle represents the area in (B). **(B)** Location of the sampled stratigraphic sections along the Capo Colonna Peninsula. **(C)** Field view of part of the Capo Colonna terrace (object of this study), in the background the Cutro terrace.

7.1.2 Coralline algae facies

Coralline algae (Division Rhodophyta) figure among the main carbonate productors of the Mediterranean Sea since the Pliocene, able to produce relevant (in thickness and extension) carbonate bodies (Basso, 1998; Ballesteros, 2006). They can form free branched to rounded nodules forming bed-form stacks (called mäerl rhodoliths) or can develop as crusts around small hard substrates (praline rhodoliths) that can merge each other resulting in complex large-scale low-relief calcareous buildups (i.e. Coralligenous), whose primary framework is mostly represented by crustose algae (Basso, 1998; Ballesteros, 2006; Bracchi *et al.*, 2014; 2016, and ref. therein). The term "coralligenous" was firstly used by Marion (1883) to indicate hard calcareous formations with calcareous algae and the octocoral *Corallium rubrum,* which gave the name of the biocoenosis. This coral was then regarded as not-diagnostic of this habitat, so the coralligenous was properly defined as a calcareous biogenic formation mainly produced by the encrusting action of coralline red algae and, subordinately, by several other animal taxa (Pérès and Picard, 1964; Ballesteros, 2006; Bracchi *et al.*, 2022).

Mäerl facies is typical of moderate to high energy setting of the circalittoral zone. This habitat can occur as facies of the Coastal Detritus Biocoenosis, but also as the Fine Gravels and Coarse Sands under the Influence of Bottom Currents Biocoenosis. Mäerl biostromal beds are considered "mobile coralligenous", as the stabilization of rhodolite/mäerl beds can led to the development of coralligenous buildups (i.e., de plateau) (Basso, 1998; Relini, 2009).

Typical coralligenous buildups develop from relatively deep subtidal sciaphilic conditions (i.e., circalittoral zone), up to shallower (i.e., infralittoral zone, up to 4 meters; Bracchi *et al.*, 2014). For these reasons, the coralligenous is now regarded as a wider ecological complex, rather than a strictly

defined biocoenosis, hosting several micro- and macro-habitats with a rich biodiversity (i.e., at least 1666 species; Ballesteros, 2006; Bracchi *et al.*, 2014, 2022). Coralligenous biocoenosis can colonizes, other than hard substrates, even mobile substrates that, consequently, after the algal encrusting action, are turned in a new biogenic rocky sea-bottom (i.e., "*coralligene de plateau*" of Pérès and Picard, 1964). Indeed, coralligenous is considered the climax habitat of the circalittoral zone of the Mediterranean Sea, second only to the shallower infralittoral *Posidonia* meadows.

7.1.3 Micrites and microbialites

Micrite is a common component of all the calcareous deposits, both detrital and bioconstructed. Micrite was defined as microcrystalline calcite made of < 4 μm sized calcite particles (Folk, 1959) but, through time, the term was used to indicate mud sized calcites with both a detrital origin (allochthonous micrite, resulting from micro-disarticulation of calcareous organisms, whitings, and bioerosion) and in-situ precipitated (autochthonous micrite), triggered by either biotic or abiotic processes in marine or continental settings (Tucker and Wright, 1990; Flügel, 2004; Riding and Virgone, 2020; Borrelli *et al.*, 2024; Perri *et al.*, 2024a). Autochthonous biologically mediated micrite can originate either by the presence of degrading organic substrates or induced by microbial metabolic activities; in both cases these bio-sedimentary carbonate deposits are defined as *microbialites* (Wolf, 1965; Burne and Moore, 1987; Riding, 2000, 2011). A large variety of microbial taxa and communities are involved in the microbialites formation in many sedimentary systems, spanning from almost totally microbial-produced carbonate factories forming large scale depositional systems, to a minor contribute for example in clastic or evaporitic sedimentary, or diagenetic, environments.

Microbialites were dominant reef builder during the Proterozoic, while in the Phanerozoic they become a component of metazoan-algal (coralgal) reefs (Riding *et al.*, 1991), occasionally representing the main reef builders like in platform margin to slope settings of stressed environments, such as the microbial carbonate factories of the Pennsylvanian (Della Porta *et al.*, 2017), the Tethyan upper Triassic (Perri *et al.*, 2017, 2019; Borrelli *et al.*, 2023b), and the Messinian salinity crisis in the Mediterranean (Borrelli *et al.*, 2021).

The microbialite development in association with modern coralgal reefs was commonly reported as minor microbialitic crusts in cryptic environments (Westphal *et al.*, 2010, and ref. therein). Larger volumes are reported in tropical reefs: as tardive reef overgrowth developed during environmental changes during deglacial sea level rises (Camoin *et al.*, 1999, 2006); as a diachronous development some meters below the living reef zone (Seard *et al.*, 2011); and finally, as coeval and interlayered with coralgal framework in photic zone (Westphal *et al.*, 2010). Microbialitic and skeletal component relationship in reefs is suggested to be mutually advantaging, as the coralgal framework provides suitable environment to be colonized by microbial communities which in turn stabilize and strengthen the reef, also contributing to its volumetric growth (Seard *et al.*, 2011).

The temperate Mediterranean modern bioconstructions are mostly represented by the coralligenous facies, and secondarily by shallow water red algae rims, vermetids trottoirs, polychaetas reefs (Pérès and Picard, 1964). In these low-relief neritic bioherms, the presence and the possible syngenetic role of the microbialites is a topic poorly investigated. In modern living

coralligenous bioconstructions of south Italy, a minor quantity of lithified autochthonous micrite (deriving from microbial activity and degradation of sponge tissues) inside the skeletal framework, was suggested to strengthen the algal framework contributing to the reef development, thanks to their syngenetic cementation (Bracchi *et al.*, 2022; Cipriani *et al.*, 2024).

In addition, the microbial mediated precipitation of micrite can represents the main process responsible for the early cementation of several mobile marine detrital substrates, even in high energetic environments. However, this process is supposed only characteristic of shallow, warm waters of tropical carbonate sedimentary systems (e.g. Diaz and Eberli, 2022, and ref. therein), even if it has been detected also in mid-latitude temperate seas (see *Chapter 6*).

Finally, in the present work, a micro-scale facies characterization of the Capo Colonna red algae dominated deposits is provided. Combining field work with petrographic and SEM-EDS analysis a reconstruction of the depositional and diagenetic history of these MIS 5a/c deposits is proposed, with a specific focus on the role of autochthonous micrite in the development of the bioconstructed facies and associated deposits.

7.2 METHODS

Five stratigraphic sections were measured, described, and sampled, using a stratigraphic/sedimentologic approach along the northern side of the Capo Colonna peninsula (**Fig. 1**). Sections were named, from the west to the east: Section 1 (39.031667 17.174943), Section 2 (39.030375 17.181662), Section 3 (39.026088 17.199457), Section 4 (39.027118 17.202814), and Section 5 (39.029327 17.204958) (**Fig. 1B**). The whole outcrop has a good lateral continuity allowing a good correlation of the measured sections. Sampling was achieved considering the lateral and vertical variability of the deposits attempting, as much as possible, to sample equidistant points along the vertical direction.

40 thin sections were prepared from 34 selected hand samples, following a traditional protocol after resin embedding, and analysed with a traditional petrographic optical microscope (Zeiss, Axioscop - 40). Scanning Electron Microscopy (SEM) was performed at University of Calabria using a ZEISS Crossbeam 350, operating in a range of 5–20 kV with a working distance between 6 mm and 15 mm. Analyses were mainly focused on the micritic microfacies and performed on selected subsamples, both on fresh broken surfaces and thin sections, after carbon coating. During SEM observations the semiquantitative elemental composition of selected points were obtained by an energy dispersion spectrometer (EDS) EDAX OCTANE Elite Plus operating at 20 kV and with a working distance of ca 12 mm. During EDS analysis, C-enriched areas (detected as more C-enriched relative to the uniformly carbon-coated background) were used to check the occurrence of residual organic matter remains.

7.3 RESULTS

7.3.1 Stratigraphic sections

A short description of the measured stratigraphic sections is here reported, along with the logs in Figure 2. In the same Figure 2 the main lateral stratigraphical correlations are also reported, which are discussed in paragraph 7.4.

Section 1 is made of a 3 m thick homogeneous whitish fine sands resting on a thin medium-fine basal conglomerate, in turn overlying the Cutro marly clay Formation (**Fig. 2**; **3A**). The succession does not contain fossils, except rare bioturbations, and randomly shows the presence of sparse centimetric cemented layers. Sands are overlain by a 1 m thick fining upward concave-cross stratified sandstones.

In Section 2 the Cutro marly clay Formation is overlain by a 0.5-1 m thick basal coarse conglomerate, composed of centimetric pebbles in a sandy matrix (**Fig. 2**; **3B**). In the upper part of this level, tabular boulders (up to 40 cm thick and 1 meter wide) occur, consisting of bioclastic sandstones and medium-fine conglomerates with lithodome boreholes (ichnospecies *Gastrochaenolites lapidicus*) along their surfaces, including internal models of *Lithophaga* sp. The following 2 m are composed of millimetric to centimetric thick braided to isolated red calcareous algal crusts, interbedded with discontinuous layers and pockets of bioclastic sandstone that becomes more abundant upward. Above, a 50 cm thick cross-stratified sandstone, rich in gastropods and containing cm-thick very cemented levels, closes the succession.

Section 3 is characterized at the base by the Cutro marly clay Formation followed by a 5-20 cm thick basal conglomerate (**Fig. 2**; **3C**). This latter is overlain by a 10-20 cm thick bioclastic sandstone encrusted at the top by centimetric laminar red algae with common lithodome boreholes. Upward, a domal body ca 1.20 m thick, laterally extending for several meters occurs. It is composed by a dense framework of mostly laminar and crustose coralline algae, and subordinately bryozoans, encrusting and binding bioclastic sediment and many others skeletal component (e.g. serpulids, molluscs, see below). This bioconstructed body (corresponding with the "algal boundstones" of Nalin and Massari, 2009) is laterally interdigitated, and then topped, with sand- to gravel-size cemented bioclastic detritus (containing also large molluscs) with slightly concave upward cross-lamination. The succession continues with another ca 1.2 m thick domal bioconstruction equivalent to the previous one, finally covered by ca 1.2 m thick cross-stratified bioclastic sandstone, rich in terrigenous clasts and fossil traces.

Section 4 starts with a 5-50 cm thick fine shell bed composed of mostly molluscs mixed with a minor clastic conglomeratic component, erosively resting on bioclastic sandstones belonging to the previous depositional cycle of the terrace (Zecchin *et al.*, 2004) (**Fig. 2**; **3D**). The succession continues with few cm thick bioclastic sandstone layers, followed by a well cemented, up to 80 cm thick, reddish coralline algal tabular rudstone (**Fig. 3E**). Upward, a 1.8 m thick bioconstruction, very similar to those in the section 3, dominated by massive red algae crusts, locally accompanied by bryozoan and serpulid colonies, is observed (**Fig. 3F, 3G**). This body passes laterally and upward to the bioclastic sandstone, which is also present in the inter-skeletal cavities of the bioconstructions, containing gastropods, serpulids, and some corals (**Fig. 3H**).

Section 5 erosively lies on the cross-stratified calcarenites belonging to the previous stratigraphic cycle (Zecchin *et al.*, 2004) and starts with a 1 m thick shell bed similar to the section 4 one (**Fig. 2**). Then ca. 2 m of coralline algal bioconstructions, interfingered with coarse sandstone close the succession.

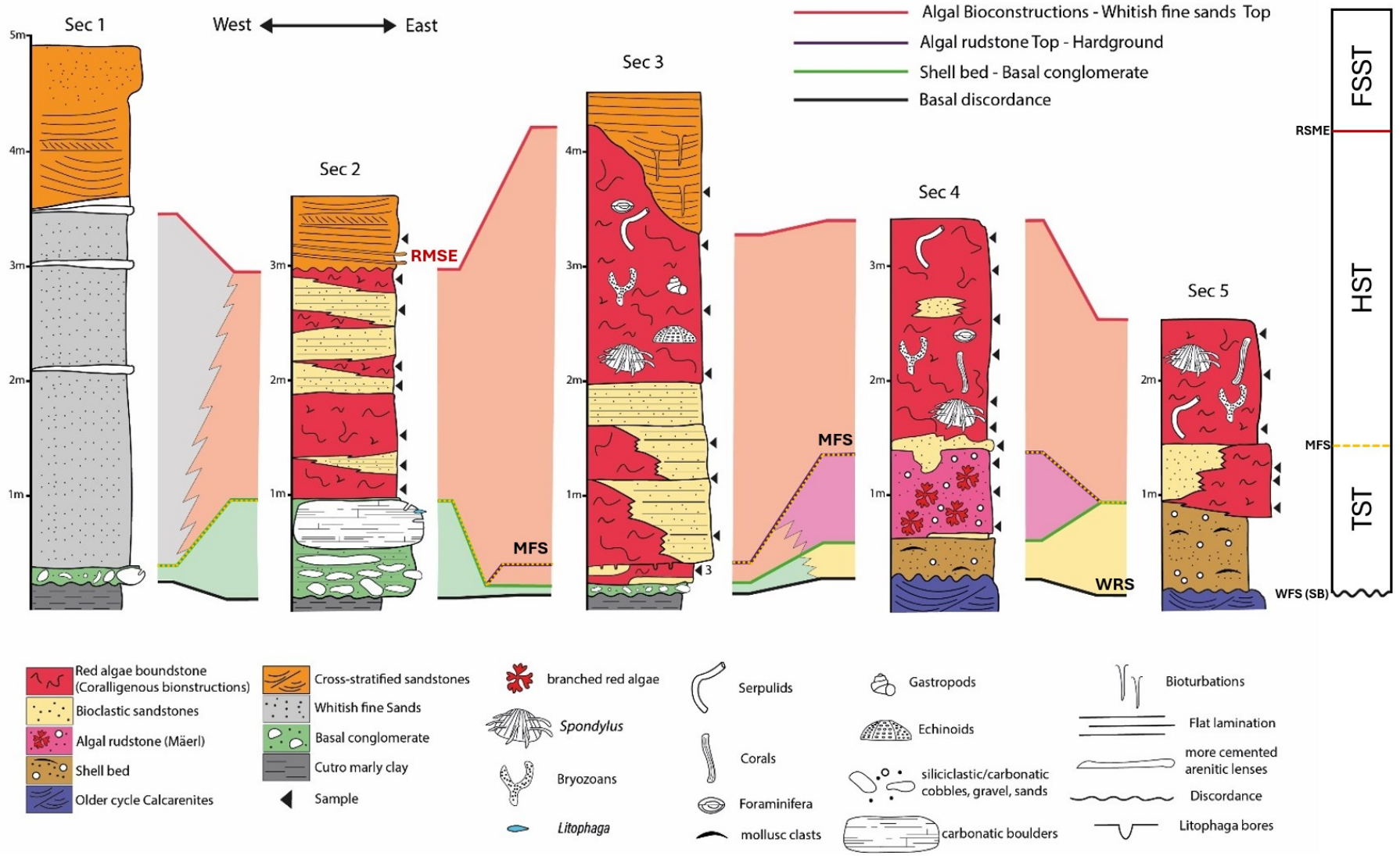

Figure 2. Measured stratigraphic sections along the Capo Colonna terrace outcrops. Lateral correlations are described and discussed in Paragraph 7.4. WFS: wave ravinement surface; MFS: Maximum Flooding Surface; RSME: Regressive Surface of Marine Erosion; TST: Transgressive System Tract; HTS: Highstand System Tract; FSST: Falling Stage System Tract.

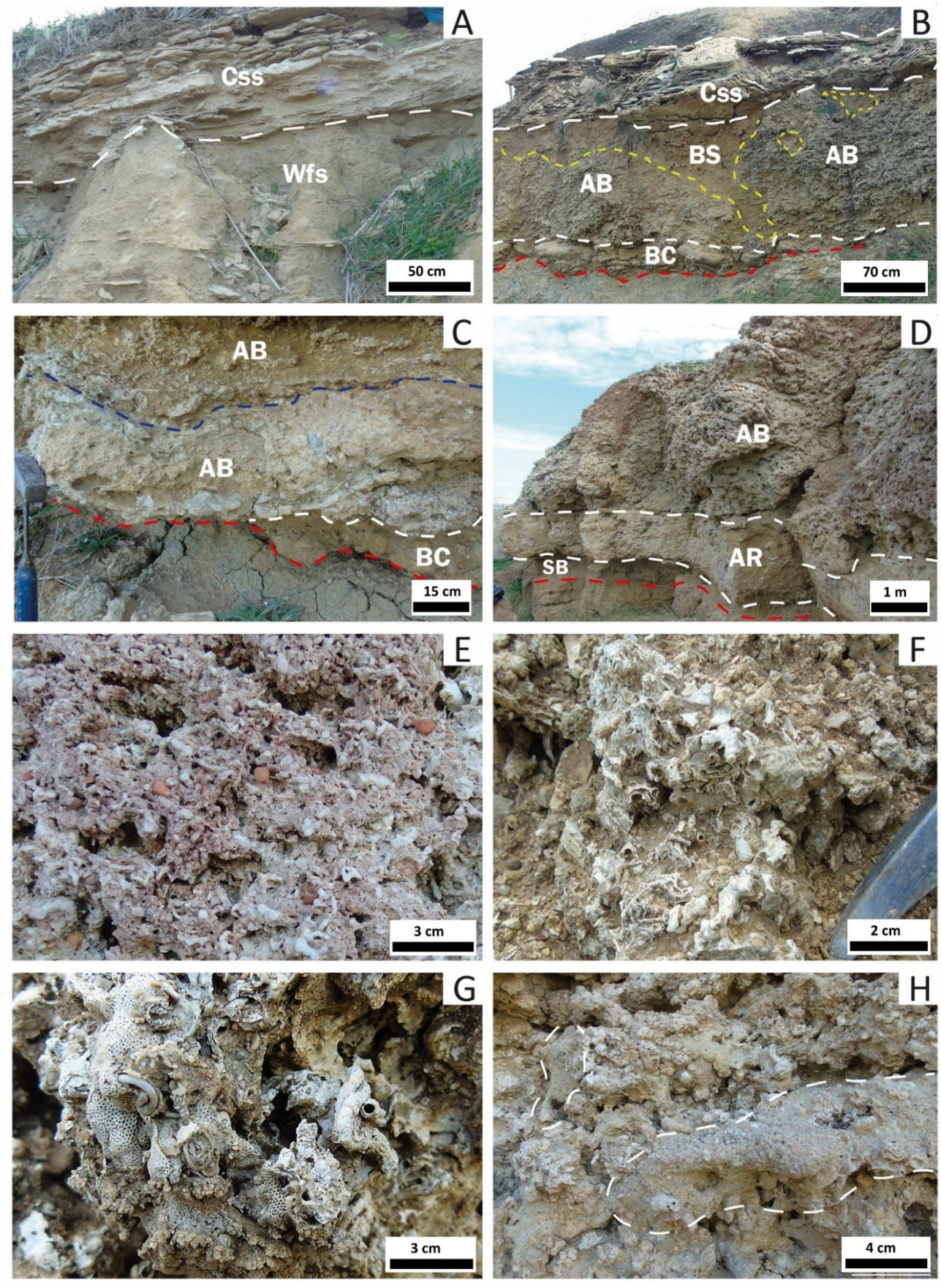
A
Css
Wfs
50 cm
B
Css
BS
AB
AB
BC
70 cm
C
AB
AB
BC
15 cm
D
AB
SB
AR
1 m
E
3 cm
F
2 cm
G
3 cm
H
4 cm

< Figure 3 (previous page). Field views of selected features of the measured stratigraphic sections. **(A)** Detail of the upper levels of Section 1, Wfs (Whitish fine sands), Css (Cross stratified sandstones). **(B)** Section 2: BC (Basal Conglomerate), AB (Algal Bioconstructions) BS (bioclastic sandstone), Css (Cross stratified sandstones), red dashed line indicates the basal unconformity. **(C)** Lower portion of Section 3: BC (Basal Conglomerate), algal boundstones bodies (AB) separated by a discontinuity with lithodome boreholes (blue dashed line). **(D)** Section 4 is composed by the upward succession of: SB (Shell Bed), AR (Algal rudstone), AB (Algal Bioconstructions). **(E)** Algal rudstone (mäerl) facies made of free branched red algae and siliciclastic grains. **(F)** General appearance of red algae bioconstructions of Section 4, with laminar encrusting algae and sediment fillings. **(G)** Detail of crustose and leafy algal crusts with frequent bryozoans (yellow arrow) and serpulids (blue arrow) at Section 5. **(H)** Algal bioconstruction and lateral/cavity filling bioclastic sandstones (areas surrounded by the white dashed line) at Section 4.

7.3.2 Bio-sedimentary facies

A total of 6 main bio-sedimentary facies were defined in the whole succession, after the integration of field work and microscopy analyses (**Tab. 1**). All these facies are here described, including microfacies characterization, which however are mostly focused on coralline calcareous algae bioconstructions.

1) ***Basal Conglomerate (BC).*** This facies, always present at the base of the stratigraphic sequence in the western sections (i.e. Section 1 to 3), lies above an erosional surface representing the base of the terrace succession (**Fig. 3B, C**). This deposit has an irregular thickness, ranging from 0.5 to 1 m. It is characterized by locally overlapped gravel to boulder-size crystalline and calcareous clasts, from generally elongated and flattened to rounded, with a matrix composed by a quartz bearing sandstone rich in bioclasts. This deposit is generally well cemented and can be structureless to rarely flat-laminated.

2) ***Shell bed (SB).*** Shell bed facies is observed in the easternmost sections (Section 4 and Section 5), where it represents the basal layer of the terrace sequence (**Fig. 3D**). It consists of an easily erodible, structureless stratum (up to 1 m thick) composed by a rudstone in which molluscs (especially bivalves *Pecten jacobaeus,* Ostreidae indet., up to 10 cm in size) are the most represented bioclasts, with rarer barnacles, gastropods, branched and reticulate bryozoan fragments, and very rare rhodoliths. The deposit also hosts minor siliciclastic coarse-grained components similar to that of the BC facies.

3) ***Algal rudstone (AR).*** This facies consists of a well cemented, homogeneous, and laterally discontinuous tabular rudstone layer from 40 cm to 80 cm in thickness, observed only in the distal Section 4 above the SB facies (**Fig. 3D**). It is formed by a red algae accumulation, with rare molluscs and bryozoan fragments (**Fig. 3E**). Red algae are essentially free melobesioids forming centimetric nodules with generally branched morphologies and smoothed-edge appearance, belonging to the taxa *Lithothamnion corallioides, Phymatolithon* sp., *Lithophyllum* sp. and *Lithothamnion* sp., as identified by Bracchi *et al.*, (2014), embedded in a gravel- to sand-size siliciclastic matrix. The uppermost part of this body shows erosional pockets filled by

bioclastic coarse sandstone, the bioclasts of which are mostly made of millimetric free branches of red algae with an elongated to rounded shape, bryozoans (i.e., fragments of bilaminate species and of colonies) and foraminifera (mainly benthonic) (**Fig. 4A**, **B**). Molluscs fragments and shells are rare and represented mainly by Pectinidae and Ostreidae or observed as internal models or as empty moulds. Finally, occasional clasts of barnacles, vermetids, serpulids, echinoids, and corals were detected. Terrigenous clasts, which represent a minority component, consist of mono to poly-crystalline mica and quartz, mostly equidimensional and rounded, ranging from coarse sand to gravel, at the base of the layer, to fine sand/silt, in its upper part. The layer is well cemented thanks to the diffuse presence of non-isopachous rims of micritic cement that envelops and binds most of the clasts, both biogenic and terrigenous (**Fig. 4B**) (see also paragraph 7.3.3). Further cementation is provided by sparitic to microsparitic mosaics of calcite cement, frequently occluding the remaining porosity.

This facies can be referred to the Modern counterpart called *mäerl bed* (Bracchi *et al.*, 2014).

4) ***Algal bioconstructions (AB).*** This is a complex bio-sedimentary facies representing the most common type of deposit in the whole studied succession (**Fig. 3B-D**). It is essentially characterized by a dense autochthonous and connected skeletal boundstone dominated by crustose coralline algae - with many others minor skeletal component - which form low-relief build-ups including a variable amount of trapped and bounded detrital sediment. More in detail, red algae form centimetres thick massive to laminated crusts (**Fig. 3F**), while bryozoans (encrusting and branching erect) and serpulids are very frequent, at places forming very dense encrustations (**Fig. 3G**).

Red algae boundstones are dominated by sub-parallel, concentric, to irregular crustose algal thalli of the following genuses/species, as identified by Bracchi *et al.* (2014): dominant *Mesophyllum alternans*, and subordinate *Mesophyllum* sp., *Lithophyllum stictaeforme*, *Lithophyllum* sp., *Lithothamnion minervae*, *Lithothamnion* sp., *Titanoderma pustulatum*, *Titanoderma* sp., *Phymatolithon* sp. .

The algal crusts are commonly separated by thin (sub millimetric – millimetric) micritic and/or terrigenous infilling (see also paragraph 7.3.2) (**Fig. 4C, D**). These crusts are often encrusted by thin (less then millimetric thick) colonies of bryozoans and foraminifera (very common *Miniacina minacea*), and vice-versa, also developing in alternate sequences (**Fig. 4E, F**). Algae thalli are also frequently bioeroded with a variable intensity, as testified by endolithic channels or a network of perforations, up to areas where the original framework is dismantled (**Fig. 5A**). Locally, the red algae framework is replaced by massive (up to centimetric thick) bryozoan zoaria, showing a regular organisation of multi-layered boxy zoecia, allowing to define local bryozoan boundstones (**Fig. 5B**). Well preserved to recrystallized serpulid calcareous tubes are sporadically associated with the red algae boundstones (**Fig. 4D, F**), even if locally they can form dense clusters, resulting in distinct serpulid boundstones (**Fig. 5C**).

The skeletal cavities of bryozoan zoaria and serpulid tubes are often partially or totally occupied by micrite, which occurs as geopetal infill concordant with the polarity of the section, or with a pendant structure (**Fig. 5C**; see also paragraph 7.3.3 and **Fig. 7B**).

In addition to skeletal boundstones, in this facies rarer microbialites have been detected. They consist of microscale (< 1 mm) flat crusts and micro mounds, composed of micrite with typical microbial fabrics, which are illustrated in detail in the paragraph 7.3.3, developed over the skeletal boundstone and the sediment.

The build-ups contain also common molluscs, such as large specimens of the sessile epifaunal *Spondylus gaederopus,* also observed both in life position (encrusting valves and articulate shells). Apart from bryozoans and serpulids, other sessile invertebrates are represented by Vermetidae indet., Scleractinia indet. (solitary corals), *Cladocora caespitosa* loose corallites and rare small colonies. Finally, regular echinids (fragments and complete tests) are also observed.

The AB facies contains irregular to lenticular cavities and pockets, both at the macro-scale (e.g., decimetric detrital infills) and at the microscale (e.g., sediment infilling the micro-cavities generated by inter- and intraskeletal cavities that constitute the skeletal framework). The filling sediment is a mixed bioclastic and terrigenous sandstone, containing a variable amount of fine gravels and silt, grain- to mud-supported, in which crustose red algae fragments represent the most abundant bioclasts. These sediments are analogous to those found in lateral contact with the bioconstructions (i.e., bioclastic sandstone facies, see below).

The above-described facies have been indicated as equivalent of the Modern *coralligenous reefs* (Nalin and Massari, 2009; Bracchi *et al.*, 2014).

5) ***Bioclastic sandstones (BS).*** Fine to coarse sandy and gravelly bioclastic sediment, more or less cemented by a micritic matrix, is associated with the red algae build-ups. This sediment results particularly abundant where the algal buildups are discontinuous (**Fig. 3B**), and generally shows a flat to low-angle cross lamination and interdigitations with the build-ups themselves (**Fig. 3H**). Moreover, such bioclastite also constitutes macro and microscale infillings of the algal boundstone cavities, resulting widespread in the boundstone framework. As the texture varies from grain- to mud-supported, the facies can be further characterized as grainstone-packstones and packstones more frequently, and wackestone-mudstones rarely.

Grainstone/packstone (**Fig. 5D**, **E**), is mostly found in lateral contact with the bioconstructions and are dominated by irregular and rounded fragments of the same crustose thalli forming the build-ups primary framework, together with bioclasts of bivalves, gastropods, bryozoan, foraminifera (both benthic and planktonic forms), rare echinoid radiola and serpulid fragments. The terrigenous clasts are represented by micas and quartz, equidimensional and rounded, while the porosity is mostly filled by sparite and microsparite (**Fig. 5D**, **E**). Packstone sediments are also found both within the bioconstruction cavities and surrounding them (**Fig. 5F**). The micritic matrix shows mostly an aphanitic/micro-peloidal fabric. Moreover, the terrigenous content is relatively common and is made of quartz, micas, lithic fragments, and rare heavy minerals (i.e., highly birefringent metamictic zircons) ranging from medium-fine sand to silt size. Erosive cavities and channels in packstone, and adjacent boundstone framework are filled by new generations of such sedimentary inputs (**Fig. 6A, B**), containing intraclasts of the same packstone (**Fig. 6C**) suggesting very early lithification. Wackestone-Mudstones show an aphanitic/micro-peloidal fabric of micrite analogous to those found in the packstone (see also paragraph 7.3.3 for details) (**Fig. 6D**).

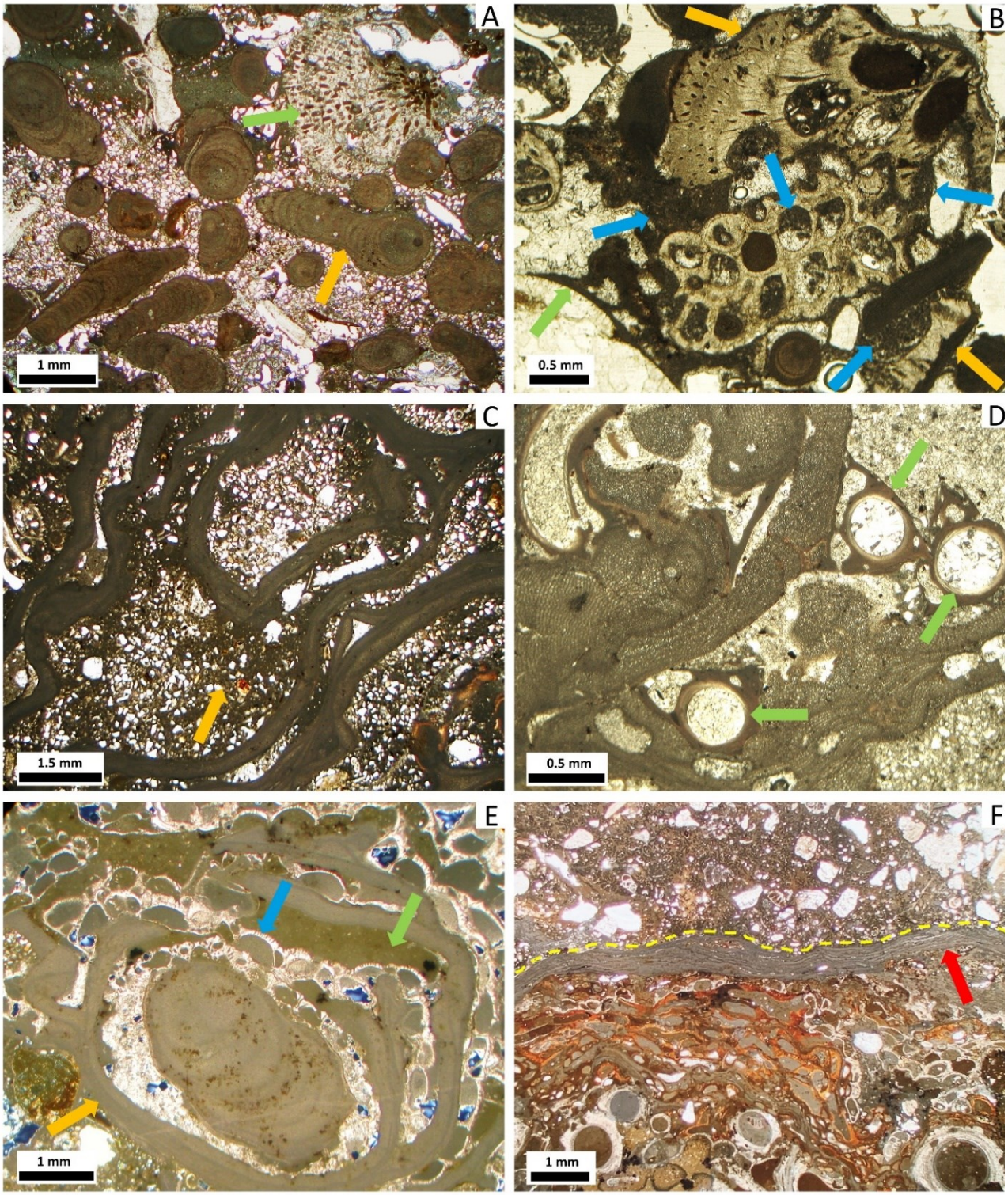

Figure 4. (A) Algal rudstone (mäerl facies): free red algae branches (yellow arrow), bryozoan bioclast (green arrow). **(B)** Detail of algal rudstone; note the discontinuous micritic rims around the quartz grain (green arrow) and bioclasts (yellow arrows), and peloidal micrites (blue arrows). **(C)** Red algae boundstone: algal thalli crusts with packstone detritus (yellow arrow). **(D)** Algal crusts with serpulids (green arrow) and grainstone-packstone infill. **(E)** Red algae crusts (yellow arrow) with encrusting foraminifera (blue arrow) and micritic (green arrow) and microspar infill. **(F)** Algal boundstone, surrounded by an algal crust (red arrow) defining the boundary with an external packstone sediment (yellow line).

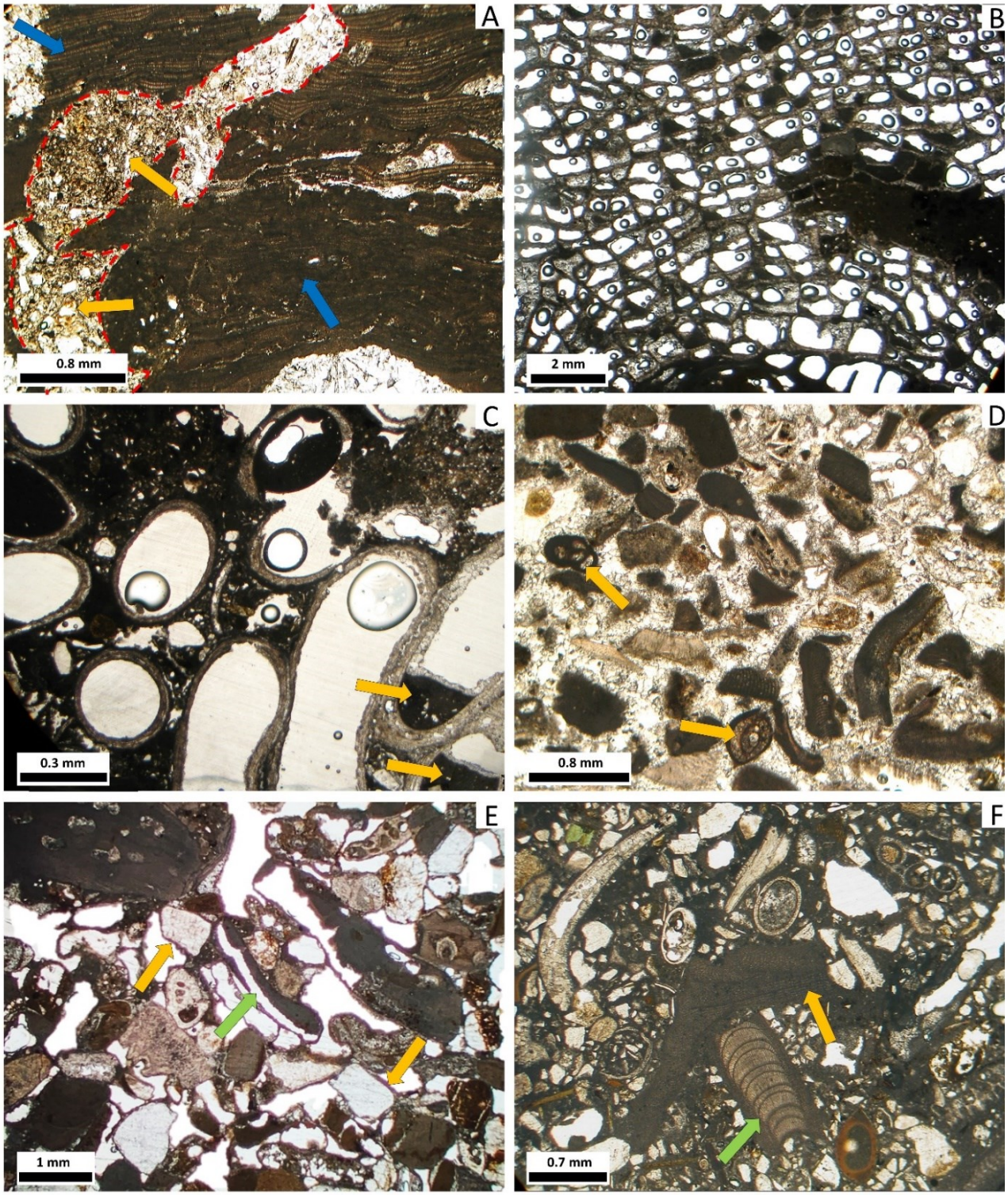

Figure 5. (A) Bioeroded red algal boundstone (blue arrows) with grainstone/packstone (yellow arrow) filling a bioerosional channel (red dashed line). **(B)** Bryozoan boundstone made of box like encrusting bryozoan partially filled by aphanitic micrite. **(C)** Serpulid boundstone with geopetal micrite infill (yellow arrows). **(D)** Grainstone associated with the bioconstruction: note benthic miliolid foraminifera (yellow arrow). **(E)** Grainstone associated with the bioconstruction, note micritic rims (yellow arrows) and dissolution voids (green arrow). **(F)** Packstone associated with the bioconstructions; encrusting algal fragment (yellow arrow), articulated algae fragment (green arrow).

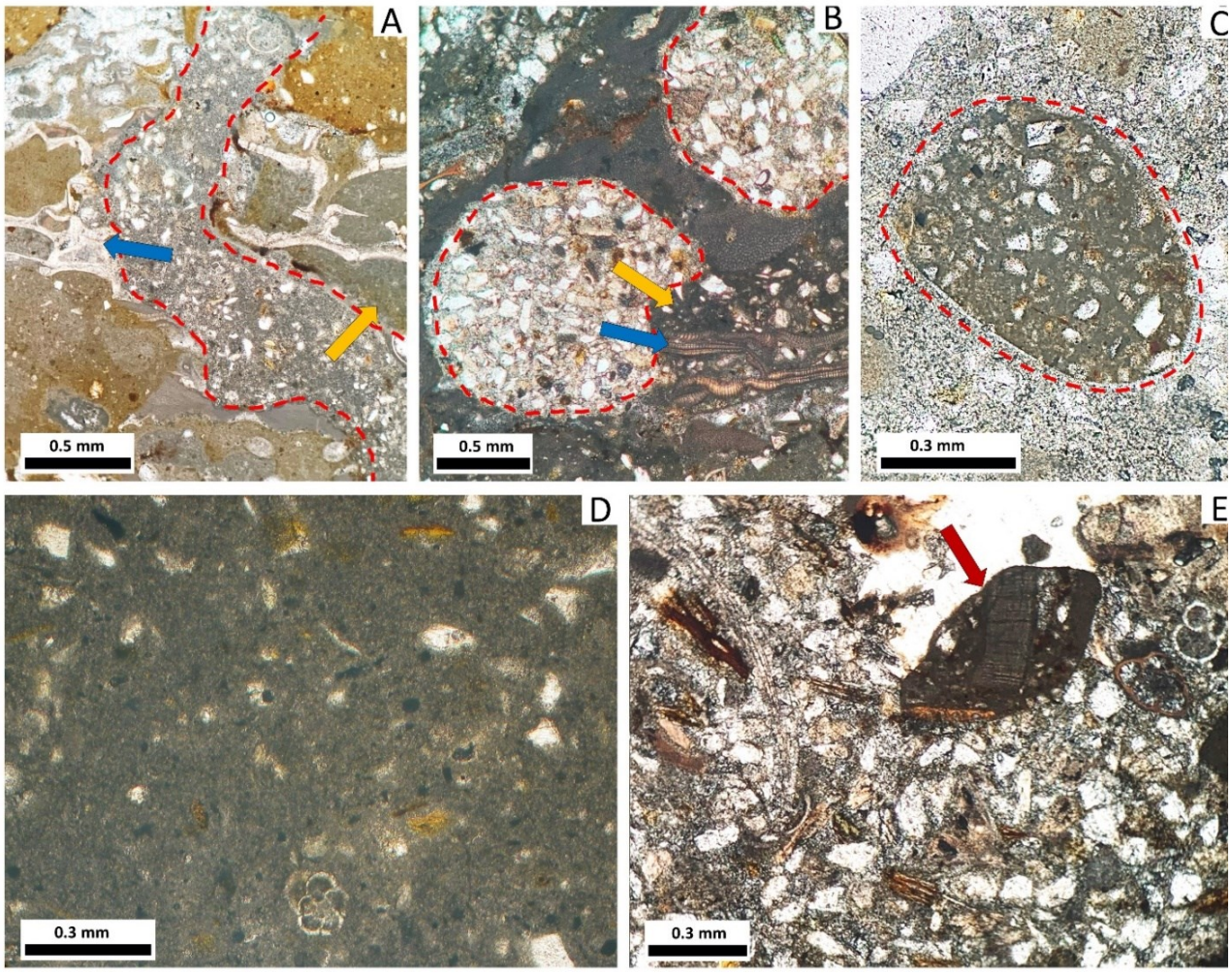

Figure 6. (A) Longitudinal section of a bioerosion channel (red dashed line) developed in the algal bioconstruction framework (blue arrow) and associated cemented packstone (yellow arrow). **(B)** Transverse sections of bioerosion channels (red dashed lines) developed in the algal bioconstruction framework (blue arrow) and associated cemented packstone (yellow arrow)**. (C)** Intraclast composed of packstone (red dashed line) within the sediments associated to the skeletal boundstone. **(D)** Aphanitic/micro-peloidal micrite in wackestone pocket. This latter is within the packstone associated with the bioconstruction framework. **(E)** Grainstone-packstone with an algal boundstone intraclast (red arrow) in the cross stratified sandstones.

Complete fossil shells of molluscs are very common in the bioclastic sandstones, e.g. valves of *Spondylus gaederopus, Manupecten* cf *pesfelis*, *Anomia ephippium*, *Venus verrucosa*, *Plagiocardium* sp., abundant *Bolma rugosa* and relative operculi, *Cerithium* sp.*, Bittium* sp., *Conus* sp., *Lima* sp., and Turridae indet., and other small gastropods.

6) ***Whitish fine sand (Wfs).*** This facies consists of loosely cemented, medium to fine whitish sand meter-thick beds. These beds generally appear massive and barren, with occasional slightly cemented layers measuring a few centimetres. Vertical burrows are locally observed (**Fig. 3A**).

7) ***Cross-stratified sandstone (Css).*** This facies consists of fine to medium bioclastic sandstone characterized by trough cross stratification, often cut by vertical burrows. The sandstone contains sparse large disarticulated *Glycymeris glycymeris* valves, *Spondylus gaederopus,* Ostreidae, and *Bolma rugosa,* the latter especially found in erosive pockets developed on the top of the AB facies. The texture varies from grainstone to packstones (**Fig. 6E**). The bioclasts are mostly composed of red algae boundstone reworked clasts, bivalves, benthic and planktic foraminifera. The terrigenous clasts are mostly represented by polygonal to rounded quartz grains.

	Facies	***Description***	***Micrite fabric***
BC	*Basal conglomerate*	Structureless to flat laminated, gravel to boulder sand-supported level.	*Not investigated*
SB	*Shell bed*	Structureless bioclastic and gravelly sand-supported level.	*Not investigated*
AR	*Algal rudstone (mäerl)*	Structureless rudstone dominated by free branched red algae, with sand to gravel terrigenous clasts.	Micritic rim cement, peloidal micrite
AB	*Algal bioconstruction (Coralligenous)*	Massive to lenticular shaped skeletal boundstones, dominated by encrusting calcareous red algae, associated with bryozoans, serpulids, and foraminifera; the bioconstructed bodies are rich in cavities, surrounded and filled by bioclastic sandstones.	Peloidal, clotted peloidal, filamentous, aphanitic/micropeloidal micrites
BS	*Bioclastic sandstones*	Bioclastic and terrigenous mixed sands to gravels lateral to the bioconstructions and filling its major cavities and the micro-scale framework spaces. Texture ranging from grainstone, packstone, and locally wackestone-mudstone enclaves.	Aphanitic/micro-peloidal, micritic rim cement
Wfs	*Whitish fine sands*	Homogeneous structureless unconsolidated sand with rare bioturbations and thin cemented levels.	*Not investigated*
Css	*Cross stratified sandstones*	Bioclastic grainstone-packstone rich in terrigenous clasts with cross stratification and vertical borings.	Aphanitic/micro-peloidal micrites, micritic rim cement

Table 1. Bio-sedimentary facies summary.

7.3.3 Micrite and cements

In the studied deposits the micritic component is widespread, and especially present in all the coralline algae bearing facies, like the algal rudstone (mäerl) and the algal bioconstructions (coralligenous) with related sediments (bioclastic sandstones). Several types of micritic fabrics and structures have been distinguished and illustrated in this paragraph; all with a possible microbial mediated genesis and an early cementation, as discussed successively in the paragraph 7.4.

In the coralligenous bioconstructions, the most common micrite fabrics vary from peloidal to clotted peloidal, and aphanitic/micropeloidal, more rarely filamentous.

Peloidal micrite consists of about 50-100 µm in diameter rounded to slightly elongated peloids, commonly infilling the skeletal cavities where it can trap and bind detrital allochthonous sediment (**Fig. 7A**), or even forming pendant bodies from the upper surface of micro-cavities in the algal boundstone (**Fig. 7B**). Moreover, this type of micrite was found also in some enclaves of the red algae rudstone facies (**Fig. 7C**).

The clotted peloidal fabric is characterized by micro-peloidal micrite clots, with less defined contours and a denser pattern than the peloidal fabric, locally observed as fillings of boundstone facies cavities (**Fig. 7D**). Furthermore, clotted peloidal with a variable amount of aphanitic micrite is sometimes observed containing accumulations of recrystallized monoaxon and triaxon calcareous sponge spicules (**Fig. 7E, F**). Clotted peloidal micrite is also the main fabric of intra-cavities micro mounds relatively common in the algal boundstone. These consist of 1-2 mm thick isolated or adjacent bodies with an irregular outline, overgrowing and enveloping the skeletal framework surfaces (**Fig. 8A-C**). A filamentous fabric of micrite can be locally detected in such microfacies (**Fig. 8B**).

More extended flat microbialitic crusts with a filamentous fabric (**Fig. 8D-F**) are frequently observed in the algal boundstone facies. These micritic crusts show thicknesses of 100-150 µm, are composed of homogeneous micritic borders extending inward as irregular micritic tubules, reminiscent of a filamentous fabric, and by a microsparitic to micropeloidal micritic inner part. These micro-crusts are frequently observed on the crustose algae surfaces, forming with them alternate sequences, or developing along erosional surfaces cutting algal framework and associated packstones (**Fig. 8D, E**). In turn, these crusts are locally encrusted by foraminifera colonies. The filamentous fabric observed in such crusts consists of micritic rod-like structures, with diameter comprised between 5 and 10 µm comparable to bacterial microfossils for morphology and size (**Fig. 8F**) (see also paragraph 7.4).

The aphanitic/micro-peloidal micrite is common in packstones and in the boundstone sedimentary infills; the fabric varies from structureless aphanitic micrite passing to distinguishable micro-peloids (**Fig. 6D**).

Micrite is also widely present in all the facies as dark micritic rims made of microcrystalline crusts developed as envelopes around all types of clasts and calcareous skeletal frameworks, showing variable thicknesses < 100 µm (**Fig. 9A-C**). In the algal rudstone (**Fig. 4B**; **9B**) these cements are more evident and envelop the majority of bioclastic and terrigenous clasts, making also bridges among them, and representing the main primary (i.e. synsedimentary) cement. Sometimes, dissolved bioclasts presence is testified by these external micritic rims, evidently more resistant to the diagenetic dissolution (**Fig. 5E**; **9B**). These micritic rims, when present, predate any other type of microbialitic pore infilling (**Fig. 9B**; **5E**). Finally, when developed around carbonate bioclasts, these rims often make transition with a progressively inward micritization front, resting indistinguishable from the micritized skeletal part (**Fig. 9C**). Moreover, both these micritic rims and the associated micritized part, are equal to the micritic rims precipitated over unaltered grain surfaces, including siliciclastic grains (**Fig. 4B**; **5E, F**).

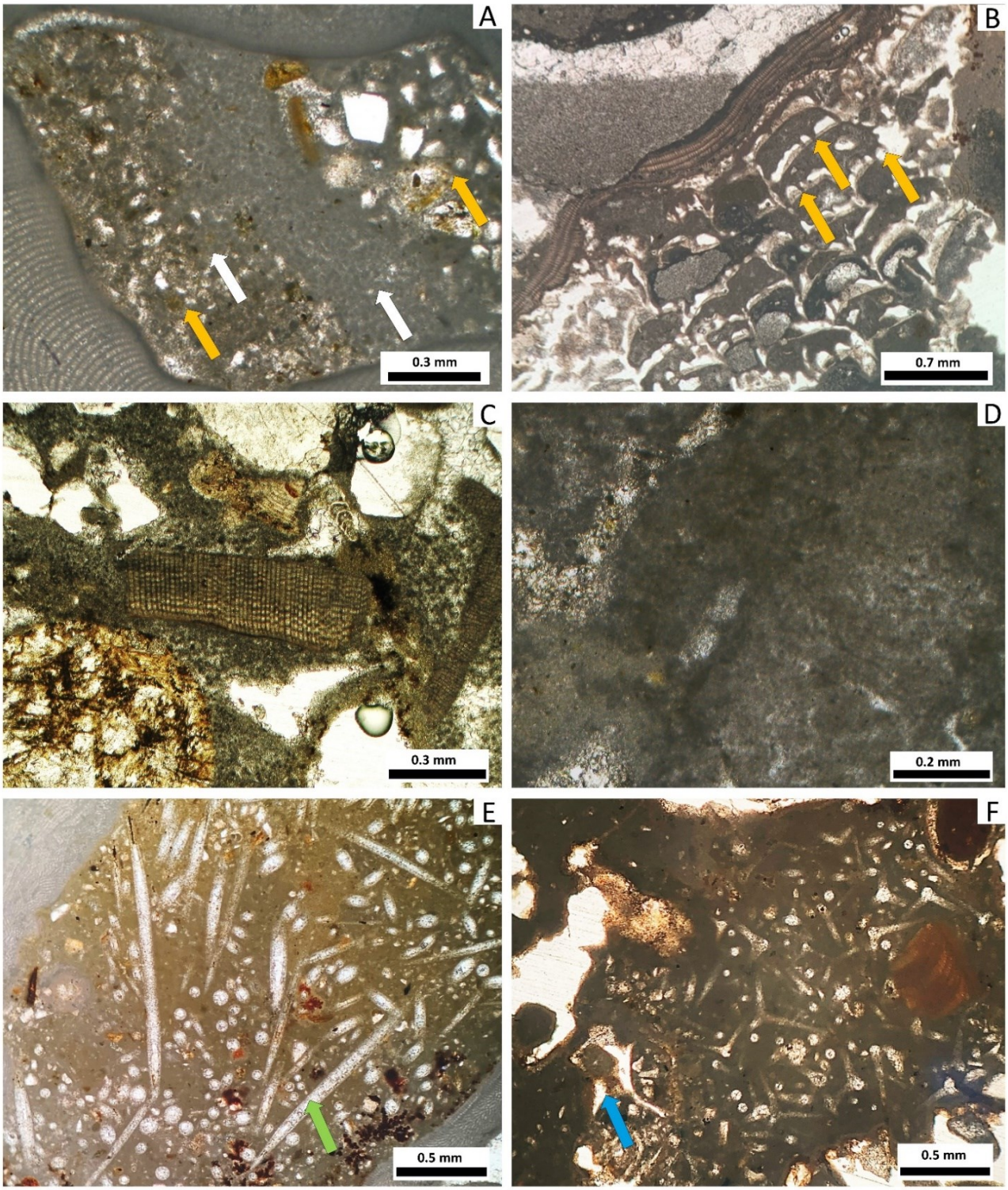

Figure 7. Fabrics of micrite. **(A)** "Pure" peloidal micrite (white arrows) with trapped sediment (yellow arrows) filling a cavity between red algal thalli. **(B)** Peloidal micrite pending inside bryozoan zoecia (yellow arrows). Compare with the geopetal structure on the top of the picture indicating the top direction. **(C)** Peloidal micrite in the algal rudstone (maerl) facies binding terrigenous and biogenic clasts. **(D)** Detail of clotted peloidal micrite in a boundstone cavity. **(E)** Sponge spicules associated with clotted peloidal micrite (green arrows). **(F)** Sponge spicules associated with aphanitic micrite (blue arrow).

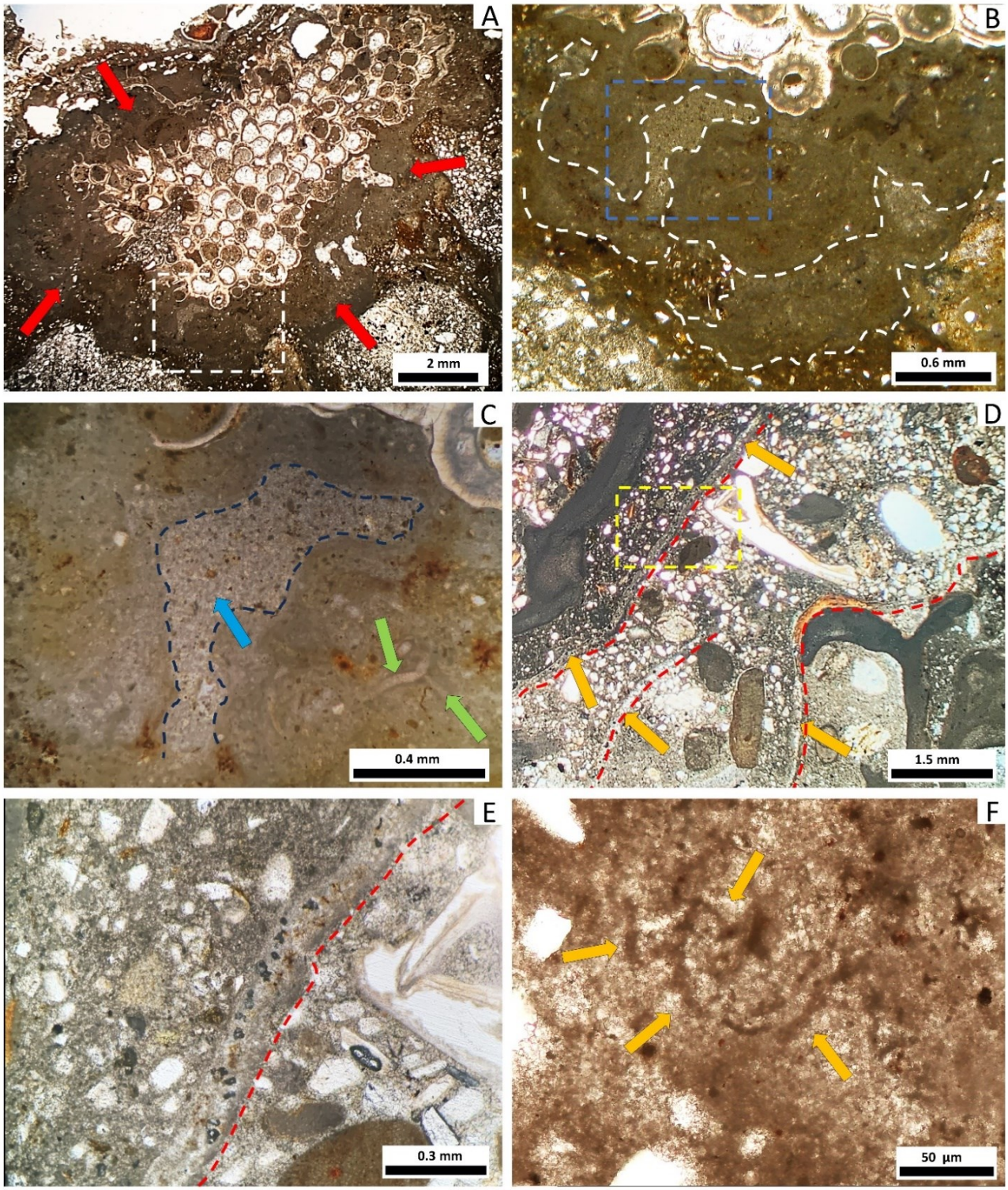

Figure 8. Fabrics of micrite. **(A)** Micro-mound microbialite (red arrows) developed over a bryozoan in the algal boundstone. White rectangle: see Fig. B. **(B)** Detail of fig. A., showing micro-mounds morphology (white dashed lines). The blue rectangle represents the field of fig. C. **(C)** Detail of Fig. B, showing a clotted peloidal fabric with sparse micritic filaments (green arrows) in the micro mounds, and a micropeloidal micrite interposed between the micro mounds (blue arrows). **(D)** Microbialitic crusts (yellow arrows) developed on erosive surfaces on algal thalli and associated sandy sediment (red dashed lines). Yellow rectangle location of Fig. E. **(E)** Detail of fig. D showing a peloidal/microsparitic composition of the crusts. **(F)** Micritized filaments (yellow arrows) immersed in micropeloidal micrite and microsparite within a microbialitic crusts.

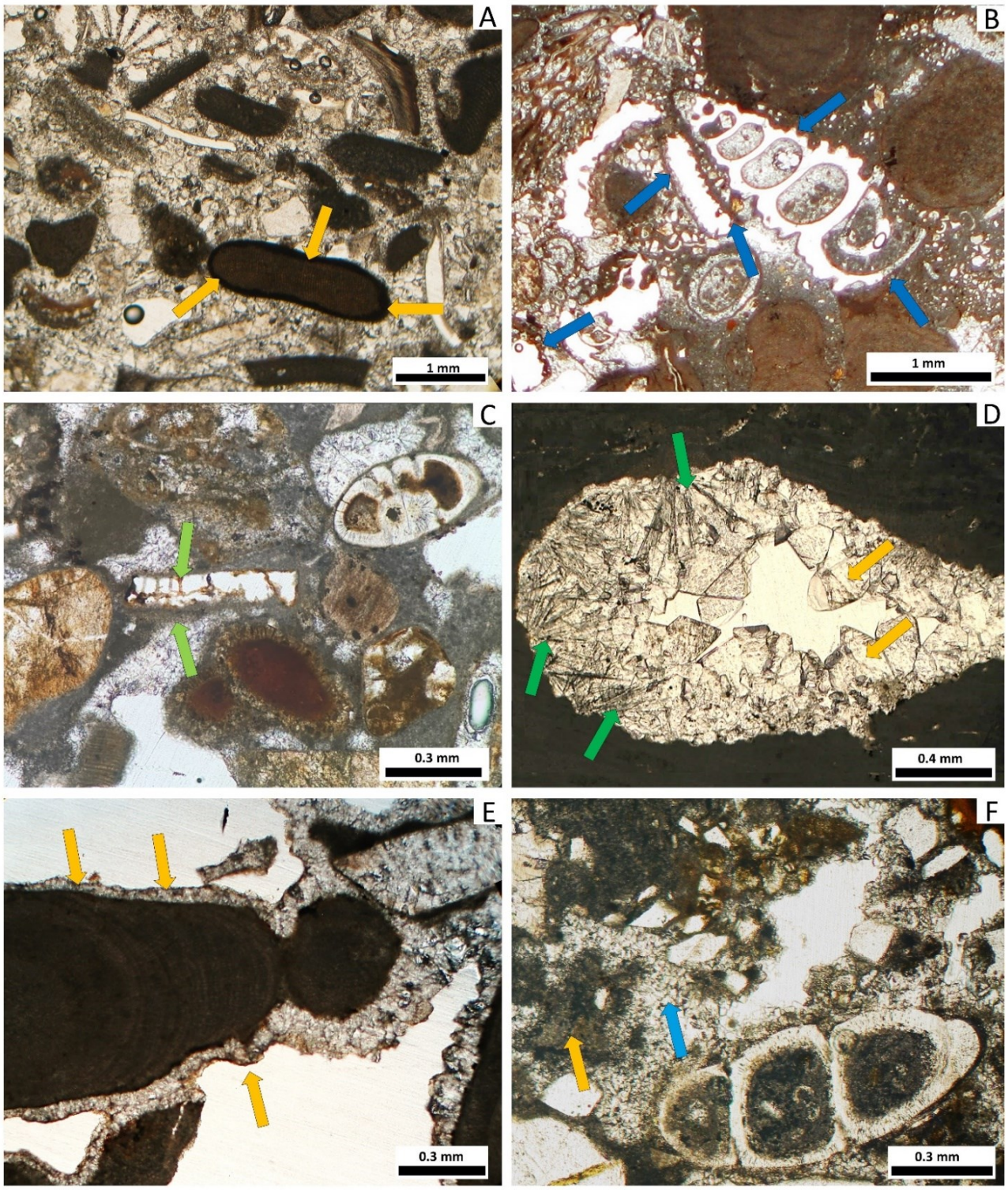

Figure 9. (A) Well developed micritic rim around an algal fragment (yellow arrows). **(B)** Micritic rims (blue arrows) around "phantom" dissolved molluscs and bioclasts**. (C)** Micritized and then dissolved bioclast making transition to micritic cement. **(D)** Primary prismatic cements relicts (green arrows) and secondary dogtooth/mosaic overgrowth (yellow arrows) in a void. **(E)** Dissolution and pseudo straight rims (yellow arrows) developed on secondary cements. **(F)** Micrite (yellow arrow) to microsparite (blue arrow) aggrading neomorphism in the packstone filling the buildups.

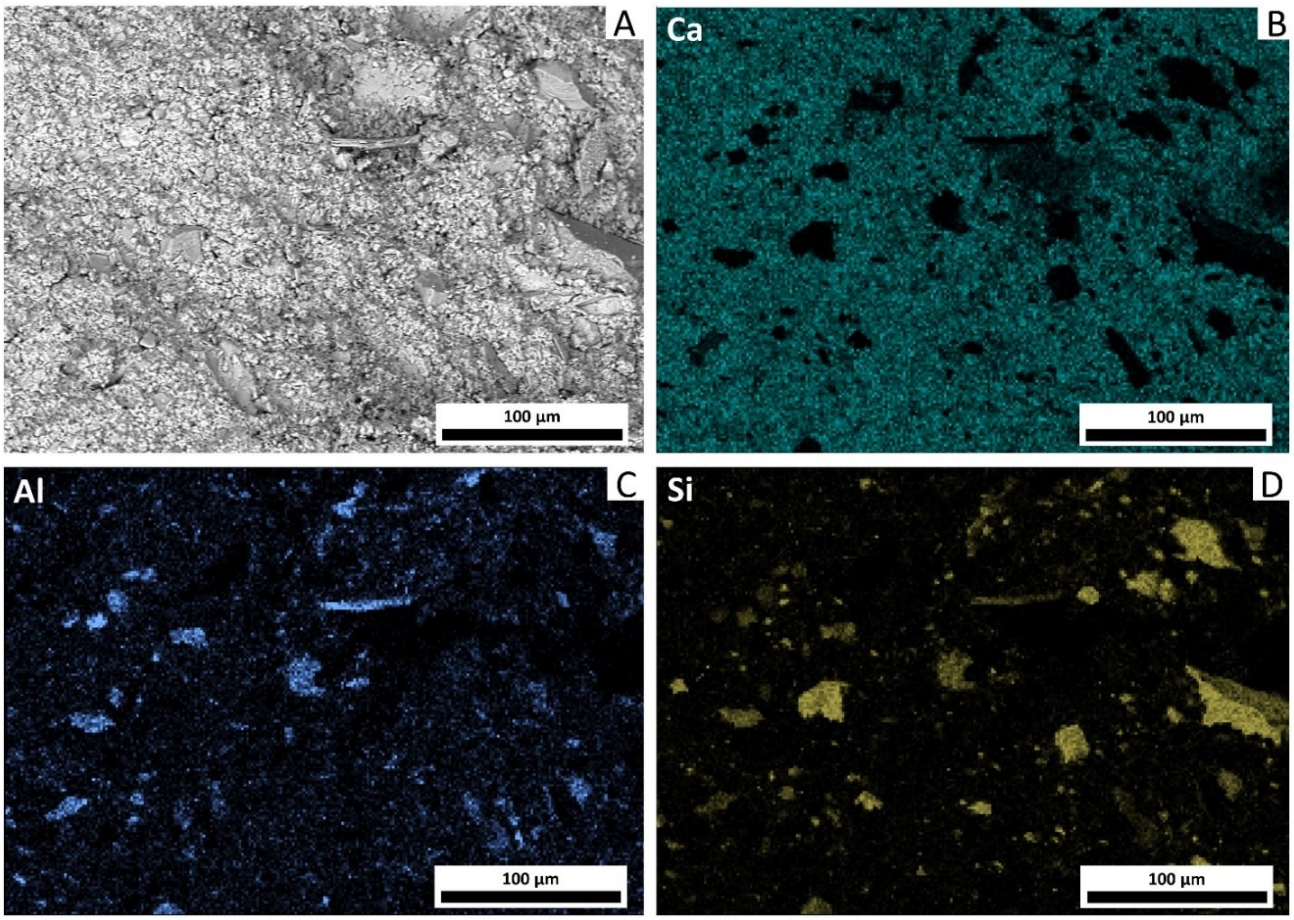

Figure 10. SEM-EDS images of the micrites (**A)** Selected area of the micrite, showing the presence of autochthons Ca carbonate micrite matrix **(B),** and scattered Al and Si (F) terrigenous clasts (**C** and **D**).

7.3.4 Non micritic cements

Rare relicts of primary marine botryoidal carbonate cements are observed (Fig. 9**D**). Conversely, secondary, relatively limpid pyramidal "dogtooth" and mosaic cements are frequently observed, partially to completely filling primary and secondary porosity across all the microfacies (Fig. 9**D**). In some cases, the external outline of dogtooth cement is partially etched, which implies circulation of aggressive water (Fig. 9**E**). In several localized areas in the algal rudstone and bioconstructions, the micrite fades to microspar suggesting neomorphic recrystallization (Fig. 9**F**).

7.3.5 Ultrastructure and composition of micrite

Despite the variety of the several described micrite types among the different facies, their ultrastructure (observed by SEM) shows substantial equal compositional and morphological features.

EDS-derived chemical elemental maps of the micrite show a homogeneous distribution pattern of Ca representing the calcareous micrite (Fig. 10**A, B**) that often surrounds, tens of micrometre-large, areas composed mainly of Si and Al (Fig. 10**C, D**). These last areas correspond with detrital siliciclastic grains (such as micas and other silicates) encased in the micrite background. The micrite is generally composed of low Mg-calcite with 1 to 4 moles % of Mg.

Micrite is constantly made of tightly packed anhedral to euhedral calcite crystals ranging in size between 1 and 4 µm (Fig. 11**A**), much smaller in comparison with terrigenous grains. Larger micrite crystals tend to develop the euhedral habitus in respect to the smaller ones that are instead

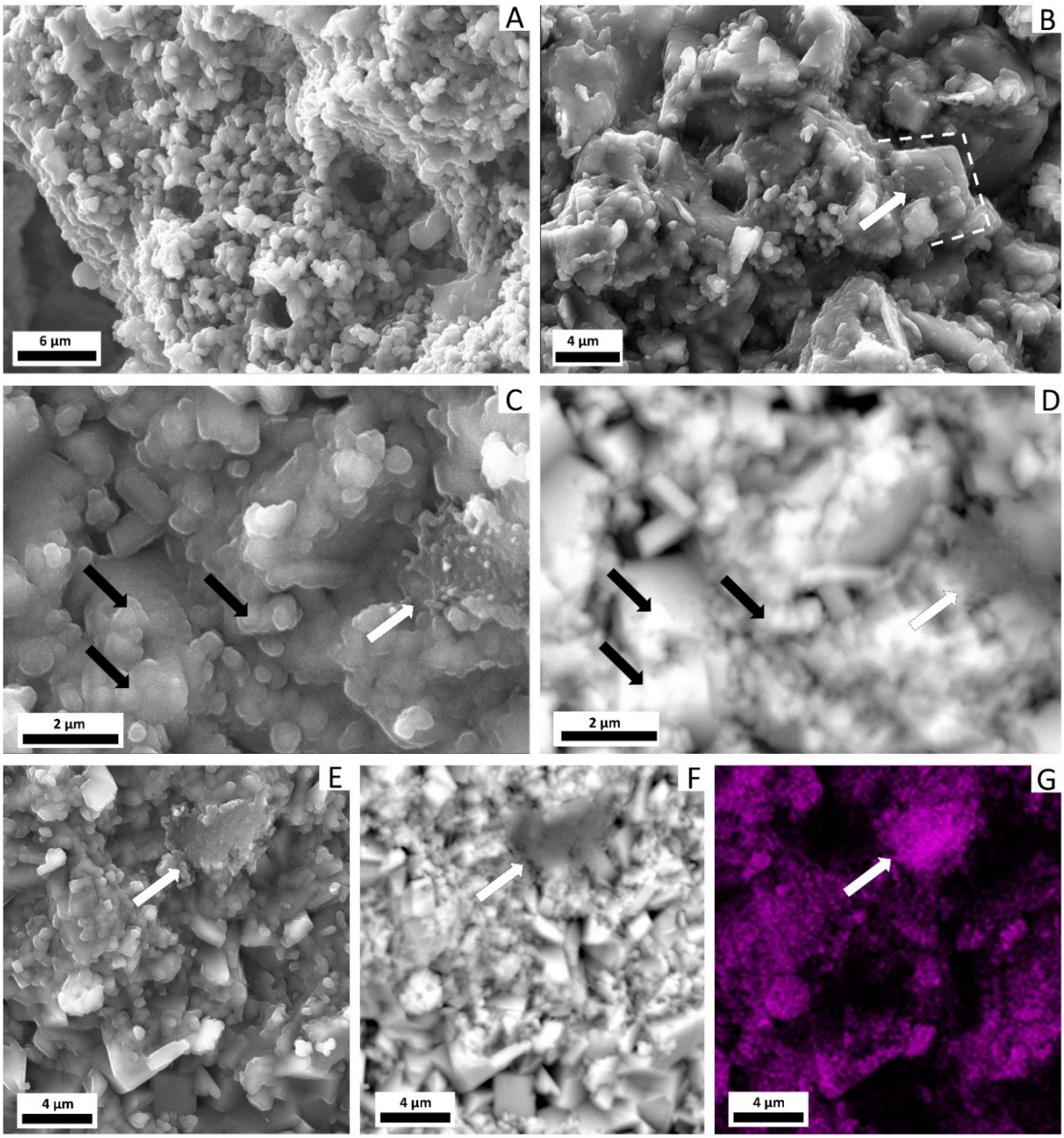

Figure 11. Ultrastructure of micrite in SEM. **(A)** Typical aspect of the micrite composed of packed 2-4 µm sized crystals. **(B)** Close-up view of micrite crystals showing anhedral smaller crystals (white arrow) passing to subhedral larger crystals (black arrow). **(C)** Micrite crystals ultrastructure composed of aggregates of nanospheres (dark arrows). Note organic matter remains (white arrow) partially mineralized by the mineral nanospheres. **(D)** Backscattered SEM view of the same field of (C) in which nanospheres and organic matter remains (are better distinguishable as their difference of density. **(E-F)** Further organic matter remains (withe arrow) in secondary and BSE SEM view. **(G)** EDS map showing the distribution of C, evidencing a relative enrichment in the area corresponding to the organic matter remain seen in Fig. E and F.

generally anhedral (Fig. 11**B**). More in detail, micrite crystals show a particular sub-crystal ultrastructure consisting of aggregates of subspherical nanocrystals in the range of 100 to 300 nm (henceforward called nanospheres) (Fig. 11**C, D**). Furthermore, micrite include diffusively dispersed

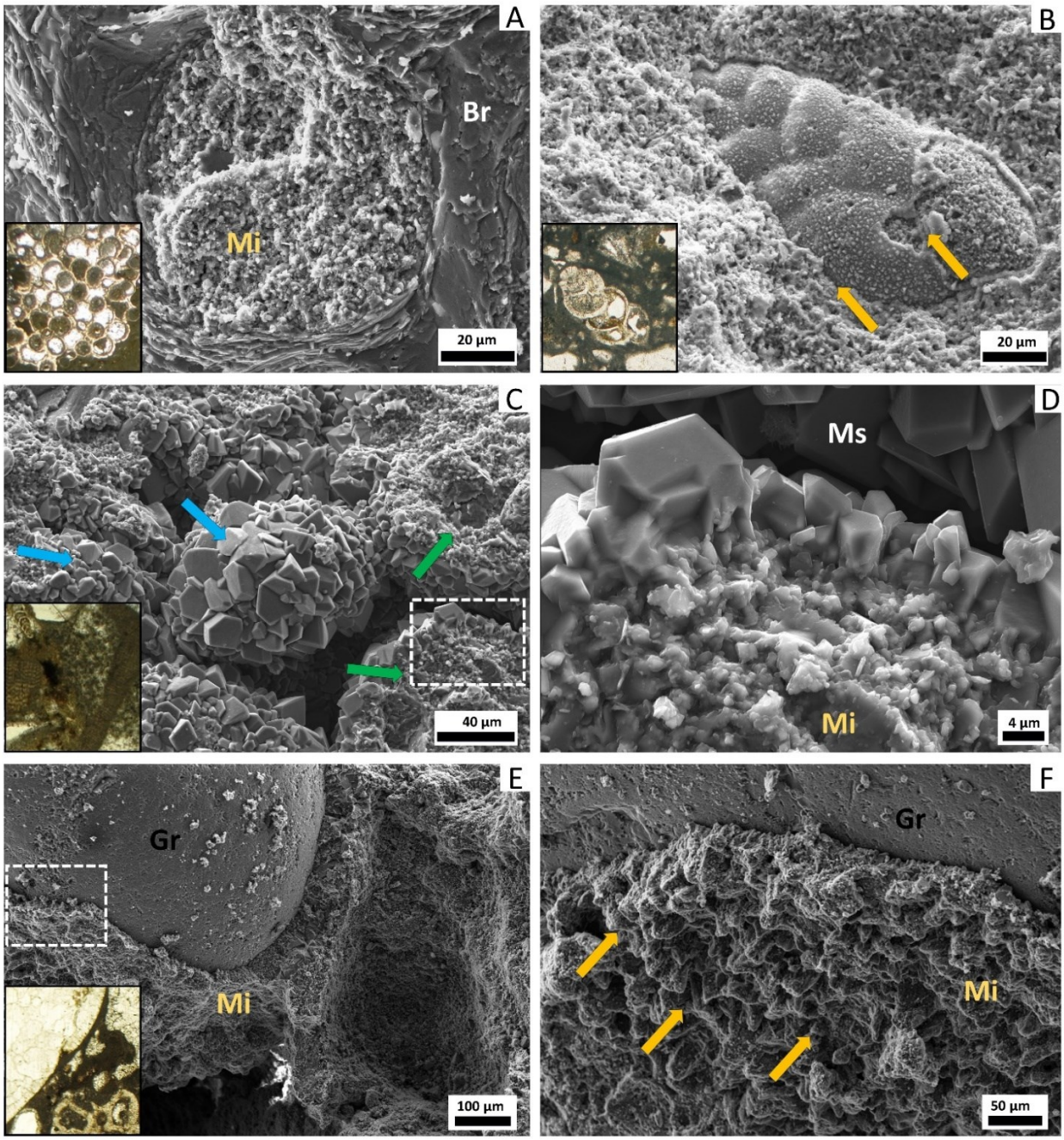

Figure 12. SEM views of micrites. In the small picture the equivalent petrographic microfacies. **(A)** Fossil bryozoan (Br) in the skeletal boundstone with zoecia filled by nanospherical micrite (Mi). **(B)** Detail of a micrite matrix formed by nanospheres aggregation, entombing a micritized biserial foraminifera, whose shell is made and filled by the same micrite nanospheres (yellow arrows). **(C)** Peloids filling a cavity of the bioconstruction, note that some peloids are broken showing the micritic inner part (green arrows), while some are covered by microspar (blue arrows). Withe the dashed rectangle: location of Fig. D. **(D)** Close-up view of C) showing peloids made of nanospheres (Mi) and covered by secondary microsparitic cements (Ms). **(E)** Micritic primary cements (Mi) surrounding a terrigenous grain (Gr) in the grainstone/packstone (algal rudstone facies). **(F)** Detail of the micritic primary cements showing micro-mound external surface (yellow arrows).

organic matter remains, characterized by irregular to sheet like C-enriched bodies of few microns in size, which some time appear partially mineralized (i.e. replaced) by the mineral nanospheres that form the micritic crystals (Fig. 11**C-G**).

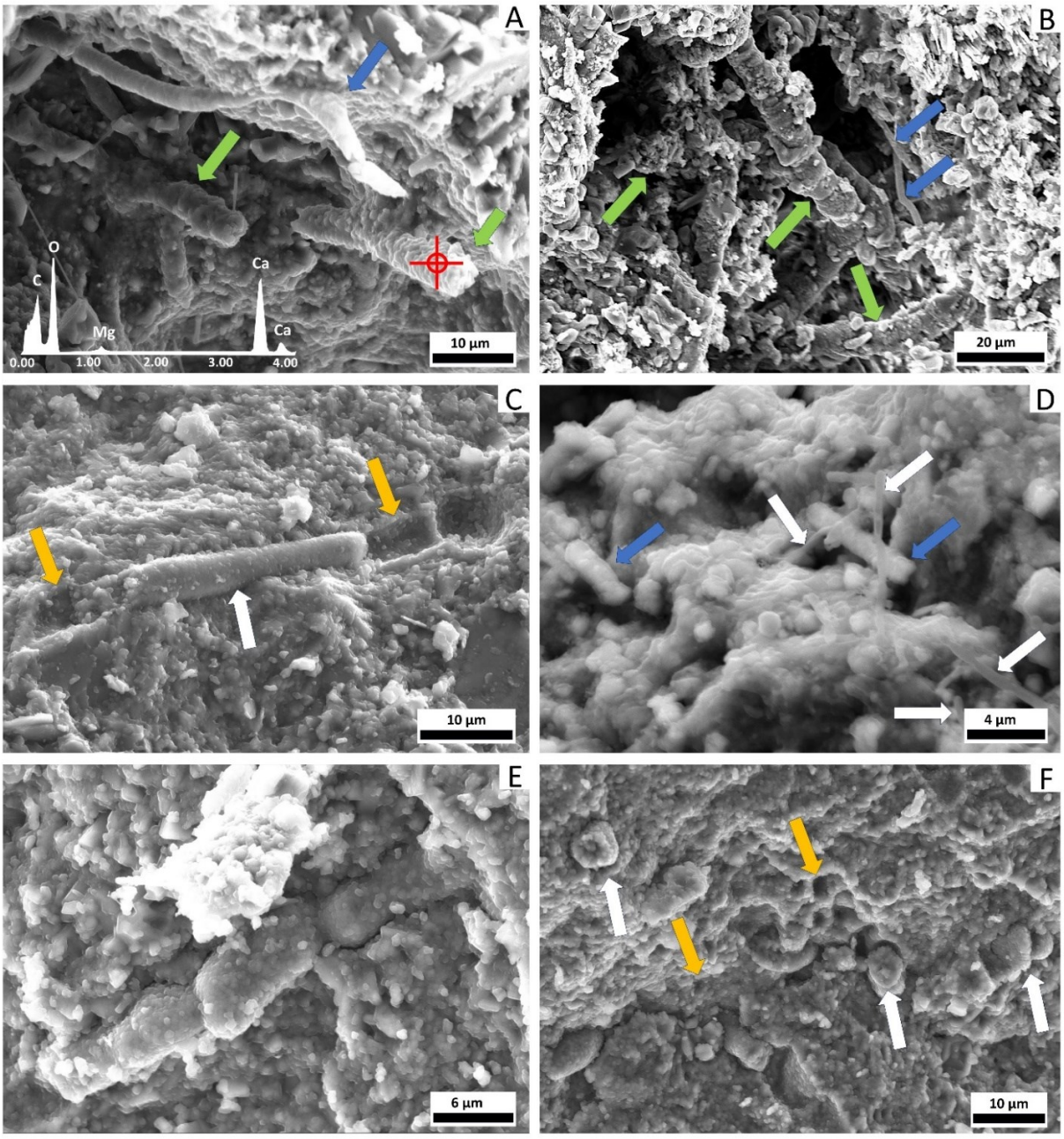

Figure 13. SEM views of bacterial fossils. **(A)** Cluster of filamentous bacterial bodies mineralized by nanospherical micrite: (type 1) filaments (green arrows), type 2 filaments (blue arrow); red point represent the spot of EDS analysis reported as spectrum. Filamentous micrite in algal boundstone facies (AB). **(B)** Filamentous bacteria showing dense (mineralized) structures: type 1 filaments (green arrows), type 2 filaments (blue arrow). Found in the AB facies. **(C)** Mineralized bacteria of type (white arrow), and relative mould (yellow arrows) impressed in the surrounding micrite made of nanospheres aggregation. Found in the AB facies. **(D)** Type 1 (blue arrows) mineralized filaments. Note organic matter filaments (white arrows). AR facies (mäerl). **(E)** Segmented filamentous bacteria fossil (type 4). AB facies. **(F)** Mineralized bacteria cells ((type 5) (white arrows) and relative subcircular moulds in the micrite matrix made of nanospheres aggregation (yellow arrows). AB facies.

Structures suggesting detrital origin of micrite, like fractures or smoothed surfaces are absent. The porosity is also apparently very reduced as the almost perfect packing of the crystals, which is also incompatible with a detrital origin.

As mentioned, the same micrite crystals, composed of nanospheres, were found to constitute all types of the observed micrite, including fillings of boundstone cavities (**Fig. 12A**), micritized bioclasts (**Fig. 12B**), and peloids (**Fig. 12C, D**). Moreover, the micritic isopachous rims enveloping and jointing adjacent clasts composing the algal Rudstone (or mäerl) facies (**Fig. 4B; 9B**) show the same nanospherical ultrastructure just described for the other types of micrite. In particular, the external surfaces of the rims are not smoothed but show mamillar micro-mounds perpendicular to the surface of the envelopes (**Fig. 12E, F**).

Finally, micritic crystals can gradually make transition to larger euhedral crystals, around 5-20 µm in size (definable as microsparite in thin section), which do not show the typical nanospherical ultrastructure of micrite, but a solid homogeneous crystal body (e.g., **Fig. 12C, D**).

Further SEM observations show that all the above described micrites, in addition to organic matter remains (**Fig. 11C, D**), host several mineralized structures that are comparable to possible fossilized bacteria (see paragraph 7.4) (**Fig. 13**). Five main morphotypes were recognized:

- **Type 1**) tubiform rod-like to slightly curved filaments, with a diameter of 5 to 10 µm (**Fig. 13A-C**), locally present in dense colony-like clusters (e.g. **Fig. 13B**); these correspond with the micritic filaments observed in thin section (**Fig. 8F**);
- **Type 2**) thin curved tubiform filaments with a diameter of 2-3 µm (**Fig. 13A, C, D**);
- **Type 3**) very thin mineralized filaments with a diameter of about 0.5 µm (**Fig. 13D**);
- **Type 4**) segmented filaments made of about 15 µm long and around 5 µm in diameter subunits (possible mineralized cells) (**Fig. 13E**);
- **Type 5**) subspherical to sub ovoidal (coccoids) mineralized bodies with a diameter of 5-10 µm (**Fig. 13F**).

In many other areas filamentous and spheric bodies of similar sizes are preserved as straight to subcircular empty moulds in the micrite (**Fig. 11A, B**; **13C, F**). The structure and the composition of all these mineralized bacterial-like bodies is made of the same nanospheres constituting the rest of micrite including organic matter remains, which is Calcite with a low percentage of Mg (i.e., from 1 to 4 %) (see an example of EDS spectrum in **Fig. 13A**).

7.4 DISCUSSON

7.4.1 Stratigraphic correlation and interpretation

The studied marine deposits represent a terraced transgressive-regressive cycle, deposited during the Late Pleistocene (age of around 100 to 80 Ky), which unconformably lie on the Pliocene/Lower Pleistocene Cutro marly clay Formation and, partially, on the residual deposits of a previous transgressive/regressive cycle of the same terrace (Zecchin *et al.*, 2009, and ref. therein).

The studied cycle starts with an erosive surface followed by a basal conglomerate (Section 1, 2, 3) making lateral transition to shell beds (Section 4, 5) accumulated during a shore retreat above a ravinement surface, produced by the action of waves and storms (wave ravinement surface - WRS) (e.g., Hwang and Heller, 2002; Zecchin *et al.*, 2019; 2021). This shore retreating provoked the

deposition of different kind of sediments in the western (Section 1, 2, 3) respect to the eastern sector (Section 4, 5), indicating an eastward deepening and a westward shallowing up to possible subaerial conditions. The effect of this transgression directly influenced the successive deposits represented by deeper marine facies such as the algal rudstone (i.e. the mäerl, depositing typically between 40 to 60 m in the modern Mediterranean; Bracchi *et al.*, 2014) (**Fig. 3E**) that, as its sedimentological characters, can be considered a biostromal body (see below). In lateral transition with the mäerl, toward shallower water, small-scale algal bioconstructions formed (Section 3; **Fig. 2**). These show the common presence of *Gastrochaenolites lapidicus* lithophagous boreholes (e.g. Bracchi *et al.*, 2014) (**Fig. 3C**). The marine transgression also reached the westernmost sectors (Section 1, 2) as testified by the presence of lithophagous boreholes in the clasts and boulders of the basal conglomerate bed indicating an increased water coverage (**Fig. 2**), and the possible development of a hardground surface probably due to an interruption, or a drastic reduction, of the clastic sedimentation, and the consequent early cementation of the mobile sediments (Nalin and Massari, 2009; Bracchi *et al.*, 2014). As a whole, all these sediments are representative of a transgressive system tract (TST) limited, at the top by a maximum flooding surface (MFS) (**Fig. 2**) (e.g., Zecchin *et al.*, 2009). It should be considered that other authors reported deeper detrital facies in the central palaeoshelf sector, which would imply a lower position of the MFS. In this case, the hardground (and so the mäerl top) formation would be constrained during the regressive phase (Nalin and Massari, 2009; Bracchi *et al.*, 2014).

Widespread algal bioconstructions and associated bioclastic sandstone follows in the succession (**Fig. 2**). This facies association can be interpreted as infralittoral coralligenous (Nalin and Massari, 2009; Bracchi *et al.*, 2014). The dimensions and density of the bioconstructions is variable along the studied transect that, as defined above, represents an eastward deepening shelf. In particular, they are more continuous but thinner in the easternmost part (Section 4, 5) while they tend to be thicker but with more interlayered bioclastic sandstones in the westernmost part (Section 2, 3). The bioclastic sandstones associated with the bioconstructions are composed of a mixed siliciclastic-carbonate sediment, indicating as source both the erosive processes affecting the bioconstructions, and the terrigenous sediment supply. The irregular lateral transition between the algal bioconstructions and the bioclastic sandstones results in frequent interdigitations, marked by stratification surfaces that can be followed from the sandy bodies through the bioconstructions. This feature indicates a low relief of the algal reefs in respect to the seabed, estimable in the order of some tens of centimetres, with a height/width ratio generally < 0,1, rather than high relief domal bioconstructions raising from the seabed with a height/width ratio of >> 0,1 (**Fig. 14**) (cf with Zecchin and Caffau, 2011). Moreover, the bioclastic sandstones are found as lenses within the calcareous bodies and infillings of the frequent macro and microcavities produced by the complex three-dimensional structure of the calcareous framework. The buildups and related sediments constitute the main sedimentary body of the Capo Colonna succession, being laterally well developed and continuous, except in the westernmost part where the presence of loose whitish fine sands, lateral to the bioconstructions, testifies the shallowing of the shelf, up to a possible shoreface environment. All these deposits generally testify shallower environmental setting, compared to the transgressive deposits below them (see above), testifying a depositional regression during a highstand system tract (HST) formation. Lastly, in the easternmost part of the terrace (Section 5) the absence of the

algal rudstone (mäerl), could indicate an eastward resumed shallower seabed. This can possibly be explained by the existence of a relief or an ancient promontory in the palaeocoastline.

Finally, above the HST deposits, a marked erosional surface can be considered the sequence boundary closing the Capo Colonna terrace transgressive-regressive cycle. Only locally cross-stratified shoreface sandstones follow the erosional surface.

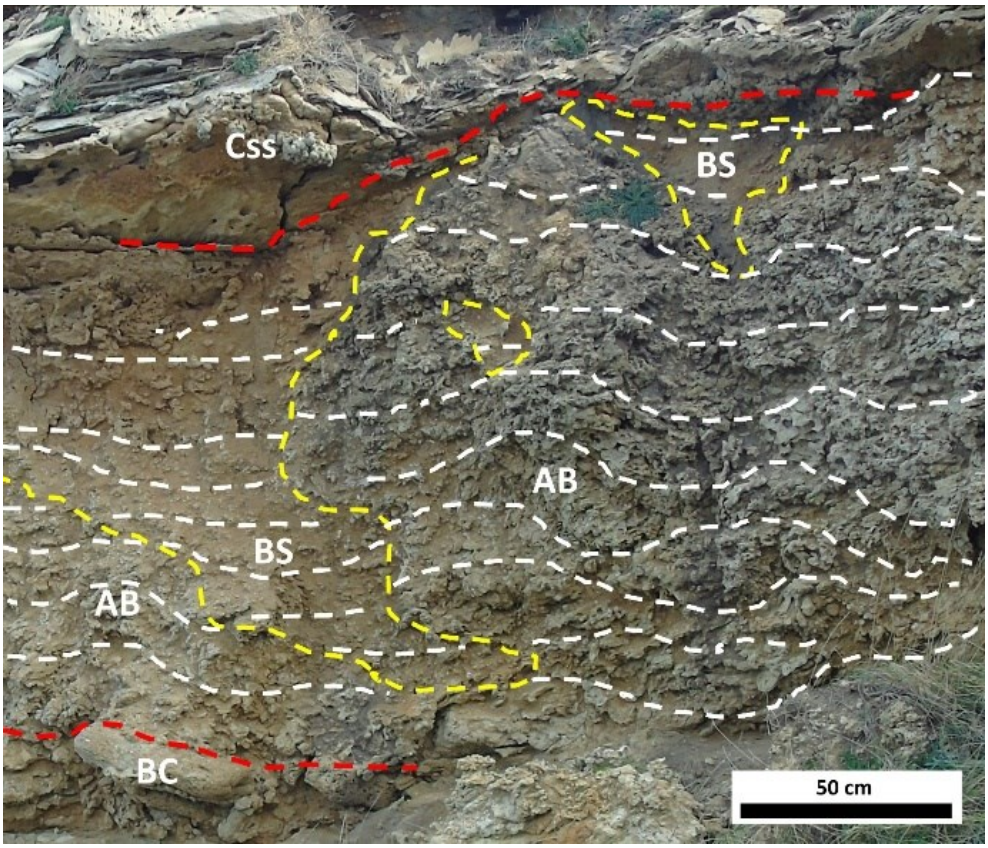

Figure 14. Section 2, field photo showing the lateral contact between Algal Boundstones (AB) and Bioclastic Sandstones (BS) (yellow dashed lines) forming the coralligenous facies association. Stratal surfaces inside (white dashed lines) evidence the low relief of the bioconstructions. Red dashed lines indicate the lower and upper boundaries of the coralligenous, lying over the basal conglomerate (BC) and overlaid by cross stratified sandstones (Css).

7.4.2 Late diagenesis

Late diagenetic phenomena are not intense. Selective dissolution, testified by dissolution voids, mostly developed on mollusc shells (**Fig. 9B**), is often accompanied by calcite reprecipitation testified by spathic dogtooth cements, and/or mosaic cements (filling the remnant primary or secondary porosity; **Fig. 9C**; **12C**, **D**). Often, micrite fades into a lighter microsparite due to aggrading neomorphism, in particular in the algal rudstone (**Fig. 9F**). As the succession is represented by raised terrace deposits located in an uplifting area, late diagenetic phenomena can be placed in a meteoric rather than a marine context. Dogtooth cements (typical of meteoric-phreatic environments) indicate that the succession has escaped from the marine environment after being buried for some time within a stable aquifer (Tucker and Wright, 1990). Finally, the partial dissolution of dogtooth cements (**Fig. 9E**), took place after the exposure to rainwater in subaerial environment.

7.4.3 Bio-sedimentary processes and role of micrite in the formation of calcareous algal bioconstructions and associated sediments

The primary framework of the studied bioconstructions is always dominated by red coralline algae (**Fig. 4C-E; 5A**) (as in the analogous present coralligenous bioconstructions, Bracchi *et al.*, 2014), at places replaced by bryozoans, encrusting foraminifera, and serpulids (**Fig. 4D- F**; **5B, C**) that, despite their abundance, are invariably subordinate in respect to algae. Consequently, still in accordance with modern coralligenous (e.g., Rosso and Sanfilippo, 2009), these latter frame-builders should more properly be considered as secondary bioconstructors. Moreover, the common occurrence of microbial mediated autochthonous micrite in the studied bioconstructions and associated sediments, implies that this belongs to the secondary framework too (**Fig. 7; 8; 9**), since it's a synsedimentary hard component contributing to the coralligenous stabilization and growth (see below for a further discussion on micrite origin and role).

Such a complex framework traps and binds a variable amount of sandy sediment, of a variable granulometry from coarse silts to fine gravels. The dominant biological component of this detritus, e.g. benthic foraminifera, molluscs, erect bryozoans, echinoids, geniculate algae, etc., including large shells (e.g., **Fig. 5D-F**), account for a fauna and flora that was hosted by the bioconstructions and/or surrounded them. In such bioclastic detritus, the presence of lithified fragments of the bioconstructions themselves, testifies that physical and/or biological processes of erosion were active during the formation of these deposits (e.g., **Fig. 5D-F**). Moreover, these erosive processes are demonstrated by the common presence of truncated surfaces recolonized by similar organisms (**Fig. 6A-C**), or by cavities filled by successive sediments (**Fig. 8D, E**).

Bracchi *et al.* (2014) inferred a relatively shallow depth (infralittoral) for the development of the here studied coralligenous, so the wave and/or storm action may be considered the main physical factor for such erosive phenomena. In addition, bioerosive processes, most probably due to endolithic organisms like Clionidae sponges, were also effective. This is testified by the not rare occurrence of sponge chambers and channels cutting across the calcareous framework (**Fig. 6A**, **B**), sometimes occurring with a dense pattern (**Fig. 5A**), in analogy with what happens in the modern coralligenous (Ballesteros, 2006).

As already suggested by previous papers (e.g., Wehrmann, 1998; Relini, 2009), even the autochthonous mäerl beds can be considered bioconstructions, as they can be regarded as biostromal body with a primary framework composed of free branched algal thalli accumulating in tabular beds (e.g., Wehrmann, 1998). In the studied deposits microbial mediated autochthonous micrite, very similar to those in the coralligenous facies, has been also detected. On this base, a role of secondary framework, which contributes to the stabilization of the mäerl bed, is inferred for the microbial micrite.

In fact, the micrite found in the Capo Colonna algal bioconstructions (both coralligenous and mäerl), is always microbial mediated and early cemented, showing the typical fabrics of microbialites (Riding, 2000; Défarge, 2011; Konhauser and Riding, 2012): 1) peloidal and clotted peloidal; filling cavities and forming micro-mounds and crusts with local filamentous fabric (**Fig. 4B; 7; 8**) in all subfacies; 2) structureless aphanitic/micropeloidal, incorporating detrital grains and representing the dark matrix of the bioclastic sandstone associated with the bioconstructions (e.g., **Fig. 4C, F**; **5C,**

F; **6D**; **8C**); 3) micritic rims binding bioclasts and terrigenous grains in both the bioclastic sandstone and rudstone (mäerl) (**Fig. 4B**; **5D, E**; **9A, B**).

In addition to the petrographic microbialitic fabrics, the rest of the dataset obtained confirms that all these types of micrite can be interpreted as an *in-situ* microbial mediated precipitate, rather than a detrital mud, as demonstrated by their: 1) nanoscale mineral structure; 2) the fossil evidence of the presence of a microbial community.

In particular, in terms of mineral nanostructure, the micrite is invariably made of the aggregation of nanospheres in the range of 100 to 300 nm (**Fig. 11C**), which are widely accepted as evidence of microbial-induced authigenic precipitates in several marine and non-marine sedimentary environments (e.g., Perri and Spadafora, 2011; Perri *et al.*, 2012a, b). Moreover, these nanosphere have been also defined as amorphous calcium carbonate or "ACC", which is still considered a characteristic and diagnostic nanostructure of modern and fossil microbial carbonates (e.g., Obst *et al.*, 2009; Ihli *et al.*, 2014; Diaz *et al.*, 2017).

In particular, such mechanism of crystal nucleation and growth substantially differs from a "classic" abiotic crystal development (Niederberger and Colfen, 2006). Indeed, in the studied case, the first generation of micrite deposition is characterized by the aggregation of nanospheres forming mostly anhedral crystals, and this morphological character is strongly in contrast with the euhedral, solid, and uniform crystal nanostructure that typifies the inorganic late diagenetic precipitates, such as the larger neomorphic microsparites and sparites crystals (**Fig. 12C, D**). In addition, these nanosphere are also found to constitute the micritized part of shells and their micritic infillings (**Fig. 12B**). This proves that also the formation of this type of micrite is a direct result of a microbial endolithic activity that evidently can also mediate the micrite formation (see “constructive” and “destructive” bioerosion *sensu* Perry, 1999).

Regarding the fossil evidence of the presence of a microbial community, widespread fossilized bacterial bodies, which showed different morphotypes, were detected, indicating a variegated microbial community inhabiting the microhabitats inside the bioconstructions and the sediments (**Fig. 13**). Moreover, the same nanospherical mineral structure above discussed, characterizes the fossilized bacterial cell (**Fig. 13**), but also organic matter remains that could represent mineralized EPS. In particular, these remains are sometime partially mineralized by mineral nanospheres confirming that the precipitation of the micrite takes place as a replacing product of the organic matter precursors (**Fig. 11C-F**). In fact, considering the role of the microbial cell walls (bacteria, algae and fungi), but also viruses and even bacterial vesicles, together with the secreted EPS, in the bio-mediated mineralization phenomena, a clear genetic link between an inferred benthic microbial community associated with the coralligenous metazoans/algal community, and the studied micrites can be inferred (Riding, 2000; Van Lith *et al.*, 2003; Benzerara *et al.*, 2006, 2010; Perri and Tucker, 2007; Perry *et al.*, 2007; Bontognali *et al.*, 2008; Sánchez-Román *et al.*, 2008; Dupraz *et al.*, 2009; Pedley *et al.*, 2009; Konhauser and Riding, 2012; Manzo *et al.*, 2012; Bahniuk *et al.*, 2015; Perri *et al.* 2022; Słowakiewicz *et al.*, 2023).

Finally, part of the deposition of the micrite may have been triggered by the degradation of non-living organic substrates (biologically influenced mineralization, *sensu* Dupraz *et al.*, 2009), such as sponges decaying tissues (Reitner *et al.*, 1995; Neuweiler *et al.*, 2007; Cipriani *et al.*, 2024). This is

testified in the studied deposits by the common accumulations of spicules surrounded by a fine clotted peloidal to aphanitic micrite matrix (**Fig. 7E, F**).

The role of microbial mediated the micrite in the growth of the bioconstructions could have been various, depending on the locus and the time of their develop: peloidal and clotted peloidal micrite with local filamentous fabric, infill cavities and form micro-mounds and crusts into primary cavities of the skeletal framework (**Fig. 7A, B**; **12C, D**). This can indicate that these fabrics are possibly the result of micrite precipitation, mediated by microbial biofilms living among algal/metazoans organic tissues, in cryptic micro-environments. In this case is more probably that microbial community was dominated by heterotrophic organisms as the absence of light, taking advantage of the abundance of organic matter deriving from dead organisms. The result could be a very early contribute to the binding, and consequently hardening, of the main skeletal framework.

The aphanitic/micropeloidal micrite very often includes terrigenous and bioclastic detritus, which can even prevail in respect to the micrite. However, even if trapped and bound detrital grains in these microbialites are present, as seen, there is evidence of their *in situ* microbial origin, allowing to interpret these micrites also as an autochthonous precipitate (**Fig. 10**; **12B, E, F**). Moreover, the presence of larger (even millimetric) detrital grains, immersed in a chemically, mineralogically, and morphologically homogeneous, micritic matrix, characterized by *in situ* nanospheres aggregation, highlighting a clear genetic difference in between the carbonate matrix and the grains. This allows to interpret the latter as allochthonous elements transported by water movements, and incorporated into autochthonous very fine micrite that can't be mobilized by currents and waves as early cemented; as commonly happens in numerous microbial carbonates in several contexts, which trap and bind large amount of grains (e.g. Reid *et al.*, 2000). It can be inferred an effect of mobile-sediment stabilization, for such microbial community associated with detrital sediments; that, moreover, explains the apparent contradiction between the coarse terrigenous grain size and the very fine matrix.

Finally, the authigenic precipitation of these micrites is consistent with proofs that testify their very early cementation such as: 1) erosive surfaces developed both on the skeletal framework and the interbedded micrites themselves (**Fig. 6A, B**); 2) microbial micritic intraclasts detected within the detritus included in the framework (**Fig. 6C**); 3) the microbialitic micro mounds and crusts grew both on algal thalli and on erosive surfaces developed on the micrites and entombed clasts (**Fig. 8**). All these features imply that the microbial micrite must have already been well cemented to be eroded and colonized, and to have formed intraclasts resedimented in a second sedimentary input. Consequently, the microbial communities that mediated the precipitation of syn-sedimentary micrite can be defined as secondary "frame-builder".

In addition to this widespread microbial micrite precipitation, the detrital facies are also very frequently characterized by the occurrence of micritic rims surrounding the grains (e.g., **Fig. 4B**; **9A, B**). This micritic rims are interpreted as primary microcrystalline cements that provide early cementation of the sediment, as their origin can also be traced back to microbial mediation in marine phreatic to vadose palaeoenvironment (Perry, 1999; Hillgärtner *et al.*, 2001). In fact, as shown by Diaz and Eberli (2022), in tropical shallow-water environments of carbonate systems of the Bahamas and Australia, the biological stabilization of the granules via microbial biofilm, is due to the biomediated precipitation of syn-sedimentary micritic envelopes.

In our bioclastic sandstones and in the algal rudstone (mäerl), such a biomediated micritic cement origin is testified by the occurrence of mineralized microbial filaments (i.e., possible bacterial microfossils), and by the biomediated nanospherical structure of the mineral (see discussion above). Moreover, during their development around the carbonate bioclasts, micritic rims fades into micritized areas. This indicates the occurrence of microbial endolithic organisms acting from outside to the interior of the carbonate grains, resulting both in the micritization and in the development of the micritic rims connecting adjacent grains (Reid and Macintyre, 2000; Diaz and Eberli, 2022, and ref. therein). Moreover, the outer surface of such micritic rims is characterized by micro-mounds growing perpendicular to the grain surfaces, and this growth style is also consistent with a microbial mediated genesis of these cements, which is also suggested by the presence of bacterial fossils (**Fig. 12E, F**; **13D**). In the rudstone algal facies (mäerl) these microbial mediated micritic rim cements, even if associated with a major terrigenous input (quartz and clay minerals), confirms that the microbial communities that mediated the syn-sedimentary micritic calcium carbonate precipitation were widespread in the whole habitat.

By contrast, the early cementation here inferred for the MIS 5 Capo Colonna mäerl seems not in accordance with the modern counterparts, since this deposit is considered a semi-rigid, soft biogenic bottom with frequent movements and overturning of the algal thalli, due to waves, bottom currents, and bioturbation, necessary to allow light to reach all the thalli surface and to contrast burial and biogenic encrustation (Steneck, 1986; Hinojosa-Arango *et al.*, 2009, and ref. therein). However, to explain the evidence of an early cementation, it cannot be excluded that microbial micrite precipitation took place in the shallow buried (few decimetres) dead accumulation of thalli, rather than in the uppermost living layer.

Finally, the micritic rims found in the detrital facies (mäerl rudstone, bioclastic sandstones) and less in the bioconstructed facies, have never been reported in Mediterranean infra-circalittoral deposits, but only in warmer tropical areas (Diaz and Eberli, 2022). These could suggest tropical conditions in Mediterranean during this period, as supported by the presence of the tropical molluscs *Thetystrombus latus* and *Cardita rufescens* (= *C. senegalensis*) (Nalin *et al.*, 2012). However, the same type of micritic cements were found in MIS 5e (the warmest MIS 5) coastal deposits of the Mar Piccolo of Taranto (east side of the same Ionian Sea) that include the same tropical fauna. Here it can be proposed that, even if not proper tropical conditions were reached during the MIS 5e, the sea surface temperature in this area was about 2 °C warmer respect to today, allowing the occurrence of these tropical-like microbial mediated marine early cements and the settlement of tropical pioneer species (see *Chapters 4 and 6*).

7.5 CONCLUSIONS

The last interglacial (MIS 5a/c) outcropping deposits of the raised Capo Colonna marine terrace, consist of a transgressive-regressive sedimentary cycle that, particularly during the regressive phase, recorded the occurrence of coralline algae-dominated bioconstructed bodies. These are characterized by calcareous low-relief domal bioherms and tabular biostromes, which have been interpreted as analogous to modern coralligenous and mäerl hard sea-bottom habitats.

Encrusting laminar red coralline algae form the primary skeletal framework of the bioherms, while bryozoans, encrusting foraminifera and serpulids, very often associated with algae, act as secondary frame-builders. Autochthonous mäerl tabular beds are mainly composed of a well cemented rudstone of free branched coralline red algae. A variable amount of sandy (actually from coarse silt to fine gravel granulometric range) bioclastic sediment is laterally interbedded with the bioconstructions, and also fills cavities and pockets typically developing on the bioconstructions. A complex fauna and flora should have inhabited these habitats, now testified mostly by abundant molluscan shells of both sessile and vagile forms.

Autochthonous synsedimentary microbial-mediated micrite has been abundantly detected in all sub-facies of the bioconstructions, whereas detrital mud particles accumulation (i.e. allochthonous micrite) seems substantially absent. In the coralligenous facies, microbial micrite is present with a peloidal, clotted peloidal, and filamentous fabrics, which commonly develop in the micro-cavities of the skeletal framework. Whereas the biostromal mäerl algal rudstones is rich in thin micritic rims and peloidal micrite, coating and cementing all the fine and coarse clasts. Furthermore, aphanitic-micropeloidal microbial micrite frequently fills the skeletal framework cavities where it also traps and binds a variable amount of grains. Even the sandy detrital sediment, laterally associated with the bioconstructions, can be *locus* of microbial micritic growth, as micritic rims frequently surround partially to totally micritized bioclasts and terrigenous grains, similarly to the process of synsedimentary detrital seabed hardening, due to microbial micritic cements that commonly form in tropical shallow-water carbonate environments.

All these autochthonous early-lithified micrites consist of mineral nanospheres (100-300 nm in size) coalescing into subhedral microcrystals replacing and mineralizing both microbial cells (present with several morphological types) and extracellular substances. This implies their biologically mediated origin, but also the widespread presence of lithifying microbial biofilms along the seabed and within almost all types of substrata, as they colonized both the cavities of the skeletal framework of the bioconstructions and the associated sediment intergranular space.

In conclusion, such biofilms, thanks to the metabolic processes of the microorganisms that induced the pervasive micritic carbonate precipitation, significantly contributed to the process of early cementation of all these deposits.

CHAPTER 8 - Late Pleistocene SST evolution in the Central Mediterranean based on *Cladocora caespitosa* geochemical proxies (work in progress)

This project is at an initial phase due to the end of the time allowed for the closure of the PhD course. Therefore, in this chapter it is reported what has been done and future prospectives.

Introduction. *Cladocora caespitosa* fossils samples, sampled along raised terraces cropping out along the southern Tyrrhenian and Ionian Sea, were screened for diagenesis, and prepared for geochemical analysis with the aim of reconstructing the mean and seasonal sea surface temperatures along the main Late Pleistocene warm phases.

As seen, the Quaternary period (2.65 – 0 Ma) was characterized by a progressive cooling and a contemporaneous increased climatic instability, consisting of a periodic alternance of glacial and interglacial periods, triggered by Earth orbital cycles and recorded by oxygen stable isotope variations, on which the Marine Isotope Stages (MIS) are based (Emiliani, 1955; Shackleton, 1967; Shackleton and Opdyke, 1973; Lisiecki and Raymo, 2005; Railsback *et al.*, 2015). Understanding the past climate variability is a key theme for understanding the present-day climate change; for example, the Last interglacial (MIS 5e) is considered as a good analogous for the prediction of the ongoing global warming (IPCC, 2007, 2023).

Climate fluctuations are recorded by the geomorphological features of tectonically active (uplifting) coastal areas, resulting in terraced deposits formations (e.g., Cerrone *et al.* 2021), and by changes in geochemical composition of skeletal minerals of marine organisms such as foraminifera, molluscs, corals, among many others (Wierzbowski, 2021), recording both ocean water variations and on Sea Surface Temperature (SST) changes. Among biogenic carbonates, scleractinian corals are commonly used as geobiological archives for palaeoenvironmental reconstructions, as their aragonitic skeleton records a series of geochemical proxies such as trace elements (e.g., Sr/Ca; Silenzi *et al.* 2005; Montagna *et al.*, 2007; Royle *et al.*, 2015b), stable isotopes (Ghosh *et al.*, 2006; Thiagarajan *et al.*, 2011; Royle *et al.*, 2015a; Kimball, 2016; Spooner *et al.*, 2016 and references therein), and also the growth parameters (Periano *et al.*, 1999; Peirano *et al.*, 2009; Kruzic *et al.*, 2012), which can be used for SST reconstructions. Moreover, scleractinian corals incorporate Uranium during its growth, making also feasible accurate U-series datings (Dai Pra and Stearns, 1977; Thiagarajan *et al.*, 2011; Amorosi *et al.*, 2014; Spooner *et al.*, 2016; Cerrone *et al.*, 2021).

For the Mediterranean area, one of the most useful palaeoclimatic and palaeoenvironmental archive is the coral *Cladocora caespitosa* (Linnaeus, 1767) (Scleractinia, incertae sedis - Faviidae? Caryophyllidae?) (Silenzi *et al.*, 2005; Montagna *et al.*, 2007; Royle *et al.*, 2015a,b). This endemic Mediterranean hermatypic zooxanthellate coral, grows in a dendroid-phacelloid form resulting in typical pillow-like colonies, and living in the infralittoral zone associated with algal hard bottoms, generally most abundant from 4 to 10 m (Periano *et al.*, 2004). *C. caespitosa* is present in the Mediterranean from the Late Pliocene, representing – especially during warm phases – an important reef builder (Bianchi and Morri, 2003; Peirano *et al.*, 2004; Peirano *et al.*, 2009; Zanchetta *et al.*, 2019).

Sampled fossiliferous sites. Sites with *C. caespitosa* occurrences reported in the literature in Calabria and near regions were selected to cover as much time span across the Late Pleistocene and, partially, across the Middle Pleistocene (**Fig. 1**; **Fig. 2**).

In the Tyrrhenian coastline of the northern Calabria (CS) and Basilicata (PO), and in the Ionian coastline of central Calabria (KR), several raised marine terraces are well exposed and, for most of them, there is also a good agreement on their absolute age, based on radiometric ages, indicating an overall age from MIS 6 to (likely) MIS 3, therefore encompassing the whole MIS 5 warm-relatively warm substages (Bracchi *et al.*, 2016; Cerrone *et al.*, 2021) (**Fig. 1**).

Cerrone *et al.* (2021) radiometrically dated with U/Th methodology well preserved (calcite < 5 %) *C. caespitosa* corallites at many sites of the Basilicata-Calabria Tyrrhenian coastline, from north to south: Fiumicello (FIU) (Maratea, PO; MIS 6, 161 ka); Torre Fiuzzi (TFZ) (Praja a Mare, CS; MIS 5e, 120 ka); Scalea (SLC) (CS; MIS 5c, 98 ka); Grotta del Prete (GRP) (San Nicola Arcella, CS; Mis 5a, 83.8 ka) (**Fig. 1**). Other sites with *C. caespitosa,* not included in the paper of Cerrone *et al.* (2021), are: Ginnasio (GIN), at Praia al Mare, few kilometres north to Torre Fiuzzi, possibly MIS 5e in age based on geomorphology (Robustelli, pers. comm., 2023), Torre Talao (TAL), few km south to Scalea, dated to MIS 7 (Carobene *et al.*, 1986), and Capo Tirone (TIR) (Belvedere Marittimo, CS), where a very small marine terraced deposits crop out along the modern coastline (**Fig. 1**). In almost all these sites, the palaeoenvironmental framework consist in shallow water rocky hard substrates colonized mainly by corals and lithophagous bivalves (evident as *Gastrochaenolites* ichnogenus) and, locally, by subordinate red algae and encrusting bivalves (*Spondylus* sp., *Ostrea* sp.); these transgressive deposits are usually covered by regressive deposits (Cerrone *et al.*, 2021). As these corals lived in very similar palaeoenvironment, the terrace succession gives the opportunity to study geochemical proxies on the same archive, in very similar marine setting. All the sites were sampled in the spring, 2023, except the site FIU, yet to be added to the samples.

Moving to the Ionian coastline of Calabria, at Le Castella (LCA) (KR) (**Fig. 1**), a *C. caespitosa* bed was dated to MIS 5c to MIS 3. A MIS 5a/c (87 +- 10 ka) was derived from U/Th ages (Belluomini *et al.*, 1988), supported by amino acid racemization (MIS 5c; Gliozzi, 1987) and stratigraphic consideration (MIS 5a, Palmentola *et al.*, 1990). More recently, attribution to MIS 3 was supported by luminescence datings of around 43-48 ka (Mauz and Hassler, 2000), and around 63 ka (Nalin *et al.*, 2020), and stratigraphic observations (Zecchin *et al.*, 2004), indicative of a general about 50 ka, correlative with MIS 3.3 (Zecchin *et al.*, 2016, 2020). At this site, sampled during 2021, a shallow water red algae buildup deposit (coralligenous) crops our, associated to small *C. caespitosa* colonies on the top that locally represents the main framework builder, and then overlaid and buried by a regressive bioclastic arenite (Bracchi *et al.*, 2016).

Other fossil corals from Tarsia (TAR) and Diamante (DIA), sampled Bernasconi *et al.* (1997, 2015), are already available for the study (**Fig. 1**). At DIA, located south of the area studied by Cerrone *et al.* (2021), a natural coastal cave with coralgal association crops out, possibly dated to MIS 9 (at least 306 ka with $^{230}Th/^{234}U$; Carobene *et al.*, 1986; Bernasconi *et al.*, 2015). Well preserved corals from this site have been already used for SST estimation (Sr/Ca-derived mean annual SST of 12-18 °C; Bernasconi *et al.*, 2015). Moving to TAR, located in the Northern Calabria hinterland, a massive coral bank is exposed in an abandoned quarry, possibly Sicilian in age (Upper Calabrian, 1.2 – 0.8 Ma)

(Bernasconi *et al.*, 1997, and ref. therein), but a refined age should be added. Corals are found in a non-cemented muddy fine matrix and are easily removed by washing.

Finally, a modern coral sample (POL) was found beached at Santa Maria di Pollina (PA, NW Sicily) (**Fig. 1**), where a similar modern shallow water rocky bottom with living small colonies was found, giving the chance to compare fossil and modern specimens of the same species.

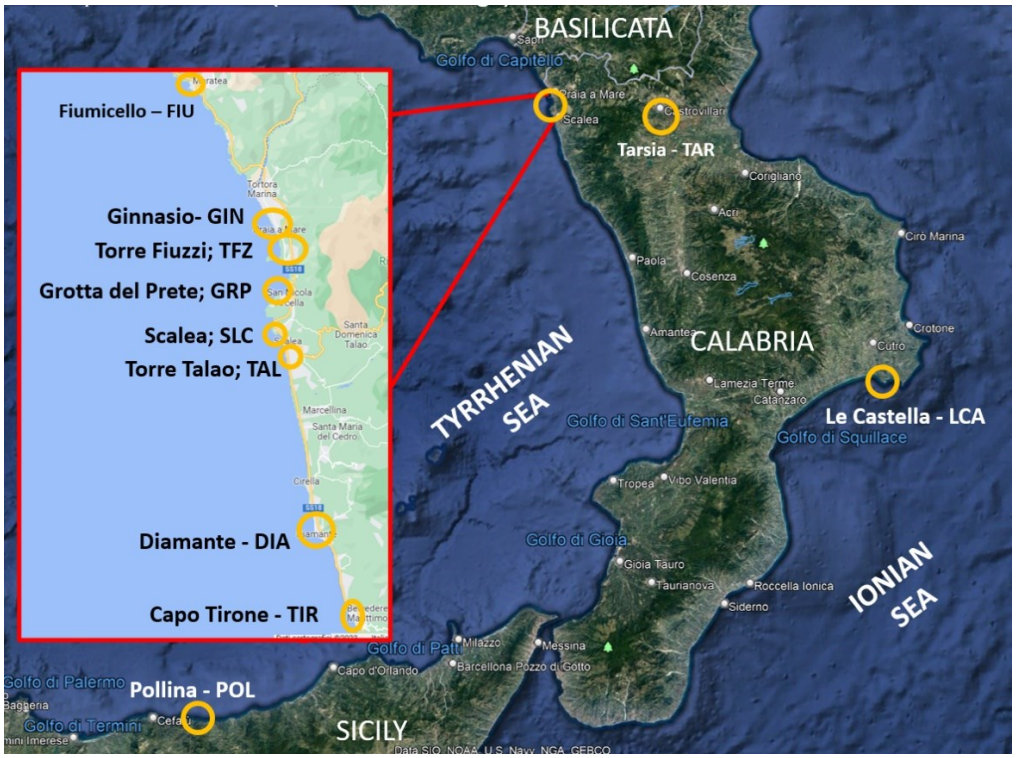

Figure 1. Location of all the selected sites with *Cladocora caespitosa,* from modern to Middle Pleistocene.

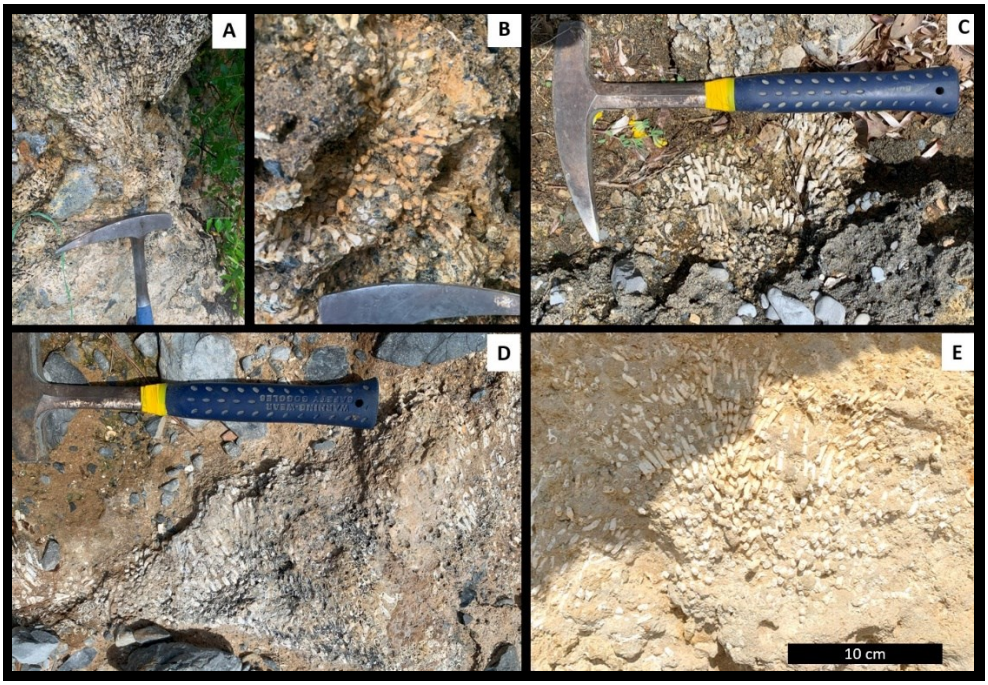

Figure 2. Some outcrops. **(A)** Ginnasio (GIN); **(B)** Torre Fiuzzi (TFZ); **(C)** Grotta del Prete (GRP); **(C)** Scalea (SLC); **(E)** Le Castella (LCA).

Preparation of the samples. Corallites from LCA and TAR were easily separable from the colony samples, buried in a uncemented fine sedimentary matrix. Those from TFZ, GRP, and GIN, instead, where more hardly cemented, but still separable. Instead, corallites were hardly cemented and not extractable at SLC, TIR, TAL, DIA. All the samples were mechanically prepared by removing external sediment and washed with ultrasonic cleaning for 10 minutes. Then, one to three corallites per site, each around 1 cm long, were chosen, selecting among those exhibiting the best degree of preservation (e.g., whitish colour, no bioerosion or encrustations, no shining recrystallized broken surfaces, the less possible detrital infill) (**Fig. 3**).

Figure 3. Some of the samples prepared for XRD screening.

Screening for diagenesis. In order to find well preserved (Calcite < 5 %) corallites for each sample, a small portion of each corallite was removed from one of its two ends to perform a bulk XRD analysis to assess the percentage of diagenetic calcite. For cemented colonies, powder samples were obtained drilling sectioned samples. Explorative XRD analysis were performed for a first preservation check. The percentage of diagenetic calcite was just 2 % in TAR, 5 % in LCA and MPT, around 10 % in GIN, TFZ, and GRP, 18-19 % in SLC and TIR, 25 % in TAL, and 45 % in DIA.

For the samples with a well constrained ages (i.e., TFZ, SLC, GRP, and LCA) further XRDs were run to find at least a well-preserved corallite, selecting three corals per site. Results of these corallites are shown in **Table 1**. The modern coral POL1, surprisingly, did not return a 100 % aragonitic composition; it is suspected a possible contamination from external encrusting red algae. LCA were all pristine, with 100 % aragonite. GRP returned only a 100 % aragonitic corallite. For SLC, the best result is around 90 %. TFZ returned a 100 % aragonitic corallite. These results are encouraging as at least a well-preserved coral per sample was found, and further may be added to the analysis.

SST estimation for MIS 3, LCA. A coral from Le Castella was preliminary analysed for geochemical proxies. Three points were micro-drilled on the external polished surface (**Fig. 4**). The analysis returned a mean $\delta^{18}O$ of -1,90 ± 0,15 ‰, and a mean $\delta^{13}C$ of -3.51 ± 0.43 ‰ (**Tab. 2**). These value, falling into or nearly near to the typical present-day samples, return reliable mean SST of 18.7 ± 0.7

°C (using the equation of Royle *et al.*, 2015a, with a $\delta^{18}O_w$ derived from an SSS of 38 psu like the modern Mediterranean), or 18.7 ± 1.0 °C (using the equation of Silenzi *et al.*, 2005). The similarity of the results, derived from different equations, suggests that this is a good estimate.

Age	Samples (18/09/23)	% pristine aragonite	% diagenetic calcite
MIS 1*	***POL1***	91.6	8.4
Likely MIS 3	***LCA1***	100	0
	LCA2	100	0
	LCA3	100	0
MIS 5a	***GRP1***	90	10
	GRP2	100	0
	GRP3	75	25
MIS 5c	***SLC1***	65.7	34.3
	SLC2	74.1	25.9
	SLC3	90.4	9.6
MIS 5e	***TFZ1***	96.4	3.6
	TFZ2	100	0
	TFZ3	92.6	9.6

Table 1. Selected samples. Inferred ages from Cerrone et a. (2021); * modern.

	$\delta^{13}C$	$\delta^{18}O$
LC_a	-4,00	-1,91
LC_b	-3,32	-1,74
LC_c	-3,20	-2,04
MEAN	*-3,51*	*-1,90*
St. Dev	*0,43*	*0,15*

Table 2. LC coral stable sotope values

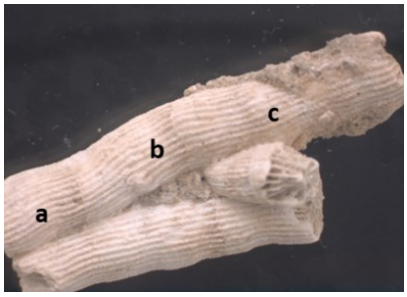

Figure 4. Sampled points for stable isotopes (LC sample)

Future analysis. All the sites will be sampled (to date, FIU was not sampled), and a representative number (e.g., at least 3) well-preserved corallites will be searched for each site. Then, geochemical analyses will be performed for SST calculating. $\delta^{18}O$ analysis could be performed for finding the seasonal growth pattern and to calculate SST, by sampling at least 2 measures/mm with microdrilling. The conventional stable isotope analysis or $\delta^{18}O$ (e.g., Urey, 1947; McCrea, 1950; Epstein *et al.*, 1953) is frequently used for the estimation past seawater temperatures. Due to the dependence of the skeletal $\delta^{18}O$ on both SST and the composition of the surrounding seawater

($\delta^{18}O_w$) that is unknown, (Wierzbowki, 2021; Huntington and Petersen, 2023), reliable SST estimates are prevented unless the method is coupled with other SST proxies, possibly trace elements net of their incertitude. This point could be solved by Sr/Ca or Mg/Ca analyses, which can be performed with EPMA or with Laster Ablation. Anyway, as indicated by Royle *et al.* (2015b), this proxy is not useful for absolute temperature estimations due to vital effects. In addition, isotope analysis on corals is also affected by vital effects. This problem is partially solved calibrating specific equations for the studied species, e.g. Royle *et al.* (2015a) for *C. caespitosa* - but there is still the lack of knowledge of the $\delta^{18}O_w$ that must be constrained to gain a reliable SST estimation.

A possibility could be represented by the application of clumped analysis (Ghosh *et al.*, 2006). The SST estimations, based on the Δ47 parameter, require no assumption for the past $\delta^{18}O$ of the seawater (Anderson *et al.*, 2021; Huntington and Petersen, 2023). Clumped analysis has been applied to both shallow and deep hermatypic and ahermatypic corals but, again, vital effects related non-equilibrium calcification were unfortunately found, most likely controlled by the CO_2 hydration/hydroxylation fractionation processes during the calcification (Ghosh *et al.*, 2006; Thiagarajan *et al.*, 2011; Saenger *et al.*, 2012; Kimball *et al.*, 2016; Spooner *et al.*, 2016). Albeit also biased by vital effects, carbonate clumped analysis remains undoubtedly the best to use when considering samples of different ages or sites, and different unknown $\delta^{18}O_w$, but of the same species. Indeed, Kimball *et al.* (2016) suggested taxa-specific vital effect, and thus different Δ47-SST relationships. More in detail, as suggested by Spooner et al (2016), it would be ideal to calibrate a specie or genus specific equation for a proper application of clumped isotope analysis for SST estimations.

Summarizing, a Δ47-SST equation based on recent or, possibly, living *C. caespitosa* individuals could be calibrated, hopefully evaluating and correcting the vital effects. This may help to use this isotopic proxy on fossil corals to estimate past SST. Moreover, reliable SST estimates could be used to back-calculate the $\delta^{18}O_w$ during the various MISs, and to compare them to the global variation curves. This, hopefully, will add new insights on the use of *C. caespitosa* as palaeoclimatic archive, and add new palaeotemperature data for the Mediterranean Sea, hoping to contribute to the understanding of the past response to climate change in this land-locked, fast warming basin (Belkin, 2009), strongly treated by the global warming.

CHAPTER 9 - GENERAL CONCLUSION

In conclusion, it is here discussed how the data and interpretations presented in the thesis, could give a contribute to the post-global warming modelling in the central Mediterranean; since the study of the past environmental conditions can indeed provide several insights on the effect of climate changes on the fauna, flora, and substrate of modern analogue environments (Bertini *et al.*, 2022).

As previously reminded, only the MIS 5e is generally regarded as a good model for the current climate change, due to its warmer global conditions compared to today (Overpeck *et al.*, 2006; Rohling *et al.*, 2008; Siddall and Valdes, 2011; Antonioli *et al.*, 2017; Fischer *et al.*, 2018; IPCC, 2023; Albano *et al.*, 2024). The younger MIS 5a and MIS 5c, known as "Neotyrrhenian" interstadials, do not exhibit pronounced peaks in the oxygen isotopic benthic stacks (Lisiecki and Raymo, 2007). However, local climatic reconstructions (including the Mediterranean area) suggest either cooler or warmer conditions in respect to today (e.g., Pérez Folgado *et al.*, 2004; Oppo *et al.*, 2006; Väliranta *et al.*, 2009; Helmens, 2014; Ilyashuk, *et al.*, 2020).

Therefore, the study of any MIS 5 deposit can be useful to provide insights into the potential impacts of contemporary climate change on analogous modern environments, as long as a local estimation of the palaeotemperature is provided.

9.1 MIS 5e SST temperature estimation and modern Global warming

A multiproxy palaeotemperature estimation (based on biogeographical affinity of the molluscan fauna, trace elements, coral growth rates, oxygen stable isotopes) was conducted on the MIS 5e coastal deposits of the MP (see *Chapter 5*). Moreover, a further attempt to estimate MIS 5e to MIS 3 SSTs is object of work in progress (see *Chapter 8*).

Albeit all the proxies used suffered of various uncertainties, suggesting caution when approaching palaeoclimatic reconstruction with a single proxy, a mean annual SST value of approximately 21 °C, was estimated in the Taranto gulf. This implies that the during the MIS 5e the SST was ca + 2 °C than the modern, with a possibly similar to today seasonality. This estimated mean annual temperature is in line with the estimations obtained in the open sea Mediterranean deposits for the same period with different proxies (Rohling *et al.*, 2002; Pérez-Folgado *et al.*, 2004; Marino *et al.*, 2007; Kandiano *et al.* (2014); Martrat *et al.* (2014).

According to recent estimates, the whole Mediterranean waters are warming at around 0.041 °C/year, responsible of an increment of around +1.5 °C registered from 1982 to 2018. In particular, the Ionian Sea is warming at 0.037 °C/year, (Pisano *et al.*, 2020).

This suggests that the SST of the Ionian Sea in the Taranto gulf estimated in this thesis (i.e. +2 °C than today), could be reached around the end of the century, if the rate of temperature growth is assumed constant.

9.2 Possible global warming effects on the molluscan fauna

The palaeotemperature estimations must be framed in a palaeoenvironmental setting, provided by the palaeoecological study achieved through the palaeobiocoenotic approach, in order to figure out possible changes on these environments due to global warming. A quantitative study, performed

on samples from the Taranto coast (*Chapter 4*), reconstructed the overall conditions during the deposition of the studied calcarenitic level: dominantly infralittoral sandy to gravelly bioclastic (dominant indications of Well Sorted Fine Sands - SFBC, locally influenced by Coastal Detritic - DC), vegetated bottom (either represented by marine phanerogams - HP - and/or algae - AP), locally more sheltered and exposed, with a smaller contribution from nearby biocoenoses, probably linked to lateral environmental variations.

The environmental setting depicted for MIS 5e Taranto Sea differs from the modern semi-closed Mar Piccolo (MP) and the nearby Mar Grande (MG), because today they are severely affected by human impact, pollution, mud deposition, and instability bottom conditions (Matarrese *et al.*, 2004; Mastrototaro *et al.*, 2008). In fact, comparing fossil and modern data, the present-day molluscan fauna is impoverished than during MIS 5e interval: 49 species were detected in MPT and MG (Mastrototaro *et al.* (2008), whereas 120 species were found in the MP fossil assemblage (net of the possibly increased number by time-averaging phenomena in the fossil assemblage, which cannot be ruled out).

For this reason, a fossil-modern comparison was carried out with modern associations coming from pristine and undisturbed coastal areas, such as marine protected areas, choosing environmental settings similar to the average conditions inferred for the MIS 5e calcarenite. Donnarumma *et al.* (2018) provided lists of molluscs from the marine protected areas (MPAs) of the southern Tyrrhenian Sea and the Ionian Sea, in four habitats: 1) mobile, predominantly sandy and muddy (SB, confrontable with SFBC and similar palaeobiotopes), 2) *Posidonia* meadows (HP), 3) hard photophilic (PHB, that is AP, photophilic algae), and 3) hard sciaphilic bottoms (SHB, that is C, Coralligenous).

The MIS 5e mollusc fauna shows a predominance of sandy-detritic palaeobiotopes, at least partially vegetated, allowing a comparison with SB and HP species lists. Also considering the molluscan indications (AP related species) and the microbial early cementation evidence, which at least locally must have hardened the seabed, the presence of hard bottom AP spots is hence expected. Instead, species from modern C hard bottoms, represented by one accidental species found in the MP fossil assemblage, were removed as there is no evidence of algal bioconstructed habitats in the MP area during MIS 5e.

Hence, the diversity of modern SB, HP, and AP habitats of these modern areas was compared to the MIS 5e of the MP. For a more direct comparison, the SB, HP, and AP species lists of the modern MPAs (reflecting the mean modern conditions), and those of the three samples from MP (T5, T13, and T17) (reflecting the mean MIS 5e conditions) were averaged.

The modern and fossil mean assemblage has a very similar species richness (Margalef's) index (d) (13.44 and 13.92, respectively). Diversity Shannon's index (H') and Evenness Pielou's index (J') of modern mean assemblages (3.48 and 0.78) are very similar, only slightly higher than those of the fossil one (3.38 and 0.71) (**Tab. 1**). All considering, the overall diversity indexes are not strongly different.

	S	N	d	H'	J'
MODERN MPAs	106	742	13.44	3.48	0.78
MIS 5e MP	120	5174	13.92	3.38	0.71

Table 1. Number of species (S) and of individuals (N); Margalef's species richness (d), diversity (H'), and evenness (J') from modern averaged sandy-photophilic vegetated assemblages from marine protected areas (MPAs) (Donnarumma *et al.*, 2018) and MIS 5e averaged samples of the Mar Piccolo (MP) (*Chapter 4*).

In addition, the preferred SST ranges of the whole molluscan assemblages provided by OBIS (2023) database were used to compare modern MPAs and the fossil assemblage of the MP (see *Chapter 4*). The comparison shows that both the graphs are very similar, with the temperature of about 20 °C being the most represented (**Fig. 1**). For a further comparison, the data relative of the species list of Mastrototaro *et al.*, (2008) were similarly plotted; also in this case, there are not marked differences with the MP or the MPAs plot (**Fig. 1, Fig. 2**). Even if the number of species and the environments are different, the similar shape of the curves confirms that this is a valid indicator of the thermal preference of the molluscan assemblages.

This fossil-modern comparison indicates that the modern and fossils faunas, even if only partially similar taxonomically, point toward a preference for the same temperature (around 20 °C). In a retrospective perspective, this may indicate that the MIS 5e SST (+ 2 °C warmer that the modern area temperature), was not warm enough to cause drastic shifts of the taxonomical composition of the community toward the increasing of species preferring higher temperatures, apart the entrance of the Senegalese Fauna, favoured by slightly warmer temperatures and acclimatized in waters cooler than their optimal conditions.

In a future perspective, it is possible to hypothesize that the autochthonous central Mediterranean fauna could not undergo drastic taxonomical reorganizations in consequence of + 2 °C of increase of the SST but will be resilient to the climate change as it was during MIS 5e.

Clearly it must be remembered that the modern global warming is markedly different from that characterizing the penultimate deglaciation, as they feature different time scales and linked to different causes (e.g., increased insolation versus increased anthropogenic climalterant gas emissions).

Furthermore, other relevant ecological processes, such as the invasion of alien species facilitated by direct and indirect human activities, are influencing the Mediterranean biota (e.g., Lessepsian migration and ships' water ballast), and the projected recolonization of Senegalese species (Albano *et al.*, 2021, 2024). These ecological processes could have more important effects on the Mediterranean mollusc fauna than the increase in temperature alone, which could, individually, be overcome with resilience by the native fauna.

The results here presented match those of Scarponi *et al.* (2022) who found, in the semi-enclosed Adriatic Sea, a clear resilient response of shallow mollusc communities to past interglacial-glacial changes. Indeed, the palaeocommunities, studied from a biogeographic point of view, were represented by the same ratios of the biogeographic groups in the last and modern interglacial

periods (MIS 5e – MIS 1), present in different percentages during the last glacial period (MIS 2). Moreover, due to the strong similarity between the two interglacial communities, despite the higher estimated SST (+3.5 °C) during MIS 5e, the Authors stated that the projected temperature increase due to CO_2 emissions will not alter current communities, even though the anthropic impact may produce more relevant, unpredicted changes (Scarponi *et al.*, 2022).

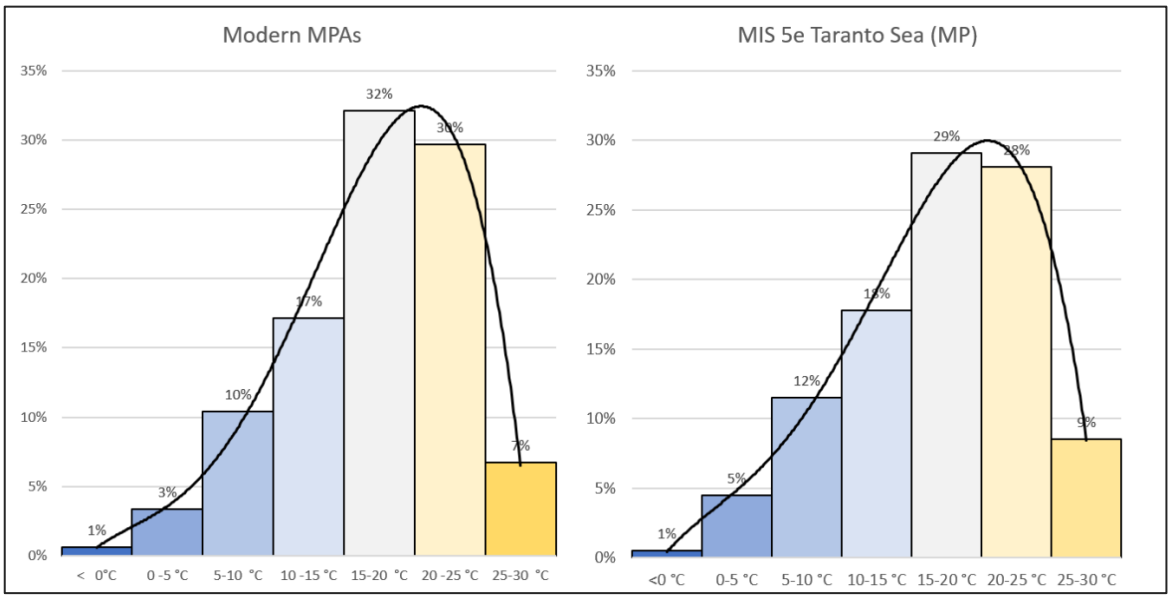

Figure 1. Comparison of preferred SST range between Modern Marine Protected areas from southern-central Italy (sandy vegetated bottoms) (modern molluscan species from Donnarumma *et al.*, 2018), and the fossil assemblage from the MIS 5e Taranto Sea (MP coastline).

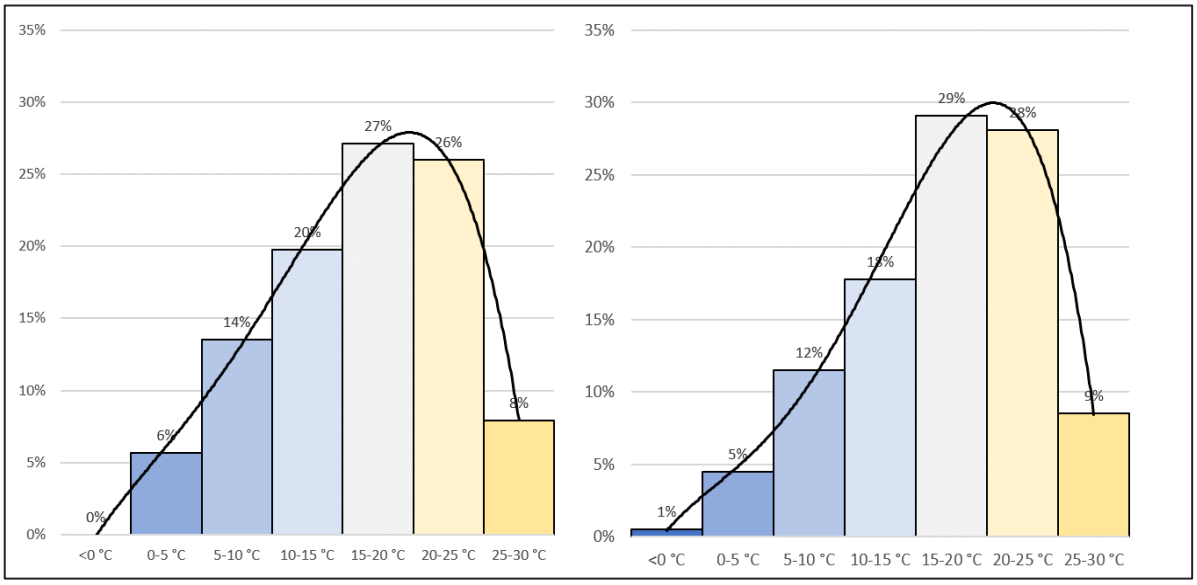

Figure 2. Comparison of preferred SST range between Modern Taranto seas (MP; Mar Piccolo, and MG, Mar Grande) (modern molluscan species from Mastrototaro *et al.*, 2008), and the fossil assemblage from the MIS 5e Taranto Sea (MP coastline).

9.3 Possible global warming effects on mobile substrates and red algae bioconstructions

The microfacies analysis performed on the MIS 5e calcarenite of Taranto, and in the MIS 5c/a sedimentary deposits of Capo Colonna, showed a common presence of micritic cements, showing several fabrics and enveloping the bioclastic sediment. The micrite is totally reconducted to a microbial mediated precipitate, due to the presence of epilithic to endolithic microbial/algal biofilm, which micritized the bioclasts and promoted early cementation of the sand grains, producing a stabilization of the shallow water mobile sediment. Such early hardening of the seabed, most likely produced small patches that served as solid substrate for the growth of autochthonous epilithic taxa (e.g., articulated calcareous algae, *Spondylus gaederopus*¸ oysters, barnacles, serpulids).

Moreover, the contribute of the microbial micritic cement appears crucial in the develop of coralline algae bioconstruction (coralligenous and maerl), confirming that the synsedimentary cementation that is well known to take places in modern Mediterranean algal reefs (Alexandersson, 1969; Bosence, 1985) is largely related to biomediated processes, as recently suggested by Bracchi *et al.* (2022) and Cipriani *et al.*, (2024) for modern coralligenous.

According to the literature data, microbial cements, and related early lithification phenomena, analogous to those found in MIS 5 of Taranto and Capo Colonna deposits, are typically associated with warm subtropical/tropical waters (mean annual SST warmer than 20-22 °C; Flugel, 2004), such as those found in the Bahamas and Northwest Australia (Diaz and Eberli, 2022). These micritic cements are, in fact, negligibly present in modern comparable facies of non-tropical domains and are totally absent in higher latitude cold temperate waters (Betlzer *et al.*, 1997). Hence, these modern cements are clearly linked to warm waters.

In the MIS 5 deposits, the recognition of such early lithification confirms warmer SST compared to present, far from tropical values. As the possible reaching of similar temperature in the next future, it is possible to hypothesize that such shallow marine cementation will become increasingly common in the modern mid-latitude Mediterranean Sea.

Microbial early cementation may occur on a larger scale, causing significant environmental changes, if the warming were further increase. The most obvious change could be a diffuse transition from soft to hard bottoms, with evident changes in the ecological and trophic relationships of the benthic life, promoting an alteration of the local coastal benthopelagic trophic interconnections, and also in the sedimentological processes that occur in coastal areas (Marcus and Boero, 1998; Danovaro, 2019).

Evaluating these possible changes, however, is far from the scope of this thesis, even if such a possibility was never considered in the scientific community (IPCC, 2023).

REFERENCES

Abe-Ouchi, A. (1996). Quaternary transition: A bifurcation in forced ice sheet oscillations? *Eos Transactions AGU, Fall Meeting Supplement*, 77(46), F415.

Aberhan, M., Fursich F.T. (1991). Paleoecology and paleoenvironments of the Pleistocene deposits of Bahia la Choya (Gulf of California, Sonora, Mexico). *Zitteliana* 18, 135- 163.

Addicott, W.O. (1969). Tertiary climatic change in the marginal northeastern Pacific Ocean. *Science*, 165(3893), 583-586.

Adhémar, J.A. (1842). Révolutions de la mer. Private publishing, France, 1842.

Aguirre, M.L. (2003). Late Pleistocene and Holocene palaeoenvironments in Golfo San Jorge, Patagonia: molluscan evidence. *Marine Geology*, 194, 3-30.

Aguirre, M.L., Richiano, S., Negro Sirch, Y. (2006). Palaeoenvironments and palaeoclimates of the Quaternary molluscan faunas from the coastal area of Bahia Vera-Camarones (Chubut, Patagonia). *Palaeogeography, Palaeoclimatology, Palaeoecology*, 229, 251– 286.

Alabiso, G., Giacomini, M., Milillo, M., Ricci, P. (2005). The Taranto Sea System: 8 years of chemical-physical measurements. *Biologia Marina Mediterranea*, 12, 369-373.

Albano P.G., Steger, J., Bošnjak M., Dunne B., Guifarro Z., Turapova, Hua Q., Kaufman D.S., Rilov G., Zuschin M. (2021). Native biodiversity collapse in the eastern Mediterranean. *Proceedings of the Royal Society B,* 288:20202469.

Albano, P. G., Schultz, L., Wessely, J., Taviani, M., Dullinger, S., Danise, S. (2024). The dawn of the tropical Atlantic invasion into the Mediterranean Sea. Proceedings of the National Academy of Sciences, 121(15), e2320687121.

Alexandersson, E.T. (1969). Recent littoral and sublittoral high-Mg calcite lithification in the Mediterranean. Sedimentology 12, 47-61.

Amorosi, A., Antonioli, F., Bertini, A., Marabini, S., Mastronuzzi, G., Montagna, P., Negri, A., Rossi, V., Scarponi, D., Taviani, M., Angeletti, L., Piva, A., Vai, G.B. (2014). The Middle-Upper Pleistocene Fronte Section (Taranto, Italy): An exceptionally preserved marine record of the Last Interglacial. *Global and Planetary Change*, 119, 23-38.

Anderson, N.T., Kelson, J. R., Kele, S., Daëron, M., Bonifacie, M., Horita, J., ..., Bergmann, K.D. (2021). A unified clumped isotope thermometer calibration (0.5–1,100 C) using carbonate-based standardization. *Geophysical Research Letters*, 48(7), e2020GL092069.

Antonioli, F. (2012). Sea level change in western-central Mediterranean since 300 kyr: comparing global sea level curves with observed data. *Alpine and Mediterranean Quaternary*, 25(1), 15-23.

Antonioli, F., Deino, A., Ferranti, F., Keller, J., Marabini, S., Mastronuzzi, G., Negri, A., Piva, A., Vai, G.B., Vigliotti L., (2008). Lo studio della sezione "Il Fronte" per la definizione del Piano Tarentiano (Puglia, Italy). *Il Quaternario, Italian Journal of Quaternary Sciences*, 21, 35-38.

Antonioli, F., Anzidei, M., Amorosi, A., Lo Presti, V., Mastronuzzi, G., Deiana, G., De Falco, G., Fontana, A., Fontolan, G., Lisco, S., Marsico, A., Moretti, M., Orrù, P.E., Sannino, G.M., Serpelloni, E., Vecchio, A. (2017). Sea-level rise and potential drowning of the Italian coastal plains: Flooding risk scenarios for 2100. *Quaternary Science Reviews*, 158, 29-43.

Ardovini, R., Cossignani, T. (2004). West African Seashells (including Azores, Madeira and Canary Is.). Museo Malacologico Piceno – Cupra Marittima. L'Informatore Piceno, Ancona, 319 pp.

Arrhenius, S. (1896). XXXI. On the influence of carbonic acid in the air upon the temperature of the ground. *The London, Edinburgh, and Dublin Philosophical Magazine and Journal of Science*, 41(251), 237-276.

Ávila, S.P., Melo, C., Silva, L., Ramalho, R.S., Quartau, R., Hipolito, A., Cordeiro, R., Rebelo, A.C., Madeira, P., Rovere, A., Hearty, P.J., Henriques, D., da Silva, C.M., de Frias Martins, A.M., Zazo, C. (2015). A review of

the MIS 5e highstand deposits from Santa Maria Island (Azores, NE Atlantic): palaeobiodiversity, palaeoecology and palaeobiogeography. *Quaternary Science Reviews*, 114, 126-148.

Ávila, S.P., Melo, C., Berning, B., Cordeiro, R., Landau, B., da Silva, C.M. (2016). *Persististrombus coronatus* (Mollusca: Strombidae) in the lower Pliocene of Santa Maria Island (Azores, NE Atlantic): paleoecology, paleoclimatology and paleobiogeographic implications. *Palaeogeography, Palaeoclimatology, Palaeoecology*, 441, 912-923.

Bahniuk, A., McKenzie, J.A., Perri, E., Bontognali, T.R.R., Vögeli, N., Rezende, C.E., Rangel, T.P. and Vasconcelos, C., (2015). Characterization of environmental conditions during microbial Mg-carbonate precipitation and early diagenetic dolomite crust formation: Brejo do Espinho, Rio de Janeiro, Brazil. Geological Society of London Special Publication 418, 243–259.

Bajnóczi, B., Schöll-Barna, G., Kalicz, N., Siklósi, Z., Hourmouziadis, G. H., Ifantidis, F., Kyparissi-Apostolika A., Pappa, M., Veropoulidou, Ziota, C. (2013). Tracing the source of Late Neolithic *Spondylus* shell ornaments by stable isotope geochemistry and cathodoluminescence microscopy. *Journal of Archaeological Science*, 40(2), 874-882.

Ballesteros, E. (2006). Mediterranean Coralligenous Assemblages. *Oceanography and Marine Biology: An Annual Review* 44, 123–195.

Bardají, T., Goy, J.L., Zazo, C., Hillaire-Marcel, C., Dabrio, C.J., Cabero, A., Ghaleb, B., Silva, P.G., Lario J. (2009). Sea level and climate changes during OIS 5e in the Western Mediterranean. *Geomorphology*, 104, 22–37.

Barrier, P., Di Geronimo S., Zibrowius H., Raisson G. (1990). Faune Sénégalienne du paléoescarpment du Capo Vaticano (Calabre Méridionale). Implications néotectoniques. *Proceedings of the Fourth Symposium on Ecology and Paleoecology of Benthic Communities*, 511-526.

Barrios, M.S., de Santiago Buey, C., Romero, E.G., Pozas, J.M. (2001). Textural and structural modifications of saponite from Cerro del Aguila by acid treatment. *Clay minerals*, 36(4), 483-488.

Basso, D. (1998). Deep rhodolith distribution in the Pontian Islands, Italy: a model for the paleoecology of a temperate sea. *Palaeogeography, Palaeoclimatology, Palaeoecology* 137, 173-187.

Basso, D., Corselli, C. (2002). Community versus biocoenosis in multivariate anaylsis of benthic molluscan thanatocoenoses. *Rivista Italiana di Paleontologia e Stratigrafia* 108 (1), 153-172.

Basso D., Brusoni, F. (2004). The molluscan assemblage of a transitional environment: the Mediterranean maërl from off the Elba Island (Tuscan Archipelago, Tyrrhenian Sea). *Bollettino Malacologico*, 40 (1-4), 37-45.

Basso, D., Bernasconi, M.P., Robba, E., Marozzo, S. (2008). Environmental evolution of the Marsala Sound, Sicily, during the last 6000 years. *Journal of Coastal Research*, 24 (1), 177-197.

Bathurst, R.G.C. (1974). Marine diagenesis of shallow water calcium carbonate sediments. *Annual Review of Earth and Planetary Sciences,* 2(1), 257-274.

Battipaglia, G., Jäggi, M., Saurer, M., Siegwolf, R. T., Cotrufo, M. F. (2008). Climatic sensitivity of δ18O in the wood and cellulose of tree rings: Results from a mixed stand of Acer pseudoplatanus L. and Fagus sylvatica L. *Palaeogeography, Palaeoclimatology, Palaeoecology*, 261(1-2), 193-202.

Beaty C.B. (1978). The Causes of Glaciation. *American Scientist*, 66(4), 452-459.

Belkin I.M. (2009). Rapid warming of Large Marine Ecosystems. *Progress in Oceanography*, 81, 207–213

Belluomini, G., Gliozzi, E., Ruggieri, G., Branca, M., Delitala, L. (1988). First dates on the terraces of the Crotone peninsula (Calabria, southern Italy). *Bollettino della Società Geologica Italiana* 107, 249–254.

Belluomini, G., Caldara, M., Casini, C., Cerasoli, M., Manfra, L., Mastronuzzi, G., Palmentola, G., Sansò, P., Tuccimei, P., Vesica, P.L. (2002). The age of Late Pleistocene shorelines and tectonic activity of Taranto area, Southern Italy. *Quaternary Science Reviews*, 21, 525–547.

Benigni, C., Corselli, C. (1981). Paleocomunità a Molluschi bentonici del Pliocene di Volpedo (Alessandria). *Rivista Italiana di Paleontologia e Stratigrafia*, 87(4).

Benzerara, K., Menguy, N., López-García, P., Yoon, T.-H., Kazmierczak, J., Tyliszczak, T., Guyot, F., Brown, G.E., 2006. Nanoscale detection of organic signatures in carbonate microbialites. Proceedings of the National Academy of Sciences, USA 103, 9440–9445.

Benzerara, K., Meibom, A., Gautier, Q., Kazmierczak, J., Stolarski, J., Menguy, N., Brown, G.E., 2010. Nanotextures of aragonite in stromatolites from the quasimarine Satonda crater lake, Indonesia. Geological Society of London Special Publication 336, 211–224.

Benzi, R., Parisi, G., Sutera, A., Vulpiani, A. (1982). Stochastic resonance in climatic change. *Tellus*, 34(1), 10-16.

Berger, A., Loutre, M. F. (1991). Insolation values for the climate of the last 10 million years. *Quaternary Science Reviews*, 10(4), 297-317.

Berger, W.H., Jansen, E. (1994). Mid-Pleistocene climate shift: the Nansen connection. In: Johannessen *et al.* (eds). The Polar Oceans and their Role in Shaping the Global Environment. *AGU Geophysical Monographs*, 85, 295–311.

Bernasconi, M.P., Robba E. (1993). Molluscan palaeoecology and sedimentological features: an integrated approach from the Miocene Meduna section, northern Italy, *Palaeogeography, Palaeoclimatology, Palaeoecology* 100 (3), 267-290.

Bernasconi, M.P., Stanley, D.J. (1997). Molluscan Biofacies, Their Distributions and Current Erosion on the Nile Delta Shelf. *Journal of Coastal Research* 13 (4), 1201-1212.

Bernasconi, M. P., Corselli, C., Carobene, L. (1997). A bank of the scleractinian coral *Cladocora caespitosa* in the Pleistocene of the Crati valley (Calabria, Southern Italy): growth versus environmental conditions. *Bollettino della Società Paleontologica Italiana*, 36, 53-62.

Bernasconi, M.P., Stanley D.J. (2014). Post-Greek Coastline Shifts Interpreted by Biostratigraphic Analysis on Hipponion's Seismotectonically Active Margin, Calabria, Italy. *Journal of Coastal Research*, 30(1), 1–12.

Bernasconi, M. P., Cefalà, M., Perri, E. (2015). Mid-latitude coralgal bioconstruction and endolithic microbialites: environmental significance during Quaternary climate variations. *Facies*, 61, 1-18.

Bertini, A., Martinetto, E. (2011). Reconstruction of vegetation transects for the Messinian–Piacenzian of Italy by means of comparative analysis of pollen, leaf and carpological records. *Palaeogeography, Palaeoclimatology, Palaeoecology*, 304(3-4), 230-246.

Bertini, A., Erba, E., Marino, M. (2022). Paleoclimatologia. In. Società Paleontologica Italiana (cur.), Manuale di Paleontologia. Seconda edizione. Idelson-Gnocchi, Napoli, pp. 411-440

Betzler, C., Brachert, T. C., Nebelsick, J. (1997). The warm temperate carbonate province: a review of the facies, zonations, and delimitations. *Courier Forschungsinstitut Senckenberg*, 201, 83-99.

Biagi, V., Corselli, C. (1984). Contributo alla conoscenza della malcofauna di un fondo SFBC (Pérès & Picard, 1964). *Bollettino Malacologico* 20 (8-9), 117-130.

Bianchi, C. N., Morri, C. (2003). Global sea warming and "tropicalization" of the Mediterranean Sea: biogeographic and ecological aspects. *Biogeographia. The Journal of Integrative Biogeography,* 24(1).

Birks, H.J.B., Birks, H.H. (1980). Quaternary Palaeoecology, E. Arnold, London.

Bigelow, N.H. (2013). Pollen Records, Late Pleistocene | Northern North America. Encyclopedia of Quaternary Science (Second Edition), 39-51.

Biswas, O., Ghosh, R., Agrawal, S., Morthekai, P., Paruya, D. K., Mukherjee, B., ..., Bera, S. (2021). A comprehensive calibrated phytolith based climatic index from the Himalaya and its application in palaeotemperature reconstruction. *Science of the Total Environment*, 750, 142280.

Boenzi, F., Caldara, M., Pennetta L. (1985). La trasgressione tirreniana nei dintorni di Castellaneta (Taranto). *Geologia Applicata e Idrogeologia*, 20, 163-175.

Bontognali, T.R.R., Vasconcelos, C., Warthmann, R.J., Dupraz, C., Bernasconi, S.M. and McKenzie, J.A. (2008). Microbes produce nanobacteria-like structures, avoiding cell entombment. Geology 36, 663–666.

Bonifay, F., Mars, P. (1959). Le Tyrrhènien dans le cadre de la chronologie quaternaire Mèditerranèenne. *Bulletin Societè Géologique France* 7(1), 62– 78.

Borghi, M., Vecchi, G. (2005). La malacofauna plio-pleistocenica del Torrente Stirone (PR): Cerithiidae – Turritellidae. *Parva Naturalia*, 7, 3-46.

Borrelli, M., Perri, E., Critelli, S., Gindre-Chanu L. (2021). The onset of the Messinian Salinity Crisis in the central Mediterranean recorded by pre-salt carbonate/evaporite deposition. *Sedimentology*, 68, 1159-1197.

Borrelli, M., Perri, E., Avagliano, D., Coraggio, F., Critelli, S. (2022). Paleogeographic and sedimentary evolution of North Calabrian basins during the Messinian Salinity Crisis (South Italy). *Marine and Petroleum Geology*, 141, 105726.

Borrelli, M., Perri, E., Morsilli, M., Critelli, S. (2023a). Late Permian-Triassic sedimentary evolution of the Southern Adriatic area based on wells and cores analysis. *Marine and Petroleum Geology*, 150, 106-154.

Borrelli, M., Manzo, E., Santagati, P., Perri, E. (2023b). Biosedimentary and palaeoecological characterization of Norian bioconstructions (Western Tethys, North Calabria). *Rendiconti Online della Società Geologica Italiana*, 59, 49-55.

Borrelli, M., Santagati, P., Guerrieri, S., Perri, E. (2024). Mid-latitude microbial-mediated modern beachrock formation (Santa Maria di Ricadi - Southern Italy). *Rendiconti Società Geologica Italiana*.

Bosence, D.W.J. (1985). The "Coralligène" of the Mediterranean—a Recent analog for Tertiary coralline algal limestones. *In Paleoalgology: Contemporary research and applications*, pp. 216-225. Berlin, Heidelberg: Springer Berlin Heidelberg.

Bottjer, D. J. (2016). Paleoecology: past, present and future. John Wiley & Sons, 222 pp.

Bracchi, V.A., Nalin, R., Basso, D. (2014). Paleoecology and dynamics of coralline dominated facies during a Pleistocene transgressive–regressive cycle (Capo Colonna marine terrace, Southern Italy). *Palaeogeography, Palaeoclimatology, Palaeoecology*, 414, 296–309.

Bracchi, V.A., Nalin, R., Basso D. (2016). Morpho-structural Heterogeneity of Shallow-Water Coralligenous in a Pleistocene Marine Terrace (Le Castella, Italy). *Palaeogeography, Palaeoclimatology, Palaeoecology*, 454, 101–112.

Bracchi, A.V., Bulegato, S., Basso D. (2020). Palaeoecology of the Pinna nobilis biofacies along the Stirone River (Early Pleistocene, Northern Italy). *Bollettino della Società Paleontologica Italiana*, 59(1), 41-55.

Bracchi, V.A., Bazzicalupo, P., Fallati, L., Varzi, A.G., Savini, A., Negri, M.P., ... , Basso, D. (2022). The main builders of Mediterranean coralligenous: 2D and 3D quantitative approaches for its identification. *Frontiers in Earth Science*, 10, 910522.

Brambilla, G., Galli, C., Santi, G. (1998). La fauna marina pleistocenica del Colle di Castenedolo (Brescia, Italia Settentrionale). Osservazioni cronologiche ed ambientali. *Natura bresciana*, 25, 35-62.

Brooks, S.J. (2006). Fossil midges (Diptera: Chironomidae) as palaeoclimatic indicators for the Eurasian region. *Quaternary Science Reviews*, 25(15-16), 1894-1910.

Brunetti, M.M. (2011). Il giacimento di Cava Lustrelle e la sua fauna malacologica. *Società Reggiana di Scienze Naturali, Notiziario* 2011, 21-34.

Brunetti, M.M., Vecchi, G. (2011). La malacofauna Plio-Pleistocenica del Torrente Stirone (Parma) VII. Rissoidae (II). *Parva Naturalia*, 9, 65-119.

Brunetti, M.M., Vecchi, G. (2014). La malacofauna Plio-Pleistocenica del Torrente Stirone (Parma). Parte VIII. Rissoidae (III), Adeorbidae, Caecidae, Hydrobiidae, Iravadiidae, Tornidae et Addenda. *Parva Naturalia*, 10, 69-128.

Burne, R, Moore, L. (1987). Microbialites: organosedimentary deposits of benthic microbial communities. *Palaios*, 2,241-25.

Caillon, N., Severinghaus, J.P., Jouzel, J., Barnola, J.M., Kang, J., Lipenkov, V.Y. (2003). Timing of atmospheric CO2 and Antarctic temperature changes across termination III. *Science*, 299, 1 728–731.

Caldara, M., Laviano, L. (1980). Osservazioni paleontologiche e paleoecologiche su un deposito quaternario affiorante a Punta della Penna (Mar Piccolo – Taranto). *Annali dell'Università di Ferrara. Sezione IX, Scienze geologiche e paleontologiche*, VI (suppl.), 57-71.

Caldara, M. (1986). La sezione tirreniana di Ponte del Re (Castellaneta Marina, Taranto): Analisi paleoecologica. *Atti della Società Toscana di Scienze Naturali*, Mem., Serie A, 93, 129-163.

Caley, T., Vázquez Riveiros N., Labeyrie, L., Cortijo, E., Duplessy J.C. (2021). Climate and the evolution of the ocean: the paleoceanographic data. In: Ramsteinm G., Landias, A., Bouttes, N., Sepulchre, P., Govin, A. (Eds), Paleoclimatology. Frontiers in Earth Sciences, Springer Nature Switzerland AG 2021, pp. 225-254.

Camoin, G., Gautret, P., Montaggioni, L.E., Cabioch, G. (1999). Nature and environmental significance of microbialites in Quaternary reefs: the Tahiti paradox. *Sedimentary Geology*, 126, 271-304.

Camoin, G., Cabioch G., Eisenhauer A., Braga J.C., Hamelin, B., Lericolais, G. (2006). Environmental significance of microbialites in reef environments during the last deglaciation. *Sedimentary Geology*, 185, 277–295.

Capron, E., Govin, A., Stone, E.J., Masson-Delmotte, V., Mulitza, S., Otto-Bliesner, B., *et al.* (2014). temporal and spatial structure of multi-millennial temperature changes at high latitudes during the Last Interglacial. *Quaternary Science Reviews*, 103, 116–133.

Cardellicchio, N., Annicchiarico, C., Di Leo, A.M., Giandomenico, S., Spada L. (2015). The Mar Piccolo of Taranto: an interesting marine ecosystem for the environmental problems studies. *Environmental Science and Pollution Research*, 23, 12495–12501.

Carpine, C. (1970). Ecologie de l'étage bathyal dans la Méditerranée occidentale. *Memories de l'Institut océanographique de Monac*, 2, 146.

Cerrone, C., Ascione, A., Robustelli, G., Tuccimei, P., Soligo, M., Balassone, G., Mormone, A. (2021). Late Quaternary uplift and sea level fluctuations along the Tyrrhenian margin of Basilicata-northern Calabria (southern Italy): New constraints from raised paleoshorelines. *Geomorphology*, 395, 107978.

Chafetz, H.S. (1986). Marine peloids: a product of bacterially induced precipitation. *Journal of Sedimentary* Petrology, 56, 812-817.

Chakroun, A., Zaghbib-Turki, D. (2017). Facies and fauna proxies used to reconstruct the MIS 5 and MIS 7 coastal environments in eastern Tunisia. *Geological Quarterly*, 61. DOI: http://dx.doi.org/10.7306/gq.1312.

Christ, N., Immenhauser, A., Wood, R. A., Darwich, K., Niedermayr, A. (2015). Petrography and environmental controls on the formation of Phanerozoic marine carbonate hardgrounds. *Earth-Science Reviews*, 151, 176-226.

Cipriani, M., Apollaro, C., Basso, D., Bazzicalupo, P., Bertolino, M., Bracchi, V.A., Bruno, F., Costa, G., Dominici, R., Gallo, A., Muzzupappa, M., Rosso, A., Sanfilippo, R., Sciuto, F., Vespasiano, G. Guido, A. (2024). Origin and role of non-skeletal carbonate in coralligenous build-ups: new geobiological perspectives in biomineralization processes. *Biogeosciences*, 21, 49–72, 2024

Cisneros, M., Cacho, I., Frigola, J., Canals, M., Masqué, P., Martrat, B., Casado, M., Grimalt, J. O., Pena, L. D., Margaritelli, G., Lirer, F. (2016). Sea surface temperature variability in the central-western Mediterranean Sea during the last 2700 years: a multi-proxy and multi-record approach. *Climate of the Past*, 12, 849–869.

Cita, M.B. (2008). Summary of Italian marine stages. *Episodes*, 31, 251-254.

Cita, M.B., Capotondi, L., Asioli, A. (2005). The Tyrrhenian stage in the Mediterranean: definition, usage and recognition in the deep-sea record. A proposal: *Rendiconti Accademia Nazionale dei Lincei*, serie 9 (16), 297–310.

Clark, P.U., Pollard, D. (1998). Origin of the middle Pleistocene transition by ice sheet erosion of regolith. *Paleoceanography*, 13(1), 1-9.

Cohen, K.M., Gibbard, P.L. (2022). Global chronostratigraphical correlation table for the last 2.7 million years (Poster version). Mendeley Data, V5, doi: 10.17632/dtsn3xn3n6.5

Columbu, A., Spötl, C., De Waele, J., Yu, T.L., Shen, C.C., Gázquez, F. (2019). A long record of MIS 7 and MIS 5 climate and environment from a western Mediterranean speleothem (SW Sardinia, Italy). *Quaternary Science Reviews,* 220, 230-243.

Coope, G.R. (2010). Coleopteran faunas as indicators of interglacial climates in central and southern England. *Quaternary Science Reviews*, 29(13-14), 1507-1514.

Cordeiro, R., Borges, J.P., Martins, A.M.F., Ávila, S.P. (2015). Checklist of the littoral gastropods (Mollusca Gastropoda) from the Archipelago of the Azores (NE Atlantic). *Biodiversity Journal*, 6, 855–900.

Cornu, S., Pätzold, J., Bard, E., Meco, J., Cuerda-Barcelo, J. (1993). Paleotemperature of the last interglacial period based on δ18O of Strombus bubonius from the western Mediterranean Sea. *Palaeogeography, Palaeoclimatology, Palaeoecology*, 103 (1-2), 1-20.

Corselli, C. (1981). La tanatocenosi di un fondo S.G.C.F. *Bollettino Malacologico* 17 (1-2), 1-26.

Cosel, R., von (2006a). Taxonomy of tropical West African bivalves II. Psammobiidae. *Bulletin du Muséum national d'Histoire naturelle, Paris, 4° série*, 11, 693-731.

Cosel, R., von (2006b). Taxonomy of tropical West African bivalves. VI. Remarks on Lucinidae (Mollusca, Bivalvia), with description of six new genera and eight new species. *Zoosystema*, 28(4), 805-851.

Cramer, W., Guiot, J., Fader, M., Garrabou, J., Gattuso, J. P., Iglesias, A., ... , Xoplaki, E. (2018). Climate change and interconnected risks to sustainable development in the Mediterranean. *Nature Climate Change*, 8(11), 972-980.

Critelli, S. (1999). The interplay of lithospheric flexure and thrust accommodation in forming stratigraphic sequences in the southern Apennines foreland basin system, Italy: *Memorie dell'Accademia Nazionale dei Lincei* 10, 257-326.

Critelli, S., Muto, F., Tripodi, V., Perri F. (2013). Link between thrust tectonics and sedimentation processes of stratigraphic sequences from the southern Apennines foreland basin system, Italy. *Rendiconti Online della Società Geologica Italiana* 25, 21-42.

Critelli, S., Muto, F., Perri, F., Tripodi, V. (2017). Interpreting Provenance Relations from Sandstone Detrital Modes, Southern Italy Foreland Region: stratigraphic record of the Miocene tectonic evolution. *Marine and Petroleum Geology* 87, 47-59.

Croll, J. (1864). On the physical cause of the change of climate during geological epochs. *Philosophical Magazie*, 28, 121-137.

Cutler, K.B., Edwards, R.L., Taylor, F. W., Cheng, H., Adkins, J., Gallup, C. D., ..., Bloom, A.L. (2003). Rapid sea-level fall and deep-ocean temperature change since the last interglacial period. *Earth and Planetary Science Letters*, 206(3-4), 253-271.

Dai Pra, G., Stearns, C.E. (1977). Sul Tirreniano di Taranto. Datazione sui coralli con il metodo del Th230/U234. *Geologica Romana*, 16, 231-242.

Dance, S.P. (1992). Shells. Dorling Kindersley Handbooks, London, 256 pp.

Danovaro, R. (2019). Biologia Marina. Second edition, UTET, De Agostini Scuola SpA, Novara, 485 pp.

Dauvin, J.C., Bakalem, A., Baffreau, A., Delecrin, C., Bellan, G., *et al.* (2017). The well sorted fine sand community from the western Mediterranean Sea: A resistant and resilient marine habitat under diverse human pressures. *Environmental Pollution,* 224, 336-351.

De Deckker, P., Arnold, L.J., van der Kaars, S., Bayon, G., Stuut, J. B. W., Perner, K., Santos, R.L., Uemura, R., Demuro, M. (2019). Marine Isotope Stage 4 in Australasia: A full glacial culminating 65,000 years ago–Global connections and implications for human dispersal. *Quaternary Science Reviews*, 204, 187-207.

De Torres, T., Ortiz, J. E., Arribas, I., Delgado, A., Julià, R., Martin-Rubi, J. A. (2010). Geochemistry of Persististrombus latus Gmelin from the Pleistocene Iberian Mediterranean realm. *Lethaia*, 43(2), 149-163.

Défarge, C. (2011). Organomineralization, in: Reitner, J., Thiel, V. (Eds.), Encyclopedia of Geobiology. Springer, Berlin, pp. 697-701.

Della Porta, G., Bahamonde, J.R., Kenter, J.A., Verwer, K. (2017). The Sierra del Cuera (Pennsylvanian microbial platform margin) in Asturias, north Spain. *Aapg Bulletin*, 101(4), 543-551.

Dell'Angelo, B., Sosso, M., Anistratenko, O., Anistratenko, V. (2017). Limpet-shaped gastropods of the genus *Diodora* (Vetigastropoda: Fissurellidae) from the Middle Miocene of Western Ukraine. *Acta Geologica Polonica*, 67, 235–247.

Delongueville, C., Pálsson, J., Scaillet, R., Ólafsdóttir, S.H. (2021). Mollusca (Bivalvia, Gastropoda, Polyplacophora and Scaphopoda) around Iceland: Sampling effort in research surveys in 2013-2015. *Marine and Freshwater Research in Iceland*, 41 pp.

Delongueville, C., Scaillet, R., Swinnen, F. (2019). New records of marine littoral Gastropoda and Bivalvia in the Azores Archipelago (Northeast Atlantic Ocean). *NOVAPEX*, 20, 35-43.

Denton, G.H. (2000). Does an asymmetric thermohaline–ice-sheet oscillator drive 100 000-yr glacial cycles? *Journal of Quaternary Science: Published for the Quaternary Research Association*, 15(4), 301-318.

Di Geronimo, I., Robba, E. (1976). Metodologie qualitative e quantitative per lo studio delle biocenosi e paleocomunità marine bentoniche. *Il Paleobenthos in una prospettiva paleoecologica Rapporto di lavoro* n.1, 1-36.

Di Geronimo, I., Robba, E. (1989). The structure of benthic communities in relation to basin stability. In: A. Boriani, M. Bonafede, G.B. Piccardo and G.B. Vai (Editors), The Lithosphere in Italy (Adv. Earth Sci. Res.). *Annali Convegno Accademia Nazionale dei Lincei*, 80, 341-352.

Di Leo, A., Annicchiarico, C., Cardellicchio, N., Giandomenico, S., Conversano, M., Castellano, G., Basile F., Martinelli W., Scortichini G., Spada, L., (2014). Monitoring of PCDD/Fs and dioxin-like PCBs and seasonal variations in mussels from the Mar Grande and the Mar Piccolo of Taranto (Ionian Sea, Southern Italy). *Environmental Science and Pollution Research*, 21, 13196-13207.

Diaz, M.R., Eberli, G.P., Blackwelder, P., Phillips, B., Swart, P.K. (2017). Microbially mediated organomineralization in the formation of ooids. *Geology*, 45(9), 771-774.

Diaz M.R., Eberli G.P. (2022). Microbial contribution to early marine cementation. *Sedimentology*, 69, 798–822.

Dickens, G.R. (2003). Rethinking the global carbon cycle with a large, dynamic and microbially mediated gas hydrate capacitor. *Earth and Planetary Science Letters*, 213(3–4), 169–183.

Dominici, S. (1994). Regressive-transgressive cycles from the Pliocene of the San Miniato area (Tuscany, Italy): paleoecology and sequence stratigraphy. Studies on Ecology and Paleoecology of Benthic Communities. Bollettino della Società Paleotologica Italiana, Special Volume 2, 117-126.

Dominici, S., Forli, M., Bogi, C., Guerrini, A., Benvenuti, M. (2020). Paleobiology from Museum collections: comparing historical and novel data on Upper Miocene molluscs of the Livorno Hills. *Rivista Italiana di Paleontologia e Stratigrafia*, 126, 65-109.

Donnarumma, L., Sandulli, R., Appolloni, L., Russo, G.F. (2018). Assessing molluscs functional diversity within different coastal habitats of Mediterranean marine protected areas. *Ecological Questions*, 29(3), 35-51.

Doughty, A.M., Kaplan, M.R., Peltier, C., Barker, S. (2021). A maximum in global glacier extent during MIS 4. *Quaternary Science Reviews*, 261, 106948.

Dowsett, H.J., Robinson, M.M. (2009). Mid-Pliocene equatorial Pacific Sea surface temperature reconstruction: a multi-proxy perspective. *Philosophical Transactions of the Royal Society*, 367, 109-125.

Dumitru, O.A., Polyak, V.J., Asmerom, Y. *et al.* (2020). Last Interglacial (sensu lato, ~130 to 75 ka) sea level history from cave deposits: a global standardized database. Earth System Science Data Discussions 4313861: 1–25.

Dunham, R.J. (1962). Classification of Carbonate Rocks According to Depositional Texture. In: Ham, W.E., Ed., Classification of Carbonate Rocks, AAPG, Tulsa, 108-121.

Duplessy, J. C., Lalou, C., Vinot, A.C. (1970). Differential isotopic fractionation in benthic foraminifera and paleotemperatures reassessed. *Science*, 168(3928), 250-251.

Duplessy, J.C., Roche, D.M., Kageyama, M. (2007). The deep ocean during the last interglacial period. *Science*, 316, 89–91.

Dupraz, C., Reid, R. P., Braissant, O., Decho, A. W., Norman, R.S., Visscher, P.T. (2009). Processes of carbonate precipitation in modern microbial mats. *Earth-Science Reviews*, 96(3), 141-162.

Dutton, A., Bard, E., Antonioli, F., Esat, T.M., Lambeck, K., McCulloch, M.T. (2009). Phasing and amplitude of sea-level and climate change during the penultimate interglacial. *Nature Geoscience*, 2(5), 355-359.

Dutton, A., Lambeck, K. (2012). Ice Volume and Sea Level During the Last Interglacial. *Science*, 337(6091), 216-219.

Dutton, A., Carlson, A.E, Long, A.J., Milne, G.A., P. U. Clark, P.I., DeConto, R., Horton, B.P., S. Rahmstorf, S., Raymo, M.E. (2015). Sea-level rise due to polar ice-sheet mass loss during past warm periods. *Science*, 349(6244), aaa4019.

Edwards, T.W.D., Fritz, P. (1986). Assessing meteoric water composition and relative humidity from18O and2H in wood cellulose: paleoclimatic implications for southern Ontario, Canada. *Applied Geochemistry*, 1(6), 715-723.

Eisenberg, J.M. (1983). Conchiglie. Atlanti della natura, Istituto geografico De Agostini, Novara, 224 pp.

El-Shazly, A., Elsayed, M.K., Pascucci, V. (2016). MIS 5 coastal carbonate diagenesis in the northern and southern Mediterranean Sea. Rapp. Comm. int. Mer Médit. 41, 55.

Emiliani, C. (1955). Pleistocene temperatures. *Journal of Geology*, 63, 538–578.

Emiliani, C. (1972). The Last Interglacial: Paleotemperatures and Chronology. *Science, New Series*, 171(3971), 571-573.

Epstein, S., Buchsbaum, R., Lowenstam, H. A., Urey, H.C. (1953). Revised carbonate-water isotopic temperature scale. *Geological Society of America Bulletin*, 64(11), 1315-1326.

Fabricius, F.H. (1977). Origin of marine ooids and grapestones. *Contributions to Sedimentology*, 7, 1–113.

Ferranti, L., Antonioli, F., Mauz, B., Amorosi, A., Dai Pra, G., Mastronuzzi, G., Monaco, C., Orrù, P., Pappalardo, M., Radtke, U., Renda, P., Romano, P., Sansò, P., Verrubbi, V. (2006). Markers of the last interglacial sea-level high stand along the coast of Italy: tectonic implications. *Quaternary International*, 145, 30-54.

Ferrero, E., Merlino, B., Provera, A., Martinetto, E. (2005). Associazione a molluschi marini e vegetali terrestri del Pliocene di Castellengo (Biella, Italia NW). *Rendiconti della Società Paleontogica Italiana,* 2, 87-106.

Finné, M., Woodbridge, J., Labuhn, I., Roberts, C.N., (2019). Holocene hydro-climatic variability in the Mediterranean: A synthetic multi-proxy reconstruction. *The Holocene*, 29, 847–863.

Fischer, H., Meissner, K. J., Mix, A. C., Abram, N. J., Austermann, J., Brovkin, V ., Capron, E., Colombaroli, D., Daniau, A.L., Dyez, K.A., Felis, T., Finkelstein, S.A., Jaccard, S.L., McClymont, E.L., Rovere, A., Sutter, J., Wolff, E.W., Affolter, S., Bakker, P., Ballesteros-Cánovas, J.A., Barbante, C., Caley, T., Carlson, A.E., Churakova (Sidorova), O., Cortese, G., Cumming, B.F., Davis, B.A.S., Vernal, A., Emile-Geay, J., Fritz, S.C., Gierz, P., Gottschalk, J., Holloway, M.D., Joos, F., Kucera, M., Loutre M.F., Lunt, D.J., Marcisz, K., Marlon, J.R., Martinez, P., Masson-Delmotte, V., Nehrbass-Ahles, C., Otto-Bliesner, B.L., Raible, C.C., Risebrobakken, B., Goñi M.F.S., Arrigo, J.S., Sarnthein, M., Sjolte, J., Thomas F. Stocker, T.F., Patricio A. Velasquez Alvárez1, Tinner, W., Valdes, P.J., Vogel, H., Wanner, H., Yan, Q.,Yu, Z., Ziegler, M., Zhou, L. (2018). Palaeoclimate constraints on the impact of 2 °C anthropogenic warming and beyond. *Nature Geoscience*, 11(7), 474-485.

Flügel, E. (2004). Microfacies of Carbonates Rocks. Springer Berlin, Heidelberg, 976 pp.

Fluteau, F., Sepulchre, P. (2021). Climate Evolution on the Geological Timescale and the Role of Paleogeographic Changes. In: Ramsteinm G., Landias, A., Bouttes, N., Sepulchre, P., Govin, A. (Eds),

Paleoclimatology. Frontiers in Earth Sciences, Springer Nature Switzerland AG 2021 Paleoclimatology (2021), 255-269.

Folk, R.L. (1959). Practical petrographic classification of limestones. *Bulletin of the American Association of Petroleum Geologists*, 43(1), 1-38.

Folk, R.L., Lynch L.F. (2001). Organic matter, putative nannobacteria and the formation of ooids and hardgrounds. *Sedimentology*, 48(2), 215-229.

Fornos, J.J., Ahr, W.M. (1997). Temperate carbonates on a modern, low-energy, isolated ramp; the Balearic platform, Spain. *Journal of Sedimentary Research*, 67(2), 364-373.

France-Lanord, C., Derry, L.A. (1997). Organic carbon burial forcing of the carbon cycle from Himalayan erosion. *Nature*, 390(6655), 65-67.

Francés, G., Mena, A., Diz, P. (2018). Climate change at different time levels. EduCO2cean Magazine, 2(2), 20 – 46

Freitas, P., Clarke, L.J., Kennedy, H., Richardson, C., Abrantes, F. (2005). Mg/Ca, Sr/Ca, and stable-isotope ($\delta^{18}O$ and $\delta^{13}C$) ratio profiles from the fan mussel *Pinna nobilis*: Seasonal records and temperature relationships. *Geochemistry, Geophysics, Geosystems*, 6, Q04D14.

Garilli, V. (2011). Mediterranean Quaternary interglacial molluscan assemblages: Palaeobiogeographical and palaeoceanographical responses to climate change. *Palaeogeography, Palaeoclimatology, Palaeoecology*, 312, 98–114.

Ghisotti, F. (1968). *Clanculus corallinus*. Società Italiana di Malacologia, Schede Malacologiche del Mediterraneo, *Serie 03Af01*, 4 pp.

Ghisotti, F., Melone, G.C. (1975). Catalogo illustrato delle conchiglie marine del Mediterraneo. *Conchiglie*, 208 pp.

Ghosh, P., Adkins, J., Affek, H., Balta, B., Guo, W., Schauble, E. A., ..., Eiler, J.M. (2006). $^{13}C–^{18}O$ bonds in carbonate minerals: A new kind of paleothermometer. *Geochimica et Cosmochimica Acta*, 70(6), 1439-1456.

Gianolla, D., Negri, M., Basso, D., Sciunnach, D. (2010). Malacological response to Pleistocene sea-level change in the Northern Po Plain, N. Italy: detailed palaeoenvironmental reconstructions from two Lombardian cores. *Rivista Italiana di Paleontologia e Stratigrafia*, 116 (1), 79-102.

Gignoux, M. (1913). Les formations marines miocenes et quaternaries dell'Italie du Sud et de la Sicilie. *Annales de l'Universté de Lyon*, 1 (36), 1-693.

Gindre-Chanu, L., Perri, E., Sharp, R.I., Peacock, D.C.P., Swart, R., Poulsen, R., Ferreira H., Machado, V. (2016). Origin and diagenetic evolution of gypsum and microbialitic carbonates in the Late Sag of the Namibe Basin (SW Angola). *Sedimentary Geology,* 342, 133–153.

Gindre-Chanu, L., Borrelli, M., Caruso, A., Critelli S., Perri, E. (2020). Carbonate/evaporitic sedimentation during the Messinian salinity crisis in active accretionary wedge basins of the northern Calabria, southern Italy. *Marine and Petroleum Geology*, 112, 104066.

Gliozzi, E. (1987). I terrazzi marini del Pleistocene superiore della penisola di Crotone (Calabria). *Geologica Romana*, 26, 17-79.

Goddéris. Y., Ramstein, G., Le Hir, G. (2021). The Phanerozoic Climate. In: Ramsteinm G., Landias, A., Bouttes, N., Sepulchre, P., Govin, A. (Eds), Paleoclimatology. Frontiers in Earth Sciences, Springer Nature Switzerland AG 2021, 359-383.

Gofas, S., Moreno, D., Salas, C. (coords.) (2011). Moluscos marinos de Andalucía. Volumen I, II. Servicio de Publicaciones e Intercambio Científico, Universidad de Málaga, 809 pp.

Graham, A.F.R.S. (1988). Mollusks: Prosobranch and Pyramidellid Gastropods. Synopses of the British Fauna (New Series) 2 (Second edition), 662 pp.

Grauel, A.L., Bernasconi, S.M. (2010). Core-top calibration of $\delta^{18}O$ and $\delta^{13}C$ of *G. ruber* (white) and *U. mediterranea* along the southern Adriatic coast of Italy. *Marine Micropaleontology*, 77(3-4), 175-186 .

Grossman, E.L., Ku, T.L. (1986). Oxygen and carbon isotope fractionation in biogenic aragonite: temperature effects. *Chemical Geology: Isotope Geoscience Section*, 59, 59-74.

Gruszczyński, M., Marshall, J. D., Goldring, R., Coleman, M. L., Małkowski, K., Gaździcka, E., ... Gatt, P. (2008). Hiatal surfaces from the Miocene Globigerina Limestone Formation of Malta: Biostratigraphy, sedimentology, trace fossils and early diagenesis. *Palaeogeography, Palaeoclimatology, Palaeoecology*, 270(3-4), 239-251.

Guallart, J., Templado, J. (2012). *Pinna nobilis*. En: VV.AA., Bases ecológicas preliminares para la conservación de las especies de interés comunitario en España: Invertebrados. Ministerio de Agricultura, Alimentación y Medio Ambiente, Madrid, 81 pp.

Guiot, J., Pons, A., de Beaulieu, J.L., Reille, M. (1989). A 140,000-year continental climate reconstruction from two European pollen records. *Nature*, 338(6213), 309-313.

Guiter, F., Andrieu-Ponel, V., de Beaulieu, J.L., Cheddadi, R., Calvez, M., Ponel, P., Reille, M., Keller, T., Goeury, C. (2003). The last climatic cycles in Western Europe: a comparison between long continuous lacustrine sequences from France and other terrestrial records. *Quaternary International*, 111, 59–4.

Guo, Z., Wilson, M., Dingwell, D.B., Liu, J. (2021). India-Asia collision as a driver of atmospheric CO2 in the Cenozoic. *Nature Communications*, 12(1), 3891.

Hall, C.A., (1964). Shallow-water marine climates and molluscan provinces. *Ecology*, 45, 226-234.

Hammer, Ø, and David A.T. Harper, D.A.T. (2006). Paleobiogeography and paleoecology. In Paleontological Data Analysis, Wiley-Blackwell, 184-251.

Hansson, H.G. (1998). NEAT (North East Atlantic Taxa): Scandinavian marine Mollusca Check-List. *Internet edition*, 120 pp. Available at: https://www.gu.se/sites/default/files/2020-10/NEAT%2AMollusca.pdf

Harmelin, J.G., Schlenz, R. (1964). Contribution preliminaire l'etude des peuplements du sediments des herbies de Phanerogames marines dela Mediterranee. *Recueil des Travaux de la Station Marine d'Endoume, 13.*

Harzhauser, M., Kronenberg, G. (2013). The Neogene Strombid Gastropod Persististrombus in the Paratethys Sea. *Acta Palaeontologica Polonica*, 58, 785-802.

Hays, J.D., Imbrie, J., Shackleton, N.J. (1976). Variations in the Earth's Orbit: Pacemaker of the Ice Ages: For 500,000 years, major climatic changes have followed variations in obliquity and precession. *Science*, 194(4270), 1121-1132.

Hearty, P.J., Dai Pra, G. (1992). The Age and Stratigraphy of Middle Pleistocene and Younger Deposits along the Gulf of Taranto (Southeast Italy). *Journal of Coastal Research*, 8(4), 882-905.

HELCOM (2012). Checklist of Baltic Sea Macro-species. *Baltic Sea Environment Proceedings*, 130, 203 pp.

Helmens, K.F., (2014). The Last Interglacial Glacial cycle (MIS 5-2) re-examined based on long proxy records from central and northern Europe. *Quaternary Science Reviews*, 86, 115e143.

Hillgärtner, H., Dupraz, C., Hug, W. (2001). Microbially induced cementation of carbonate sands: are micritic meniscus cements good indicators of vadose diagenesis? *Sedimentology*, 48(1), 117-131.

Hinojosa-Arango, G., Maggs, C.A., Johnson, M.P. (2009). Like a rolling stone: the mobility of maerl (Corallinaceae) and the neutrality of the associated assemblages. *Ecology*, 90(2), 517-528.

Hoffman, J.S., Clark, P.U., Parnell, A.C., He, F. (2017). Regional and global sea-surface temperatures during the last interglaciation. *Science*, 355(6322), 276-279.

Høsæter, T. (1986). An annotated check-list of marine molluscs of the Norwegian coast and adjacent waters. *Sarsia*, 71, 73-145.

Huntington, K.W., Petersen, S.V. (2023). Frontiers of Carbonate Clumped Isotope Thermometry. *Annual Review of Earth and Planetary Sciences*, 51, 611-641.

Hutson, W.H. (1980). The Agulhas current during the late Pleistocene: Analysis of modern faunal analogs. *Science*, 207, 64–66.

Huybers, P. (2009). Pleistocene glacial variability as a chaotic response to obliquity forcing. *Climate of the Past*, 5(3), 481-488.

Huybers, P., Wunsch, C. (2005). Obliquity pacing of the late Pleistocene glacial terminations. *Nature*, 434(7032), 491-494.

Hwang, I. G., Heller, P.L. (2002). Anatomy of a transgressive lag: Panther Tongue sandstone, Star Point formation, central Utah. Sedimentology, 49(5), 977-999.

Ihli, J., Wong, W.C. Noel, E.H., Kim, Y.Y., Kulak, A.N., Christenson, H.K., Duer, M.J., Meldrum F.C. (2014). Dehydration and crystallization of amorphous calcium carbonate in solution and air. *Nature Communications*, 5, 3169.

Ilyashuk, E. A., Ilyashuk, B. P., Heiri, O., Spötl, C. (2020). Summer temperatures and lake development during the MIS 5a interstadial: new data from the Unterangerberg palaeolake in the Eastern Alps, Austria. *Palaeogeography, Palaeoclimatology, Palaeoecology*, 560, 110020.

Imbrie, J., Kipp, N.G. (1971). A new micropaleontological method for quantitative paleoclimatology: application to a Late Pleistocene Caribbean core. In: Turekian, K.K. (Ed.), The Late Cenozoic Glacial Ages. Yale *University Press, New Haven and London*, 71–181.

Imbrie, J., Berger, A., Boyle, E.A., Clemens, S.C., Duffy, A., Howard, W.R., ..., Toggweiler, J.R. (1993). On the structure and origin of major glaciation cycles 2. The 100,000-year cycle. *Paleoceanography*, 8(6), 699-735.

IPCC (2007). Summary for policymakers. Contribution of Working Group I to the Fourth Assessment Report of the Intergovernmental Panel on Climate Change. In: Solomon, S., Qin, D., Manning, M., Chen, Z., Marquis, M., Averyt, K.B., Tignor, M., Miller, H.L. (Eds.), Climate Change 2007: the Physical Science Basis. Cambridge University Press, Cambridge, United Kingdom and New York, NY, USA.

IPCC (2023). Summary for Policymakers. In: Climate Change 2023: Synthesis Report. Contribution of Working Groups I, II and III to the Sixth Assessment Report of the Intergovernmental Panel on Climate Change [Core Writing Team, H. Lee and J. Romero (eds.)]. IPCC, Geneva, Switzerland, 1-34, doi: 10.59327/IPCC/AR6-9789291691647.001

Issel, A. (1914). Lembi fossiliferi quaternarie recenti nella Sardegna meridionale. *Accademia Nazionale dei Lincei, Serie 5*, 759-770.

Jansen, E., Sjoholm, J. (1991). Reconstruction of glaciation over the 6 Myr from ice-borne deposits in the Norwegian Sea. *Nature*, 349, 600–603.

Jansen, E., Overpeck, J., Briffa, K.R., Duplessy, J.C., Joos, F., Masson-Delmotte, V., Olago, D., Otto-Bliesner, B., Peltier, W.R., Rahmstorf, S., Ramesh, R., Raynaud, D., Rind, D., Solomina, O., Villalba, R., Zhang, D. (2007). Palaeoclimate. In: Climate Change 2007: The Physical Science Basis. Contribution of Working Group I to the Fourth Assessment Report of the Intergovernmental Panel on Climate Change. [Solomon, S., D. Qin, M. Manning, Z. Chen, M. Marquis, K.B. Averyt, M. Tignor and H.L. Miller (eds.)]. *Cambridge University Press, Cambridge, United Kingdom and New York, NY, USA*.

Jarret, M. (2009). The usefulness of mollusk shells in paleoclimate research: an Introduction of the techniques and a presentation of Eocene climate data. *Georgia Geological Society Guidebook*, 29, 43-50.

Joussaume, S., Duplessy, J.C. (2021). The Climate System: Its Functioning and History. In: Ramsteinm G., Landias, A., Bouttes, N., Sepulchre, P., Govin, A. (Eds), Paleoclimatology. *Frontiers in Earth Sciences, Springer Nature Switzerland AG 2021*, 1-22.

Jouzel, J., Lorius, C., Petit, J.R., Genthon, C., Barkov, N.I., Kotlyakov, V.M., Petrov, V.M., (1987). Vostok ice core: a continuous isotope temperature record over the last climatic cycle (160,000 years). *Nature*, 329(6138), 403-408.

Judd, E.J., Tierney, J.E., Huber, B.T., Wing, S.L., Lunt, D.J., Ford, H.L., Inglis, G.N., McClymont, E.L., O'Brien, C.L., Rattanasriampaipong, R., Si, W., Staitis, M.L., Thirumalai, K., Anagnostou, E., Cramwinckel, M.J., Dawson, R.R., Evans, D., Gray, W.R., Grossman, E.L., Henehan, M.J., Hupp, B.N., MacLeod, K.G., O'Connor, L.K., Sánchez Montes, M.L., Song, H., Zhang, Y.G. (2022). The PhanSST global database of Phanerozoic sea surface temperature proxy data. *Scientific Data*, 9, 753.

Kandiano, E.S., Bauch, H.A., Fahl, K. (2014). Last interglacial surface water structure in the western Mediterranean (Balearic) Sea: Climatic variability and link between low and high latitudes. *Global and Planetary Change*, 123, 67-76.

Kellner, L. (2003). A new species of *Gibberula* Swainson, 1840 (Cystiscidae) from Cape Verde Islands. (Mollusca: Gastropoda). *Club Conchylia lnformationen*, 35, 7-9.

Kennedy, H., Richardson, C.A., Duarte, C.M., Kennedy, D.P. (2001). Oxygen and carbon stable isotopic profiles on the fan mussel, *Pinna nobilis*, and reconstruction of sea surface temperature in the Mediterranean. *Marine Biology*, 139, 1115-1124.

Kennett, J.P., Cannariato, K.G., Hendy, I.L., Behl, R.J. (2003). Methane Hydrates in Quaternary Climate Change: The Clathrate Gun Hypothesis. *In Special Publications Series, American Geophysical Union, Washington, DC,* 54.

Kindler, P., Davaud, E., Strasser, A. (1997). Tyrrhenian coastal deposits from Sardinia (Italy): a petrographic record of high sea levels and shifting climate belts during the last interglacial (isotopic substage 5e). *Palaeogeography, Palaeoclimatology, Palaeoecology* 133, 1-25.

Kimball, J., Eagle, R., Dunbar, R. (2016). Carbonate "clumped" isotope signatures in aragonitic scleractinian and calcitic gorgonian deep-sea corals. *Biogeosciences*, 13, 6487–6505.

Köhler, P.F. Joos, S. Gerber, R. Knutti (2005). Simulating changes in vegetation distribution, land carbon storage, and atmospheric CO_2 in response to a collapse of the North Atlantic thermohaline circulation. *Climate Dynamics*, 25(7–8), 689–708.

Kobluk, D.R., Risk M.J. (1977). Micritization and Carbonate-Grain Binding by Endolithic Algae. *The American Association of Petroleum Geologists Bulletin*, 61(7), 1069-1082.

Konhauser, K.O., Newman, D.K., Kappler A. (2005). The potential significance of microbial Fe (III) reduction during deposition of Precambrian banded iron formations. *Geobiology*, 3(3), 167-177.

Konhauser, K., Riding, R. (2012). Bacterial biomineralization. *Fundamentals of Geobiology*, 105-130.

Koulouri, P., Dounas, C., Arvanitidis, C., Koutsoubas, D., Eleftheriou, A. (2006). Molluscan diversity along a Mediterranean soft bottom sublittoral ecsotone. *Scientia Marina*, 70(4), 573-583.

Kružić, P., Sršen, P., Benković, L. (2012). The impact of seawater temperature on coral growth parameters of the colonial coral Cladocora caespitosa (Anthozoa, Scleractinia) in the eastern Adriatic Sea. *Facies*, 58, 477–491.

Kukla, G.J., Bender M.L., de Beaulieu J.L., Bond G., Broecker, W.S., Cleveringa, P., Gavin, J.E., Herbert, T.D., Imbrie, J., Jouzel, J., Keigwin, L.D., Knudsen, K.L., McManus, J.F., Merkt, J., Muhs, D.R., Muller, H., Poore, R.Z., Porter, S.C., Seret, G., Shackleton, N.J., Turner, C., Tzedakis, P.C., Winograd, I.J. (2002). Last Interglacial Climates". *USGS Staff - Published Research*, 174.

La Mesa, G., Paglialonga, A., Tunesi, L. (2019). Manuali per il monitoraggio di specie e habitat di interesse comunitario (Direttiva 92/43/CEE e Direttiva 09/147/CE) in Italia: ambiente marino. *ISPRA, Serie Manuali e linee guida*, 190/2019.

Labeyrie, L.D., Duplessy, J.C., Blanc, P.L. (1987). Variations in mode of formation and temperature of oceanic deep waters over the past 125,000 years. *Nature*, 327(6122), 477-482

Laskar, J., Robutel, P., Joutel, F., Gastineau, M., Correia, A. C., Levrard, B. (2004). A long-term numerical solution for the insolation quantities of the Earth. *Astronomy & Astrophysics*, 428(1), 261-285.

Lemche, H. (1948). Northern and Arctic Tectibranch Gastropods. I. The larval shells II. A revision of the Cephalaspid species. Det *Kongelige Danske Videnskabernes Selskab, Biologiske Skrifter*, 5, 136 pp.

Limaye, R.B., Kumaran, K.P.N., Nair, K.M., Padmalal, D. (2007). Non-pollen palynomorphs as potential palaeoenvironmental indicators in the Late Quaternary sediments of the west coast of India. *Current Science*, 1370-1382.

Lisiecki, L.E., Raymo, M.E. (2005). A pliocene-pleistocene stack of 57 globally distributed benthic d18O records. *Paleoceanography*, 20, PA1003.

Liu, L., Jie, D., Liu, H., Gao, G., Li, D., Li, N. (2021). An evaluation of soil phytoliths for reconstructing plant communities and palaeoclimate in the northern temperate region. *European Journal of Soil Science*, 72(2), 900-917.

Lopes, E.P. (2010). Recent data on marine bivalves (Mollusca, Bivalvia) of the Cape Verde Islands, with records of six species new to the archipelago. *Zoologia Caboverdiana*, 1, 59-70.

Maier, E., Titschack, J. (2010). *Spondylus gaederopus*: A new Mediterranean climate archive — Based on high-resolution oxygen and carbon isotope analyses. *Palaeogeography, Palaeoclimatology, Palaeoecology*, 291, 228–238.

Manzo, E., Perri, E. Tucker, M.E. (2012). Carbonate deposition in a fluvial tufa system: processes and products (Corvino Valley – southern Italy). Sedimentology 59, 553–577.

Marcus, N.H., & Boero, F. (1998). Minireview: The importance of benthic-pelagic coupling and the forgotten role of life cycles in coastal aquatic systems. *Limnology and Oceanography*, 43(5), 763-768.

MARGO Project Members. (2009). Constraints on the magnitude and patterns of ocean cooling at the last glacial maximum. *Nature Geoscience,* https://doi.org/10.1038/NGEO411.

Mariani, L., Coletti, G., Mateu-Vicens, G., Bosio, G., Collareta, A., Khokhlova, A., Di Cencio, A., Casati, S., Malinverno, E. (2022). Testing an indirect palaeo-seagrass indicator: Benthic foraminifera from the Lower Pleistocene Posidonia meadow of Fauglia (Tuscany, Italy). *Marine Micropaleontology*, 173, 102126,

Marina, P., Urra, J., Rueda, J.L., Salas, C. (2012). Composition and structure of the molluscan assemblage associated with a *Cymodocea nodosa* bed in south-eastern Spain: seasonal and diel variation. *Helgol Marine Research*, 66, 585–599.

Marino, G., Rohling, E. J., Rijpstra, W.I.C., Sangiorgi, F., Schouten, S., Damsté, J.S.S. (2007). Aegean Sea as driver of hydrographic and ecological changes in the eastern Mediterranean. *Geology*, 35(8), 675-678.

Marion, A.F. (1883). Esquisse d'une topographie zoologique du Golf de Marseille. *Annales Musée d'Historie Naturelle Marseille*, 1, 108 pp.

Martinis, B., Robba E. (1971). Note Illustrative della carta geologica d'Italia alla scala 1:100.000, foglio 202 Taranto, arti grafiche ditta E. di Mauro, Cava Tirrenia, 9-26.

Martinson, D.G., Pisias, N.G., Hays, J.D., Imbrie, J., Moore, T. C., Shackleton, N.J. (1987). Age dating and the orbital theory of the ice ages: development of a high-resolution 0 to 300,000-year Chronostratigraphy. *Quaternary research*, 27(1), 1-29.

Martrat, B., Grimalt, J.O., Lopez-Martinez, C., Cacho, I., Sierro, F.J., Flores, J.A., Zahn, R., Canals, M., Curtis, J.H., Hodell, D.A. (2004). Abrupt temperature changes in the Western Mediterranean over the past 250,000 years. *Science*, 306(5702), 1762-1765.

Martrat, B., Jimenez-Amat, P., Zahn, R., Grimalt, J.O. (2014). Similarities and dissimilarities between the last two deglaciations and interglaciations in the North Atlantic region. *Quaternary Science Reviews*, 99, 122-134.

Maslin, M., Seidov, D., Lowe, J. (2001). Synthesis of the nature and causes of rapid climate transitions during the Quaternary. *Geophysical Monograph-American Geophysical Union*, 126, 9-52.

Maslin, M.A., Ridgwell, A.J. (2005). Mid-Pleistocene revolution and the 'eccentricity myth'. *Geological Society, London, Special Publications*, 247(1), 19-34.

Mastrototaro, F., Giove, A., D'Onghia, G., Tursi, A., Matarrese, A., Gadetta, V. (2008). Benthic diversity of the soft bottoms in a semi-enclosed basin of the Mediterranean Sea. *Journal of the Marine Biological Association of the United Kingdom*, 88(2), 247–252.

Matarrese, A., Mastrototaro, F., D'Onghia, G., Maiorano, P., Tursi, A. (2004). Mapping of the benthic communities in the Taranto seas using side-scan sonar and an underwater video camera. *Chemistry and Ecology*, 20(5), 377–386.

Mauz, B., Hassler, U. (2000). Luminescence chronology of Late Pleistocene raised beaches in southern Italy: new data of relative sea-level changes. *Marine Geology*, 170, 187 – 203.

May, R.M. (1981). Patterns in multi-species communities. In May, R.M. (ed.), *Theoretical Ecology: Principles and Applications,* Blackwell, Oxford, UK, 197–227.

McCrea, J.M. (1950). On the isotopic chemistry of carbonates and a paleotemperature scale. *The Journal of Chemical Physics*, 18(6), 849-857.

McInerney, F.A., Wing, S.L. (2011). The Paleocene-Eocene thermal maximum: A perturbation of carbon cycle, climate, and biosphere with implications for the future. *Annual Review of Earth and Planetary Sciences*, 39, 489–516.

McIntyre, A., Ruddiman, W.F. (1972). Northeast Atlantic Post-Eemian paleooceanography: a predictive analog of the future. *Quaternary Research*, 2, 350–354.

McManus, J.F., Oppo, D.W., Cullen, J.L. (1999). A 0.5-million-year record of millennial-scale climate variability in the North Atlantic. *Science*, 283, 971–975.

McManus, J.F., Oppo, D.W., Keigwin, L.D., Cullen, J.L., Bond, G.C. (2002). Thermohaline circulation and prolonged interglacial warmth in the North Atlantic. *Quaternary Research*, 58(1), 17-21.

Meco, J., (2008). Historia geológica del clima en Canarias. Joaquín Meco, Las Palmas de Gran Canaria, 296 pp.

Meco, J., Guillou, H., Carracedo, J.C., Lomoschitz, A., Ramos, A.J.G., Rodríguez-Yánez, J.J. (2002). The maximum warmings of the Pleistocene world climate recorded in the Canary Islands. *Palaeogeography, Palaeoclimatology, Palaeoecology*, 185, 197-210.

Melis, R., Bernasconi, M.P., Colizza, E., Di Rita, F., Equini Schneider E., Forte, E., Montenegro, M.E., Pugliese, N., Ricci, M. (2015). Late Holocene palaeoenvironmental evolution of the northern harbour at the Elaiussa Sebaste archaeological site (south-eastern Turkey): evidence from core ELA6. *Turkish Journal of Earth Sciences*, 24(6), 566-584.

Miao, Y., Jin, H., Liu, B., Herrmann, M., Sun, Z., Wang, Y. (2015). Holocene climate change on the northeastern Tibetan Plateau inferred from mountain-slope pollen and non-pollen palynomorphs. *Review of Palaeobotany and Palynology*, 221, 22-31.

Michel, J., Westphal, H., Cosel, R., von (2011). The mollusk fauna of soft sediments from the tropical, upwelling-influenced shelf of Mauritania (Northwestern Africa). *Palaios*, 26, 447-460.

Milankovitch, M. (1941). Kanon der Erdbestrahlung und seine Andwendung auf das Eiszeiten-problem. pp. 633.

Monegatti, P., Raffi, S. (2001). Taxonomic diversity and stratigraphic distribution of Mediterranean Pliocene bivalves. *Palaeogeography, Palaeoclimatology, Palaeoecology*, 165, 171–193.

Monnin, E., Indermühle, A., Dällenbach, A., Flückiger, J., Stauffer, B., Stocker, T., *et al.* (2001). Atmospheric CO_2 concentrations over the last glacial termination. *Science*, 291, 112–114.

Montagna, P., McCulloch, M., Mazzoli, C., Silenzi, S., Odorico, R. (2007). The non-tropical coral Cladocora caespitosa as the new climate archive for the Mediterranean: high-resolution (~weekly) trace element systematics. *Quaternary Science Reviews*, 26, 441–462.

Montefalcone, M., Tunesi, L., Ouerghi, A. (2021). A review of the classification systems for marine benthic habitats and the new updated Barcelona Convention classification for the Mediterranean. *Marine Environmental Research*, 169, 105387.

Montesinos, M., Ramos, A.J., Lomoschitz, A., Coca, J., Redondo, A., Betancort, J.F., Meco, J. (2014). Extralimital Senegalese species during Marine Isotope Stages 5.5 and 11 in the Canary Islands (29°N): sea surface temperature estimates. *Palaeogeography, Palaeoclimatology, Palaeoecology*, 410, 153-163.

Moore, C.H. (1977). Beach rock origin: some geochemical, mineralogical and petrographical considerations. *Geoscience and Man*, 18, 155–163.

Morad, S. (1998). Carbonate cementation in sandstones: distribution patterns and geochemical evolution. *Special pubblications, The International Association of Sedimentologists*, 26, 1-26.

Müller, P.J., Kirst, G., Ruhland, G., von Storch, I., Rosell-Mele, A., (1998). Calibration of the alkenone paleotemperature index U37K' based on core-tops from the eastern South Atlantic and the global ocean (60°N-60°S). *Geochimica et Cosmochimica Acta*, 62, 1757–1772.

Mutti, M., Bernoulli, D. (2003). Early marine lithification and hardground development on a Miocene ramp (Maiella, Italy): key surfaces to track changes in trophic resources in nontropical carbonate settings. *Journal of Sedimentary Research*, 73(2), 296-308.

Nalin, R., Basso, D., Massari, F. (2006). Pleistocene coralline algal build-ups (coralligène de plateau) and associated bioclastic deposits in the sedimentary cover of Cutro marine terrace (Calabria, southern Italy). *Geological Society, London Special Publication*, 255, 11–22.

Nalin, R., Massari, F. (2009). Facies and stratigraphic anatomy of a temperate carbonate sequence (Capo Colonna terrace, Late Pleistocene, Southern Italy). *Journal of Sedimentary Research*, 79, 210-225.

Nalin, R., Bracchi, V. A., Basso, D., Massari, F. (2012). *Persististrombus latus* (Gmelin) in the upper Pleistocene deposits of the marine terraces of the Crotone peninsula (southern Italy). *Italian journal of geosciences*, 131(1), 95-101.

Nalin, R., Lamothe, M., Auclair, M., Massari, F. (2020). Chronology of the marine terraces of the Crotone Peninsula (Calabria, southern Italy) by means of infrared-stimulated luminescence (IRSL). *Marine and Petroleum Geology*, 122, 104645.

Negri, A., Amorosi, A., Antonioli, F., Bertini, A., Florindo, F., Lurcock, P.C., Marabini, S., Mastronuzzi, G., Regattieri, E., Rossi, V., Scarponi, D., Taviani, M., Zanchetta, G., Vai, G.B. (2015). A potential global boundary stratotype section and point (GSSP) for the Tarentian Stage, Upper Pleistocene, from the Taranto area (Italy): Results and future perspectives. *Quaternary International*, 383(5), 145-157.

Nelson, C.S. (1988). An introductory perspective on non-tropical shelf carbonates. Sedimentary Geology 60, 3-12.

Nelson, C.S., James, N.P. (2000). Marine cements in mid-Tertiary cool-water shelf limestones of New Zealand and southern Australia. Sedimentology 47, 609-629.

Nessim, R.B., Tadros, H.R., Abou Taleb, A.E., Moawad, M.N. (2015). Chemistry of the Egyptian Mediterranean coastal waters. *The Egyptian Journal of Aquatic Research*, 41(1), 1-10.

Neuweiler, F., Daoust, I., Bourque, P. A., Burdige, D. (2007). Degradative Calcification of a Modern Siliceous Sponge from the Great Bahama Bank, The Bahamas: A Guide for Interpretation of Ancient Sponge-Bearing Limestones. *Journal of Sedimentary Research*, 77, 552–563.

Niederberger, M., Colfen, H. (2006). Oriented attachment and mesocrystals: non-classical crystallization mechanisms based on nanoparticle assembly. Physical Chemistry Chemical Physics 8, 3271–3287.

OBIS (2023). Ocean Biodiversity Information System. Intergovernmental Oceanographic Commission of UNESCO. Accessed: 30/05/2023. Available from: https://obis.org/.

Obreht, I., De Vleeschouwer, D., Wörmer, L., Kucera, M., Varma, D., Prange, M., Laepple, T., Wendt, J., Nadini-Weiss, S.D., Schulz, H., Hinrichs, K.U. (2022). Last Interglacial decadal sea surface temperature variability in the eastern Mediterranean. *Nature Geoscience*, 15(10), 812-818.

Obst, M., Dynes, J. J., Lawrence, J. R., Swerhone, G. D., Benzerara, K., Karunakaran, C., Karunakaran, A., Kaznatcheev, K., Tyliszczak, K., Hitchcock, A.P. (2009). Precipitation of amorphous $CaCO_3$ (aragonite-like)

by cyanobacteria: a STXM study of the influence of EPS on the nucleation process. *Geochimica et Cosmochimica Acta*, 73(14), 4180-4198.

Olausson, E. (1965). Evidence of climatic changes in North Atlantic deep-sea cores, with remarks on isotopic paleotemperature analysis. *Progress in Oceanography*, 3, 221-252.

Oliver, P.G., Cosel, R., von (1992). Taxonomy of Tropical West African Bivalves, IV. Arcidae. *Bulletin du Muséum national d'Histoire naturelle, Paris,* 4° série, 14, 293-381.

Oliver, P.G., Holmes, A.M., Killeen, I.J., Turner, J.A. (2016). Marine Bivalve Shells of the British Isles. Amgueddfa Cymru - National Museum Wales. Accessed: 25/02/2022. Available from: http://naturalhistory.museumwales.ac.uk/britishbivalves.

Oppo, D.W., McManus, J.F., Cullen, J.L. (2006). Evolution and demise of the last Interglacial warmth in the subpolar North Atlantic. *Quaternary Science Reviews*, 25, 3268–3277.

O'Reilly, S.S., Mariotti, G., Winter, A.R., Newman, S.A., Matys, E.D., McDermott, F., Pruss, S.B., Bosak, T., Summons, R.E., Klepac-Ceraj, V. (2017). Molecular biosignatures reveal common benthic microbial sources of organic matter in ooids and grapestones from Pigeon Cay, The Bahamas. *Geobiology*, 15(1), 112-130.

Overpeck, J.T., Otto-Bliesner, B.L., Miller, G.H., Muhs, D.R., Alley, R.B., Kiehl, J.T., (2006). Paleoclimatic evidence for future ice-sheet instability and rapid sea-level rise. *Science*, 311(5768), 1747-1750.

Ovtos, E.G. (2015). The Last Interglacial Stage: Definitions and marine highstand, North America and Eurasia. *Quaternary International* 383, 158e173.

Paillard, D. (1998). The timing of Pleistocene glaciations from a simple multiple-state climate model. *Nature*, 391, 378–381.

Paillard, D. (2021). Climate and Astronomical Cycles. In: Ramsteinm G., Landias, A., Bouttes, N., Sepulchre, P., Govin, A. (Eds), Paleoclimatology. Frontiers in Earth Sciences, Springer Nature Switzerland AG 2021, 1-22.

Paillard, D., Parrenin, F. (2004). The Antarctic ice sheet and the triggering of deglaciations. *Earth and Planetary Science Letters*, 227(3-4), 263-271.

Palerud, R., Gulliksen, B., Brattegar, T., Sneli, J.A., Vader, W. (2004). The marine macro-organisms in Svalbard waters. Norwegian Polar Institute, Skrifter, 201, 56 pp.

Palmentola, G., Carobene, L., Mastronuzzi, G., Sansò, P. (1990). I terrazzi marini Pleistocenici della Penisola di Crotone (Calabria). *Geografia Fisica e Dinamica Quaternaria*, 13, 75-80.

Parenzan, P. (1974). Carta d'identità delle conchiglie del Mediterraneo. Volume secondo – Bivalvi. Bios Taras Editrice, Taranto, 546 pp.

Pavia, G., Dulai, A., Festa, A., Gennari, R., Pavia, M., Carnevale, G. (2022). Palaeontology of the Upper Pliocene marine deposits of Rio Vaccaruzza, Villalvernia (Piedmont, NW Italy). *Rivista Italiana di Paleontologia e Stratigrafia* (*Research in Paleontology and Stratigraphy*), 128(1), 129-210.

Pedley, H.M., Bennett, S.M. (1985). Phosphorites, hardgrounds and syndepositional solution subsidence: a palaeoenvironmental model from the Miocene of the Maltese Islands. *Sedimentary Geology*, 45(1-2), 1-34.

Pedley, M., Rogerson, M., Middleton, R. (2009). Freshwater calcite precipitates from in vitro mesocosm flume experiments: a case for biomediation of tufas. Sedimentology 56, 511–527.

Peharda, M., Gillikin, D. P., Schöne, B. R., Verheyden, A., Uvanović, H., Markulin, K., Šarić, T., Janeković, I., Župan, I. (2022). Nitrogen Isotope Sclerochronology—Insights Into Coastal Environmental Conditions and *Pinna nobilis* Ecology. *Frontiers in marine science*, 8, 816879.

Peirano, A., Kružić, P., Mastronuzzi, G. (2009). Growth of Mediterranean reef of *Cladocora caespitosa* (L.) in the Late Quaternary and climate inferences. *Facies*, 55, 325–333.

Peppe, D.J., Baumgartner, A., Flynn, A., Blonder, B. (2018). Reconstructing paleoclimate and paleoecology using fossil leaves. *Methods in paleoecology: Reconstructing Cenozoic terrestrial environments and ecological communities*, 289-317.

Pérès, J.M. (1967). The mediterranean benthos. Oceanography and Marine Biology: an annual review.

Pérès, J.M. (1982). Zonations and organismic assemblages. In: Kinne, O., *Marine Ecology, A Comprehensive, Integrated Treatise on Life in Oceans and Coastal Water*s, 5(1), 642.

Pérès J.M., Picard J. (1964). Noveau manuel de bionomie benthique de la Méditerraneée. *Recueil des Travaux de la Station Marine d'Endoume,* 31, 1-137.

Pérès-Folgado, M., Sierro, F. J., Flores, J. A., Grimalt, J. O., Zahn, R. (2004). Paleoclimatic variations in foraminifer assemblages from the Alboran Sea (Western Mediterranean) during the last 150 ka in ODP Site 977. *Marine Geology*, 212(1-4), 113-131.

Perri, E. Tucker, M. (2007). Bacterial fossils and microbial dolomite in Triassic stromatolites. *Geology*, 35, 207–210.

Perri, E., Spadafora, A. (2011). Evidence of microbial biomineralization in modern and ancient stromatolites. *Stromatolites: interaction of microbes with sediments*, 631-649.

Perri, E., Manzo, E., Maurice, E., Tucker M.E. (2012a). Multi-scale study of the role of the biofilm in the formation of minerals and fabrics in calcareous tufa. *Sedimentary Geology*, 263-264, 16–29.

Perri, E., Tucker, M.E., Spadafora, A. (2012b). Carbonate organo-mineral micro-and ultrastructures in sub-fossil stromatolites: Marion Lake, South Australia. *Geobiology*, 10(2), 105-117.

Perri, E., Borrelli, M., Spadafora, A., Critelli S. (2017). The role of microbialitic facies in the micro- and nano-pore system of dolomitized carbonate platforms (Upper Triassic e Southern Italy). *Marine and Petroleum Geology*, 88, 1-17.

Perri, E., Tucker, M.E., Słowakiewicz, M., Whitaker, F., Bowen, L., Perrotta, I.D. (2018). Carbonate and silicate biomineralization in a hypersaline microbial mat (Mesaieed sabkha, Qatar): roles of bacteria, extracellular polymeric substances and viruses. *Sedimentology*, 65(4), 1213-1245.

Perri, E., Borrelli, M., Bernasconi, M.P., Gindre-Chanu, L., Spadafora, A., Critelli, S. (2019). Microbial-dominated carbonate depositional systems: a biosedimentary and stratigraphic reconstruction in the Late Triassic of Western Tethys (northern Calabria, Italy). *Facies*, 65(3), 31.

Perri, E., Słowakiewicz, M., Perrotta, I.D., Tucker, M.E. (2022). Biomineralization processes in modern calcareous tufa: Possible roles of viruses, vesicles and extracellular polymeric substances (Corvino Valley–Southern Italy). *Sedimentology*, 69(2), 399-422.

Perri, E., Borrelli, M., Heimhofer, U., Umbro, B., Santagati, P., Le Pera, E. (2024a). Microbial dominated Ca-carbonates in a giant Pliocene cold-seep system (Crotone Basin – South Italy). *Sedimentology*. doi: 10.1111/sed.13192

Perri, E., Borrelli, M., Robustelli, G., Manzo, E., Guerrieri, S., Santagati, P. (2024b). Microbially Induced Ca-Carbonate Authigenic Deposition in the Mercure Palaeolake (Middle Pleistocene - Southern Italy). *Rendiconti Online Società Geologica Italiana*, 63. https://doi.org/10.3301/ROL.2024.24.

Perry, C.T. (1999). Biofilm-related calcification, sediment trapping and constructive micrite envelopes: a criterion for the recognition of ancient grass-bed environments? *Sedimentology*, 46(1), 33-45.

Perry, R.S., Mcloughlin, N., Lynne, B.Y. Sephton, M.A., Oliver, J.D., Perry, C.C., Campbell, K., Engel, M.H., Farmer, J.D., Brasier, M.D., Staley, J.T. (2007). Defining biominerals and organominerals: direct and indirect indicators of life. *Sedimentary Geology*, 201(1-2), 157-179.

Petit, J.R., Jouzel, J., Raynaud, D., Barkov, N.I., Barnola, J.M., Basile, I., *et al.* (1999). Climate and atmospheric history of the past 420,000 years from the Vostok Ice Core, Antarctica. *Nature*, 399, 429–436.

Piani, P. (1984). Revisione del genere *Emarginula* Lamarck, 1801 in Mediterraneo. *Lavori della Società Italiana di Malacologia*, 21, 193-238.

Piazza, M., Robba, E. (1998). Autochthonous biofacies in the Pliocene Loreto Basin, BaJja California Sur, Mexico. *Rivista Italiana di Paleontologia e Stratigrafia*, 104(1), 227-262.

Picard, J. (1965). Recherches qualitatives sur les Biocenoses marines des substrats meubles draglables de la region de Marseillaise. *Recueil des Travaux de la Station Marine d'Endoume*, 36, 160 pp.

Picard, J. (1985). Reflexion sur les ecosystemes marins benthiques: hierarchisation, dynamique spatio-temporelle. *Tethis*, 11(3-4), 230-242.

Pierre, C. (1999). The oxygen and carbon isotope distribution in the Mediterranean water masses. *Marine Geology*, 153, 41–55.

Pisano, A., Marullo, S., Artale, V., Falcini, F., Yang, C., Leonelli, F. E., ... & Buongiorno Nardelli, B. (2020). New evidence of Mediterranean climate change and variability from sea surface temperature observations. *Remote Sensing*, 12(1), 132.

Plikk, A., Engels, S., Luoto, T. P., Nazarova, L., Salonen, J. S., Helmens, K.F. (2019). Chironomid-based temperature reconstruction for the Eemian Interglacial (MIS 5e) at Sokli, northeast Finland. *Journal of Paleolimnology*, 61, 355-371.

Poggiani, L., Mattioli, G., Micali, P. (2004). I Molluschi marini conchiferi della Provincia di Pesaro e Urbino. *I Quaderni dell'Ambiente*, 17, 175 pp.

Prada, F., Yam, R., Levy, O., Caroselli, E., Falini, G., Dubinsky, Z., Goffredo, S., Shemesh, A. (2019). Kinetic and metabolic isotope effects in zooxanthellate and non-zooxanthellate Mediterranean corals along a wide latitudinal gradient. *Frontiers in Marine Science*, 6, 522.

Prahl, F.G., Wakeham, S.G. (1987). Calibration of unsaturation patterns in long-chain ketone compositions for palaeotemperature assessment. *Nature*, 330(6146), 367-369.

Prahl, F.G., Muehlhausen, L.A., Zahnle, D.L. (1988). Further evaluation of long-chain alkenones as indicators of paleoceanographic conditions. *Geochimica et Cosmochimica Acta*, 52(9), 2303-2310.

Prell, W.L. (1985). The stability of low latitude sea surface temperatures: an evaluation of the CLIMAP reconstruction with emphasis on positive SST anomalies. U.S. Dept. of Energy, Washington D.C.

Preston, F. (1948). The commonness and rarity of species. *Ecology*, 29, 254–283.

Purdy, E.G. (1963). Recent calcium carbonate facies of the Great Bahama Bank. 2. Sedimentary facies. The *Journal of Geology*, 71(4), 472-497.

Raffi, S., Stanley, S.M., Marasti, R., (1985). Biogeographic patterns and Plio-Pleistocene extinction of Bivalvia in the Mediterranean and Southern North Sea. *Paleobiology*, 11, 368-388.

Raffi, S., Serpagli, E. (1994). Introduzione alla Paleontologia. UTET, Scienze della Terra, Torino, 654 pp.

Ragaini, L., Mariani, R. (1992). Analisi paleoecologica della malacofauna pliocenica di Camino Tondo (Grosseto, Italia). *Atti della Società Toscana di Scienze Naturali, Memorie, Serie A,* 99, 1-27.

Ragaini, L., Ficini, F., Zanchetta, G., Regattieri, E., Perchiazzi, N., Dallai, L. (2019). Mineralogy and oxygen isotope profile of *Pelecyora gigas* (Veneridae, Bivalvia) from Tuscan Pliocene. *Alpine and Mediterranean Quaternary*, 32(1), 5-13.

Ragazzola, F., Caragnano, A., Basso, D., Schmidt, D.N., Fietzke, J. (2020). Establishing temperate crustose Early Holocene coralline algae as archives for palaeoenvironmental reconstructions of the shallow water habitats of the Mediterranean Sea. *Palaeontology*, 63, 155–170.

Railsback, L.B., Gibbard, P.L., Head, M.J., Voarintsoa, N.R.G., Toucanne, S. (2015). An optimized scheme of lettered marine isotope substages for the last 1.0 million years, and the climatostratigraphic nature of isotope stages and substages. *Quaternary Science Reviews*, 111, 94-106.

Raymo, M.E. (1997). The timing of major climate terminations. *Paleoceanography*, 12, 577–585.

Raymo, M.E., Ruddiman, W.F., Froelich, P. N. (1988). Influence of late Cenozoic mountain building on ocean geochemical cycles. *Geology*, 16(7), 649-653.

Reich, S., Di Martino, E., Todd, J. A., Wesselingh, F. P., Renema, W. (2015). Indirect paleo-seagrass indicators (IPSIs): a review. *Earth-Science Reviews*, 143, 161-186.

Reid, R.P, Macintyre, I.G. (2000). Microboring versus recrystallization: further insight into the micritization process. *Journal of Sedimentary Research*, 70, 24–28.

Reitner, J., Gautret, P., Marin, F., Neuweiler, F. (1995). Automicrites in modern marine microbialite. Formation model via organic matrices (Lizard Island, Great Barrier Reef, Australia). *Bulletin de l'Institut océanographique de Monaco*, 14, 237–264.

Reijmer, J.J.G. (2021). Marine carbonate factories: Review and update. Sedimentology, 68(5), 1729-1796.

Relini, G. (2009). Biocostruzioni marine. Elementi di architettura naturale. *Quaderni Habitat*, 22, 160 pp.

Repetto, G., Bianco, I., Franchino, G., Lacroce, L., Orlando, F., Gallo, L.M., Bittarello, E. (2017). Popolamento a molluschi marini in ghiaie feldspatiche di cava all'interno di un relitto. *Rivista piemontese di Storia naturale*, 38, 131-146.

Repetto, G., Balistreri, P., Bevilacqua, A., Violanti D. (2020). *Persististrombus latus* (Gmelin, 1791) (Gastropoda: Strombidae) nel "Tirreniano" dell'isola di Favignana (Arcipelago delle Egadi, Sicilia ovest). *Rivista piemontese di Storia naturale*, 41, 3-22.

Riding, R. (2000). Microbial carbonates: the geological record of calcified bacterial–algal mats and biofilms. *Sedimentology*, 47, 179-214.

Riding, R. (2011). Microbialites, stromatolites, and thrombolites. In: Reitner J., Thiel V. (Eds.), Encyclopedia of Geobiology. Encyclopedia of Earth Sciences Series. Springer, Heidelberg, pp. 635-654.

Riding, R., Martin, J.M., Braga, J. C. (1991). Coral-stromatolite reef framework, upper Miocene, Almería, Spain. *Sedimentology*, 38(5), 799-818.

Riding R., Virgone A. (2020). Hybrid Carbonates: in situ abiotic, microbial and skeletal co-precipitates. *Earth-Science Reviews*, 208, 103300.

Rixen, M., Beckers, J. M., Levitus, S., Antonov, J., Boyer, T., Maillard, C., ..., Zavatarelli, M. (2005). The Western Mediterranean Deep Water: a proxy for climate change. *Geophysical Research Letters*, 32(12).

Roberts, N. (1998). The Holocene. An environmental history, Blackwell, Oxford.

Rohling, E.J., Cane, T.R., Cooke, S., Sprovieri, M., Bouloubassi, I., Emeis, K.C ., Schiebel, R., Kroon, D., Jorissen, F.J., Lorre, A., Kemp, A.E.S. (2002). African monsoon variability during the previous interglacial maximum. *Earth and Planetary Science Letters*, 202(1), 61-75.

Rohling, E.J., Grant, K., Hemleben, C.H., Siddall, M., Hoogakker, B.A.A., Bolshaw, M., Kucera, M., (2008). High rates of sea-level rise during the last interglacial period. *Nature Geoscience*, 1(1), 38-42.

Rosen, B.R. (1999). Paleoclimatic implications of the energy hypothesis from Neogene corals of the Mediterranean region. In: Agusti, J. Rook, L., Andrews, P. (eds) The evolution of Neogene terrestrial ecosystems in Europe. Cambridge University Press, Cambridge.

Rosenthal, Y., Linsley, B. (2006). Mg/Ca and Sr/Ca Paleothermometry from calcareous marine fossils, Encyclopedia of Quaternary Sciences, Elsevier Ltd, 20 pp.

Rosewater, J. (1975). An Annotated List of the Marine Mollusks of Ascension Island, South Atlantic Ocean. *Smithsonian Contributions to Zoology*, 189, 41 pp.

Rosso, A., Sanfilippo, R. (2009). The contribution of bryozoans and serpuloideans to coralligenous concretions from SE Sicily. In: UNEP-MAP-RAC/SPA, *Proceedings of the First Symposium on the Coralligenous and other calcareous bio-concretions of the Mediterranean Sea* (Tabarka, 15-16 January 2009), 123-128.

Royer, D.L. (2006). CO_2-forced climate thresholds during the Phanerozoic. *Geochimica et Cosmochimica Acta*, 70(23), 5665-5675.

Royle, S.H., Andrews, J.E., Marca-Bell, A., Turner, J., Kružić, P. (2015a). Seasonality in sea surface temperatures from $\delta^{18}O$ in Cladocora caespitosa: modern Adriatic to late Pleistocene, Gulf of Corinth. *Journal of Quaternary Science*, 30, 298-311.

Royle, S.H., Andrews, J.E., Turner, J., Kružić, P. (2015b). Environmental and diagenetic records from trace elements in the Mediterranean coral Cladocora caespitosa. *Palaeogeography, Palaeoclimatology, Palaeoecology*, 440, 734–749.

Rueda, J.L., Gofas, S., Urra, J., Salas, C. (2009). A highly diverse molluscan assemblage associated with eelgrass beds (*Zostera marina* L.) in the Alboran Sea: Micro-habitat preference, feeding guilds and biogeographic al distribution. *Scientia Marina*, 73, 679-700.

Rull, V. (2010). Ecology and palaeoecology: two approaches, one objective. *The Open Ecology Journal*, 3(1).

Russo, F., Gautret, P., Mastandrea, A., Perri, E. (2006). Syndepositional cements associated with nannofossils in the Marmolada Massif: Evidences of microbially mediated primary marine cements? (Middle Triassic, Dolomites, Italy). *Sedimentary Geology,* 185, 267-275.

Russo, P. (2021). La Famiglia Naticidae Guilding, 1834 (Gastropoda: Caenogastropoda) del Mare Mediterraneo. *Alleryana*, 39, 33-58.

Ryan, D.D., Clement, A.J.H., Jankowski, N.R., Stocchi, P. (2021). The last interglacial sea-level record of Aotearoa New Zealand, Earth System Scientific Data, 13, 3399–3437.

Sabelli, B. (1980). Conchiglie. Caratteristiche e ambienti di vita dei molluschi. Arnoldo Mondadori Editore, Milano, 502 pp.

Saenger, C., Affek, H., Felis, T., Thiagarajan, N., Lough, J.M., Holcomb, M. (2012). Carbonate clumped isotope variability in shallow water corals: Temperature dependence and growth-related vital effects. *Geochemica et Cosmochimica Acta*, 99, 224-242.

Sánchez-Goñi, M.F., Bakker, P., Desprat, S., Carlson, A.E., Van Meerbeeck, C.J., Peyron, O., Naughton, F., Fletcher, W.J., Eynaud, F., Rossignol, L., Renssen, H. (2012). European climate optimum and enhanced Greenland melt during the Last Interglacial. *Geology*, 40, 627–630.

Sánchez-Román, M., Vasconcelos, C., Schmid, T., Dittrich M., McKenzie, J.A., Zenobi, R., Rivadeneyra, M.A. (2008). Aerobic microbial dolomite at the nanometer scale: implications for the geologic record. *Geology* 36, 879–882.

Scarponi, D., Nawrot, R., Azzarone, M., Pellegrini, C., Gamberi, F., Trincardi, F., Kowalewski, M., 2022. Resilient biotic response to long-term climate change in the Adriatic Sea. Global Change Biology, 28(13), 4041-4053.

Scholle P.A., Ulmer-Scholle, D.S. (2003). A color guide to the petrography of carbonate rocks: grains, textures, porosity, diagenesis. *American Association of Petroleum Geologists, Memoir*, *77* (Vol. 77), 1-470.

Scotese, C., Song, H., Mills, B., van der Meer, D. (2021). Phanerozoic Paleotemperatures: The Earth's Changing Climate during the Last 540 million years. *Earth-Science Reviews*, 215, 10.1016.

Scotti, G., Chemello, R., Riggio, S. (1995). Benthic malacofauna of a shallow marine lagoon: the ''Stagnone di Marsala'' (Western Sicily). In: *Abstract 12th Interational. Malacological Congress, Vigo, Spain. Vigo: Unitas Malacologia, CSIC*, 256–257.

Seard, C., Camoin, G., Yokoyama, Y., Matsuzaki, H., Durand, N., Bard, E., Sepulcre, S., Deschamps, P. (2011). Microbialite development patterns in the last deglacial reefs from Tahiti (French Polynesia; IODP Expedition #310): Implications on reef framework architecture. *Marine Geology,* 27, 63–86.

Seppä, H., Bennett, K.D. (2003). Quaternary pollen analysis: recent progress in palaeoecology and palaeoclimatology. *Progress in Physical Geography*, 27, 548-79.

Sepulchre, P. (2002). Paleoclimatology and Paleoecology. Evolution of phylogenetic tree of life. Available at: https://www.eolss.net/ebooklib/sc_cart.aspx?File=E6-71-90-01

Shackleton, N.J. (1967). Oxygen isotope analyses and Pleistocene temperatures re-assessed. *Nature*, 215(5096), 15-17.

Shackleton, N.J. (1969). The last interglacial in the marine and terrestrial records. Proceedings of the *Royal Society of London. Series B. Biological Sciences*, 174(1034), 135-154.

Shackleton, N.J. (1987). Oxygen isotopes, ice volume and sea level. *Quaternary Science Reviews*, 6(3-4), 183-190.

Shackleton, N.J., Opdyke, N. D. (1973). Oxygen isotope and palaeomagnetic stratigraphy of Equatorial Pacific core V28-238: Oxygen isotope temperatures and ice volumes on a 105 year and 106 year scale. *Quaternary research*, 3(1), 39-55.

Shackleton, N.J., Sánchez-Goñi, M.F., Pailler, D., Lancelot, Y. (2003). Marine isotope substage 5e and the Eemian interglacial. *Global and Planetary Change*, 36(3), 151-155.

Shaltout, M., Omstedt, A. (2014). Recent sea surface temperature trends and future scenarios for the Mediterranean Sea. *Oceanologia*, 56, 411–443.

Sugihara, G. (1980). Minimal community structure: an explanation of species abundance patterns. The *American Naturalist*, 116(6), 770-787.

Suosaari, E.P., Lascu, I., Oehlert, A.M., Parlanti, P., Mugnaioli, E., Gemmi, M., Machabee, P.F., Piggot, A.M. Palma, A.T., Reid, R.P. (2022). Authigenic clays as precursors to carbonate precipitation in saline lakes of Salar de Llamara, Northern Chile. *Communications Earth & Environment*, 3: 325.

Siddall, M., Rohling, E.J., Thompson, W.G., Waelbroeck, C. (2008). Marine isotope stage 3 sea level fluctuations: Data synthesis and new outlook. *Reviews of Geophysics*, 46(4).

Siddall, M., Valdes, P. J. (2011). Implications of ocean expansion. *Nature Climate Change*, 1(6), 299-300.

Siegenthaler, U., Stocker, T. F., Monnin, E., Lüthi, D., Schwander, J., Stauffer, B., *et al.* (2005). Stable carbon cycle-climate relationship during the Late Pleistocene. *Science*, 310(5752), 1313–1317.

Silenzi, S., Bard, E., Montagna, P., Antonioli, F. (2005). Isotopic and elemental records in a non-tropical coral (Cladocora caespitosa): discovery of a new high-resolution climate archive for the Mediterranean Sea. *Global and Planetary Change*, 49, 94– 120.

Słowakiewicz, M., Perri, E., Tagliasacchi, E., Działak, P., Borkowski, A., Gradziński, M., Działak, P., Borkowski, A., Gradziński, M., Kele, S., Tucker, M.E. (2023). Viruses participate in the organomineralization of travertines. *Scientific Reports* 13(1), 11663.

Spada, G. (1970). Contributo alla malacofauna della biocenosi a Posidonia oceanica lungo le coste italiane. *Conchiglie*, 7(9-10), 125-135.

Spada, G., Sabelli B., Morandi V. (1973). Contributo alla conoscenza della malacofauna marina dell'Isola di Lampedusa. *Conchiglie*, 9(3-4), 29-67.

Spano, C. (1989). Macrofauna circalitorale del Pliocene inferiore di Capo S. Marco (Sardegna occidentale). *Rivista Italiana di Paleontologia e Stratigrafia*, 95(2), 137-172.

Spano, C., Puddu, B., Murgia, D. (2002). Autoecologia e ambiente dei molluschi marini alloctoni raccolti in spiagge delle coste meridionale e sud-orientale della Sardegna. *Rendiconti Seminario Facoltà Scienze Università Cagliari*, 72(2), 29-65.

Spooner, P.T., Guo, W., Robinson, L.F., Thiagarajan, N., Hendry, K.R., Rosenheim, B.E., Leng, M.J. (2016). Clumped isotope composition of cold-water corals: A role for vital effects? *Geochimica et Cosmochimica Acta*, 179, 123-141.

Spratt, R.M., Lisiecki, L E. (2016). A Late Pleistocene sea level stack. *Climate of the Past*, 12(4), 1079–1092.

Steneck, R.S. (1986). The ecology of coralline algal crusts: convergent patterns and adaptative strategies. *Annual review of ecology and systematics*, 17(1), 273-303.

Stirling, C.H., Esat, T.M., Lambeck, K., McCulloch, M.T. (1998). Timing and duration of the last interglacial: evidence for a restricted interval of widespread coral reef growth. *Earth and Planetary Science Letters*, 160, 745–762.

Sugihara, G. (1980). Minimal community structure: an explanation of species abundance patterns. *The American Naturalist*, *116*(6), 770-787.

Taviani, M. (2015). Unpersisting *Persististrombus*: a Mediterranean story. *Vieraea*, 42, 9-18.

Tebble, N. (1976). British Bivalve Seashells. A Handbook for Identification. Second Edition. Trustess of the British Museum (Natural History), London, 212 pp.

Thiagarajan, N., Adkins, J., Eiler, J. (2011). Carbonate clumped isotope thermometry of deep-sea corals and implications for vital effects. *Geochimica et Cosmochimica Acta*, 75, 4416–4425.

Thompson, S.B., Creveling, J.R. (2021). A global database of marine isotope substage 5a and 5c marine terraces and paleoshoreline indicators. *Earth System Science Data*, 13, 3467–3490.

Thunell, R.C., Williams, D.F. (1989). Glacial-Holocene salinity changes in the Mediterranean Sea: hydrographic and depositional effects. *Nature*, 338, 493-496.

Tomašových, A., Gallmetzer, I., Haselmair, A., Kaufman, D. S., Mavrič, B., Zuschin, M. (2019). A decline in molluscan carbonate production driven by the loss of vegetated habitats encoded in the Holocene sedimentary record of the Gulf of Trieste. *Sedimentology*, 66(3), 781-807.

Tomassetti, L., Brandano, M., Mateu-Vicens, G. (2022). 3D modelling of the upper Tortonian-lower Messinian shallow ramp carbonates of the Hyblean domain (Central Mediterranean, Faro Santa Croce, Sicily). *Marine and Petroleum Geology*, 135, 105393.

Tucker M.E., Wright V.P. (1990). Carbonate *Sedimentology*. Blackwell Scientific Publications, Oxford, U.K, 482 pp.

UNEP/MAP-RAC/SPA (2015). Handbook for interpreting types of marine habitat for the selection of sites to be included in the national inventories of natural sites of conservation interest. Bellan-Santini D., Bellan G., Bitar G., Harmelin J.G., Pergent G. Ed. RAC/SPA, 168 pp. + Annex.

Urey, H.C. (1947). The thermodynamic properties of isotopic substances. *Journal of the Chemical Society (Resumed*), 562-581.

Uvanović, H., Schöne, B.R., Markulin, K., Janeković, I., Peharda, M. (2021). Venerid bivalve Venus verrucosa as a high-resolution archive of seawater temperature in the Mediterranean Sea. *Palaeogeography, Palaeoclimatology, Palaeoecology*, 561, 110057.

Valenzano, E., Scardino, G., Cipriano, G., Fago, P., Capolongo, D., De Giosa, F., Lisco, S., Mele, D., Moretti, M., Mastronuzzi, G. (2018). Holocene morpho-sedimentary evolution of the Mar Piccolo Basin (Taranto, Southern Italy). *Geografia Fisica e Dinamica Quaternaria*, 119-135.

Väliranta, M., Birks, H. H., Helmens, K., Engels, S., Piirainen, M. (2009). Early Weichselian interstadial (MIS 5c) summer temperatures were higher than today in northern Fennoscandia. Quaternary Science Reviews, 28(9-10), 777-782.

Van der Kooij, B., Immenhauser, A., Steuber, T., Bahamonde Rionda, J.R., Merino Tome, O. (2010). Controlling factors of volumetrically important marine carbonate cementation in deep slope settings. *Sedimentology*, 57(6), 1491-1525.

van Lith, Y., Warthmann, R., Vasconcelos, C., McKenzie, J.A. (2003). Microbial fossilization in carbonate sediments: a result of the bacterial surface involvement in dolomite precipitation. *Sedimentology*, 50, 237–245.

Veron, J.E.N., Stafford-Smith, M. (2000). Corals of the World: Australian Institute of Marine Science Townsville MC. Qld, Australia.

Vertino, A., Stolarski, J., Bosellini, F.R., Taviani, M. (2014). Mediterranean corals through time: from Miocene to Present. *The Mediterranean Sea: Its history and present challenges*, 257-274.

Voskuil, R.P.A., Onverwagt, W.J.H. (1989). Inventariasation of the recent European and West African Cardiidae (Mollusca, Bivalvia). *Gloria Maris*, 28, 49-96.

Waelbroeck, C., Labeyrie, L., Duplessy, J. C., Guiot, J., Labracherie, M., Leclaire, H., Duprat, J. (1998). Improving past sea surface temperature estimates based on planktonic fossil faunas. *Paleoceanography*, 13(3), 272-283.

West, C.F., Burchell, M., Andrus, C.F.T. (2018). Molluscs and paleoenvironmental reconstruction in island and coastal settings: Variability, seasonality, and sampling. *Zooarchaeology in practice: Case studies in methodology and interpretation in archaeofaunal analysis*, 191-208.

Wehrmann, A. (1998). Modern cool-water carbonates on a coastal platform of northern Brittany, France: Carbonate production in macrophytic systems and sedimentary dynamics of bioclastic facies. Senckenbergiana maritima 28, 151-166.

Westphal, H., K. Heindel, K., Brandano, M., Peckmann, J. (2010). Genesis of microbialites as contemporaneous framework components of deglacial coral reefs, Tahiti (IODP 310). *Facies,* 56, 337–352.

Wierzbowski, H. (2021). Advances and challenges in palaeoenvironmental studies based on oxygen isotope composition of skeletal carbonates and phosphates. *Geosciences*, 11(10), 419.

Willeit, M., Ganopolski, A., Calov, R., Brovkin, V. (2019). Mid-Pleistocene transition in glacial cycles explained by declining CO2 and regolith removal. *Science Advances*, 5(4), eaav7337.

Whittaker, R.H. (1965). Dominance and Diversity in Land Plant Communities: Numerical relations of species express the importance of competition in community function and evolution. *Science*, 147(3655), 250-260.

Whittle, G.L., Kendall, C.G.S., Dill, R.F., Rouch, L. (1993). Carbonate cement fabric displayed: a traverse across the margin of the Bahamas Platform near Lee Stocking Island in the Exuma Cays. *Marine Geology*, 110, 213–243.

Wolf, K.H. (1965). Gradational sedimentary products of calcareous algae. *Sedimentology*, 5, 1-37.

WoRMS Editorial Board (2022). World Register of Marine Species. Available from https://www.marinespecies.org at VLIZ. Accessed 2022-12-30. doi:10.14284/170 .

Wye, K.R. (1991). The Encyclopedia of Shells. Knickerbocker Press, New York, 288 pp.

Zachos, J.C., Shackleton, N.J., Revenaugh, J.S., Pälike, H., Flower, B.P. (2001). Climate response to orbital forcing across the oligocene-miocene boundary. *Science*, 292, 274–278.

Zachos, J.C., Dickens, G.R., Zeebe, R.E. (2008). An early Cenozoic perspective on greenhouse warming and carbon-cycle dynamics. *Nature*, 451(7176), 279-283.

Zanchetta, G., Bini, M., Montagna, P., Regattieri, E., Ragaini, L., Da Prato, S., Ciampalini, A., Dallai, L., Leone, G. (2019). Stable isotope composition of fossil ahermatypic coral *Cladocora caespitosa* (L.) from Pleistocene raised marine terraces of The Livorno area (Central Italy). *Alpine and Mediterranean Quaternary*, 32, 73 – 86.

Zecchin, M., Nalin, R., Roda, C. (2004). Raised Pleistocene marine terraces of the Crotone peninsula (Calabria, Southern Italy): facies analysis and organization of their deposits. *Sedimentary Geology*, 172, 165 – 185.

Zecchin, M., Civile, D., Caffau, M., Roda, C. (2009). Facies and cycle architecture of a Pleistocene marine terrace (Crotone, southern Italy): A sedimentary response to late Quaternary, high-frequency glacio-eustatic changes. *Sedimentary Geology*, 216, 138–157.

Zecchin, M., Caffau, M. (2011). Key features of mixed carbonate-siliciclastic shallow-marine systems: the case of capo Colonna terrace (southern Italy). *Italian Journal of Geosciences*, 130 (3), 370–379.

Zecchin, M., Caffau, M., Civile, D., Critelli, S., Di Stefano, A., Maniscalco, R., Muto, F., Sturiale, G., Roda, C. (2012). The Plio-Pleistocene evolution of the Crotone Basin (southern Italy): interplay between sedimentation, tectonics and eustasy in the frame of Calabrian Arc migration. *Earth-Science Reviews*, 115(4), 273-303.

Zecchin, M., Caffau, M., Ceramicola, S. (2016). Interplay between regional uplift and glacio-eustasy in the Crotone Basin (Calabria, southern Italy) since 0.45 Ma: a review. *Global and Planetary Change* 143, 196–213.

Zecchin, M., Catuneanu, O., & Caffau, M. (2019). Wave-ravinement surfaces: classification and key characteristics. Earth-science reviews, 188, 210-239.

Zecchin, M., Civile, D., Caffau, M., Critelli, S., Muto, F., Mangano, G., Ceramicola, S. (2020). Sedimentary evolution of the Neogene-Quaternary Crotone Basin (southern Italy) and relationships with large-scale tectonics: A sequence stratigraphic approach. *Marine and Petroleum Geology*, 117, 104381.

Zecchin, M., Caffau, M., Catuneanu, O. (2021). Recognizing maximum flooding surfaces in shallow-water deposits: An integrated sedimentological and micropaleontological approach (Crotone Basin, southern Italy). *Marine and Petroleum Geology*, 133, 105225.

Zenone, A., Alagna, A., D'anna, G., Kovalev, A., Kreitschitz, A., Badalamenti, F., Gorb, S.N. (2020). Biological adhesion in seagrasses: the role of substrate roughness in *Posidonia oceanica* (L.) Delile seedling anchorage via adhesive root hairs. *Marine Environmental Research*, 160, 105012.

Ringraziamenti

A conclusione di questa tesi di dottorato, desidero esprimere la mia più sincera gratitudine a tutti coloro che mi hanno supportato durante questo percorso formativo.

Un sentito ringraziamento ai miei Supervisori, Prof. Edoardo Perri e Prof.ssa Maria Pia Bernasconi, per i preziosi insegnamenti ricevuti nel corso di questi anni e per il tempo dedicato alla discussione e revisione delle bozze. Grazie per avermi guidato con pazienza e competenza attraverso le varie esperienze formative che ho avuto l'opportunità di intraprendere in questo triennio.

Ringrazio i revisori Prof.ssa Silvia Danise e Prof.ssa Stefania Lisco per gli utili commenti e correzioni apportate alla bozza della tesi.

Desidero ringraziare il Dott. Mariano Davoli per le analisi al SEM effettuate presso il laboratorio di quest'Ateneo, la Prof.ssa Giovanna Scopelliti per le analisi isotopiche effettuate presso l'Università di Palermo, ed il Prof. Roberto Pizzolotto per l'aiuto con le elaborazioni dei dati. Ringrazio inoltre il Prof. Salvatore Critelli, coordinatore del corso di Dottorato, per le attività formative predisposte.

Un sincero ringraziamento va anche ai miei colleghi Mario e Salvatore per il loro prezioso aiuto in tutte le fasi.

Infine, desidero rivolgere un ringraziamento a tutta la mia famiglia, in particolare ai miei genitori, a mio fratello, ai miei zii, alla mia fidanzata, per il loro costante e incondizionato supporto durante questi tre anni. Il loro affetto e la loro fiducia in me riposta sono da sempre stati fonti inesauribile di motivazione e forza, senza di cui non avrei potuto raggiungere alcun traguardo. Grazie a tutti di cuore!

APPENDIXES: Molluscan fauna from the MIS 5e calcarenite (TA)

Appendix I: abundances and relative abundances of the molluscan species

Molluscan species listed in systematic order and with the WoRMS Editorial Board (2022) nomenclature.

MOLLUSCAN SPECIES	ABUNDANCE			RELATIVE ABUNDANCE		
	T5	T13	T17	T5	T13	T17
BIVALVIA						
Nucula nucleus (Linnaeus, 1758)	55	5	33	1,80%	0,32%	6,17%
Lembulus pella (Linnaeus, 1758)	55	40	3	1,80%	2,53%	0,56%
Arca noae Linnaeus, 1758	23	10	3	0,75%	0,63%	0,56%
Barbatia barbata (Linnaeus, 1758)	1	0	5	0,03%	0,00%	0,93%
Acar clathrata (Defrance, 1816)	0	3	3	0,00%	0,19%	0,56%
Anadara corbuloides (Monterosato, 1881)	2	1	0	0,07%	0,06%	0,00%
Striarca lactea (Linnaeus, 1758)	0	0	1	0,00%	0,00%	0,19%
Glycymeris bimaculata (Poli, 1795)	0	11	0	0,00%	0,70%	0,00%
Glycymeris glycymeris (Linnaeus, 1758)	10	44	5	0,33%	2,78%	0,93%
Pinna nobilis Linnaeus, 1758	6	3	0	0,20%	0,19%	0,00%
Pecten jacobaeus (Linnaeus, 1758)	0	8	1	0,00%	0,51%	0,19%
Mimachlamys varia (Linnaeus, 1758)	4	15	22	0,13%	0,95%	4,11%
Flexopecten flexuosus (Poli, 1795)	3	0	1	0,10%	0,00%	0,19%
Flexopecten glaber (Linnaeus, 1758)	2	9	4	0,07%	0,57%	0,75%
Spondylus gaederopus Linnaeus, 1758	8	2	5	0,26%	0,13%	0,93%
Ostrea edulis Linnaeus, 1758	4	1	0	0,13%	0,06%	0,00%
Ostrea stentina Payraudeau, 1826	11	8	0	0,36%	0,51%	0,00%
Hyotissa hyotis (Linnaeus, 1758)	0	0	15	0,00%	0,00%	2,80%
Ctena decussata (O. G. Costa, 1829)	0	1	5	0,00%	0,06%	0,93%
Loripes lacteus (Linnaeus, 1758)	40	3	3	1,31%	0,19%	0,56%
Lucinella divaricata (Linnaeus, 1758)	71	332	21	2,32%	21,01%	3,93%
Loripinus fragilis (Philippi, 1836)	128	25	17	4,18%	1,58%	3,18%
Myrtea spinifera (Montagu, 1803)	5	1	0	0,16%	0,06%	0,00%
Chama gryphoides Linnaeus, 1758	1	2	3	0,03%	0,13%	0,56%
Hemilepton nitidum (W. Turton, 1822)	6	0	0	0,20%	0,00%	0,00%
Cardita rufescens Lamarck, 1819	0	2	6	0,00%	0,13%	1,12%
Glans trapezia (Linnaeus, 1767)	0	6	7	0,00%	0,38%	1,31%
Cardites antiquatus (Linnaeus, 1758)	0	1	0	0,00%	0,06%	0,00%
Acanthocardia aculeata (Linnaeus, 1758)	1	2	0	0,03%	0,13%	0,00%
Acanthocardia echinata (Linnaeus, 1758)	7	0	0	0,23%	0,00%	0,00%
Acanthocardia paucicostata (G. B. Sowerby II, 1834)	55	0	0	1,80%	0,00%	0,00%
Acanthocardia tuberculata (Linnaeus, 1758)	0	20	12	0,00%	1,27%	2,24%
Parvicardium exiguum (Gmelin, 1791)	119	34	18	3,89%	2,15%	3,36%
Papillicardium papillosum (Poli, 1791)	17	67	13	0,56%	4,24%	2,43%
Laevicardium crassum (Gmelin, 1791)	0	6	0	0,00%	0,38%	0,00%

Cerastoderma glaucum (Bruguière, 1789)	0	2	0	0,00%	0,13%	0,00%
Spisula subtruncata (da Costa, 1778)	72	56	0	2,35%	3,54%	0,00%
Lutraria oblonga (Gmelin, 1791)	0	1	3	0,00%	0,06%	0,56%
Macomangulus tenuis (da Costa, 1778)	18	0	0	0,59%	0,00%	0,00%
Moerella distorta (Poli, 1791)	1	0	0	0,03%	0,00%	0,00%
Moerella pulchella (Lamarck, 1818)	928	69	22	30,34%	4,37%	4,11%
Gari fervensis (Gmelin, 1791)	1	1	0	0,03%	0,06%	0,00%
Abra alba (W. Wood, 1802)	91	3	0	2,97%	0,19%	0,00%
Azorinus chamasolen (da Costa, 1778)	6	0	0	0,20%	0,00%	0,00%
Venus casina Linnaeus, 1758	5	3	2	0,16%	0,19%	0,37%
Venus verrucosa Linnaeus, 1758	1	29	1	0,03%	1,84%	0,19%
Timoclea ovata (Pennant, 1777)	0	2	0	0,00%	0,13%	0,00%
Gouldia minima (Montagu, 1803)	29	109	132	0,95%	6,90%	24,67%
Dosinia exoleta (Linnaeus, 1758)	0	14	0	0,00%	0,89%	0,00%
Dosinia lupinus (Linnaeus, 1758)	20	0	0	0,65%	0,00%	0,00%
Pitar rudis (Poli, 1795)	44	12	0	1,44%	0,76%	0,00%
Callista chione (Linnaeus, 1758)	3	69	4	0,10%	4,37%	0,75%
Mysia undata (Pennant, 1777)	0	10	6	0,00%	0,63%	1,12%
Varicorbula gibba (Olivi, 1792)	286	108	44	9,35%	6,84%	8,22%
GASTROPODA						
Tectura virginea (O. F. Müller, 1776)	0	3	0	0,00%	0,19%	0,00%
S*maragdia viridis* (Linnaeus, 1758)	1	12	0	0,03%	0,76%	0,00%
Diodora graeca (Linnaeus, 1758)	1	3	11	0,03%	0,19%	2,06%
Diodora italica (Defrance, 1820)	2	0	0	0,07%	0,00%	0,00%
Emarginula octaviana Coen, 1939	0	1	3	0,00%	0,06%	0,56%
Haliotis tuberculata Linnaeus, 1758	0	0	3	0,00%	0,00%	0,56%
Clanculus corallinus (Gmelin, 1791)	0	8	6	0,00%	0,51%	1,12%
Gibbula ardens (Salis Marschlins, 1793)	0	10	4	0,00%	0,63%	0,75%
Gibbula guttadauri (Philippi, 1836)	0	0	1	0,00%	0,00%	0,19%
Gibbula magus (Linnaeus, 1758)	0	4	5	0,00%	0,25%	0,93%
Steromphala racketti (Payraudeau, 1826)	1	0	0	0,03%	0,00%	0,00%
Jujubinus striatus (Linnaeus, 1758)	0	2	0	0,00%	0,13%	0,00%
Calliostoma laugieri (Payraudeau, 1826)	1	13	22	0,03%	0,82%	4,11%
Calliostoma zizyphinum (Linnaeus, 1758)	0	3	0	0,00%	0,19%	0,00%
Tricolia pullus pullus (Linnaeus, 1758);	1	6	0	0,03%	0,38%	0,00%
Cerithium vulgatum Bruguière, 1792	28	39	4	0,92%	2,47%	0,75%
Bittium latreillii (Payraudeau, 1826)	20	28	33	0,65%	1,77%	6,17%
Bittium reticulatum (da Costa, 1778)	36	4	0	1,18%	0,25%	0,00%
Turritellinella tricarinata (Brocchi, 1814)	11	1	0	0,36%	0,06%	0,00%
Turritella turbona Monterosato, 1877	0	3	0	0,00%	0,19%	0,00%
Rissoa monodonta Philippi, 1836	27	62	3	0,88%	3,92%	0,56%
Rissoa violacea Desmarest, 1814	0	2	0	0,00%	0,13%	0,00%
Alvania geryonia (Nardo, 1847)	3	9	4	0,10%	0,57%	0,75%
Alvania lineata Risso, 1826	4	0	3	0,13%	0,00%	0,56%
Pusillina group *(Pusillina* Monterosato, 1884)	204	86	1	6,67%	5,44%	0,19%
Thetystrombus latus (Gmelin, 1791)	0	5	0	0,00%	0,32%	0,00%
Calyptraea chinensis (Linnaeus, 1758)	3	12	2	0,10%	0,76%	0,37%
Naticarius stercusmuscarum (Gmelin, 1791)	3	2	0	0,10%	0,13%	0,00%

Cryptonatica affinis (Gmelin, 1791)	0	1	0	0,00%	0,06%	0,00%
Euspira guilleminii (Payraudeau, 1826)	0	7	0	0,00%	0,44%	0,00%
Euspira macilenta (Philippi, 1844)	35	11	0	1,14%	0,70%	0,00%
Euspira montagui (Forbes, 1838)	0	2	0	0,00%	0,13%	0,00%
Monoplex parthenopeus (Salis Marschlins, 1793)	0	1	0	0,00%	0,06%	0,00%
Eulima glabra (da Costa, 1778)	2	0	0	0,07%	0,00%	0,00%
Bolinus brandaris (Linnaeus, 1758)	6	0	0	0,20%	0,00%	0,00%
Hexaplex trunculus (Linnaeus, 1758)	8	6	0	0,26%	0,38%	0,00%
Ocinebrina aciculata (Lamarck, 1822)	1	0	0	0,03%	0,00%	0,00%
Stramonita haemastoma (Linnaeus, 1767)	1	0	0	0,03%	0,00%	0,00%
Tritia incrassata (Strøm, 1768)	252	29	3	8,24%	1,84%	0,56%
Tritia mutabilis (Linnaeus, 1758)	0	4	0	0,00%	0,25%	0,00%
Columbella rustica (Linnaeus, 1758)	3	1	0	0,10%	0,06%	0,00%
Gibberula philippii (Monterosato, 1878)	1	0	0	0,03%	0,00%	0,00%
Granulina clandestina (Brocchi, 1814)	1	0	0	0,03%	0,00%	0,00%
Bivetiella cancellata (Linnaeus, 1767)	0	1	0	0,00%	0,06%	0,00%
Conus ermineus Born, 1778	0	5	0	0,00%	0,32%	0,00%
Conus ventricosus Gmelin, 1791	1	0	0	0,03%	0,00%	0,00%
Sorgenfreispira brachystoma (Philippi, 1844)	29	*2*	1	0,95%	0,13%	0,19%
Mangelia attenuata (Montagu, 1803)	7	1	0	0,23%	0,06%	0,00%
Mangelia cf *costata* (Pennant, 1777)	2	0	0	0,07%	0,00%	0,00%
Mangelia costulata Risso, 1826	2	0	0	0,07%	0,00%	0,00%
Mangelia cf *taeniata* (Deshayes, 1835)	1	0	0	0,03%	0,00%	0,00%
Parthenina terebellum (Philippi, 1844)	1	0	0	0,03%	0,00%	0,00%
Megastomia conoidea (Brocchi, 1814)	1	2	0	0,03%	0,13%	0,00%
Turbonilla acuta (Donovan, 1804)	4	0	0	0,13%	0,00%	0,00%
Pyrgiscus crenatus (T. Brown, 1827)	1	0	0	0,03%	0,00%	0,00%
Acteon tornatilis (Linnaeus, 1758)	3	1	0	0,10%	0,06%	0,00%
Retusa mammillata (Philippi, 1836)	0	2	0	0,00%	0,13%	0,00%
Retusa nitidula (Lovén, 1846)	1	3	0	0,03%	0,19%	0,00%
Bulla cf *striata* Bruguière, 1792	1	0	0	0,03%	0,00%	0,00%
Ringicula auriculata (Ménard de la Groye, 1811)	12	2	0	0,39%	0,13%	0,00%
Haminoea hydatis (Linnaeus, 1758)	0	*2*	0	0,00%	0,13%	0,00%
Weinkauffia turgidula (Forbes, 1844)	3	0	0	0,10%	0,00%	0,00%
SCAPHOPODA						
Antalis dentalis (Linnaeus, 1758)	2	3	1	0,07%	0,19%	0,19%
Antalis inaequicostata (Dautzenberg, 1891)	182	19	4	5,95%	1,20%	0,75%
Fustiaria rubescens (Deshayes, 1826)	10	5	1	0,33%	0,32%	0,19%
Dischides politus (S. Wood, 1842)	1	2	0	0,03%	0,13%	0,00%

Appendix II: biogeographical ranges and preferred SST ranges

List of identified species. Biogeographical ranges: Boreal-Celtic (*BC*), Lusitanian (*L*), Mauretanic-Senegalese (*MS*); "*" indicates species today absent in the Mediterranean but present outside it in the Lusitanian province. Species common to all the three samples are underlined. Preferential SST ranges (checked on OBIS, 2023) of each species.

Species/taxa	Biogeographic range			Preferred SST range (°C)						
	BC	*L*	*MS*	-5 – 0	0-5	5-10	10-15	15-20	20-25	25-30
Tectura virginea (O. F. Müller, 1776)	+	+	+			+	+	+	+	
Smaragdia viridis (Linnaeus, 1758)	+	+	+					+	+	+
Diodora graeca (Linnaeus, 1758)	+	+				+	+	+	+	
Diodora italica (Defrance, 1820)		+						+	+	
Emarginula octaviana Coen, 1939		+	+					+	+	+
Haliotis tuberculata Linnaeus, 1758	+	+	+				+	+	+	+
Clanculus corallinus (Gmelin, 1791)		+						+	+	
Gibbula ardens (Salis Marschlins, 1793)		+						+	+	
Gibbula guttadauri (Philippi, 1836)		+						+	+	
Gibbula magus (Linnaeus, 1758)	+	+	+			+	+	+	+	+
Steromphala racketti (Payraudeau, 1826)		+						+	+	
Jujubinus striatus (Linnaeus, 1758)	+	+					+	+	+	+
Calliostoma laugieri (Payraudeau, 1826)		+						+	+	
Calliostoma zizyphinum (Linnaeus, 1758)	+	+				+	+	+	+	
Tricolia pullus pullus (Linnaeus, 1758);	+	+	+					+	+	
Cerithium vulgatum Bruguière, 1792		+	+				+	+	+	+
Bittium latreillii (Payraudeau, 1826)		+					+	+	+	
Bittium reticulatum (da Costa, 1778)	+	+	+			+	+	+	+	+
Turritellinella tricarinata (Brocchi, 1814)	+	+			+	+	+	+	+	

Turritella turbona Monterosato, 1877	+	+		
Rissoa monodonta Philippi, 1836		+		
Rissoa violacea Desmarest, 1814	+	+		
Alvania geryonia (Nardo, 1847)		+		
Alvania lineata Risso, 1826		+		
Pusillina group (gen. Pusillina Monterosato, 1884)	+	+	+	
Thetystrombus latus (Gmelin, 1791)			+	
Calyptraea chinensis (Linnaeus, 1758)	+	+	+	
Naticarius stercusmuscarum (Gmelin, 1791)		+		
Cryptonatica affinis (Gmelin, 1791)	+	+		
Euspira guilleminii (Payraudeau, 1826)		+		
Euspira macilenta (Philippi, 1844)		+		
Euspira montagui (Forbes, 1838)	+	+		
Monoplex parthenopeus (Salis Marschlins, 1793)		+	+	
Eulima glabra (da Costa, 1778)	+	+	+	
Bolinus brandaris (Linnaeus, 1758)		+		
Hexaplex trunculus (Linnaeus, 1758)		+		
Ocinebrina aciculata (Lamarck, 1822)	+	+		
Stramonita haemastoma (Linnaeus, 1767)		+	+	
Tritia incrassata (Strøm, 1768)	+	+		
Tritia mutabilis (Linnaeus, 1758)		+		
Columbella rustica (Linnaeus, 1758)		+	+	
Gibberula philippii (Monterosato, 1878)		+		
Granulina clandestina (Brocchi, 1814)		+		
Bivetiella cancellata (Linnaeus, 1767)		+	+	
Conus ermineus Born, 1778		+*	+	

Conus ventricosus Gmelin, 1791		+	+	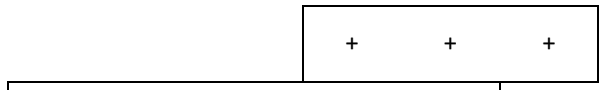
Sorgenfreispira brachystoma (Philippi, 1844)	+	+		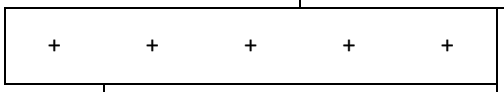
Mangelia attenuata (Montagu, 1803)	+	+		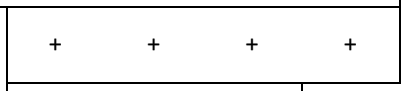
Mangelia cf *costata* (Pennant, 1777)	+	+		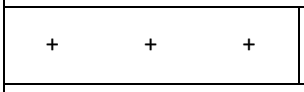
Mangelia costulata Risso, 1826	+	+		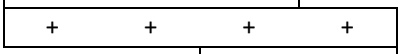
Mangelia cf *taeniata* (Deshayes, 1835)		+		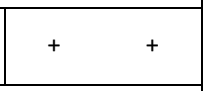
Parthenina terebellum (Philippi, 1844)	+	+		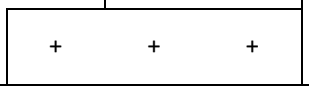
Megastomia conoidea (Brocchi, 1814)	+	+		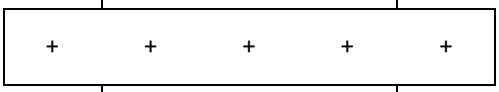
Turbonilla acuta (Donovan, 1804)	+	+		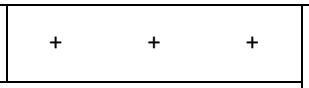
Pyrgiscus crenatus (T. Brown, 1827)	+	+		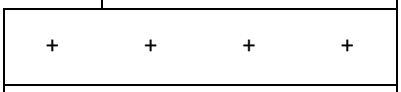
Acteon tornatilis (Linnaeus, 1758)	+	+	+	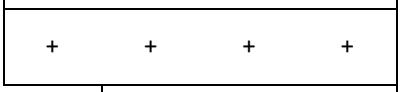
Retusa mammillata (Philippi, 1836)	+	+		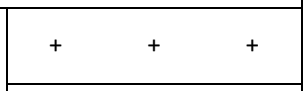
Retusa nitidula (Lovén, 1846)	+	+		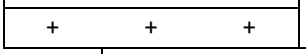
Bulla cf *striata* Bruguière, 1792		+	+	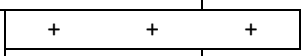
Ringicula auriculata (Ménard de la Groye, 1811)		+	+	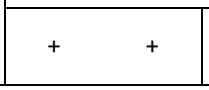
Haminoea hydatis (Linnaeus, 1758)		+	+	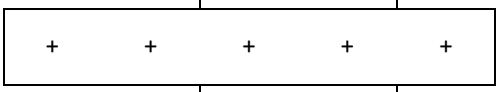
Weinkauffia turgidula (Forbes, 1844)		+	+	
Nucula nucleus (Linnaeus, 1758)	+	+	+	
Lembulus pella (Linnaeus, 1758)		+	+	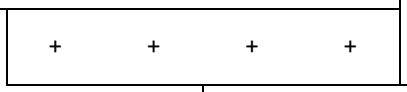
Arca noae Linnaeus, 1758		+	+	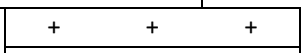
Barbatia barbata (Linnaeus, 1758)		+	+	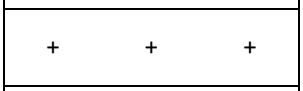
Acar clathrata (Defrance, 1816)		+	+	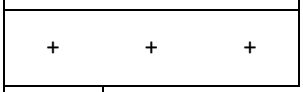
Anadara corbuloides (Monterosato, 1881)		+	+	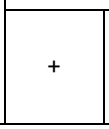
Striarca lactea (Linnaeus, 1758)	+	+	+	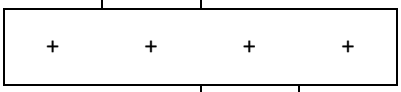
Glycymeris bimaculata (Poli, 1795)		+		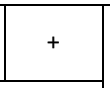
Glycymeris glycymeris (Linnaeus, 1758)	+	+		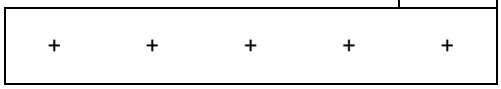

Pinna nobilis Linnaeus, 1758		+								+	+		
Pecten jacobaeus (Linnaeus, 1758)		+	+						+	+	+	+	
Mimachlamys varia (Linnaeus, 1758)	+	+	+				+	+	+	+	+		
Flexopecten flexuosus (Poli, 1795)		+								+	+		
Flexopecten glaber (Linnaeus, 1758)		+							+	+	+		
Spondylus gaederopus Linnaeus, 1758		+	+							+	+		
Ostrea edulis Linnaeus, 1758	+	+				+	+	+	+	+			
Ostrea stentina Payraudeau, 1826		+	+							+	+	+	
Hyotissa hyotis (Linnaeus, 1758)			+						+	+	+	+	
Ctena decussata (O. G. Costa, 1829)	+	+	+						+	+	+		
Loripes lacteus (Linnaeus, 1758)	+	+	+	*nd*	*nd*	*nd*	*nd*	*nd*	*nd*	*nd*	*nd*	*nd*	
Lucinella divaricata (Linnaeus, 1758)	+	+							+	+	+		
Loripinus fragilis (Philippi, 1836)		+	+							+	+		
Myrtea spinifera (Montagu, 1803)	+	+	+			+	+	+	+	+			
Chama gryphoides Linnaeus, 1758		+	+							+	+	+	
Hemilepton nitidum (W. Turton, 1822)	+	+					+	+	+	+			
Cardita rufescens Lamarck, 1819		+*	+									+	
Glans trapezia (Linnaeus, 1767)		+	+							+	+		
Cardites antiquatus (Linnaeus, 1758)		+								+	+	+	
Acanthocardia aculeata (Linnaeus, 1758)	+	+					+	+	+				
Acanthocardia echinata (Linnaeus, 1758)	+	+				+	+	+	+	+			
Acanthocardia paucicostata (G. B. Sowerby II, 1834)	+	+							+	+	+		
Acanthocardia tuberculata (Linnaeus, 1758)	+	+							+	+	+		
Parvicardium exiguum (Gmelin, 1791)	+	+				+	+	+	+	+			
Papillicardium papillosum (Poli, 1791)	+	+	+						+	+	+		

Laevicardium crassum (Gmelin, 1791)	+	+	+	+	+	+	+	+	+	
Cerastoderma glaucum (Bruguière, 1789)	+	+			+	+	+	+		
Spisula subtruncata (da Costa, 1778)	+	+	+		+	+	+			
Lutraria oblonga (Gmelin, 1791)	+	+	+			+	+			
Macomangulus tenuis (da Costa, 1778)	+	+		+	+	+	+	+	+	
Moerella distorta (Poli, 1791)		+	+					+	+	
Moerella pulchella (Lamarck, 1818)		+	+					+	+	
Gari fervensis (Gmelin, 1791)	+	+	+	+	+	+	+	+		
Abra alba (W. Wood, 1802)	+	+	+		+	+	+	+	+	
Azorinus chamasolen (da Costa, 1778)	+	+	+	+	+	+	+	+	+	
Venus casina Linnaeus, 1758	+	+	+		+	+	+	+	+	+
Venus verrucosa Linnaeus, 1758	+	+	+		+	+	+	+		
Timoclea ovata (Pennant, 1777)	+	+	+	+	+	+	+	+		
Gouldia minima (Montagu, 1803)	+	+	+	+	+	+	+	+		
Dosinia lupinus (Linnaeus, 1758)	+	+	+		+	+	+	+	+	
Desini exoleta (Linnaeus, 1758)	+	+	+	+	+	+	+	+	+	+
Pitar rudis (Poli, 1795)	+	+	+			+	+	+		
Callista chione (Linnaeus, 1758)	+	+				+	+	+	+	
Mysia undata (Pennant, 1777)	+	+		+	+	+	+	+		
Varicorbula gibba (Olivi, 1792)	+	+	+		+	+	+	+		
Antalis dentalis (Linnaeus, 1758)	+	+				+	+	+		
Antalis inaequicostata (Dautzenberg, 1891)		+						+	+	
Fustiaria rubescens (Deshayes, 1826)		+	+					+	+	
Dischides politus (S. Wood, 1842)		+	+					+	+	

Appendix III: photographs of molluscan and other taxa

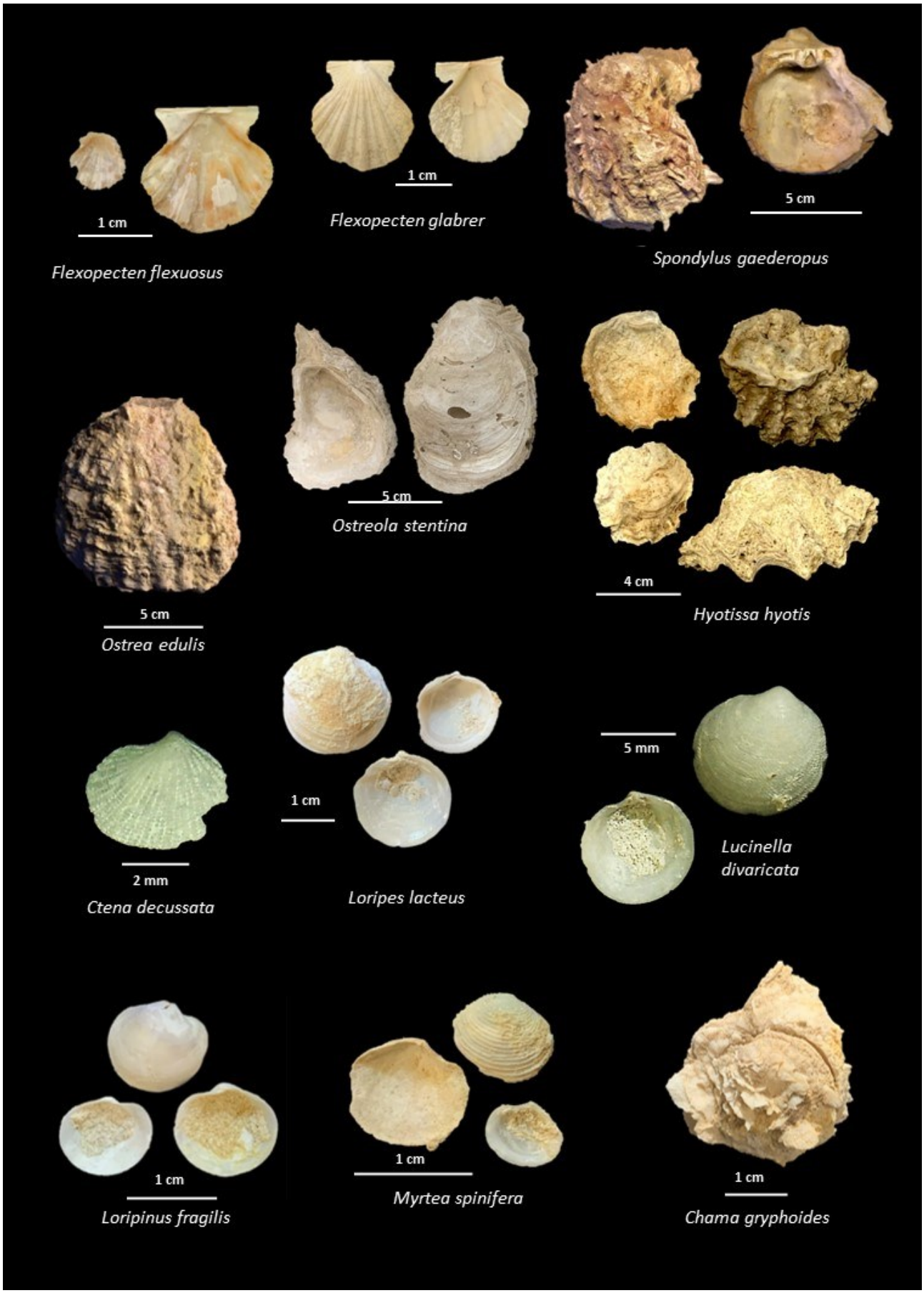
1 cm
Flexopecten flexuosus
1 cm
Flexopecten glabrer
5 cm
Spondylus gaederopus
5 cm
Ostrea edulis
5 cm
Ostreola stentina
4 cm
Hyotissa hyotis
2 mm
Ctena decussata
1 cm
Loripes lacteus
5 mm
Lucinella divaricata
1 cm
Loripinus fragilis
1 cm
Myrtea spinifera
1 cm
Chama gryphoides


2 mm
Hemilepton nitidum
1 cm
Cardita rufescens
2 mm
Glans trapezia
5 mm
Cardites antiquatus
1 cm
Acanthocardia aculeata
2 cm
Acanthocardia echinata
2 cm
Acanthocardia paucicostata
5 mm
Acanthocardia tubercolata
5 mm
Parvicardium exiguum
2 cm
Papillicardium papillosum
1 cm
Laevicardium crassum
2 cm
Cerastoderma glaucum
1 cm
Spisula subtruncata
1 cm
Lutraria oblonga
1 cm
Macomangulus tenuis


5 mm
Moerella distorta
1 cm
Moerella pulchella
5 mm
Gari fervensis
1 cm
Abra alba
2 cm
Azorinus chamasolen
5 mm
Venus casina
5 cm
Venus verrucosa
5 mm
Timoclea ovata
5 mm
Gouldia minima
2 cm
Dosinia exoleta
1 cm
Dosinia lupinus
5 mm
Pitar rudis
5 cm
Callista chione
1 cm
Mysia undata
5 mm
Varicorbula gibba


GASTROPODS
2 mm
Tectura virginea
2 mm
Smaragdia viridis
2 mm
Diodora graeca
1 cm
Diodora italica
2 mm
Emarginula octaviana
5 mm
Haliotis tuberculata
2 mm
Clanculus corallinus
5 mm
Gibbula ardens
1 mm
Gibbula guttadauri
5 mm
Gibbula magus
5 mm
Steromphala racketti
2 mm
Jujubinus striatus
2 mm
Calliostoma laugieri
2 mm
Calliostoma zizyphinum
2 mm
Tricolia pullus pullus
1 cm
Cerithium vulgatum

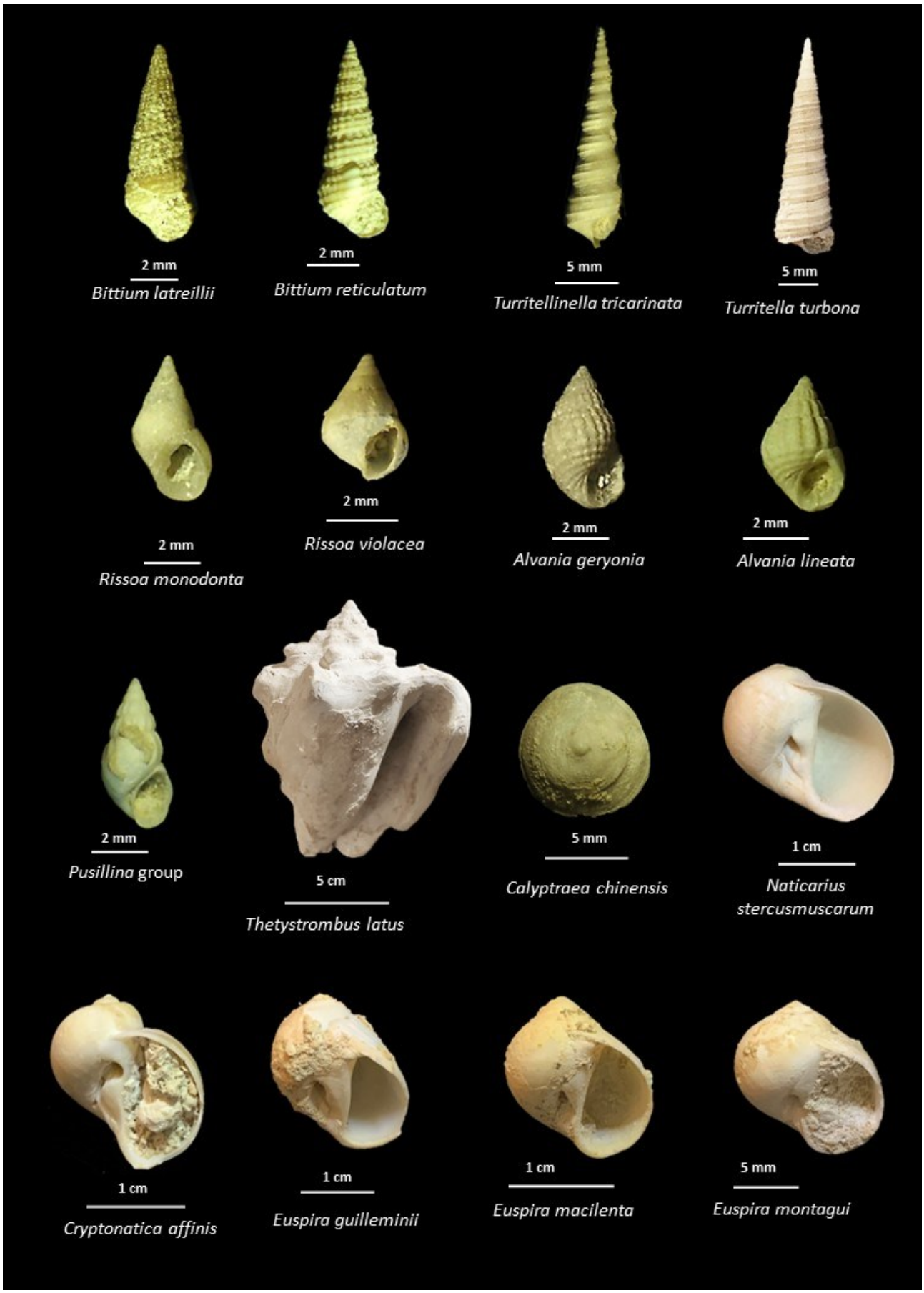
2 mm
Bittium latreillii
2 mm
Bittium reticulatum
5 mm
Turritellinella tricarinata
5 mm
Turritella turbona
2 mm
Rissoa monodonta
2 mm
Rissoa violacea
2 mm
Alvania geryonia
2 mm
Alvania lineata
2 mm
Pusillina group
5 cm
Thetystrombus latus
5 mm
Calyptraea chinensis
1 cm
Naticarius stercusmuscarum
1 cm
Cryptonatica affinis
1 cm
Euspira guilleminii
1 cm
Euspira macilenta
5 mm
Euspira montagui

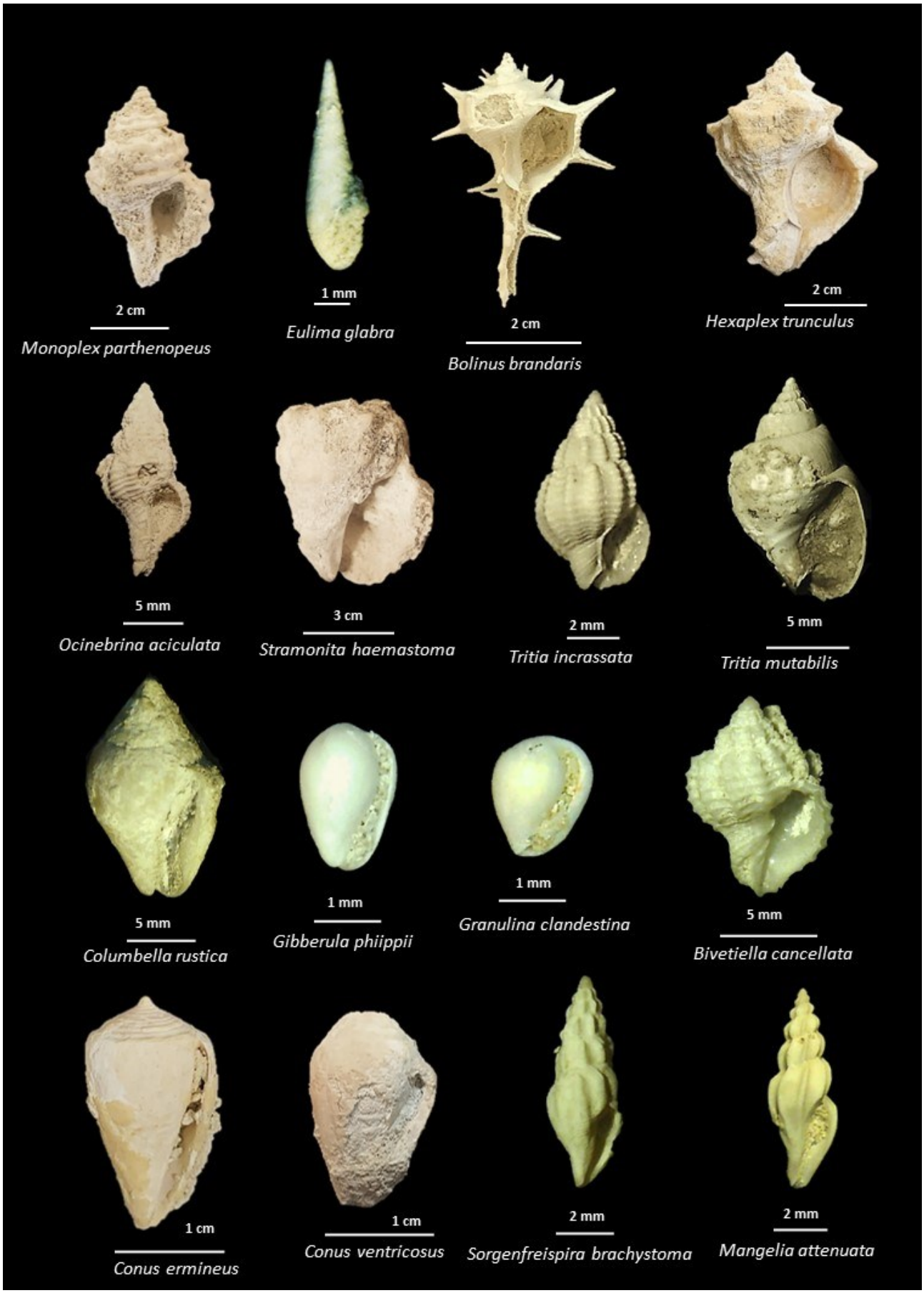
2 cm
Monoplex parthenopeus
1 mm
Eulima glabra
2 cm
Bolinus brandaris
2 cm
Hexaplex trunculus
5 mm
Ocinebrina aciculata
3 cm
Stramonita haemastoma
2 mm
Tritia incrassata
5 mm
Tritia mutabilis
5 mm
Columbella rustica
1 mm
Gibberula phiippii
1 mm
Granulina clandestina
5 mm
Bivetiella cancellata
1 cm
Conus ermineus
1 cm
Conus ventricosus
2 mm
Sorgenfreispira brachystoma
2 mm
Mangelia attenuata

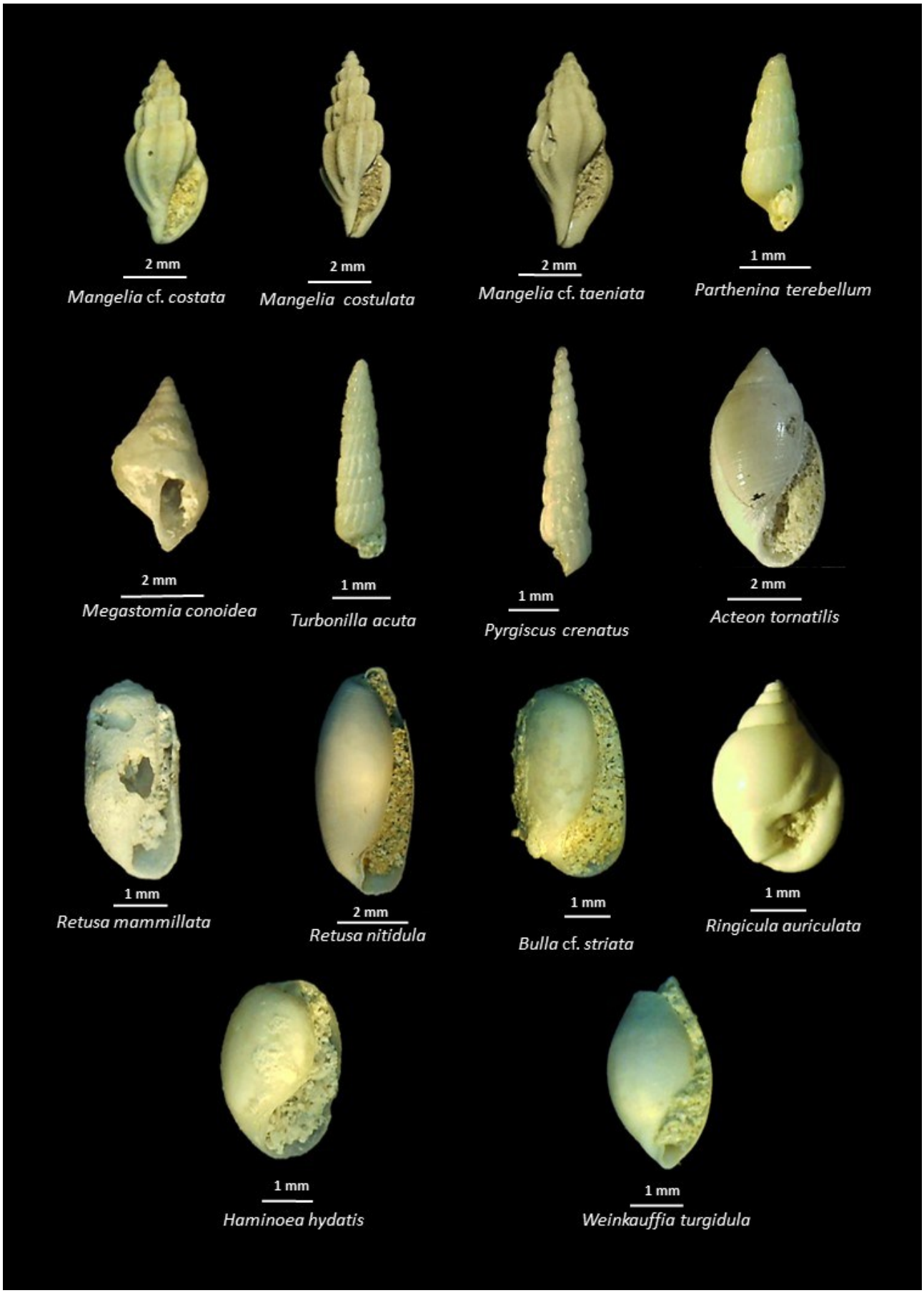
2 mm
Mangelia cf. costata
2 mm
Mangelia costulata
2 mm
Mangelia cf. taeniata
1 mm
Parthenina terebellum
2 mm
Megastomia conoidea
1 mm
Turbonilla acuta
1 mm
Pyrgiscus crenatus
2 mm
Acteon tornatilis
1 mm
Retusa mammillata
2 mm
Retusa nitidula
1 mm
Bulla cf. striata
1 mm
Ringicula auriculata
1 mm
Haminoea hydatis
1 mm
Weinkauffia turgidula

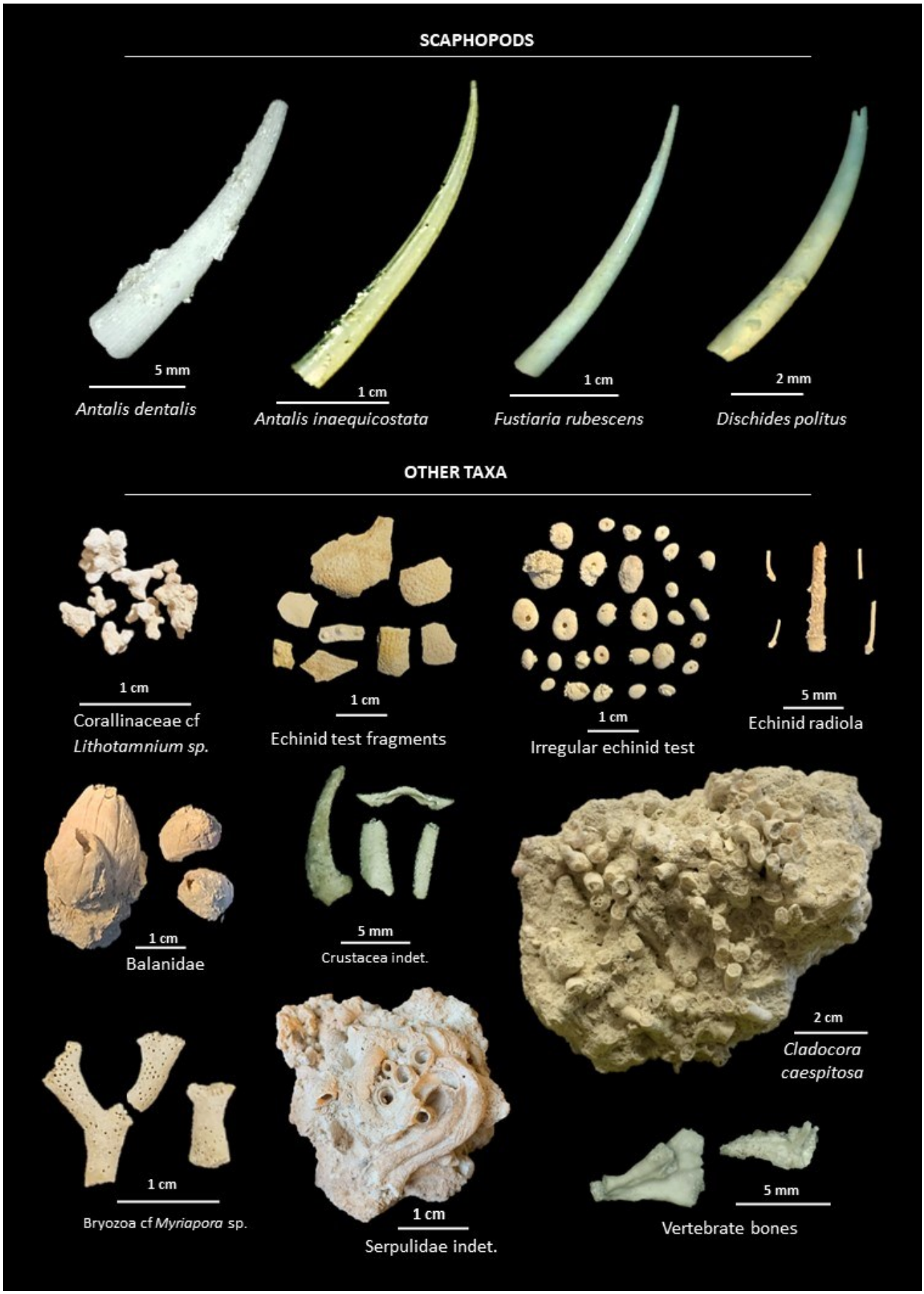
SCAPHOPODS
5 mm
Antalis dentalis
1 cm
Antalis inaequicostata
1 cm
Fustiaria rubescens
2 mm
Dischides politus
OTHER TAXA
1 cm
Corallinaceae cf
Lithotamnium sp.
1 cm
Echinid test fragments
1 cm
Irregular echinid test
5 mm
Echinid radiola
1 cm
Balanidae
5 mm
Crustacea indet.
2 cm
Cladocora
caespitosa
1 cm
Bryozoa cf Myriapora sp.
1 cm
Serpulidae indet.
5 mm
Vertebrate bones